Author/s:
Robinson, Jessica Louise

Title:
Structural and Regulatory Changes to the Mouse Y Chromosome

Date:
2020

Persistent Link:
https://hdl.handle.net/11343/243791

Structural and Regulatory Changes to the Mouse Y Chromosome

by Jessica Louise Robinson
ORCID 0000-0001-6199-2515

Submitted in total fulfilment of the requirements of the degree of Doctor of Philosophy

March 2020

Murdoch Children's Research Institute
Department of Paediatrics
Faculty of Medicine, Dentistry and Health Sciences
The University of Melbourne

Abstract

The X chromosome and the Y chromosome are the sex chromosomes of mammals. While the X chromosome carries many genes with functions beyond sex, the Y chromosome is relatively gene poor. It serves as the trigger for development of a male embryo, with its genes having roles in testis determination and function. The sex chromosomes exist as a pair; in females, this pair are XX, and in males, XY.

Two different mouse Y chromosomes were the focus of this project. The first was a transgenic fluorescent reporter Y chromosome, *Ddx3y*^{mKate2}, which was created to be used as a tool in chromosome instability research. The second was the naturally occurring Y chromosome from the A/HeJ inbred mouse strain, Y$^{A/HeJ}$. The work associated with these two Y chromosomes comprised the two studies in this project.

The *Ddx3y*^{mKate2} Y chromosome was generated by targeted insertion of a transgene cassette containing the red fluorescent protein gene, *mKate2*, into the mouse Y chromosome adjacent to the *Ddx3y* locus. This was selected as the relatively broad expression of *Ddx3y* indicated a permissive environment for expression of the *mKate2* transgene. As male mice are XY, all male *Ddx3y*^{mKate2} mice carried the fluorescent reporter. The mKate2 fluorescence in this strain has been previously assessed, revealing that the reporter was detectable from the preimplantation embryo, through to sexual maturity. To finalise the characterisation of the *Ddx3y*^{mKate2} mouse, this study assessed the fluorescence in the *Ddx3y*^{mKate2} male in advanced age. Additionally, this study characterised another transgenic reporter strain, *Hprt*$^{DsRed\text{-}Express}$, to serve as a comparison. To demonstrate the utility of the *Ddx3y*^{mKate2} reporter, the *Ddx3y*^{mKate2} Y chromosome was crossed onto two known chromosome instability backgrounds: the *Trp53* knockout and *Cenpagfp* fusion knock-in backgrounds. Following *in vivo* and *in vitro* experiments, it was determined that the *Cenpagfp* background was the better background to model the *Ddx3y*^{mKate2} reporter Y chromosome; however, more work using this genetic background in embryonic stem cells is advised for assessing the *Ddx3y*^{mKate2} reporter Y chromosome.

The Y$^{A/HeJ}$ chromosome from the inbred A/HeJ strain was causally associated with a disturbance in the testis determination pathway. The Y$^{A/HeJ}$ chromosome resulted in a subset of male mice having developed either ovotestes (gonads containing ovarian and testicular tissue) or abnormally small testes without epididymal sperm. It was confirmed that the Y$^{A/HeJ}$ chromosome still carried the testis triggering gene, *Sry*. The gonadal and cytological abnormalities associated with this Y chromosome lead to the speculation that there was a structural change at or near its centromere. This study extended the characterisation of the A/HeJ phenotype, including identification of an age-related decline in male gonad mass, as well as assessment of the Y$^{A/HeJ}$ chromosome. It was confirmed that the structural change to the Y$^{A/HeJ}$ chromosome was a halving of the *Rbmy* tandem repeat array. This was predicted to adversely affect *Sry* gene expression during testis determination, resulting in the A/HeJ gonadal phenotype. Assessment of *Sry* regulation and gene expression from the Y$^{A/HeJ}$ chromosome is recommended to complete the work associated with this Y chromosome.

Declaration of Work Completed

Declaration

This is to certify that:

i. The thesis comprises only my original work towards the PhD except where indicated in the Preface,

ii. Due acknowledgement has been made in the text to all other material used

iii. The thesis is fewer than 100,000 words in length, exclusive of tables, maps, bibliographies and appendices

Jessica Robinson

March 2020

Preface

Pursuant to the regulations governing the degree of Doctor of Philosophy at the University of Melbourne, I hereby submit:

i. The author's contribution to Chapter 3 was 98%. Miss Alison Graham (Murdoch Children's Research Institute) collected and fixed the E17.5 *Ddx3y*^{mKate2} embryo tissues, which was sectioned and stained by the author.

ii. The author's contribution to Chapter 5 was 99%. Miss Alison Graham (Murdoch Children's Research Institute) assisted with imaging of abnormal A/HeJ genitalia.

iii. The author's contribution to Chapter 6 was 85%. Miss Alison Graham (Murdoch Children's Research Institute) collected all genital ridge samples assessed in the preliminary bisulfite sequencing, including dissections, DNA extracting, bisulfite conversion and mass cleavage. Initial processing of the preliminary bisulfite sequencing data was also performed by Miss Alison Graham, with subsequent analysis of the data performed by the author. Additionally, approximately 5% of the genital ridge samples assessed in the methylation-dependent Droplet Digital PCR and bisulfite sequencing were dissected by Miss Alison Graham.

Therefore, the author's overall contribution to the work presented in this thesis was 93%.

Acknowledgements

I would like to thank Doctor Paul Kalitsis and Doctor Damien Hudson for the opportunity to undertake my PhD in their laboratory. I would also like to that my advisory committee, Doctor Alex Combers and Doctor Don Newgreen, for their support and advice during my studies. I would like to extend my thanks to past and present members of the Chromosome Research Group: Doctor Thian Thian Beh, Doctor Christian Nielsen, Doctor Tao Zhang and Miss Alison Graham, for their support over the years.

A special thanks goes to Miss Alison Graham for her assistance both in the laboratory and beyond, including her continued assistance and support over this journey. Her exceptional input has been invaluable to my PhD adventure.

I would also like to thank my colleagues and friends, Ms Michelle Scurr, Ms Louise O'Connor, Doctor Astrid Glaser and Doctor Jaya Vikraman for their support and friendship. I also thank Doctor Matt Burton for his assistance regarding confocal microscopy and cell sorting, and the Animal House staff for their on-going assistance managing our mouse colonies.

Last, and certainly not least, a profound thank you to my family, without whom I would have been unable to pursue this journey: Tasha Robinson, Dean Robinson, Ben Robinson, and our dogs, Buster and Murphy. Your ongoing support and encouragement have been integral to my ability to undertake my PhD, and I cannot conceive of having done this without you.

Table of Contents

List of Figures

List of Tables

Abbreviations

Abbreviation	Definition
µg	Microgram
µL	Microlitre
µM	Micromolar
α	Alpha
ABC	Avidin/Biotin Complex
ABS	Absolute Quantification
AEC	Animal Ethics Committee
AGD	Anogenital Distance
BAC	Bacterial Artificial Chromosome
BLAST	Basic Local Alignment Search Tool
bp	Basepair
C	Cytosine
C-terminal	Carbon-terminal
CAIS	Complete Androgen Insensitivity Syndrome
Cenpa	Centromere Protein A
CMV-CAG	Cytomegalovirus-Chicken Beta Actin
CNV	Copy Number Variation
CO_2	Carbon Dioxide
CpG	CG Dinucleotide
CRISPR	Clustered Regularly Interspaced Short Palindromic Repeats
d	Days (post-natal)
DAB	3,3'-diaminobenzidine
DAPI	4',6-diamonding-2-phenyliodine
ddPCR	Droplet Digital PCR
Ddx3y	DEAD (Aspargine-Glutamate-Alanine-Asparagine) Box Polypeptide 3, Y Chromosome-linked
dH_2O	Deionised water
DMEM	Dulbecco's Modified Eagle Medium
DMU	Disease Model Unit, also referred to as the Animal Facility of MCRI
DNA	Deoxyribonucleic Acid
dNTP	Deoxyribonucleoside triphosphate
dpc	Days Post-Coitum
DQ	Direct Quantification
DSD	Disorder of Sex Determination

E	Embryonic Day
EDTA	Ethylenediaminetetraacetic acid
EGFP or eGFP	Enhanced GFP
EpiS	Epiblast Stem (cell)
ES	Embryonic Stem (cell)
EtOH	Ethanol
FACS	Fluorescence-Activated Cell Sorting
FBS	Foetal Bovine Serum
FISH	Fluorescence *in situ* Hybridisation
G	Gauge
G1	Gap 1 (Phase)
GFP	Green Fluorescent Protein
HBSS	Hank's Buffered Saline Solution
HMG	High Mobility Group
Hprt	Hypoxathine Guanine Phosphoribosyl Transferase
ICM	Inner Cell Mass
IHC	Immunohistochemistry
iPS	Induced Pluripotent Stem (cell)
kb	Kilobase
KCl	Potassium Chloride
kDa	Kilodalton
KO	Knockout
lncRNA	Long non-coding RNA
M	Molar
Mb	Megabase
^{m}C	Methylcytosine
MCRI	Murdoch Children's Research Institute
$MgCl_2$	Magnesium Chloride
mL	Millilitre
mM	Millimolar
mm	Millimetre
mRNA	Messenger RNA
ms	Millisecond
MSCI	Meiotic Sex Chromatin Inactivation
MSUC	Meiotic Sex Unpaired Chromatin
N-terminal	Nitrogen-terminal
NCBI	National Center for Biotechnology Information

Neo^R	Neomycin Resistance
ng	Nanogram
NLS	Nuclear Localisation Signal
nm	Nanometre
NP40	Nonidet P40
NTC	No Template Control
ORF	Open Reading Frame
p	Short (arm of chromosome)
PAIS	Partial Androgen Insensitivity Syndrome
PAR	Pseudoautosomal Region
PBS	Phosphate Buffered Saline
PCR	Polymerase Chain Reaction
PEV	Position Effect Variegation
PFA	Paraformaldehyde
PGC	Primordial Germ Cell
PGK	Phosphoglycerate Kinase
PMEF	Primary Mouse Embryonic Fibroblast
PMSC	Post-Meiotic Sex Chromatin
q	Long (arm of chromosome)
Rbmy	RNA-Binding Motif Protein, Y Chromosome
RBC	Red Blood Cell
RNA	Ribonucleic Acid
S phase	Synthesis Phase
SAP	Shrimp Alkaline Phosphatase
SD	Standard Deviation
SDS	Sodium Dodecyl Sulfate
SEM	Standard Error of the Mean
Sox9	Sry-Related HMG (High Mobility Group) Box 9
Sry	Sex Determining Region of the Y Chromosome
SSC	Saline Sodium Citrate
T	Thymine
TBE (buffer)	Tris-Borate-EDTA
TE	Trophectoderm
TE (buffer)	Tris-EDTA
TNB	Tris-NaCl-Blocking (buffer)
Trp53	Tumour Repressor Protein 53
ts	Tail Somites

U	Units (of enzyme); Uracil
v/v	Volume per volume
XCI	X Chromosome Inactivation
Ymin	Y Chromosome Minor Satellite (DNA)
Yp	Short arm of the Y chromosome
Yq	Long arm of the Y chromosome
x g	Multiplied by the force of gravity ('times' gravity)

Chapter 1: Introduction

1.1. Introduction

The experiments detailed in this thesis were performed to assess two different mouse Y chromosomes. The first Y chromosome assessed was a transgenic fluorescent reporter Y chromosome generated by targeted insertion of a gene cassette containing the red fluorescent protein gene, *mKate2*. The gene cassette was inserted into the short arm of the Y chromosome adjacent to the *Ddx3y* gene to create the *Ddx3y*^{mKate2} reporter Y chromosome, with the aim that this could be used as a tool in chromosome instability research. All male mice in the resulting transgenic *Ddx3y*^{mKate2} strain carry the reporter Y chromosome.

Previously, the *Ddx3y*^{mKate2} reporter mouse strain had been assessed for the characteristics of the fluorescence from the reporter[5] so as to better inform future researchers on its usefulness. This previous characterisation has been summarised in Sections 1.1.6.1.2 and 3.1.1.2. The work performed on the *Ddx3y*^{mKate2} reporter strain in this study focused on two aims: to finalise the characterisation of the *Ddx3y*^{mKate2} mouse, including comparison to another transgenic mouse strain, *Hprt*$^{DsRed\text{-}Express}$; and to model the *Ddx3y*^{mKate2} reporter Y chromosome on known chromosome instability backgrounds to demonstrate its utility.

The second study in this project focused on the Y$^{A/HeJ}$ chromosome, a naturally-occurring Y chromosome which was identified in the inbred A/HeJ mouse strain. This Y chromosome had previously been causally-linked to abnormal gonads in A/HeJ mice[2], despite carrying the testis triggering gene *Sry*[2]. The original characterisation of the Y$^{A/HeJ}$ chromosome speculated that there was a structural defect or change at or near the centromere[2]. This defect was predicted to adversely affect the testis determination pathway in embryos carrying the Y$^{A/HeJ}$ chromosome, leading to the abnormal gonads (ovotestes and small testes) observed in adults[2]. The work in this study extended the characterisation of the phenotype associated with the Y$^{A/HeJ}$ chromosome, as well as assessed the Y$^{A/HeJ}$ chromosome for a change in the *Rbmy* repeat array, which was hypothesised to be the locus of the predicted structural change. The *Sry* locus on the Y$^{A/HeJ}$ chromosome was also assessed for changes in its methylation during the window of testis determination.

This chapter will provide background on chromosomes, focusing specifically on the mouse Y chromosome and its role in male sex determination. The details of mouse embryogenesis, including testis determination during gestation, will also be explored. Additionally, a brief background on each of the mouse strains examined in this project will be outlined. Finally, the respective aims and hypotheses of the two studies of this thesis's project will be stated.

1.1.1. Chromosomes

In eukaryotes, the instructions for life, genes, are encoded in DNA[7] which is organised into discrete structures known as chromosomes[7]. Chromosomes reside in the nucleus, a membrane-bound structure in the cell[8], with the sum of all chromosomes within a cell is referred to as its karyotype. For the majority of the cell cycle (interphase), chromosomes exist in a relaxed state in nuclear domains called chromosome territories[9-11], which are comprised of higher-order chromatin units[10]. These territories are spatially limited, and serve an important role in transcription, by bringing genes and their enhancers into close physical proximity[9,12]. When the cell begins cell division (mitosis/meiosis) following DNA replication, its chromosomes become distinct entities through a combination of compaction (Figure 1.1A) and topological rearrangements[13], including organisation into a series of loops mediated by the condensin protein complexes[13-15].

The functional unit of chromatin is the nucleosome, a complex of DNA with histone protein octamers[16]. These octamers are composed of four dimers, two of histone H2A-H2B and two of histone H3-H4[17,18]; the DNA wraps around the histone octamer to form the nucleosome[19]. Adjacent nucleosomes are separated from one another by linker DNA, between 10 base pairs (bp) and 80 bp of sequence, associated with histone H1, giving a 10 nm fibre[19,20] with a "beads on a string appearance". The nucleosomes then coil in on themselves, to generate a higher-order fibre with a 30 nm diameter[19], which in turn forms a helical chromatin fibre in interphase. This process results in the condensed chromosome structure that is prepared to undergo nuclear division.

A chromosome consists of chromosome arms, a centromere and telomeres. The chromosome arms contain the genes the chromosome carries, as well as sequence between genes. The centromere is the primary constriction of the chromosome between the chromosome arms and is the site of kinetochore assembly[21] in preparation for division. The telomeres cap the ends of the chromosome arms to protect the coding regions.

There are four broad types of chromosomes: metacentric, submetacentric, acrocentric and telocentric. Metacentric chromosomes consist of short (p or 'petite' ('small' in French)) and long (q or 'queue' (the next letter after p)) arms which are similar in length (Figure 1.1B), which are similar in length, and as such the centromere is in the centre of the condensed chromosome[22]. In the case of submetacentric chromosomes, the short arm is noticeably shorter than the long arm, resulting in the centromere no longer being centrally located on the chromosome[22]. For acrocentric chromosomes, where the short arm is substantially shorter than the long arm, the centromere is far closer to one end of the chromosome than the other[21,23]. Telocentric chromosomes do not possess a short arm, consisting only of a long arm, with the centromere located at the end of the chromosome[23]. Duplicated long arms of telocentric chromosomes therefore join at the end of this chromosome arm[23].

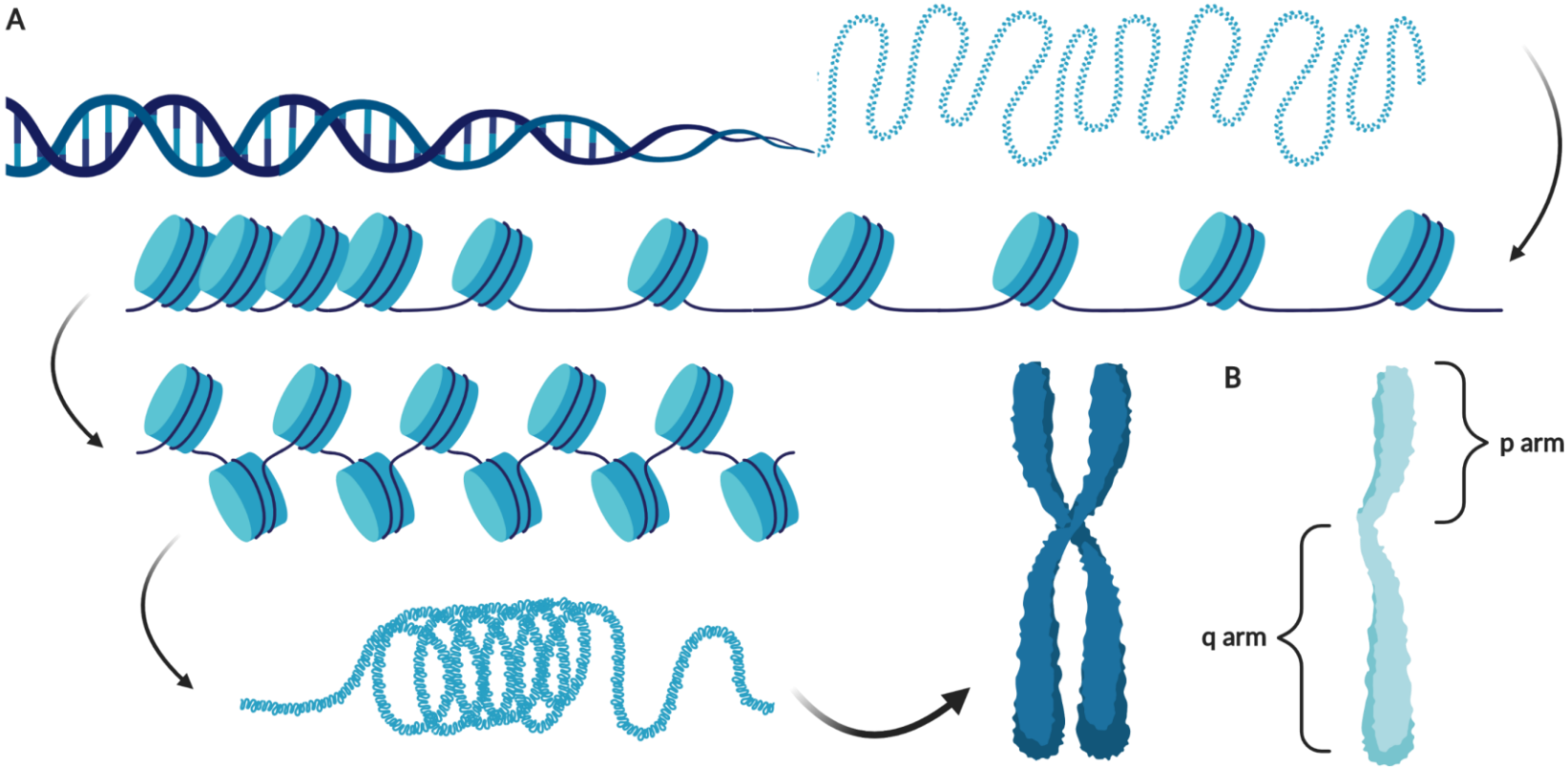

Figure 1.1 - Compaction of DNA into Eukaryotic Chromosomes

(A) The primary sequence of the eukaryotic genome begins as a double stranded sequence (upper left). This then coils itself tightly (upper right) in order to enable winding of the DNA around histone octamers to form nucleosomes (middle right), the functional unit of chromatin. These nucleosomes have a 'bead on a string' appearance, and then begin to compact (upper middle left, lower middle left) to form chromatin fibres (bottom left). The chromatin fibres then undergo further compaction, eventually forming the condensed metaphase chromosome (bottom right). Not to scale. (B) Eukaryotic chromosomes are composed of a long (q) arm and a short (p) arm, with the exception of telocentric chromosomes which only have a long arm (not shown). These chromosome arms join at the centromere, represented as the primary constriction of the condensed chromosome.

1.1.1.1. The Centromere

In preparation for nuclear division, each chromosome arm is duplicated, forming a pair of sister chromatids. Duplicated sister chromatids, and the long and short chromosome arms, are all joined to one another at the centromere, appearing as a constriction on the chromosome. The centromere is a region of DNA typically composed of adenosine-thymine (AT)-rich tandem repeat satellite sequence[21]. In mice, this sequence is referred to as minor satellite DNA[24], while in humans it is referred to as alpha (α) satellite DNA[25]. Centromere satellite DNA repeat sequences can vary in size between chromosomes and species[26], ranging from 90 kb to many Mb in size[24]. This sequence is the base upon which centromere proteins assemble to aid cohesion between chromosome arms and sister chromatids. However, despite the fact that this satellite DNA typically identifies the canonical centromere, functional centromere locations are specified by the assembly of certain constitutive proteins.

Some centromere proteins are constitutive to the centromere, residing in the region and specifying its location throughout the cell cycle. One such constitutive protein is Centromere Protein A (*Cenpa*)[27,28], a mammalian histone H3-like protein that is found only at the centromere[24,29]. At the centromere, a subunit of *Cenpa* heterodimerises with histone H4[29], and this heterodimer combines with two heterodimers of histone H2A and H2B, to form a *Cenpa* nucleosome at the centromere[29]. *Cenpa* was the first identified centromeric protein, and remains at the centromere in the nucleosome structure throughout the cell cycle[27,28]. The presence of Cenpa protein is the primary epigenetic determinant of the centromere[23,24,28]. While centromeric DNA sequences exhibit a wide range of sequence divergence[26], the Cenpa protein is highly evolutionary conserved between species[26], highlighting its importance in chromosome biology.

Other proteins are transiently associated with the centromere, coming to the region specified by Cenpa as the cell prepares for division, to assemble a scaffold structure known as the kinetochore[21]. The kinetochore is a multi-protein complex composed of at least one hundred proteins[21], and forms the point of connection between the duplicated chromosome and the nuclear division machinery of the cell[21,29]. This is achieved by attachment of the spindle microtubules to the outer kinetochore[29]. In mice, the kinetochore binds between five and seven microtubules per chromosome[30], whereas human kinetochores bind approximately 20 microtubules per chromosome[31]. Attachment of sufficient spindle microtubules to all chromosomes is required for a cell to proceed through division, representing a metaphase-anaphase checkpoint[29]. The function of this checkpoint is to ensure that the sister chromatids of all chromosomes will be effectively separated[29], and hence the correct number of chromosomes will migrate to each pole of the dividing cell.

1.1.1.2. Cell Division

There are two types of nuclear division: mitosis and meiosis. Mitosis is a process which produces genetically identical daughter cells, by dividing duplicated sister chromatids between the resulting daughter cells. Meiosis, meanwhile, is the process of halving the genome to produce genetically distinct haploid daughter cells. This process involves facilitating recombination between homologous chromosomes, followed by the first meiotic division, dividing homologues between the resulting daughter cells. This is followed by the second division which then separates sister chromatids between daughter cells, which now contain a haploid genome[32]. Meiosis occurs in the germ cells, which are then able to combine to generate a diploid (two chromosome sets) offspring (refer to Section 1.1.4).

In mammals, diploidy is the normal genetic state, with changes from the diploid chromosome number being deleterious. However, other organisms, such as angiosperm plants[33], have more than two copies of their chromosome complement (polyploid)[33]. Euploidy refers to the state of having the correct number of chromosomes, while aneuploidy refers to having an abnormal number of whole chromosomes, including gains or losses of chromosomes[34].

Aneuploidy is highly associated with cancers[35] and birth defects or miscarriages[36], with an estimated 35% of spontaneous abortions being due to aneuploidy in the conceptus[36]. Additionally, in humans, approximately 75% of haematopoietic cancers and 90% of solid tumours are aneuploid[35]. Aneuploidy may present as full aneuploidy, affecting all cells in an organism[32], but may also be mosaic aneuploidy; that is, the change/s to the karyotype are not present in all cells in an organism[32,34]. Monosomy is the condition in which a diploid cell or organism has only a single copy of a particular chromosome[32]. This typically results from the loss of one whole chromosome out of the homologous pair during cell division[32]. Autosomal monosomy in mammals is typically lethal, as autosomes carry many essential genes[32].

Contrasting to monosomy, it is also possible for cells or animals to gain additional whole chromosomes[34]. The term used to describe these abnormal chromosome numbers depends on the number of homologous chromosomes following the gain event: trisomy is the presence of three homologous chromosomes in an otherwise diploid cell[34], tetrasomy is the presence of four homologues in a cell[34], and so forth. Many of these conditions in which additional autosomal homologues are present also result in lethality[34]. Some chromosome aneuploidies, however are survivable in a cell, or in an animal, and may allow the affected individual to reach full-term gestation before the onset of lethality, such as trisomy of chromosome 13 or chromosome 18 in humans[34]. Some aneuploidies even allow survival into adulthood, such as trisomy of chromosome 21 in humans, which results in Downs Syndrome[34].

Regarding sex chromosomes, the impact of aneuploidy can differ. The sex chromosomes

(explored further in Section 1.1.2) in mammals are the X and Y chromosomes, with the Y chromosome being essential for testis determination. From these two chromosomes, the sex chromosome configuration can be XX, in which the sex chromosome pair is homologous, or can be XY, in which both the X and Y chromosomes are hemizygous. It is possible for a cell or animal to experience sex chromosome monosomy[34] in the XY system of sex determination. However, it is only X chromosome monosomy that is potentially survivable in a cell or animal[32], as the X chromosome contains many genes that serve metabolic or housekeeping functions unrelated to sex determination.

Total absence of the X chromosome and these essential genes is lethal, but having a single X chromosome can be survivable[32], as in mammals only a single X chromosome is active in a single cell[37]. Additional X chromosomes are silenced by a mechanism called X chromosome inactivation (XCI, discussed further in Section 1.1.2.1), which serves to ensure equal X chromosome gene dosage between XX and XY individuals[37]. The Y chromosome, in contrast, is typically able to be lost from a cell or animal with little impact on viability (discussed further in Section 1.1.2.2).

1.1.2. The Sex Chromosomes

The presence of the Y chromosome is required for the development of a male in mammals[38,39]. Despite being relatively gene-poor, the Y chromosome contains genes related to testis determination and spermatogenesis[40]. This is in contrast to its partner, the X chromosome, which contains many essential genes, such as housekeeping and metabolic genes[21,41,42]. It is for this reason that the Y chromosome is considered 'non-essential' in terms of cell viability, as its loss does not result in cell lethality. Loss of the Y chromosome can, however, have adverse effects on an organism due to the resulting X chromosome monosomy.

For example, loss of the Y chromosome (or the inactive X chromosome) in humans results in a condition known as Turner's Syndrome, occurring in one in 2500 live born girls[43]. The 45,XO females exhibit many congenital problems, such as cardiovascular and renal problems, infertility, short stature[35,43-45], and in cases where loss of the Y chromosome has been mosaic[43,45], potential to develop gonadoblastoma, a cancer of the gonads[35,43-45]. This cancer is associated with retention of Y chromosome material in cells of the gonadal tissue[43]. In contrast, loss of the Y chromosome in mice does not adversely affect the mouse, with the resulting 39,XO females being both viable and fertile[46].

The mammalian X chromosome and Y chromosome originated from an ancestral pair of autosomes[40,47,48], but these two chromosomes diverged from one another between 160 million and 166 million years ago[49-51]. Due to their joint origin from a homologous pair, there are genes which have homologues on both the X chromosome and Y chromosome, such as *Rbmx* and *Rbmy* or *Ddx3x* and *Ddx3y*, respectively. In addition to these homologues, the X chromosome and Y chromosome

also share a region of homology, called the pseudoautosomal region, or PAR[52,53]. This region facilitates pairing between the X chromosome and Y chromosome in male meiosis[41,54]. X chromosomes in XX individuals, meanwhile, pair along their entire length[36], as they are homologues. In mice, there is one PAR on the Y chromosome of approximately 700 kb in size[55-57], which has a corresponding PAR on the X chromosome, while in humans there are two PARs, with a major PAR of approximately 2.7 Mb in length[58] at the tip of the short arm of both sex chromosomes, and a minor PAR at the tip of the long arms (approximately 330 kb)[58]. Typically, only the larger PAR on the human sex chromosomes is used in meiotic recombination[58]. Outside of the PAR, the sex chromosomes share little homology[59,60].

Over the course of the evolution of the XY system of sex determination, the Y chromosome has progressively lost much of its gene content[52,59], retaining few genes which largely have their functions restricted to determination, development and function of the male reproductive system[52,59]. The genes that have remained on the Y chromosome are associated with testis determination and function, with sex determination (the commitment of an organism to develop as either a male or female) resulting from the sex chromosome constitution[39]. Male organisms develop from XY embryos, and females, from XX embryos[38].

The evolutionary selective pressure is different on the X and Y chromosomes. Gene stability over time is facilitated by homology directed repair between homologous chromosomes, such that gross mutations on a single chromosome are often repaired using the homologue as a template[52]. Additionally, recombination between homologous sites on chromosome pairs maintains persistence of genes[21,52]. In this way, the X chromosome has an advantage, as it is able to undergo these processes in XX individuals, adding to its stability over time[52]. The Y chromosome, in contrast, does not have a homologue, being hemizygous in males[21,41,52]; as such, it does not have a homologous partner to use as a template to correct any defects[21,41]. This results in a higher susceptibility to genetic drift relative to autosomes and the X chromosome[21,61], as it is the largest region of the genome at which variation can only occur as a result of mutational incidents[61]. The effective population size of the Y chromosome is one quarter that of each of the autosomes[21,61].

1.1.2.1. Mouse X Chromosome Inactivation

Due to the difference in the number of X chromosomes between the sexes, it is essential that the X chromosome gene dose is equalised between males and females[37]. This is needed because cells which have two (or more) active X chromosomes will experience a deleterious overdose of X chromosome-linked genes[62]. To ensure that the gene dosage from the X chromosome is equal between the sexes, the phenomenon known as X chromosome inactivation (XCI) evolved, which results in only one X chromosome being active per cell[37]. All remaining X chromosomes in a given cell become transcriptionally silenced or 'inactivated'[37,62]. As this project focuses on mice, only mouse XCI is discussed in this section.

The main element in the process of XCI is a long non-coding RNA (lncRNA) called *Xist*[37,62]. *Xist* is expressed from the inactive X chromosome and acts to inactivate that chromosome by coating it[37], condensing it into a structure known as a Barr body[63] which is transcriptionally silenced[37,62]. In a cell with more than one X chromosome, all bar one will undergo XCI to form Barr bodies. For example, an XXX individual (X chromosome trisomy) would have a single active X chromosome and two Barr bodies per cell[64]. This would also be the case in cells carrying a Y chromosome and additional X chromosome/s, such as XXY, as these cells also require only a single active X chromosome[65]. However, while the cells have a mechanism to inactivate additional X chromosomes, having more than one or two X chromosomes in a cell or animal can still result in deleterious effects[64,65]. Multiple copies of the Y chromosome does not appear to exert much negative effect on the cell or animal, although 47,XYY humans are at higher risk of delayed development and learning difficulties[66].

Two types of XCI are observed in mice: imprinted XCI and random XCI. Imprinted XCI is observed in the early preimplantation embryo (discussed further in Section 1.1.4), in which the paternal X chromosome in an embryo is preferentially inactivated, and hence silent in all cells of the embryo. This is due to preferential transcription of the *Xist* RNA from the paternal X chromosome[67], inactivating this chromosome. The level of *Xist* RNA from the paternal locus does not reach levels sufficient to inactivate this X chromosome until approximately the four-cell stage[67], as two-cell embryos show gene activity from paternal X chromosome loci[67] following embryonic genome activation at this stage[68-71].

The paternal X chromosome is later reactivated in the post-implantation embryo, at which point the second type of XCI is established: random XCI[62,72-74]. This manifests as either the maternal or paternal X chromosome being inactivated at random in each cell of the organism[37,62], although the stage at which this happens varies between species. In mice, random XCI occurs in the embryo proper following implantation into the uterine wall[37,62,75].

1.1.2.2. The Mouse Y Chromosome

The mouse Y chromosome is acrocentric, possessing a long arm and a very short arm. The majority of the genes on the Y chromosome are contained on the short arm, with the long arm being predominantly made up of ampliconic repeats (repeated DNA/gene units)[76] (Figure 1.2). Indeed, 98.0% of the euchromatic DNA of the mouse Y chromosome (89.5 Mb, 99.9% of whole chromosome) is gene-dense ampliconic sequence[76]. This large amount of euchromatin on the mouse Y chromosome aligns this chromosome more closely to the composition of the mouse autosomes than to Y chromosomes of other species[76]. The human Y chromosome, for example, is comprised of only approximately 40% euchromatin (22.8 Mb[76] of the total 57 Mb[77]).

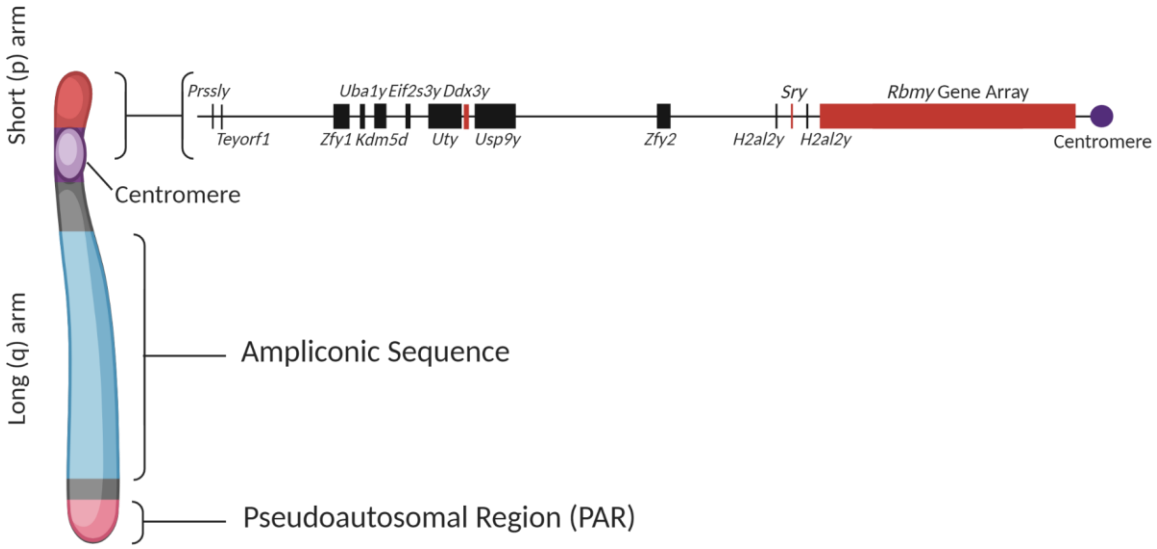

Figure 1.2 - Schematic of the Mouse Y Chromosome

The mouse Y chromosome is acrocentric, having a long arm which is primarily composed of ampliconic sequence (blue), and a gene-rich short arm (red). These arms join at the centromere (purple), the primary constriction of the condensed chromosome, and the site at which the division machinery of the cell attaches to the chromosome. The long arm of the mouse Y chromosome also contains the pseudoautosomal region (PAR, pink), a region of homology to the mouse X chromosome which facilitates pairing of the sex chromosomes in male meiosis. The genes of interest in this project (*Ddx3y*, *Sry*, and *Rbmy*) are highlighted in the map of short arm genes (right). Not to scale.

The centromere of the mouse Y chromosome is composed of approximately 90 kb of minor satellite repeat DNA specific to the Y chromosome, termed Y minor or Ymin sequence[21,24]. This centromeric sequence on the mouse Y chromosome exhibits greater divergence than the divergence observed at mouse autosomal and X chromosome centromeres[21,24,26], and the 90 kb array is composed of a 2.3 kb higher order repeat unit present in multiple copies[21]. The 90 kb array of centromeric DNA lies between the short arm (3.5 Mb) and long arm (86.0 Mb) of the chromosome[76]. This Ymin satellite sequence interacts with the centromeric protein Cenpa[21].

The long arm of the mouse Y chromosome (Figure 1.2) consists of ampliconic sequence acquired following the divergence of the X and Y chromosomes, accounting for 86.4 Mb of the 89.6 Mb of the mouse Y chromosome[76]. This ampliconic sequence contains a 0.5 Mb ampliconic region that is present in approximately 200 copies[76], as well as a pair of each of 7 Mb and 4.5 Mb tandem repeats[76]. The long arm ampliconic repeat element contains three protein coding families: *Sly* (*Sycp3*-like Y chromosome-linked, 132 gene copies), *Srsy* (Serine-rich, secreted, Y chromosome-linked, 197 gene copies) and *Ssty* (Spermiogenesis specific transcript of the Y1, 317 gene copies)[76]. *Sly* and *Ssty* are related to autosomal genes in the mouse, on chromosome 10 (*Sycp3*, Synaptonemal complex protein 3) and chromosome 13 (*Spin1*, Spindlin 1), respectively[76,78,79].

From the centromere of the mouse Y chromosome, the short arm (Figure 1.2) contains a large region comprised of a tandem repeat array of multiple copies of the RNA-binding motif protein (Y Chromosome-linked) gene, *Rbmy*. This region spans approximately 1.1 Mb of sequence[76], and current estimates put the number of repeats at 30 gene units[76]. Beyond this lies the testis determining gene, *Sry* (Sex determining Region of the Y), which is located inside an inverted repeat of the gene *H2al2* (*H2al2b* and *H2al2c*, downstream and upstream of *Sry*, respectively)[76], a histone H2A homologue. Towards the telomere of the short arm, there are several genes involved in spermatogenesis and spermiogenesis, the processes associated with generation and maturation of the male gametes (refer to Section 1.1.5.2.1). These genes include *Usp9y* (Ubiquitin specific peptidase 9, Y chromosome, involved in germ cell development[76,80]), *Zfy1* and *Zfy2* (Zinc finger protein 1 and 2, Y Chromosome-linked, involved in meiosis and formation of sperm[76,81,82]), and *Eif2s3y* (Eukaryotic translation initiation factor 2, subunit 3, structural gene Y Chromosome-linked, involved in differentiation of spermatogonia stem cells[76,83]). The last genes on the Y chromosome short arm before the telomere are the single copy genes *Prssly* (protease, serine-like, Chr Y[76]) and *Teyorf1* (testis expressed, Chromosome Y open reading frame 1[76]), both of which are expressed in the germ cells of the testis[76].

Three gene regions are of interest in this thesis: *Ddx3y*, *Sry*, and the *Rbmy* tandem repeat array. *Ddx3y* is relevant to the first study (the *Ddx3y*^{mKate2} reporter mouse), while *Sry* and the *Rbmy* array are relevant to the second study (the A/HeJ mouse).

Ddx3y (DEAD[Asparganine-Glutamine-Alanine-Asparganine]-box polypeptide 3, Y chromosome-linked) is an RNA helicase that functions in RNA metabolism[38,84]. This gene has been

shown to be involved to the development and maintenance of early male germ cells (gonocytes)[85,86] in mouse embryos, and is highly important for the early zygotic divisions of male mouse embryos[87]. *Ddx3y* is relatively unique amongst mouse Y chromosome genes, being broadly expressed in many stages and tissues in the male[86] (Figure 3.2). The majority of Y chromosome genes in the mouse typically have their expression restricted to the male reproductive system, whereas *Ddx3y* produces a long ubiquitously-expressed transcript[86,88]. Other Y chromosome genes which have a broad expression profile are *Eif2s3y*, *Kdm5d* and *Uty*[76].

The *Sry* (Sex determining region of the Y Chromosome) gene is a transcription factor[45,89,90] that is transiently expressed in the undifferentiated bipotential genital ridge during embryogenesis[91]. Expression of this gene is the molecular trigger for commitment of the bipotential gonad to the testis determination pathway, and its expression is tightly regulated spatiotemporally in the genital ridge[91]. The function of *Sry* is explored in more detail in Section 1.1.5.2.

Rbmy (RNA-binding motif protein, Y Chromosome-linked) is an RNA binding protein involved in RNA metabolism within the male germline, with its expression restricted to the testis in mice[92], specifically to the nuclei of germ cells[93]. This gene is present in multiple copies of the open reading frame (ORF) arranged in a tandem repeat array adjacent to the centromere on the mouse Y chromosome short arm. This gene is explored further in Section 6.1.1.1.

1.1.3. The Mouse as a Model

The mouse has long been used as a model in biomedical research[94-96], due to the ease of housing, feeding and breeding these animals. Mice are small, and are able to be housed in groups, making them a cost-effective animal model[68,94,96,97]. Also, the short generation time (weaned at approximately three weeks of age, sexual maturity within six weeks) and production of litters (multiple offspring per pregnancy, approximately three weeks' gestation)[68,94] make these animals highly useful for multi-generational research.

The mouse shares many similarities with humans, with 17,094 mouse genes shown to have homology to human genes[98]. This is useful when selecting an animal model for research that may be generalisable to humans[94,95]. In regards to the work in this thesis, both humans and mice use the XY chromosome system for the determination of sex, with the presence of the Y chromosome sufficient to trigger development of a male. In both species, this is due to expression of the Y chromosome-linked gene, *Sry*, within the embryonic genital ridge.

However, the mouse does differ from humans in many significant ways. For example, the diploid human genome is divided amongst 46 chromosomes, including a mix of metacentric (five pairs), submetacentric (13 pairs) and acrocentric (six pairs) chromosomes[99]. The mouse, however, has its genome spread across 40 chromosomes[68], all of which are telocentric (19 autosome pairs and the X chromosome)[23], with the exception of the Y chromosome, which is acrocentric[42].

Additionally, while mice are not a perfect model for humans, with the mouse phenotype predicted from human data not always manifesting as expected, the mouse is universally accepted as the primary animal model for human genetic disorders[95].

1.1.4. Mouse Preimplantation Embryonic Development

Preimplantation development is the period of embryonic development prior to implantation of the embryo into the uterine wall of the female. Preimplantation development begins at fertilisation, the meeting of a mature spermatozoon (sperm) and an oocyte (egg)[68-70]. In mice, preimplantation development occurs over the five days following mating, with fertilisation occurring in the oviduct[68]. However, before fertilisation can take place, the gametes need to mature and be free to interact within the female reproductive tract[68-70]. The process of ovulation is briefly described below, with spermatogenesis described in Section 1.1.5.2.1.

Ovulation is the release of an oocyte from the ovary, the gonad of the female[68]. Following its release, the oocyte completes the first meiotic division within the zona pellucida, the layer of extracellular material that separates it from the follicle cells[68]. This division results in extrusion of the first polar body, a small membrane-bound structure containing minimal cytoplasm, to allow the oocyte to retain its size[68], and half of the recombinant chromosomes from the oocyte[68]. This body remains with the oocyte within the zona pellucida[68]. Following the first meiosis, the oocyte arrests in metaphase of the second meiosis until fertilisation[68].

Fertilisation occurs when a sperm penetrates the cumulus cells surrounding the oocyte, and the zona pellucida, and fuses to the membrane of the oocyte, depositing its haploid pronucleus containing its genetic material[68]. Following fusion between the two membranes, the oocyte surface alters to prevent fertilisation by additional sperm[68,100]. Fertilisation triggers the second meiotic division, resulting in extrusion of the second polar body, and the resulting haploid pronuclei from both the oocyte and sperm migrate towards the centre of the cell, now a one-cell embryo, or zygote[68,100]. These pronuclei replicate their genomes during this movement, followed by the first (mitotic) division of the zygote to form a two-cell embryo[68,100]. From this point, the haploid pronuclei do not exist, having given rise to the diploid embryonic genome, contained within a single nucleus[68].

The embryo initially relies on maternal mRNA and proteins stored in the oocyte before its own genome activates, when it can then synthesise its own biomolecules[68,100]. In mice, this embryonic genome activation (EGA) occurs at the end of G1 phase of the two-cell stage of the embryo[68-71], approximately 27 hours post-fertilisation[68], at which point maternally-derived transcripts are destroyed and replaced with embryo-derived transcripts[68]. Many of the maternal proteins do persist for longer, but eventually are also replaced[68-70]. Failure of EGA at the two-cell stage results in embryonic death, as it represents failure of an embryo to synthesise its own biomolecules, which is essential for subsequent cleavages[101]. At the two-cell stage, the two cells (blastomeres) are totipotent[102], capable of differentiating into any cell type in the mouse.

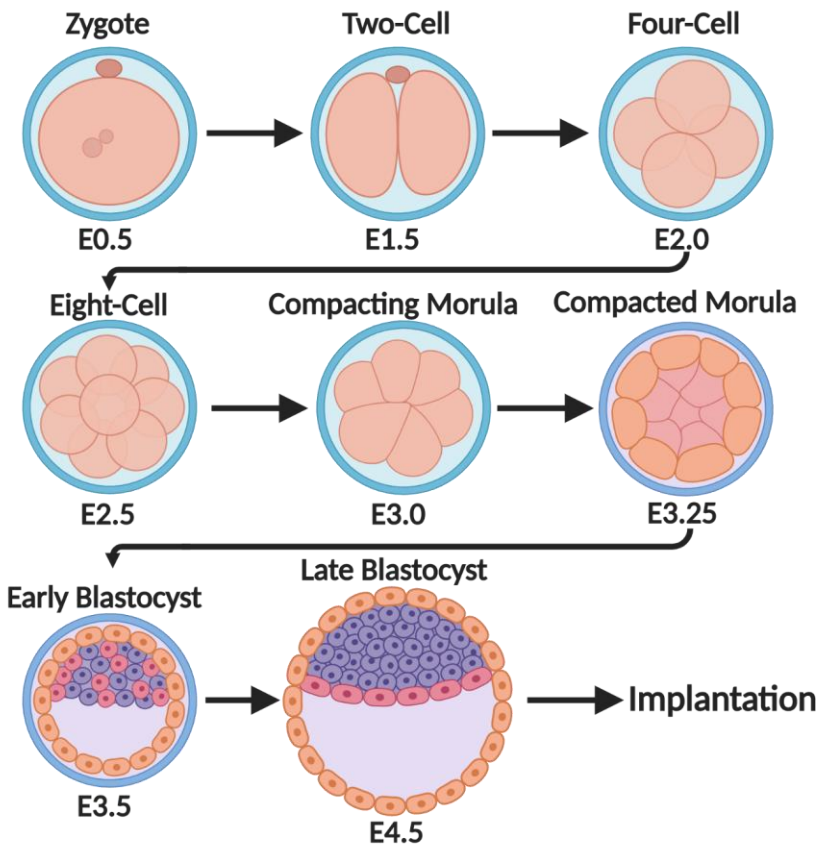

Figure 1.3 - Mouse Preimplantation Development

Preimplantation development is the period of embryonic development between fertilisation of the ovum and the implantation of the embryo into the uterine wall. In the mouse, preimplantation development occurs from fertilisation at embryonic day (E)0.0 to between E4.5 and E5.0. The one-cell embryo, a zygote (E0.5), divides to give rise to a two-cell embryo (E1.5). This embryo then undergoes two rounds of division, becoming a four-cell (E2.0) then eight-cell (E2.5) embryo. At the eight-cell stage, the embryo begins to compact (E3.25), with the boundaries between neighbouring cells (blastomeres) becoming indistinguishable. This gives rise to the morula. Additional cell divisions proceed during this morula stage, and between E3.25 and E3.5, one or more fluid-filled cavities (blastocoels) begin to appear in the embryo. At this stage the embryo is known as a blastocyst (E3.5). The blastocoels eventually form a single blastocoel, which then enlarges up until approximately E4.5. At this point, the embryo hatches out of its zona pellucida to implant into the uterine wall, ending preimplantation development (approximately E5.0).

Mice are litter animals, and as such, give birth to multiple live young[68]. This means that multiple oocytes are released at ovulation, between eight and 12, depending on the mouse strain[68]. Thus, in mice, both the release of oocytes and fertilisation by sperm are asynchronous processes[68]. Therefore, the first cleavage of these embryos will occur over the course of several hours following mating in naturally conceived pregnancies[68]. This accounts for differences in developmental stages of embryos within a single litter, sometimes up to half a days' difference[68]. In mice, the timeline for preimplantation development is counted in days post-coitum (dpc) or as embryonic days (E). In this thesis, the notation used will be embryonic days (E), with noon on the first day following mating being designated as E0.5. Figure 1.3 outlines the timeline for preimplantation embryonic development in mice.

The first two division of the preimplantation embryo (from one-cell to two-cell, and from two-cell to four-cell) are the most prone to mitotic errors[103]. In particular, these two divisions are vulnerable to non-disjunction events affecting their chromosomes[103]. This is thought to be due to the early embryo's reliance on maternally-derived transcripts and proteins[103], as, prior to and immediately following EGA[69-71], embryo-derived transcripts are in low abundance[103]. The longer duration of these two mitoses is also believed to contribute to this susceptibility to error: the first division occurs over 14 hours to 20 hours, and the second over 18 hours to 22 hours[103]. This contrasts to the approximately 10 hour duration of subsequent divisions[103]. This vulnerability to mitotic errors has been observed in strains such as the WtEiJ mouse[103], which carried a missegregation-prone Y chromosome[103,104]. This Y chromosome was particularly prone to malsegregation in the first few mitoses following fertilisation[103], resulting in mice with a mosaic sex chromosome complement[103]. This impacted on their gonadal development, resulting in a high rate of hermaphroditism and disturbed sex ratios[103,104].

From the two-cell stage onwards, the blastomeres of the embryo continue to divide in a series of mitoses without cytosolic growth[68], resulting in smaller and smaller cells contained within the zona pellucida[68]. Up until the eight-cell stage, the blastomeres are equipotent[68]; that is, all equally competent to produce any cell type in the resulting embryo and mouse. From the following stage, 16-cell, onwards, the blastomeres become gradually more developmentally restricted as differentiation of the different germ layers begins[68]. This initially consists of two lineages: the trophectoderm (TE) and the inner cell mass (ICM)[68]. This differentiation begins at the start of compaction of the embryo into a morula, at which point the boundaries between cells begin to become difficult to distinguish as the blastomeres flatten and increase their contact with one another[68,105]. The morula begins to become polarised, defining the ICM and TE lineages[68,100,105]; this fate determination eventually becomes irreversible[68,100,105]. The ICM will give rise to the embryo proper, while the TE will give rise to the extra-embryonic tissues[68,105].

Following the fifth cleavage division (32 cells), one or more fluid-filled cavities, known as blastocoels, will begin to form in the embryo, and will eventually coalesce to form a single

cavity[68,105]. This marks the change in morphology to a blastocyst. The blastocoel enlarges, during which the blastocyst is described as 'expanding'[68]. Once the blastocyst is fully expanded, it consists of a single layer of TE surrounding the fluid-filled blastocoel, with a small group of ICM cells attached to the TE at a single point[68]. A mature blastocyst has a ratio of TE:ICM cells of approximately 2:1[105]. In mice, the blastocyst is fully mature at approximately E4.5[68], and hatches from the zona pellucida to implant into the uterus at approximately E5.0[68]. This marks the end of preimplantation development.

1.1.5. Mouse Sex Determination

Following implantation of the mature blastocyst embryo (Section 1.1.4), the embryo begins its post-implantation development. This involves the differentiation and development of organ structures which will support post-natal survival after disconnection from the life support system provided by the mother's body. Part of this process is the development of the reproductive system, underpinned by sex determination, in order to propagate the next generation of the species.

1.1.5.1. Formation of the Bipotential Genital Ridge

The bipotential genital ridge arises in both male and female embryos via the same process[68,91]. The genital ridges differentiate from a medial strip of cells along the length of (adjacent to) the developing mesonephros (plural: mesonephroi)[68], a primitive excretory organ which is eventually superseded by the kidney[106]. The genital ridges are described as bipotential at this point in development as they are capable of committing to two different developmental pathways, giving rise to either the testis or ovary[68,91,107].

The bipotential genital ridge arises from the intermediate mesoderm[68]. In the mouse, the bipotential gonad and mesonephros are visible as a distinct urogenital system by approximately E10.0[68,91,108] to E10.5[108], with the genital ridge being visually distinct from the mesonephros at approximately E10.5[108]. Shortly thereafter, at E11.5, the morphology of the male and female gonads remain visually identical, despite being molecularly distinct[68,108-110] (refer Section 1.1.5.2).

As the genital ridge progenitor cells migrate to the space between the coelomic epithelium and the mesonephros, these cells also continue to proliferate[108]. These progenitors began as epithelial cells of the coelomic epithelium, before delaminating and ingressing towards the mesonephros after undergoing an epithelial-to-mesenchymal transition[107,108]. These mesenchymal cells are the progenitors that will give rise to the somatic cell populations within the differentiated gonad[108]. In males, the genital ridge also recruits additional mesonephros-derived cells to support the development of the testis vasculature[108,111-113]. These transformations and migrations describe the origin of the somatic cells in the gonad, and occur between E9.5 and E11.0[108,114].

The primordial germ cells (PGCs), however, begin to migrate at approximately E8.0, travelling to the epithelium of the hindgut from near the yolk sac[115] (arise at approximately E7.5)[108]. From the hindgut, the PGCs traverse the dorsal mesentery[108], with the first cells reaching and colonising the forming bipotential genital ridges between E10.0 and E11.0[68,108,116]. This is an active migratory process, thought to be driven by chemotaxis[68,108]. During their migration, PGCs undergo multiple divisions, dividing approximately every 16 hours[68,108,117]. Within the genital ridges, the PGCs continue to divide multiple times, such that their population reaches approximately 3,000 by E11.5[108]. By E13.5, approximately 25,000 PGCs have colonised the primordium of each gonad in the embryo[68]. The male germ cells proliferate until approximately E14.0, when they enter mitotic arrest[68].

The first overt visible signs of sexual differentiation, when a testis and ovary can be visually distinguished, appear after approximately E12.5. This occurs as the testes become characterised by striations known as testis cords, and are substantially larger than ovaries due to high rates of proliferation in the testes[68,118-120]. The ovary, meanwhile, remains morphologically ambiguous at this stage[68].

1.1.5.2. Mouse Testis Determination

As noted in Section 1.1.5.1, the male and female genital ridges are morphologically and molecularly indistinguishable up until E11.0, and become molecularly distinct from one another at E11.5[119]. The cause of this molecular difference between genital ridges of the sexes is due to the expression of the testis determining gene, *Sry*, in the somatic cells of the male genital ridge[91,107,121]. *Sry* gene expression in the mouse genital ridge is tightly regulated both temporally, across a brief window of development, and spatially, occurring in a dynamic wave across the genital ridge[91,107,121-124] (Figure 1.4).

Sry is expressed in the somatic cells of the genital ridge that are the precursors to the supporting cell lineage of the gonad, the Sertoli cells[125-127]. In XY genital ridges, *Sry* expression in these cells (pre-Sertoli cells) triggers them to commit to differentiating into Sertoli cells[91,107]. Failure to express *Sry* as required for Sertoli cell development, such as in an XX genital ridge, results in these precursor cells instead differentiating into granulosa cells[91,107], the supporting cells of the ovary. Following this cell fate commitment due to *Sry* expression, Sertoli cells in the genital ridge then orchestrate the reorganisation of the cells of the genital ridge into testis cords[119], generating morphological differences between the male and female gonads. These testis cords contain the germ cells surrounded by the Sertoli cells, and are visible as striations along the gonad from approximately E12.75-E13.0[68,91,119]. Sertoli cells also trigger the development of the germ cells and Leydig cells, the androgen-producing cells of the testis which secrete testosterone[128], as well as the testis vasculature[91,129].

The expression of *Sry* is the molecular trigger for this Sertoli cell fate, but its window of action is brief. *Sry* expression in the mouse genital ridge can only serve to trigger testis determination between E10.5 and E12.5[130,131]. Beyond E12.5, no level of *Sry* expression will be able to trigger the genital ridge to commit to testis development. Instead, the genital ridge will typically follow the ovarian pathway. The expression pattern of *Sry* in male mouse embryos has been characterised[91,107,121-124,132], both temporally and spatially, with these two aspects related to one another. *Sry* expression begins at approximately E10.5, before rapidly increasing to peak at E11.5, with *Sry* expression needing to exceed a threshold to trigger Sertoli differentiation[91]. However, concurrent with this time-related increase, the region in which *Sry* expression is detectable changes as well (Figure 1.4). *Sry* expression begins in the centre of the genital ridge at E10.5, and from there spreads outwards to each of the poles, with the entire genital ridge being *Sry*-positive at approximately E11.5[91,107,121,123,125-127,130] (Figure 1.4). From this peak, *Sry* expression declines between E11.5 and E12.5, while also ceasing to be detected from the centre of the genital ridge[119]. As the *Sry* expression levels decline as development progresses towards E12.5, its signal is no longer detectable further out from the centre of the genital ridge, with the last regions of the genital ridge that are still *Sry*-positive being the poles[91,107,121,123,125-127,130] (Figure 1.4).

This dynamic pattern of *Sry* expression is essential to mouse testis determination, as it is only at this stage that the bipotential genital ridge can be triggered to become a testis[122-124]. In a normal XY gonad, following the end of receptivity at E12.5, *Sry* expression is absent in the testis[91]. During its brief presence, the Sry protein activates its primary target, the *Sox9* (Sry-related HMG (High Mobility Group) box 9) gene[91,107,121]. It does this by binding to the recognition sequence (A/T)ACAA(T/A) within the DNA minor groove by its high mobility group (HMG) DNA binding domain[91,130,133]. It shares this domain with other *Sox* genes, including its target *Sox9*, as *Sry* is the founding member of this transcription factor gene family[91,107,130,133]. This HMG domain in Sry is highly conserved between species, as this is the functional domain of the protein, but its tail domain is not[130,134]. Once Sry has bound the sequence, it induces a bend in the double-stranded DNA at an angle of 60° to 85°[91,130,135].

Once *Sox9* has been activated by Sry, it is then capable of self-activation in the absence of Sry. *Sox9* is immediately upregulated following Sry expression[91,107,121,130], and as such its onset of expression follows the same centre-to-poles wave pattern as *Sry*[91,109,110,121-124,130]. Following this activation pattern, *Sox9* persists across the entire genital ridge, and later the whole testis, beyond the E12.5 extinction of *Sry* expression[91,109,110]. This is achieved by Sox9 binding to its own enhancer within Sertoli cells, along with the protein Nr5a1 (Nuclear Receptor subfamily 5, group A, member 1, also known as Steroidogenic Factor 1 or Sf1), to perpetuate its expression to maintain the Sertoli cell phenotype[91].

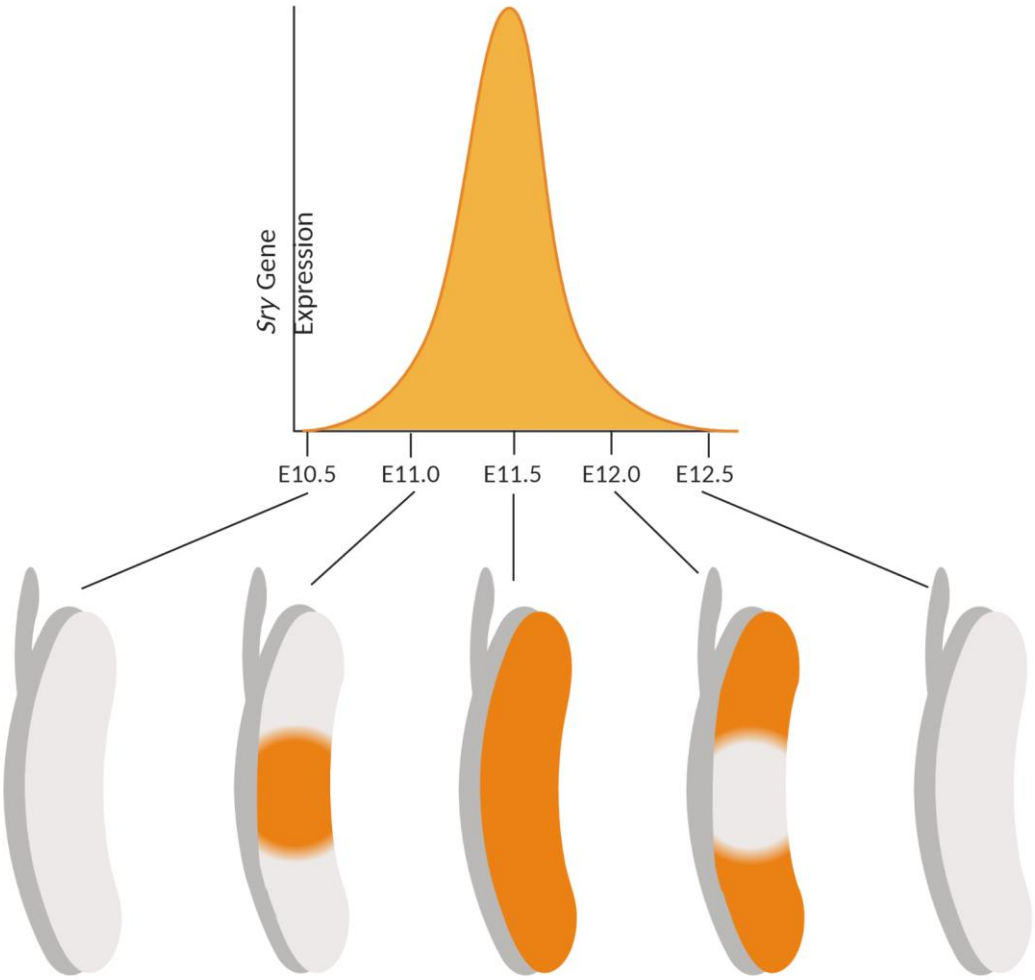

Figure 1.4 - Expression of *Sry* During Mouse Testis Determination

Sry expression in mouse testis determination is a highly dynamic process which is tightly spatiotemperally controlled. The upper graph illustrates the relative expression of *Sry* (orange) across the window of testis determination, between E10.5 and E12.5. Gene expression begins at approximately E10.5, before rapidly increasing to its peak at approximately E11.5. From this point, *Sry* expression rapidly extinguishes, to become completely absent by E12.5. Concurrent with this temporal pattern, the spatial distribution of *Sry* expression also follows a precise pattern (bottom images, left to right). *Sry* expression begins in the centre of the genital ridge (orange) proceeding out towards both poles by E11.5. As *Sry* expression declines after E11.5, spatially, the expression begins to extinguish from the centre outwards (grey), such that the last regions expressing *Sry* are the poles. By E12.5, the entire genital ridge no longer expresses *Sry*.

While the *Sry* is the trigger for testis determination, one *Sry* gene is not necessarily interchangeable for another, both between species, and, in the case of mice, between strains. For example, human *SRY* has been previously shown to not be sufficient to induce testis determination in XX mouse embryos when under control of human regulatory sequences[136], but is able to do so when used in a chimeric sequence using endogenous mouse *Sry* regulatory sequences[91,136]. *Sry* is poorly conserved between species outside of its functional domain, the HMG domain, but this gene also typically contains two nuclear localisation signals (NLSs) to direct the protein to the nucleus where it may perform its function as a transcription factor[91,130,134]. These three factors are present in the *Sry* gene in the majority of mammals, such as humans, horses, chimpanzees and mice, as they are required for *Sry* action[91].

However, mouse *Sry* differs from other species' *Sry* genes at both the N- and C-terminals of the protein. At its N-terminus, the mouse Sry protein has only two amino acids before the NLS and HMG domain[137]. This is a substantial reduction in this region relative to other species' Sry proteins, which tend to have between 30 and 60 amino acids before the NLS and HMG domain[137]; one example is human Sry, which has 57 amino acids at the N-terminus, before its first NLS[130,133]. Mouse Sry differs again at the C-terminus, having a long poly-glutamine tail[138] (223 amino acids[133]) not observed in any other species' *Sry* genes, separated from the second NLS and 79 amino acid HMG domain[139] by a bridge domain of 63 amino acids[133,139]. This poly-glutamine tail is essential for Sry to induce testis determination for several reasons, including protection of the protein from degradation, and for Sry to successfully transactivate *Sox9*[140,141].

Inbred laboratory mouse strains are a mix of two mouse strains, *Mus* (*M.*) *musculus* and *M. domesticus*, with the vast majority carrying an *M. Musculus*-derived Y chromosome[122,142]. Of interest here are the *M. domesticus* Y chromosomes, such as those found in the inbred strain AKR/J[122] and in the wild-derived *M. d. poschiavinus*[122,123,143]. While not all *M. domesticus*-derived Y chromosomes result in abnormal testis development when crossed onto the C57BL/6J background[122] ("the mouse"), these two example *M. Domesticus* Y chromosomes result in a disturbance to normal testis determination. The $Y^{AKR/J}$ chromosome leads to delayed testis cord development in C57BL/6J embryos, but their gonads do not develop ovarian tissue[122,124,144].

The *M. d. poschiavinus* Y (Y^{POS}) chromosome, however, when crossed onto the C57BL/6J background results in no normal testis development, only the development of ovaries or ovotestes (gonads composed of ovarian and testicular tissue)[122,145,146]. This is believed to be due to a difficulty in the interaction between a specific *Sry* allele and the autosomal genetic elements from another background, delaying *Sry* expression, adversely affecting testis determination[123,145]. This has been linked to the substantially reduced poly-glutamine tail in the Y^{POS} *Sry* allele, which consists of only eight glutamine residues due to a premature stop codon[130,145,147]. This results in a truncated protein, which, while capable of triggering testis determination in its own genetic context[141,147], has been shown to destabilise the Sry protein, and results in weaker transactivation activity relative to an *Sry*

gene carrying the *M. musculus* poly-glutamine domain[141,145]. Bullejos and Koopman (2005)[123] demonstrated that expression of *Sry* from the Y^{POS} chromosome was delayed relative to that from $Y^{C57BL/6J}$ when both Y chromosomes are on the C57BL/6J background, with maximal *Sry* expression detectable at 20 tail somites (ts) in C57BL/6J XY^{POS} genital ridges, compared to 18 ts in C57BL/6J $XY^{C57BL/6J}$ genital ridges[123].

This example highlights the sensitivity of the *Sry* expression profile within the mouse testis determination window. While the peak of *Sry* expression in the mouse genital ridge has been shown to be at E11.5 (18 ts), the critical time window for *Sry* expression has been demonstrated to be only approximately six hours, between 12 ts and 15 ts[148]. Therefore, the precise timing of *Sry* expression is essential to successful testis determination.

1.1.5.2.1. Spermatogenesis

Following testis determination, the Sertoli cells coordinate the reorganisation of the genital ridge into testis cords, which give rise to the seminiferous tubules of the mature testis[119]. These tubules are the site within which the process of spermatogenesis occurs. Spermatogenesis is the process by which the haploid gametes (spermatozoa) of the testis are produced by meiosis[68,149]. The seminiferous tubules of the testes consist of the supporting Sertoli cells and the stem cell population, the spermatogonia, that supply cells to the spermatogenesis pathway[68]. Meiosis in the testis proceeds from the periphery of the tubule in towards the lumen, with the successive cell divisions giving rise to different cell types[68].

Spermatogonia line the basement membrane of the seminiferous tubules, interspersed with Sertoli cells which support the spermatogonia[68]. Spermatogonia consist of two varieties: type A spermatogonia, the stem cells of the testis which are self-renewing, and type B spermatogonia, which are derived from the type A spermatogonia via mitosis and enter the meiotic pathway[68,150]. Type A spermatogonia appear within the seminiferous tubules between three and seven days after birth[68], and continually divide to replenish their population[150]. Some daughter cells of these mitoses differentiate into intermediate spermatogonia, which then differentiate into type B spermatogonia[68,151]. The type B spermatogonia are present adjacent to the basement membrane, and are smaller than type A spermatogonia[68]. These cells are also capable of undergoing mitosis to produce more type B spermatogonia, resulting in the population of these cells exceeding the population of type A spermatogonia[68].

Type B spermatogonia then enlarge and migrate from the basement membrane towards the lumen of the tubule, and divide via mitosis to yield primary spermatocytes[68]. The primary spermatocytes then undergo the first meiotic division to produce secondary spermatocytes[68,152]. During this first meiotic division, the autosomes pair with their homologues for recombination[68]. The X and Y chromosomes also pair, despite not being homologues, at a region of homology, the

PAR (refer to Section 1.1.2)[68]. Following this pairing, the X and Y chromosomes undergo meiotic sex chromosome inactivation (MSCI), in which the X and Y chromosomes become transcriptionally silenced[149,153]. This is due to the fact that the majority of these chromosomes are unpaired or 'unsynapsed', triggering the meiotic silencing of unsynapsed chromatin or MSUC mechanism[53,149,152,154-156]. This involves remodelling of the chromatin of the X and Y chromosomes to a heterochromatic state known as post-meiotic sex chromatin (PMSC)[53,149,155,156]. The sex chromosomes are also sequestered in a nuclear subdomain called the sex body or XY body, where they reside until the second meiotic division[149,157].

The secondary spermatocytes undergo the second meiotic division, in which the sister chromatids separate, producing haploid spermatids (n = 20)[68]. This marks the end of meiosis. However, the spermatids, also referred to as round spermatids, are not yet fully mature gametes[68]. Through the progression from primary and secondary spermatocytes, to the spermatid stage, the cells have progressively moved towards the lumen of the seminiferous tubule[68]. It is at the luminary surface that the spermatids are remodelled through a process called spermiogenesis into mature spermatozoa[68]. Spermiogenesis is a process of extensive differentiation where the cell extrudes much of its cytoplasm and morphologically changes from a round cell to have a distinct head, midpiece and tail, with superfluous bodies being left on the luminal surface at the completion of the process[68]. Up until the mature spermatozoa stage, at which point the sperm are ready to be released into the lumen of the seminiferous tubules, each of the cell types are characterised by cytoplasmic bridges[68]; that is, all cells are connected to one another via shared membranes[68,151]. This is the result of incomplete cytokinesis, such that the cells have a shared cytoplasm[68]. These bridges are maintained until the release of the mature sperm into the lumen in preparation for reproduction[68,151].

The spermatogenesis process results in the production of four genetically distinct haploid sperm from one stem cell (type A spermatogonium)[68], in contrast to oogenesis (refer to Section 1.1.4) which produces only a single haploid oocyte per stem cell. In the mouse, the process from spermatogonium to mature spermatozoa that are capable of fertilisation takes approximately five weeks[68].

From the lumen of the seminiferous tubules, the sperm are then able to be deposited in the reproductive tract of the female following copulation. In the mouse, approximately 5.8×10^7 spermatozoa are released per ejaculation[68]. Once the sperm are in the female reproductive tract, it takes approximately one hour post-ejaculation for the sperm to become competent for fertilising an oocyte[68]. This is because they then undergo further maturation in the form of capitation, a biochemical process within the sperm that results in the sperm then being capable of fertilisation[68].

1.1.5.2.2. XY Sex Development Disorders

As detailed in Section 1.1.5.2, the testis determination process is tightly controlled within the mouse embryo, with disruptions to this process having deleterious results on the gonads of the mouse. Disorders of sex development (DSDs) are cases in which there is congenital atypical development of the sex of an individual, referring to their chromosomal, gonadal and/or anatomical (genital) sex[157]. In humans, the incidence of DSDs is estimated to be one in 5,500, although data is limited[157].

There can be many causes of DSDs, including atypical sex chromosome constitution (deviation from either XX or XY), with Turner's syndrome, 45,X, discussed in Section 1.1.2, being a human example of this. A mouse example of this was the WtEiJ mouse[103], discussed in Section 1.1.4. Other causes may include genetic abnormalities, such as mutations in genes involved in development of the reproductive system, such as those affecting endocrine function, including complete and partial androgen insensitivity (CAIS and PAIS, respectively)[158], or downstream targets of genes involved in sex determination, such as *Sox9*[159].

However, as the focus of this thesis is on the Y chromosome, discussion of DSDs here will focus on XY DSDs, specifically gonadal DSDs due to abnormalities on the Y chromosome. XY DSDs can range from development of an intersex (human) or hermaphrodite (mouse) individual, possessing gonads consisting of both testicular and ovarian tissues (ovotestes), through to total sex reversal, in which an XY individual develops as a female, possessing ovaries (ovarian tissue only)[158]. This was observed in the C57BL/6J mice carrying the Y^{POS} chromosome[160], discussed in Section 1.1.5.2 in which all gonads developed at least some ovarian tissue, with approximately half developing only ovarian tissue (completely sex reversed)[160].

Two abnormalities of the Y chromosome that results in XY DSD have relevance to this project will be described here: abnormalities related to the *Sry* gene, and abnormalities related to the *Rbmy* gene array.

1.1.5.2.2.1. *Sry*-Related Sex Development Disorders

As *Sry* (Section 1.1.2.2) is the trigger for testis determination, mutations affecting this gene's function would result in a negative effect on testis determination. A loss of function mutation, in which *Sry* is unable to effectively perform its transcription factor role during the critical window for testis determination. This would result in formation of either an ovotestis, with some regions of the gonad being able to complete testis determination, or fully sex reversing to generate an ovary due to failure to adequately activate *Sox9* expression within the responsive period of the genital ridge, such as in the case of the Y^{POS} chromosome[146] (Section 1.1.5.2).

An example of a human condition resulting in gonadal abnormalities due to an *SRY* mutation is Swyer Syndrome, in which the affected patient experiences complete gonadal dysgenesis, where the gonads are composed of non-functional undeveloped fibrous tissue known as streak gonads[161]. These XY patients typically have normally-formed fallopian tubes and uterus, as well as female external genitalia. This disorder can be caused mutations in *SRY*, as well as other autosomal genes such as *Nr5a1*, with between 10% and 20% of gonadal dysgenesis cases being linked to *Sry*[162]. These *Sry* mutations primarily affect the functional domain of the protein, the HMG domain, and tend to be *de novo* mutations[163].

Additionally, as the dynamics of *Sry* gene expression within the testis determination window is known to be of vital importance in order to activate the testis determination pathway before the ovarian pathway activates[123], anything that causes deviation from this expression pattern will likely result in abnormal gonadal development. In 2005, a case study[164] was reported of a human XY female patient with gonadal dysgenesis due to a pericentric inversion on the Y chromosome[164]. This inversion relocated the *SRY* gene from the terminal end of the human Y chromosome short arm to the long arm[164], placing *SRY* adjacent to a heterochromatic block at Yq12[164]. The *SRY* gene itself was confirmed to have no mutations in this patient, and so it was assessed for indications of changes to its regulation[164]. *Sry* expression is regulated by methylation of cytosine residues at cytosine-guanine dinucleotide pairs, called CpGs, within its regulatory regions, in both mice and humans[132,164]. *Sry* promoter methylation is high when not expressed, and declines to allow gene expression to continue[132,164] (*Sry* methylation dynamics in mice discussed further in Section 6.1.1.2).

The *SRY* locus in the patient was assessed for methylation, and was found to be hypermethylated relative to the phenotypically normal father[164]. This hypermethylation indicated that there may have been an issue with *SRY* methylation-dependent regulation in the embryonic development of this patient[164]. This was speculated to be due to a phenomenon called position effect variegation (PEV), in which juxtaposition of euchromatin with a region of heterochromatin due to a structural rearrangement on a chromosome results in silencing of a gene in some cells (variegated silencing)[165]. This silencing is the result of heterochromatin spreading across the border between it and the euchromatin, spreading its repressive markers[165]. In the case of this patient, the euchromatic *SRY* gene locus was juxtaposed to the highly heterochromatic region from the Yq arm, likely leading to silencing of *SRY* expression during testis determination[164].

1.1.5.2.2.2. *Rbmy*-Related Sex Development Disorders

The *Rbmy* gene (Section 1.1.2.2) codes for a protein involved in nuclear RNA processing in spermatogenesis[93] expressed in the male germline, being particularly abundant in spermatogonia and spermatocytes[93,166]. This gene is present in a multicopy state, located on the long arm of the human Y chromosome and on the short arm of the mouse Y chromosome. Due to its expression in germ cells, *RBMY* deletions are associated with infertility in humans[167] due to spermatogenic

failure[167-169].

In mice, males with *Rbmy* deletions are fertile, being capable of producing sperm, but these gametes have abnormal morphology[170]. It is important to note, however, that this was only observed in mice carrying a fully penetrant *Sry* transgene, as mice with severe *Rbmy* deletions undergo sex reversal, developing as XY females[170]. The use of this transgene within the context of severe *Rbmy* deletions demonstrated that, while the *Rbmy* deletion was the cause of the sex reversal, it was not due to the absence of *Rbmy* itself. Instead, it was likely due to repression of *Sry*, as on the mouse Y chromosome, the multicopy *Rbmy* gene array lies between the heterochromatic Y chromosome centromere and the *Sry* gene. Deletions in this region may result in *Sry* repression due to PEV, as discussed in Section 1.1.5.2.2.1 referring to a human patient experiencing *SRY* silencing[164].

The mouse models that have been reported that demonstrate sex reversal due to large *Rbmy* deletions were generated by the Cattenach laboratory at the MRC Radiobiology Unit[171], with five mouse lines having been established: Y^{d1} [172], Y^{d2} [172], Y^{d3} [171,172], Y^{d5} [172] and Y^{d6} [172]. All five lines were shown to carry Y chromosomes with reductions in the *Rbmy* copy number[172], with Y^{d1} and Y^{d6} having the fewest *Rbmy* copies[172]. Additionally, genital ridges from mouse embryos carrying these deleted Y chromosomes (except for Y^{d6}) were collected at E11.5 and assessed for *Sry* expression[172]. Each of these samples had decreased *Sry* expression in the genital ridges relative to the normal XY control, with the least expression observed in the mouse line with the greatest *Rbmy* deletion (Y^{d1})[172]. This indicated both a general repressive effect on *Sry* in the context of an *Rbmy* deletion[170,172], and a relationship between the degree of *Rbmy* deletion and the degree of *Sry* repression in testis determination[170,172].

The number of *Rbmy* repeats was closely assessed in the Y^{d1} and Y^{d3} lines[170]. As was observed in all Y^{d} mouse lines, there was incomplete sex determination resulting in the majority of XY^{d} mice developing as females[170,172]. It was observed that XY^{d1} and XY^{d3} mice developed as partially fertile females[173]. Two estimates of the copy number of *Rbmy* on these two chromosomes were made based on two different assumptions. The first estimate assumed that the Y^{d1} chromosome carried at least two copies of *Rbmy*, and yielded a copy number of two for Y^{d1} and three for Y^{d3} [170]. The second estimate assumed that the control Y chromosome carried 50 repeats of *Rbmy*, as was the generally accepted estimate of the array at the time[170]. This resulted in estimates of four and six *Rbmy* repeats on these Y^{d} chromosomes, respectively[170]. However, the estimates of two and three *Rbmy* repeats for Y^{d1} and Y^{d3}, respectively, were the generally accepted estimates of the copy number on these Y chromosomes[170,173]. These severe deletions of the *Rbmy* gene array to only a few repeats on the Y^{d1} and Y^{d3} chromosomes were demonstrated to have resulted in repression of *Sry*, likely due to its increased proximity to the heterochromatic centromere, rather than due to a reduction or absence of *Rbmy* expression[170].

As the copies of *RBMY* on the human Y chromosome are located on the other arm of the chromosome to *SRY* (Yq and Yp, respectively), as opposed to being located adjacent to one another as occurs on the mouse Y chromosome, deletions of *RBMY* would affect only processes involving RBMY protein, such as the impact on spermatogenesis[167-169] (above), rather than a positional effect on *SRY*, as seen in mice.

1.1.6. Background on Mouse Strains of Interest

Two mouse strains were the focus of this project: the transgenic *Ddx3y*^{mKate2} mouse, and the classic inbred A/HeJ mouse. This section provides a brief background on each strain, as well as on an additional transgenic mouse, *Hprt*$^{DsRed\text{-}Express}$, that was also characterised in this work as a comparison to the *Ddx3y*^{mKate2} mouse.

1.1.6.1. Background of the *Ddx3y*^{mKate2} Mouse

The *Ddx3y*^{mKate2} reporter Y chromosome was generated to be used as a tool for chromosome instability research by targeted insertion of a red fluorescent protein gene, *mKate2*, to act as the reporter signal. As this reporter chromosome was a Y chromosome, all males of the *Ddx3y*^{mKate2} mouse strain carried the reporter chromosome. The Y chromosome was selected for generation of this transgenic line as it is the only chromosome of the mouse karyotype that is non-essential for viability of the cell and organism. As such, this reporter Y chromosome may be used in work that causes loss of the reporter chromosome without the concern of maintaining cell or animal viability.

The signal from the fluorescent reporter in *Ddx3y*^{mKate2} mouse has been previously characterised on a stable background[5]. This previous characterisation[5] is summarised below (Section 1.1.6.1.2), as is the creation of the reporter (Section 1.1.6.1.1).

1.1.6.1.1. Creation of the *Ddx3y*^{mKate2} Mouse

The *Ddx3y*^{mKate2} reporter Y chromosome was created by Drs Paul Kalitsis and Jeff Mann by targeted insertion of a gene cassette into the mouse Y chromosome, via homologous recombination, adjacent to the *Ddx3y* gene locus (refer to Section 1.1.2.2) on the short arm of the Y chromosome. Figure 3.1 illustrates the targeting arms, insertion cassette and target locus. The gene targeting cassette consists of a neomycin resistance gene under the control of the phosphoglycerate kinase (PGK) promoter for use as selection of successful recombinants, and the coding sequence for the red fluorescent protein mKate2 under the control of the cytomegalovirus chicken beta-actin (CMV-CAG) promoter[174] as the gene of interest to insert onto the mouse Y chromosome. The targeting arms contained homology to exons 8 to 17 of the endogenous *Ddx3y* gene locus.

This targeting construct was designed to allow targeted insertion of the fluorescent reporter (mKate2) and selection (neomycin resistance) genes into the Y chromosome such that the *Ddx3y* gene locus remains intact. This was vital, as this gene is essential for early embryonic development in the mouse embryo[87], and as such interrupting its coding sequence would render successful recombinants non-viable. This gene locus was selected for targeting as *Ddx3y* is broadly expressed across many different tissues in the mouse (refer to Figure 3.2), distinguishing it from other mouse Y chromosome genes which are expressed only in the testis. This broad expression of *Ddx3y* in multiple tissues, in both embryos and adult mice, suggests that this locus was likely to be within a permissive chromatin environment, making it an ideal region for insertion of the transgene cassette. This chromatin environment, combined with the strong promoters controlling the transgenes, was predicted to result in high expression of the fluorescent reporter gene, *mKate2*, across a broad range of tissues, giving this reporter Y chromosome versatile utility in chromosome research.

The fluorescent protein chosen to serve as the reporter transgene, mKate2, was selected for insertion due to red fluorescent proteins having many features that make them ideal for use in cell-based work. These features include reduced cytotoxicity from excitation by red to far-red light compared to green fluorescent protein (GFP)[175], as well as red light's ability to penetrate deeper into tissues[175] and low levels of background autofluorescence relative to that observed with GFP[175].

The far-red fluorescent protein mKate2 is a monomeric protein, with a molecular weight of 26 kDa[176], and exhibits 75% of the brightness observed from enhanced (E)GFP[176]. Maturing with a half-time of less than 20 minutes at cellular pH, 37°C[176], this red fluorescent protein exhibits a high level of stability across a wide range of pH values, is highly photostable, and lacks reported toxicity in animal models[176]. The excitation/emission maxima of this 232 amino acid protein is 588 nm/633 nm[176].

To target the mouse Y chromosome, the targeting construct (Figure 3.1) was electroporated into male (XY) mouse embryonic stem (ES) cells, where it was then able to insert the gene cassette into the mouse Y chromosome at the specific site at the *Ddx3y* gene locus. This was achieved via homologous recombination to generate the transgenic reporter Y chromosome, now termed *Ddx3y*^{mKate2}, using the strategy in Rohozinski et al (2002)[177]. Neomycin-resistant clones were screened for successful insertion of the transgene cassette by Southern blot hybridisation. *Ddx3y*^{mKate2}-containing ES cells were then injected into recipient 129S1/SvImJ blastocysts according to standard procedures[68] to generate chimeric blastocysts.

These chimeric embryos were then transferred into pseudopregnant recipient females to gestate. Live-born chimeric male mice were mated to 129S1/SvImJ females for germline transmission. The resulting male offspring carried the *Ddx3y*^{mKate2} Y chromosome, founding the *Ddx3y*^{mKate2} strain, and continued to be breed with 129S1/SvImJ females to generate a stable colony of *Ddx3y*^{mKate2} mice. As all *Ddx3y*^{mKate2} males carried the reporter chromosome, there was need for

routine genotyping for the transgene on the Y chromosome, an advantage of this model system.

1.1.6.1.2. Preliminary Characterisation of mKate2 Signal in the *Ddx3y*^{mKate2} Strain

Previously, this laboratory characterised the mKate2 fluorescence in the *Ddx3y*^{mKate2} mouse strain, from early preimplantation development to the mature adult mouse[5]. Based on the broad expression of the nearby *Ddx3y* gene and the strong synthetic promoter controlling the mKate2 gene, it was predicted that the fluorescent reporter would be highly expressed from early in development, and in that majority of tissues in the adult. This section gives a brief overview of the previous characterisation of the *Ddx3y*^{mKate2} mouse; further detail is contained in Section 3.1.1.2 and Figure 3.3.

The *Ddx3y*^{mKate2} mouse was assessed for mKate2 fluorescence from preimplantation development to sexual maturity. It was found that the male *Ddx3y*^{mKate2} embryo begins to exhibit detectable mKate2 fluorescence at the blastocyst stage, from the beginning of cavitation at between approximately E3.0 to 3.5[5]. This fluorescence was present across the entire midgestation embryo at E9.5[5]. Adult *Ddx3y*^{mKate2} organs were examined at six weeks of age, and revealed that all organs, bar the spleen, exhibited some degree of mKate2 fluorescence[5]. Of the organs examined, the heart and testes were the most intensely fluorescent[5]. Female samples at all stages assessed remained non-fluorescent.

To complete the assessment of the *Ddx3y*^{mKate2} mouse, the mKate2 signal needs to be assessed in advanced age, and the reporter Y chromosome should be modelled on known instability backgrounds to demonstrate its utility.

1.1.6.2. Creation of the *Hprt*$^{DsRed\text{-}Express}$ Mouse

As the *Ddx3y*^{mKate2} Y chromosome was generated to serve as a tool for chromosome instability research, it is useful to compare it against other reporter chromosomes that have been created for a similar purpose. While other fluorescent reporter chromosomes have been created and published (refer to Section 1.1.7), the variables assessed in characterisation of published reporter mice can vary between publications. To address this, the work in this thesis regarding the *Ddx3y*^{mKate2} mouse involved characterisation of another fluorescent reporter mouse strain, the *Hprt*$^{DsRed\text{-}Express}$ mouse. The aim of this characterisation was to assess similar variables as were assessed in the *Ddx3y*^{mKate2} mouse (Section 3.1.1.2), in order to enable effective comparison of the two strains.

The Hprt$^{DsRed\text{-}Express}$ reporter X chromosome was created by Dr Jeff Mann by targeted insertion of the fluorescent protein gene *DsRed-Express* (also referred to as DsRedT1[178], Clontech Inc.) into the *Hprt* (Hypoxanthine guanine Phosphoribosyl Transferase) locus on the mouse X

chromosome. This insertion was achieved using the method described in Tang et al (2002)[179], with the following modifications: the *Cre* coding sequence was replaced with the *DsRed-Express* coding sequence, and the neomycin resistance selection cassette was flanked by *loxP* sites.

DsRed-Express is a tetrameric red fluorescent protein that was derived from DsRed through targeted and random mutagenesis to mature rapidly[180] (maturation half-time of 0.7 hours[178]). This mutagenesis also served to result in a fluorescent protein that would exert a minimally cytotoxic effect on the cell, a common issue with many fluorescent proteins used for whole cell labelling, often due to aggregation of the fluorescent protein[180]. From this, DsRed-Express was found to be highly photostable with low phototoxicity[180]. This variant was found to be spectrally distinct from GFP, with reduced green emission, and is excitable by both blue and green lasers with an excitation/emission spectrum of 554 nm/586 nm[178].

Briefly, the targeting strategy to insert the reporter into the mouse X chromosome used a targeting vector containing a neomycin resistance gene under the control of the PGK promoter and the *DsRed-Express* gene under the control of the CMV-CAG promoter[174], with targeting arms to *Hprt* exons 2 and 3. The targeting construct was electroporated into 129S1/SvImJ ES cells, and the transgene cassette was integrated into the *Hprt* locus via homologous recombination, such that the coding sequence of the gene was interrupted, inactivating the *Hprt* gene[179,181]. Selection for successful recombinants was performed using neomycin resistance and Southern blot hybridisation, with recombinant ES cells injected into recipient 129S1/SvImJ blastocysts to generate chimeras. These chimeric blastocysts were transferred to pseudopregnant females as described for the *Ddx3y*^{mKate2} strain (Section 1.1.6.1.1).

In order to confirm germline transmission of the recombinant *Hprt*$^{DsRed\text{-}Express}$ X chromosome, chimeric male offspring were mated to 129S1/SvImJ females. The neomycin resistance cassette was removed by mating the resulting offspring with a 129S1/SvImJ *Cre* deleter mouse line[179]. The resulting offspring of this mating were used to establish the *Hprt*$^{DsRed\text{-}Express}$ strain, in which males or females may carry the reporter X chromosome. As such, genotyping is required for mice in this strain. To facilitate this, the reporter X chromosome is maintained in heterozygosity with the wild type (non-recombinant) X chromosome in females.

1.1.6.3. Background of the A/HeJ Mouse

The A/HeJ mouse strain is a classically inbred strain of albino mice that was separated into its own lineage separate from the closely related A/J strain prior to 1930. As with other mouse strains from the inbred A strain background, A/HeJ has had use in work involving cancer and immunology research[182,183]. The focus on A/HeJ for this project, however, is on its Y chromosome ($Y^{A/HeJ}$) and the male sex determination pathway.

This strain has previously[2] been noted to have incidence of abnormal male sex determination, with 4% of non-productive males having been identified as hermaphrodites carrying ovotestis gonads, and a further 17% of these non-productive males possessing abnormally small testes which did not produce epididymal sperm[2]. The abnormalities in the A/HeJ strain were first identified when a mouse was forwarded to the Eicher laboratory in 1993 due to its abnormal external genitalia[2]. Examination of this mouse revealed gonads consisting of ovarian and testicular tissue[2], ovotestes. The Jackson Laboratory production colony for the A/HeJ strain exhibited a slight reduction in male mice relative to females to 46.8% of the colony[2]. Examinations of non-productive males from this colony between 1993 and 2005[2] identified the above noted incidence of hermaphroditism and small testes, for an overall incidence of gonadal abnormalities of 21% in non-productive males[2].

The 2008 publication[2] characterising the defect in the A/HeJ males confirmed that the phenotype observed in these males was due solely to the $Y^{A/HeJ}$ chromosome[2]. This was confirmed through backcrossing the $Y^{A/HeJ}$ chromosome onto the inbred C57BL/6J background to generate the C57BL/6J-$Y^{A/HeJ}$ consomic line[2]. These males were mated to C57BL/6J females, and the resulting embryos were identified to also have gonadal abnormalities amongst the males[2]. Of 23 XY embryos from these crosses, five (21.7%) had at least one gonad that had developed as an ovotestis, and one (4.3%) had a testis which had not formed correctly, having attenuated cord growth[2]. This represented a 26% rate of gonadal abnormality in the E14.5 embryos.

As the causative element for these abnormalities had been linked specifically to the $Y^{A/HeJ}$ chromosome[2], the focus then shifted to that Y chromosome specifically. It was initially hypothesised that the development of ovarian tissue in A/HeJ ovotestes was due to loss of the $Y^{A/HeJ}$ chromosome from those regions[2], such as occurred in the WtEiJ mouse (Section 1.1.4). However, while the $Y^{A/HeJ}$ chromosome was found to prone to some missegregation in mitosis[2], there was no difference in retention of the Y chromosome between ovarian and testicular tissues within an ovotestis, with both having over 90% of cells analysed being XY[2].

Cytological assessments of the $Y^{A/HeJ}$ chromosome revealed that this Y chromosome has increased intracentromeric gaps between duplicated sister chromatids[2], as well as being prone to premature sister chromatid separation[2]. These observations lead the authors to hypothesise that, while the cytological defects were likely not causative of the testis determination abnormalities, the two were likely linked, having a single cause[2]. The authors speculated that there is a structural abnormality at or near the $Y^{A/HeJ}$ chromosome centromere[2], and that this structural abnormality affected sister chromatid cohesion[2], and, due to *Sry*'s proximity to the centromere, there may be an adverse effect on its expression during testis determination[2], causing these gonadal abnormalities.

1.1.7. Other Fluorescent Reporter Y Chromosomes

The mouse Y chromosome has been targeted for insertion of fluorescent protein genes in other studies to generate mouse strains in which the males exhibit fluorescence. As the *Ddx3y*^{mKate2} mouse was the focus of the first study in this project (Chapters 3 and 4), this section briefly covers two fluorescent reporter Y chromosomes and highlights the similarities and differences of these reporter strains to the *Ddx3y*^{mKate2} mouse.

The Y-GFP mouse line created by Yamamoto et al (2014)[46] was generated by insertion of a *green fluorescent protein* (*GFP*) gene into the mouse Y chromosome[46]. This was achieved by targeting a Y chromosome-specific repeat on the long arm within embryonic stem (ES) cells, which were then used to generate transgenic mice[46]. The group then confirmed that all male progeny of these transgenic mice carried the reporter Y chromosome[46]. The Y-GFP mice were assessed for GFP fluorescence at the blastocyst and midgestation stages of development[46]. While all male (and no female) embryos were fluorescent, the fluorescence was not uniform across each embryo[46]. In the blastocyst, the Y-GFP embryo had regions of greater fluorescence than the remainder of the embryo[46]. This was also observed in the midgestation embryo, with regions being either far less or far more fluorescent than the majority of the body[46]. At both stages assessed, however, the fluorescence images did not perfectly recapitulate the bright-field images[46]; instead, the GFP signal had a more grainy appearance[46]. This contrasts to the previous work on the *Ddx3y*^{mKate2} mouse (Figure 3.3A), in which all relevant structures of the embryos were clearly distinguishable in the fluorescence images[5].

The Y-Chr-eGFP mice were created by Zhao et al (2019)[184], by using CRISPR (clustered regularly interspaced short palindromic repeats) to insert the gene for enhanced (e)GFP into the mouse Y chromosome between the genes *Ddx3y* and *Uty*[184]. The gene targeting was performed within microinjected zygotes, which were then allowed to gestate to term[184]. Successful transgenic founder Y-Chr-eGFP males were detected by the presence of fluorescence in the skin of the adult male mouse, and these males were mated to produce the Y-Chr-eGFP strain[184]. Y-Chr-eGFP male embryos were assessed at the blastocyst stage, and found to be fluorescent across the entirety of the embryo[184]. Unlike the Y-GFP blastocysts above, the Y-Chr-eGFP blastocyst fluorescence images better recapitulated the bright-field images, a similarity with the *Ddx3y*^{mKate2} blastocysts[184]. However, the Y-Chr-eGFP mouse was not assessed at the midgestation or adult stages[184], unlike the previous characterisation performed for the *Ddx3y*^{mKate2} mouse (Figure 3.3)[5].

1.1.8. Hypotheses and Aims

Each of the two studies in this project have separate aims and hypotheses.

In order to demonstrate the utility of the *Ddx3y*^{mKate2} chromosome as a reporter for use in chromosome instability research, this thesis aims to:

1. Finalise the characterisation of the mKate2 signal in the *Ddx3y*^{mKate2} mouse on a stable background, including into advanced age.
2. Characterise the *Hprt*$^{DsRed\text{-}Express}$ reporter X chromosome mouse model, and to compare its characteristics to those of the *Ddx3y*^{mKate2} mouse.
3. Utilise two known chromosome instability backgrounds, the tumour suppressor protein *Trp53* knockout background and the knock-in fusion centromere protein *Cenpagfp* background, to model how the *Ddx3y*^{mKate2} reporter Y chromosome may be used in chromosome instability research.

It is hypothesised that the *Ddx3y*^{mKate2} mouse will have several strengths recommending its use in chromosome instability research.

In order to demonstrate that the cause of the male sex development defect present in the A/HeJ mouse is due to a partial deletion in the *Rbmy* gene repeat array on the Y$^{A/HeJ}$ chromosome arm, this thesis aims to:

1. Assess the male sex determination phenotype of the males in the Murdoch Children's Research Institute (MCRI) A/HeJ colony in order to extend upon the published phenotype.
2. Assess the gene copy number at the multicopy *Rbmy* locus on A/HeJ and control Y chromosomes, and characterise any copy number variation (CNV) of the *Rbmy* locus in A/HeJ males relative to the control strains, A/J and BALB/c.
3. Examine regulation of the *Sry* gene by assessing its methylation in the genital ridges of A/HeJ, A/J and BALB/c embryos during the window of testis determination.

It is hypothesised that there is a deletion within the *Rbmy* gene array on the Y$^{A/HeJ}$ chromosome, reducing its copy number. This reduction is hypothesised to adversely affect *Sry* gene expression in A/HeJ genital ridges, resulting in the gonadal phenotype observed in male A/HeJ mice.

Chapter 2: Materials and Methods

2.1. Equipment and Resources

2.1.1. List of Suppliers

Table 2.1 - List of Suppliers

Supplier	Reagents/Consumables/Equipment/Services
Agena Bioscience	SpectroCHIP, MassCLEAVE T7 Kit (T Cleavage), EpiTYPER MassARRAY system
Australian Genome Research Facility (AGRF)	Bisulfite sequencing of *Sry* promoter
Becton Dickson (BD)	BC FACSAria Cell Sorter, BD Influx Cell Sorter, FACSDiva software, BD FACS Sortware sorter software
Bioline	ISOLATE II Genomic DNA Extraction Kit
Bio-Rad	96-well semi-skirted well, Auto Droplet Generator (Auto DG), Evagreen© ddPCR Master Mix, Evagreen© ddPCR Droplet Oil, QuantaSoft software, QuantaSoft Analysis Pro (AP) software
De Novo Software	FCS Express software
Evrogen	Anti-tRFP antibody (cat.# AB233, anti-mKate2)
iNtRON Biotechnology	RedSafe™ Nucleic Acid Staining Solution (20,000x)
MCRI Flow Cytometry and Imaging Facility	Fluorescence-activated cell sorting (FACS)
MCRI Laboratory Support Services	Buffers: PBS, saturated NaCl, TBE, TE
MCRI Sequenom Platform Facility	Preliminary bisulfite sequencing of *Sry* promoter and gene
MCRI Tissue Culture Department	10% FBS DMEM, FreezeMix, FBS
Merck Millipore	EmbryoMax Filtered Light Mineral Oil
New England Biolabs (NEB)	*Hind*III, *Msp*JI, *Nla*III, *Hpy*CH4IV; associated buffers and reagents, CutSmart Buffer, Proteinase K
Promega	2x PCR Master Mix
Qiagen	10x PCR buffer, HotStarTaq Kit
Sigma Aldrich	DMEM, HBSS, Isopropanol, M2 medium
Syngene	G:BOX Chemi XX6 System (Gel Doc), Genesys software
Thermo Fisher Scientific	Nanodrop 2000 Microvolume Spectrophotometer, AmpliTaq Gold DNA Polymerase Kit, 1 M Tris pH 8.0, UltraPure™ Distilled Water, SYBR Safe DNA Gel Stain, RNase A, SuperFrost™

	Adhesive Slides
Vector Laboratories	VECTASTAIN Elite ABC Kit
WPI	Flurodish
Zymo Research	EZ DNA Methylation-Direct Kit

2.1.2. List of Databases

Table 2.2 - List of Databases

Database	URL	Reference
FPBase	https://www.fpbase.org/	Lambert, 2019[6]
UCSC Genome Browser, assembly Dec. 2011 (GRCm38/mm10)	http://genome.ucsc.edu/cgi-bin/hgGateway	Kent et al, 2002[185]
NCBI Primer BLAST	https://www.ncbi.nlm.nih.gov/tools/primer-blast/	Ye et al, 2012[186]

2.1.3. List of Primers

Table 2.3 - Primers

	Gene/Allele	Primer ID	Sequence	%GC Content	Melting Temperature	Amplicon Size
Routine Genotyping Assays	*mSry*	mSryF1	CACTGGCCTTTTCTCCTACC	55	58.9°C	349 bp
		mSryR1	CATGGCATGCTGTATTGACC	50	57.2°C	
	mHprt	HPRT-1	GTGTCGCCACACCTGACTAA	55	60°C	219 bp
		HPRT-2	ATGCCCAGCTACCAAGAAAG	50	57.9°C	
	Trp53 Wild-type (*Trp53*$^{+}$) Allele	Trp53x4f	CCACTCACCGTGCACATAAC	55	59.2°C	286 bp
		Trp53x4r	CATCACCTCACTGCATGGAC	55	58.6°C	
	Trp53 Knockout (*Trp53*$^{-}$) Allele	Trp53i7r	AGCCCAAGAGGAAACAGAGG	55	59.3°C	454 bp
		Pgk-pAf	ATTAAGGGCCAGCTCATTCC	50	57.6°C	
	Cenpa Wild-type (*Cenpa*$^{+}$) Allele	CenaI4k	GGAGCACAACTCATCCGTTC	55	58.9°C	260 bp
		CenaI4J	CGCTGGGAAAAGACTGCTCTG	57	61.5°C	
	Cenpagfp Knock-In	CenaE5r	GCATTTATATGGCGGGACTG	50	56.7°C	421 bp
		neo3utr_f	CGCCTTCTATGAAAGGTTGG	50	56.5°C	

	(*Cenpa*^{g}) Allele					
	DsRed-Express	DsR_f	CCAAGCTGAAGGTGACCAAG	55	58.8°C	303 bp
		DsR_r	CCTCCCAGCCCATAGTCTTC	60	59.2°C	
Blastocyst Genotyping Assay	*Cenpa* Wild-type (*Cenpa*$^{+}$) Allele	CaI4f1	GGGAAAAGACTGCTCTGAAGGA	50	61.2°C	301 bp
		CaI4r1	GGGGTCTAGGCTTTGTAAAATGG	48	62.9°C	
	Cenpagfp Knock-In (*Cenpa*^{g}) Allele	neo3UTRf1	GAAAGGTTGGGCTTCGGAATC	52	61.2°C	235 bp
		CaE5r1	CCATAGGGCTGAGCAATTCAC	52	61.2°C	
***Rbmy* Copy Number ddPCR Assays**	*Rbmy*	Ry1ddf	TGAACAGGGCTTCCTCACAG	55	59.6°C conventional 61.9°C ddPCR	203 bp
		Ry1ddr	CTCTACCAAGTGGGCTGCTG	60	60.4°C conventional 62.7°C ddPCR	
	Ddx3y	Dd2f	TGCCAGGTAGACAAAATGACC	48	58.2°C conventional 60.5°C ddPCR	104 bp
		Dd2r	TAGAGAGGTGGGGCTTAGGG	60	59.7°C conventional 62.1°C ddPCR	
***Sry* CpG Methylation ddPCR Assays**	*Sry* CpG -300	CpG1_1f	GTCCATCCTAAACATTAGGTACGTTA	39	58.5°C conventional 60.8°C ddPCR	98 bp
		CpG1_1r	CTTTTTCTTTGATCATTCTGTCACAAC	33	58.3°C conventional 60.5°C ddPCR	
	Sry CpG -537	CpG2_f	TCCTGAAGGAGGAGGGATAA	50	56.4°C conventional 58.8°C ddPCR	91 bp
		CpG2_r	AGAGCTAAAAGCCACTGACC	50	57.5°C conventional 59.8°C ddPCR	

Preliminary Bisulfite Sequencing of *Sry* *Inner primer GC% and T_m calculated without the tag and 10mer						
	Reverse Strand *Sry* Promoter Outer (Round 1)	SR-pro-f1	GTTAAAAGTTATTGATTAAAATGTGTTTG	21	54.6°C	452 bp
		SR-pro-r1	AAACTATAAAACCAAAACAAACTATTTC	21	54.6°C	
	Reverse Strand *Sry* Promoter Inner (Round 2)	SR-pro-tag	aggaagagagGTTAAAAGTTATTGATTAAAATGTGTTTG	21	54.6°C	421 bp (includes tag and 10mer)
		SR-pro-T7	cagtaatacgactcactatagggagaaggctAATAAATTCCATACTTATCATTTTTAACCC	23	56.0°C	
	Forward Strand *Sry* Promoter Inner (Round 1)	Spro-f1	TGATGTATTGATATGATTAAGAAAGGAA	25	55.5°C	370 bp
		Spro-r1	ATCAAACAAAACCCCTCAAATTTAT	28	56.2°C	
	Forward Strand *Sry* Promoter Inner (Round 2)	Spro-tag	aggaagagagTTTTTTATGGTGTAGATATTTATATTGGGT	23	56.4°C	343 bp (includes tag and 10mer)
		Spro-T7	cagtaatacgactcactatagggagaaggctAAAAACTACACTTTCACACTCCTTAAAA	29	58.5°C	
	Reverse Strand *Sry* Gene Outer Forward (Round 1)	SR-gen-f1	GTTTTTGTTTTATTGTAGAAGGTTGT	27	26.9°C	329 bp
		SR-gen-r1	CTAAAAAACATAAAAAACCATATCAAAC	21	54.0°C	
	Reverse Strand *Sry* Gene Inner (Round 2)	SR-gen-tag	aggaagagagTTGTTGAGGTAATTGTAGGTTGTAAAAT	29	58.2°C	340 bp (includes tag and 10mer)
		SR-gen-T7	cagtaatacgactcactatagggagaaggctTCTAAAAAACATAAAAAACCATATCAAAC	21	55.1°C	
	Forward Strand *Sry* Gene Inner (Round 1)	Sgen-f1	TAAGTTTTGGGATTGGTGATAATTGTTT	29	58.6°C	315 bp
		Sgen-r1	CAACTACAAACTATAAAATACCACTCCTC	35	58.5°C	
	Forward Strand *Sry* Gene Inner (Round 2)	Sgen-tag	aggaagagagTTGTTTAGAGAGTATGGAGGGTTATG	39	58.2°C	315 bp (includes tag and 10mer)
		Sgen-T&	cagtaatacgactcactatagggagaaggctACCACTCCTCTATAACACTTTAACCCT	41	61.2°C	

All melting temperature and %GC content values calculated using NCBI Primer BLAST tool. %GC content reported to nearest whole value.

Melting temperatures calculated for conventional PCR unless otherwise noted. Conventional PCR values were calculated using the preset values of the BLAST tool (refer to Table 2.4). ddPCR values were calculated by modifying the input values for divalent cation and dNTP concentrations as per Table 2.4, as the Evagreen© master mix contained these concentrations which deviated from conventional PCR mixes.

Table 2.4 - Changes to the NCBI Primer BLAST Settings for ddPCR conditions

Variable	Preset Value in NCBI Primer BLAST	ddPCR Evagreen© Chemistry Value
Divalent Cation Concentration	1.5	3.8
dNTP Concentration	0.6	0.8

2.1.4. Microscopes

The imaging of whole organs and embryos were performed on the Leica M205 FA stereomicroscope with the fluorescence lamp used for *Ddx3y*^{mKate2} (including intercrossed strains) and *Hprt*$^{DsRed\text{-}Express}$ related work. A/HeJ, A/J and BALB/c gonads and embryos were also imaged on this microscope, without the use of the fluorescence lamp.

Imaging of the E17.5 *Ddx3y*^{mKate2} embryo IHC tissues was performed on Zeiss Axioplan2 microscope as a single colour image.

The imaging of *Ddx3y*^{mKate2}/*Cenpagfp* and *Hprt*$^{DsRed\text{-}Express}$ preimplantation embryos was performed on the Zeiss LSM 780 confocal microscope.

2.1.5. General Equipment

Cell sorting experiments were performed primarily on the BD FACSAria FUSION cell sorter at the Murdoch Children's Research Institute (MCRI), with some sorting performed on the BD Influx cell sorter (MCRI). Sorts were performed by Dr Matthew Burton and Dr Paul Lau following experimenter input on required gating. Refer to Figures 4.2 and 4.4 for examples of gating.

Agarose gels upon which polymerase chain reaction (PCR) products were run in submarine electrophoresis tanks were imaged using the Gel Doc system (refer to Table 2.1).

All droplet digital PCR (ddPCR) experiments and optimisations were run using the Bio-Rad©

ddPCR system, consisting of the QX200 automated droplet generator ("AutoDG"), the PX1 PCR Plate heat sealer, the CX1000 96-well deep well thermocycler and the QX200 droplet reader.

DNA concentration and quality quantification was performed on the Nanodrop system (refer to Table 2.1).

2.1.6. Software

2.1.6.1. Imaging and Image Analysis Software

Images generated on the Leica M205 FA microscope were processed and analysed using the Leica Application Suite (LAS) version 4.0 software and/or Axiovision version Rel. 4.9.1 software. Digital measurement of A/HeJ and A/J gonad length and width was performed in Axiovision using the measurement tool. Images of the E17.5 *Ddx3y*^{mKate2} embryo IHC were captured and analysed using Axiovision.

Images generated on the Zeiss LSM 780 confocal microscope were processed and analysed using the Zen Black version ZEN 2.3 SP1 software, release version 14.0.0.0.

Images of agarose gels were captured using Genesys software, and analysis (see Section 2.7.1) was performed using FIJI version v1.52h software.

Figures were assembled and created using Biorender.com, with maps of the *Sry* locus generated in SnapGene Viewer version 4.0.4 software.

2.1.6.2. Statistical Software

All statistical analyses (as outlined in Section 2.9) were performed using GraphPad Prism version 7.04. This software was also used to generate all graphs presented in this work. Some bars for highlighting significant comparisons and p-values displayed on graphs were added manually to the graphs as figures were assembled, while others were added in GraphPad Prism.

2.1.6.3. Flow Cytometry/Fluorescence Activated Cell Sorting (FACS)

The software on the FACS machines were BD FACSDiva for the FACSAria and BD FACS Sortware sorter software for the Influx, with the majority of sort plots generated using these softwares. Plots of the *Ddx3y*^{mKate2}/*Trp53* knockout PMEFs were modified using FCS Express version 6, due to gating error during sorting.

2.1.6.4. Droplet Digital Polymerase Chain Reaction (ddPCR) Software

Data captured by the Bio-Rad© droplet reader was acquired using the Quantasoft software. Downstream analysis was performed using Quantasoft Analysis Pro (AP) version 1.0.596.0525 software.

2.2. Mouse Husbandry

All mice were housed in the Murdoch Children's Research Institute (MCRI) Disease Model Unit (DMU) Animal Facility ("Animal Facility"). All housing and experimental procedures were conducted under the approval of the MCRI Animal Ethics Committee (AEC), under the approval number A825, in accordance with its guidelines.

All data pertaining to mouse numbers, including litter sizes, were collected and recorded by Animal Facility staff on Microsoft Excel spreadsheets, and later on the Animal Management System (AMS) operated by the Walter + Eliza Hall Institute (WEHI). Day to day mouse handling, including cage maintenance, ear clipping, matings, routine culling and welfare handling, were performed by experienced Animal Facility staff. Culling of experimental animals for tissue or embryo collection was performed by either experienced Animal Facility staff, the PhD candidate, or another experienced researcher associated with this project.

2.2.1. Mouse Strain Information

The *Ddx3y*^{mKate2} and *Hprt*$^{DsRed\text{-}Express}$ mouse strains were both generated and maintained on a 129S1/SvImJ (Jax stock #002448[187]) background. Refer to Sections 3.1.1.1 and 3.1.2, respectively, for details of the gene targeting used to create these transgenic strains. The MCRI *Ddx3y*^{mKate2} colony used in this project was established using ES cell clone #106, with mice from the established colony used in this project. The 129S1/SvImJ strain is widely used for the generation of transgenic mouse lines, as there are many embryonic stem cell lines that have been derived from this strain, many of which have been observed to show a high frequency of germline transmission[187-189].

The *Ddx3y*^{mKate2} strain was used in generating two intercrossed strains in this project. This was achieved by crossing the *Ddx3y*^{mKate2} strain with the *Trp53* knockout (KO) and *Cenpagfp* knock-in transgenic strains. To generate the *Ddx3y*^{mKate2}/*Trp53* KO and *Ddx3y*^{mKate2}/*Cenpagfp* intercrossed mouse strains, the *Ddx3y*^{mKate2} Y chromosome was crossed onto each respective genetic background by mating *Ddx3y*^{mKate2} males with females heterozygous for the relevant transgene (*Trp53* KO allele (*Trp53*$^{-}$) or *Cenpagfp* allele (*Cenpa*^{g})). Resulting progeny constituted the *Ddx3y*^{mKate2}/*Trp53* KO and *Ddx3y*^{mKate2}/*Cenpagfp* mouse strains, respectively.

The *Trp53* knockout (KO) mouse strain was purchased from the Jackson Laboratory, where it is identified as Trp53^{Tm1Ty} (Jax stock #002101[190]). The *Trp53* KO colony maintained at MCRI was on a mixed strain background, primary component C53BL/6J (Jax stock #000664[191]), minor component from common genetic background 129S2/SvPas[192]. The *Trp53* KO strain is a transgenic mouse strain created by Jacks and colleagues[4], described in the 1994 *Current Biology* paper: "Tumor spectrum analysis in *Trp53*-mutant mice"[4], which generated the *Trp53* knockout or null allele, notated in this thesis as *Trp53*$^{-}$. Refer to Section 4.1.1 for description of its creation and associated phenotype.

The *Cenpagfp* knock-in transgenic mouse strain created by Kalitsis and colleagues[29], described in the 2003 *Chromosome Research* paper: "Partially functional Cenpa-GFP fusion protein causes increased chromosome missegregation and apoptosis during mouse embryogenesis"[29]. This involved generation of an allele for a fusion protein, Cenpagfp, with the allele notated as *Cenpa*^{g}. Refer to Section 4.1.2 for description of its creation and associated phenotype. The MCRI *Cenpagfp* colony was maintained on a BALB/cJ background (Jax stock #000651[193]).

BALB/c mice used for embryo collections in Section 2.4.2.4 were obtained from the MCRI Animal Facility BALB/c colony as required, as a BALB/c colony was not maintained by the research group. These mice were maintained on a BALB/c WEHI background, which was derived from the BALB/cJ (Jax stock #000651[193]) inbred albino strain. The BALB/c WEHI background was derived at the Walter and Eliza Hall Institute (WEHI), with mice purchased from WEHI by MCRI to establish the BALB/c colony at MCRI. In this thesis, this mouse strain is referred to as BALB/c.

The A/HeJ (Jax stock #000645[194]) and A/J (Jax stock #000646[183]) inbred albino mouse strains were obtained from the Jackson Laboratory in July 2014 and January 2014, respectively. Both are inbred strains from the A background, an albino mouse line derived from a cross between the Bagg Albino and the Cold Harbor Spring Albino strains[182]. The A/HeJ, also known as AHe and AHeston, strain diverged from the lineage leading to the A/J strain prior to 1930 at less than the 20th filial generation (F20)[182,194]. A/J is considered to be the closest related strain to A/HeJ. As BALB/c and A strains share a common ancestor due to being descended from Bagg Albino stock[195], BALB/c mice are closely related to both A/HeJ and A/J mice.

2.2.2. Breeding Strategies/Colony Maintenance

The BALB/c, A/HeJ, A/J, and *Ddx3y*^{mKate2} colonies were maintained by brother-sister matings as sexually mature mice became available, as these strains did not require specific genotype combinations for breeding. In the case of the *Ddx3y*^{mKate2} strain, all males were carriers of the transgene and therefore could mate with any female. The BALB/c, A/HeJ and A/J strains were inbred strains with no need to account for transgene transmission, and so any male was able to mate with any female, as required.

The *Trp53* KO, *Ddx3y*^{mKate2}/*Trp53* KO, *Cenpagfp* and *Ddx3y*^{mKate2}/*Cenpagfp* colonies were all maintained using brother-sister matings, in either heterozygous-heterozygous crosses or, for the *Trp53* KO and *Ddx3y*^{mKate2}/*Trp53* KO colonies, heterozygous-homozygous crosses. Homozygotes were not used in stock matings in the *Cenpagfp* and *Ddx3y*^{mKate2}/*Cenpagfp* colonies as these mice did not survive gestation (refer to Section 4.1.2). As both the *Trp53*$^{-}$ and *Cenpa*^{g} transgenes were autosomally inherited, the sex of the parent carrying the transgene was not relevant for breeding. All males in the *Ddx3y*^{mKate2}/*Trp53* KO and *Ddx3y*^{mKate2}/*Cenpagfp* colonies carried the *Ddx3y*^{mKate2} Y chromosome.

The *Hprt*$^{DsRed\text{-}Express}$ colony was also maintained using brother-sister matings, in crosses containing one wild type parent (XX or XY) and one parent carrying the *Hprt*$^{DsRed\text{-}Express}$ X chromosome (X$^{Hprt\ DsRed\text{-}Express}$X or X$^{Hprt\ DsRed\text{-}Express}$Y), with males and females both able to transmit the reporter chromosome to their progeny. Due to the impact of X chromosome inactivation (XCI, refer to Section 1.1.2.1), matings were set up such that all females born were either wild type (XX) or heterozygous for the *Hprt*$^{DsRed\text{-}Express}$ X chromosome (X$^{Hprt\ DsRed\text{-}Express}$X).

2.3. Tissue Collection from Adult Mice

2.3.1. Tissue Collection from Adult and Aged *Ddx3y*^{mKate2} Male Mice, and Adult *Hprt*$^{DsRed\text{-}Express}$ Mice

A *Ddx3y*^{mKate2} male mouse was culled at 52 weeks of age by cervical dislocation. The chest and abdominal cavities were opened using surgical scissors, and the heart, lungs, kidneys, spleen, liver and gonads were removed using surgical scissors and blunt-tipped forceps. Additionally, the head of the mouse was removed, stripped of fur/skin, and the eyes and brain were removed using blunt-tipped forceps. All harvested organs were transferred into cold PBS, imaged on the Leica M205 FA stereomicroscope (Section 2.1.4) for bright-field and mKate2 fluorescence, then discarded.

Additionally, the above organs were collected from male *Ddx3y*^{mKate2} mice aged between 53 and 125 days as described above. The carcasses of the males were stored at 4°C after euthanasia of the animals via cervical dislocation, and organs were dissected out into ice cold PBS. Organs were stored on ice in PBS until imaging at the listed times post-mortem (between 5.5 and 9 hours post-mortem, Section 3.2.1.2) as listed above, then discarded.

The above organs, as well as visceral and abdominal fat, were collected as described above from six week old male and female HprtDsRed-Express mice. The mice selected for this tissue collection were either transgenic (X$^{Hprt\ DsRed\text{-}Express}$X or X$^{Hprt\ DsRed\text{-}Express}$Y) or wildtype (XX or XY). All tissues were transferred into cold PBS, then imaged on the Leica M205 FA stereomicroscope for bright-field and DsRed-Express fluorescence, then discarded.

2.3.2. Thymus Collections from *Ddx3y*^{mKate2} /*Trp53* Knockout Mice

Trp53$^{-/-}$ mice are highly prone to developing tumours, particularly lymphomas of the thymus[180]. Seven *Ddx3y*^{mKate2}/*Trp53*$^{-/-}$ and four *Ddx3y*^{mKate2}/*Trp53*$^{+/+}$ males were culled by cervical dislocation. The chest cavities were opened using surgical scissors, and thymuses were removed from the chest cavity using surgical scissors and blunt-tipped forceps. The thymus was often initially removed with the heart and/or lungs attached, to reduce the likelihood of damaging the thymus. The thymus was then dissected away from the other organs using surgical scissors, blunt- and sharp-tipped forceps under a dissecting microscope in cold PBS; unneeded organs were discarded. Collected thymuses were imaged on the Leica M205 FA stereomicroscope for bright-field and mKate2 fluorescence. Thymuses collected for cell derivation were stored in PBS on ice until cell harvesting and derivation (Section 2.6.1).

2.3.3. Gonad Collection from Adult A/HeJ and A/J Mice

Gonads were collected opportunistically from adult A/HeJ and A/J male mice culled at a variety of ages during the course of routine colony maintenance. Mice were culled by cervical dislocation by either the researcher or experienced Animal Facility staff, and bodies of the mice were weighed prior to collection of the gonads. Briefly, the abdominal cavity was opened using blunt-tipped forceps and surgical scissors, and the gonads were removed using blunt-tipped forceps and surgical scissors. Any residual tissue such as fat remaining attached to the gonad was removed from the gonad using a scalpel blade, sharp-tipped forceps and a dissecting microscope. The right gonad was first weighed, then the left gonad was added to the balance, giving a mass value for both gonads. The mass of the left gonad was calculated as:

$$Mass\ of\ Left\ Gonad = (Mass\ of\ Both\ Gonads) - (Mass\ of\ Right\ Gonad)$$

The gonads were then transferred into ice cold PBS, then imaged using the Leica M205 FA stereomicroscope. The tails of the adult mice were clipped for later crude DNA extraction (Section 2.5.1.1) and sex genotyping (Section 2.5.2).

2.4. Embryo Collections

For the below matings to derive embryos, female mice were checked by experienced Animal Facility staff in the morning for the presence of a vaginal 'plug', indicating copulation had occurred overnight[68]. Plugged females were housed separately from the male to prevent additional copulation. Noon of the day on which the plug was observed was designated as embryonic day (E)0.5.

2.4.1. Preimplantation Embryo Collection

For *Ddx3y*^{mKate2}/*Cenpagfp* preimplantation embryos, *Ddx3y*^{mKate2}/*Cenpa*$^{+/g}$ females were mated with a *Ddx3y*^{mKate2}/*Cenpa*$^{+/g}$ male. Plugged females were collected in the afternoon of E3.5. For *Hprt*$^{DsRed\text{-}Express}$ preimplantation embryos, matings were set up between either X$^{Hprt DsRed\text{-}Express}$Y males and XX females, or XY males and X$^{Hprt DsRed\text{-}Express}$X females. Plugged females were collected at various time points between E1.5 and E4.0.

To collect embryos, females were culled via cervical dislocation, and the uterine horns were removed without the ovaries. The oviducts were flushed with M2 media using a blunted needle and a 3 mL syringe, and the reproductive tracts were flushed with M2 media from the top of the uterine horns using a sharp 25 gauge (G) needle and 3 mL syringe. Embryos between the two-cell and eight-cell stage were typically recovered from the oviducts, while all subsequent stages were recovered from the uterine horns; however, in order to maximise the yield, both structures were flushed in all collections. The preimplantation embryos were identified by use of a phase-contrast dissection microscope, and pooled in a fresh M2 media droplet using a P2 pipette. Preimplantation embryos were then washed through a minimum of three M2 media droplets to remove blood and stromal cells.

For *Ddx3y*^{mKate2}/*Cenpagfp* collections, the embryos were placed into individual M2 media droplets in a glass-bottomed Flurodish (WPI), and the droplets were then covered with sterile mineral oil. Embryos were imaged for T-PMT (transmitted light detector, bright-field), green fluorescent protein (GFP) and mKate2 fluorescence on the LSM 780 confocal microscope on a stage in a temperature-controlled, humidified chamber (37°C, 5% CO_2). Imaged embryos were removed from the M2 media droplets and transferred into individual microfuge tubes and frozen at -20°C for later DNA extraction and genotyping (refer to Section 2.5.3).

For *Hprt*$^{DsRed\text{-}Express}$ collections, the litter of embryos from an individual female were pooled together into a single M2 media droplet in a glass-bottomed Flurodish (WPI), which was then covered with sterile mineral oil. Embryos were imaged for T-PMT (bright-field) and DsRed-Express fluorescence on the LSM 780 confocal microscope on a stage in a temperature-controlled, humidified chamber (37°C, 5% CO_2). Once imaging was complete, embryos were discarded.

2.4.2. Postimplantation Embryo Collection

Post-implantation embryos were desired from the following strains: *Ddx3y*^{mKate2}, *Ddx3y*^{mKate2}/*Trp53* KO intercrossed strain, *Ddx3y*^{mKate2}/*Cenpagfp* intercrossed strain, *Hprt*$^{DsRed\text{-}Express}$, A/HeJ, A/J and BALB/c.

In order to collect post-implantation midgestation embryos, females were collected at different stages between E9.5 and E14.5, with an additional *Ddx3y*^{mKate2} embryo collected at E17.5 (Section 2.4.2.5). Plugged females were housed separately from the male until E9.5 when they were checked for pregnancy by experienced Animal Facility staff. Pregnant females were culled via cervical dislocation, and the uterine tracts were removed without the ovaries. Embryos were dissected out of the uterine tracts, decidua and embryonic membranes (chorion and amnion) using fine-tipped forceps. For E9.5 embryos, these membranes were retained and frozen (no PBS) at -20°C for later DNA extraction and genotyping (Sections 2.5.1 and 2.5.2, respectively), with the exception of *Hprt*$^{DsRed\text{-}Express}$ embryos. For *Hprt*$^{DsRed\text{-}Express}$ embryos, the whole embryo was retained and frozen (no PBS) at -20°C after imaging, for later DNA extraction from whole embryos and genotyping (Sections 2.5.1 and 2.5.2, respectively).

All embryos were imaged for bright-field on the Leica M205 FA stereomicroscope. *Ddx3y*^{mKate2}/*Cenpagfp* embryos were also imaged for mKate2 and GFP fluorescence, and *Ddx3y*^{mKate2}/*Trp53* KO embryos were imaged for mKate2 fluorescence. *Hprt*$^{DsRed\text{-}Express}$ embryos were imaged for DsRed-Express fluorescence.

2.4.2.1. Embryo Staging

Post-implantation embryos were broadly staged based on the gestational day (E9.5 to E14.5, E17.5) on which they were collected. More specific staging was determined by morphology and the number of somites in the tail of the embryo as described below.

For *Ddx3y*^{mKate2}/*Trp53* KO, *Ddx3y*^{mKate2}/*Cenpagfp* and *Hprt*$^{DsRed\text{-}Express}$ midgestation embryos, the embryos were staged based on the size and morphology of the embryo.

For A/HeJ, A/J and BALB/c embryos collected prior to E13.5, precise staging of the embryos was essential to collecting embryonic tissue at specific points in the sex development window due to the highly dynamic changes in the genital ridge across this period (refer to Section 1.1.5.2). Additionally, as the A/HeJ and A/J embryos were found during collections to be delayed by up to 12 hours relative to their expected stage, careful staging was essential to ensure the correct time points were being collected in order to precisely assess the *Sry* locus.

To stage these embryos, the size and morphology was assessed, followed by the counting of tail somites (ts)[196,197] for embryos between E10.5 and E13.0. ts were counted from the base of the hind limb with the embryo lying on its side, and counted out to the tip of the tail. To confirm the number of ts, the embryo was carefully turned onto its other side, and this count from base of hind limb to tip of tail was repeated. A discrepancy of greater than one ts between the two counts resulted in both sides of the tail being recounted. If it was not clear whether there was definitive number of ts between both sides, a value of [(n) to (n + 1)] was recorded. Embryos were grouped

according to gestational age as follows: E11.25 = 15 ts ± 1 (14 ts to 16 ts), E11.5 = 18 ts ± 1 (17 ts to 19 ts), E12.0 = 22 ts ± 1 (21 ts to 23 ts), E12.5 = 26 ts ± 1 (25 ts to 27 ts)[196]. For E14.5 embryos of these strains, gestational age was assessed by timing of collection, size and morphology. The E17.5 embryo was assessed by size and morphology by experienced Animal Facility staff.

2.4.2.2. *Ddx3y*^{mKate2}*/Cenpagfp* Embryos

For *Ddx3y*^{mKate2}/*Cenpagfp* post-implantation embryos, *Ddx3y*^{mKate2}/*Cenpa*$^{+/g}$ females were mated to *Ddx3y*^{mKate2}/*Cenpa*$^{+/g}$ males, with pregnant females collected in the afternoon of E9.5. This time point was chosen as it was before the onset of embryonic lethality in the *Cenpa*$^{g/g}$ embryos[29] (Section 4.1.2). Once imaged for fluorescence and bright-field, these embryos were preliminarily classified as male or female based on mKate2 fluorescence, and as one of three *Cenpa* genotypes (*Cenpa*$^{+/+}$, *Cenpa*$^{+/g}$ and *Cenpa*$^{g/g}$) based on GFP fluorescence and morphology (non-fluorescent/normal, faint fluorescence/normal, and faint fluorescence/malformed and small, respectively). These genotypes were then confirmed using PCR genotyping (refer to Section 2.5.2).

2.4.2.3. *Ddx3y*^{mKate2}*/Trp53* KO Embryos

For *Ddx3y*^{mKate2}/*Trp53* KO post-implantation embryos, *Ddx3y*^{mKate2}/*Trp53*$^{+/-}$ or *Ddx3y*^{mKate2}/*Trp53*$^{-/-}$ females were mated to either a *Ddx3y*^{mKate2}/*Trp53*$^{+/-}$ or *Ddx3y*^{mKate2}/*Trp53*$^{-/-}$ male, with pregnant females were collected on either E10.5, E11.5 or E12.5. Once imaged for mKate2 fluorescence and bright-field, these embryos were preliminarily classified as male or female based on mKate2 fluorescence. *Trp53* genotype (*Trp53*$^{+/+}$, *Trp53*$^{+/-}$ or *Trp53*$^{-/-}$) was ascertained by PCR genotyping (refer to Section 2.5.2). The embryos were used to derive primary mouse embryonic fibroblasts (PMEFs; procedure outlined in Section 2.6.2) that were either immediately subjected to fluorescence-activated cell sorting (FACS, Section 2.6.5) into mKate2-positive/negative populations, or were put into long term culture and/or mitotic spindle poison treatment followed by sorting based on mKate2 fluorescence as above (Section 2.6.4).

2.4.2.4. A/HeJ, A/J and BALB/c Embryos

For A/HeJ, A/J and BALB/c post-implantation embryos, males were mated with females of the same strain. Pregnant A/HeJ and A/J females were collected at 9 pm for E11.5 embryos on the day of E11.5, and at 5 pm for E12.5 embryos of both strains, and for E14.5 A/HeJ embryos, on the days of the respective stages. For BALB/c embryos, pregnant females were collected at 2 pm on the day of either E11.5, E12.5 or E14.5. Additional time points between E11.0 and E12.5 were added as required to increase proportions of different tail somite number embryos. Once imaged, these embryos were carefully staged according to Section 2.4.2.1.

For embryos between E11.0 and E13.0, the genital ridges were dissected out using fine-

pointed forceps, either attached to the mesonephroi or isolated from the mesonephroi. Paired genital ridges from each embryo were placed into individual 200 µL microfuge tubes without PBS, and frozen at -20°C. Heads and forelimb pairs were each separately retained and frozen at -20°C, no PBS, for later DNA extraction. Forelimb DNA was crudely extracted according to Section 2.5.1.1 for use in sex genotyping, while heads were retained for neat DNA extraction using the tissue lysis method in Section 2.5.1.2 for use in downstream experiments.

Genital ridge samples with mesonephroi removed were collected by Miss Alison Graham, while a subset (approximately 5%) of genital ridge samples with mesonephroi attached were also collected by Miss Alison Graham. The remainder of the genital ridge samples with mesonephroi attached were collected by the PhD candidate.

For embryos at E14.5, embryonic gonads from A/HeJ and BALB/c embryos were dissected out using fine-pointed forceps and imaged using the Leica M205 FA stereomicroscope while attached to the mesonephroi. Gonads were classified as having either 'testis', ovary' or 'testis-like' morphology based on size, shape and the presence of striations corresponding to the testis cords. Forelimbs were retained and frozen at -20°C, no PBS, for later DNA extraction (Section 2.5.1) for genotyping (Section 2.5.2).

2.4.2.5. *Ddx3y*^{mKate2} Embryo and Immunohistochemistry Staining

For the E17.5 *Ddx3y*^{mKate2} male embryo (Section 3.2.1.1), a 129S1/SvImJ female was mated to a *Ddx3y*^{mKate2}/ male, and once pregnant, was collected in the afternoon of E17.5. The embryo was anaesthetised and euthanised by experienced Animal Facility staff. The tissues of the embryo were collected and processed by Miss Alison Graham. Briefly, the head, forelimbs, heart and testis of the E17.5 embryo were fixed in 4% paraformaldehyde (PFA) overnight at 4°C, then transferred to 70% ethanol (EtOH) until processing for embedding. The structures were processed, embedded in paraffin wax and stored at 4°C.

The tissues were sectioned at 6 µM on a microtome and transferred to SuperFrost Plus glass slides by the PhD candidate. The presence of the mKate2 protein was detected by anti-mKate2 immunohistochemistry (IHC) staining of the sections. Briefly, the sections were dewaxed through xylene and rehydrated through graded EtOHs, and antigen retrieval was performed by incubation in 100°C citrate buffer for 20 minutes, followed by 30 minute incubation in the citrate buffer as it cooled to room temperature. Samples were washed in PBS and blocked for one hour in the blocking solution provided in the VECTASTAIN Elite ABC Kit.

Diluted anti-tRFP (Evrogen) antibody was added at 1:2000 to the slides and incubated at 4°C overnight to stain for the mKate2 protein. Slides were washed, incubated in 3% hydrogen peroxidase for 10 minutes, then washed before addition of a biotinylated secondary antibody provided by the

VECTASTAIN Elite ABC Kit. Slides were incubated for one hour, while the ABC reagent was prepared. Slides were washed, incubated in the ABC reagent for 30 minutes, before application of the DAB solution for approximately 30 seconds. Sections were flooded with dH_2O to stop the reaction, then counter-stained with Meyers-Haematoxylin. The slides were rinsed, dehydrated through graded EtOHs, and treated with SafSolvent. The sections were mounted with DEPEX and imaged in colour (Section 2.1.4) for mKate2 signal.

2.5. Genotyping of Mice and Mouse Embryos

2.5.1. DNA Extractions from Adult and Embryonic Mouse Tissues

DNA needed to be extracted from mouse and embryonic tissues for use in various genotyping reactions (Section 2.5.2), and in PCR-based analyses of genomic loci (Sections 2.7 and 2.8). The extraction procedure used depended on the quality of DNA required for the relevant experiment.

2.5.1.1. Routine DNA Extraction

DNA was extracted from mouse ear clips collected by experienced Animal Facility staff, and from whole embryos, using a sodium hydroxide (NaOH) extraction method. Briefly, an NaOH pellet was dissolved in 50 mL of autoclaved dH_2O, resulting in a solution with a concentration of approximately 50 mM NaOH. The solution was then filter sterilised by manual syringing through a 0.22 µm filter unit. Ear clips or embryos were thawed from -20°C storage, and 600 µL of 50 mM NaOH was added to each sample. Samples were incubated at 95°C for 10 minutes, vortexed at maximum speed for approximately 10 seconds, followed by further incubation at 95°C for five minutes. Samples were then vortexed for approximately 10 seconds at maximum speed, and allowed to cool briefly towards room temperature, then 50 µL of 1 M PCR-grade Tris, pH 8.0, was added per sample, and tubes were then inverted to mix. The resulting crude lysate was then used in routine genotyping (see Section 2.5.2).

The above NaOH DNA extraction method was modified for use on limb buds obtained from embryo collections. 60 µL of filter-sterilised 50 mM NaOH was added per tube, and 5 µL of 1 M PCR-grade Tris, pH 8.0, was added per sample following incubation (same as above), resulting in crude lysate for routine genotyping (Section 2.5.2).

2.5.1.2. Neat DNA Extraction

DNA was extracted from embryo heads using a tissue lysis method. Briefly, the samples were thawed from -20°C and 200 µL of Tissue Lysis Buffer (refer to Table 2.5) + Proteinase K (190 µL Tissue Lysis Buffer + 10 µL Proteinase K (20 mg/mL)) mixture was added to each sample. Samples were incubated at 56°C for three hours, pipetted through a P200 pipette tip to manually disaggregate the tissue, then placed back at 56°C overnight. Samples were removed from 56°C and 90 µL of saturated sodium chloride (NaCl) was added per sample, followed by inversion/shaking the tubes to mix the samples. The samples were placed at 4°C overnight to allow cell debris to precipitate out of solution. The samples were removed from 4°C and centrifuged at maximum speed in a refrigerated centrifuge at 4°C for 15 minutes. The supernatant of the samples was added to fresh 1.5 mL tubes containing 300 µL of isopropanol. The samples were mixed well by inversion and incubated at room temperature for approximately 30 minutes, then centrifuged at maximum speed for 10 minutes at room temperature. Supernatant was discarded and pellets were washed with 500 µL of 70% EtOH. Tubes were centrifuged to draw EtOH dregs to the bottom of the tube, which was then removed with a P200 pipette tip. Pellets were air dried in a laminar flow hood, and 30 µL of TE buffer + RNase A (100 ng/mL) was added per tube. Samples were incubated overnight at 37°C to aid in resuspension of DNA. Resuspended samples were stored at 4°C for short-term storage, and at -20°C for long-term storage.

DNA was extracted from midgestation embryonic membranes as above with the following alterations: incubation in Tissue Lysis Buffer + Proteinase K (same volume as above) was performed for two hours at 56°C before addition of saturated NaCl; samples were incubated at -20°C for 30 minutes; refrigerated centrifugation step was at maximum speed for 10 minutes; supernatant was decanted into 280 µL of isopropanol; pellets were resuspended in 20 µL TE buffer + RNase A (100 ng/mL).

Table 2.5 - Tissue Lysis Buffer

Reagent	Final Concentration
NaCl	100 mM
Tris HCl pH 7.5	50 mM
EDTA pH 8.0	10 mM
SDS	0.5%
dH_2O	To volume

2.5.2. Routine Genotyping

Mice born into the *Trp53* KO, *Cenpagfp* and *Hprt*$^{DsRed\text{-}Express}$ colonies (and intercrossed colonies) were routinely genotyped for the presence of their respective transgenes: the *Trp53*

knockout allele (*Trp53*$^{-}$), the *Cenpagfp* knock-in allele (*Cenpa*^{g}) or the DsRed-Express knock-in allele (*DsRed-Express*). HprtDsRed-Express, *Ddx3y*^{mKate2}/*Cenpagfp* and *Ddx3y*^{mKate2}/*Trp53* KO midgestation embryos were also genotyped for their respective transgenes using either crude DNA lysate (refer to Section 2.5.1.1, *Ddx3y*^{mKate2}/*Trp53* KO and *Hprt*$^{DsRed\text{-}Express}$ embryos) or neat DNA (refer to Section 2.5.1.2, *Ddx3y*^{mKate2}/*Cenpagfp* embryos). *Ddx3y*^{mKate2} mice did not require genotyping, as all male mice carried the transgenic *Ddx3y*^{mKate2} Y chromosome. A/HeJ and A/J mice, as well as midgestation embryos from all strains, were genotyped for sex by detection of the Y chromosome gene *Sry*, and amplification of the X chromosome *Hprt* gene as an internal control. All mice were genotyped using crude DNA lysate (Section 2.5.1.1).

Genotyping reactions were run using the Promega 2X PCR Master Mix, combined with UltraPure dH_2O, 1 µL each of 3 µM forward and reverse primers for each allele being assessed (for the *Trp53* KO and *Cenpagfp* PCRs, both the wild-type and transgene alleles for the relevant reaction; *Sry* and *Hprt* for the sexing PCR; for the *Hprt*$^{DsRed\text{-}Express}$ PCR, only the knock-in allele; refer to Table 2.3), and 1 µL of DNA, total reaction volume of 15 µL. Samples were cycled in a thermocycler according to the relevant protocol in Table 2.6.

Table 2.6 - Routine Genotyping PCR Cycling Conditions

Temperature	Duration	Cycles
95°C	2 minutes (Sexing reaction) 3 minutes (*Trp53* reaction, *DsRed-Express* reaction, *Cenpagfp* reaction)	x1
95°C	15 seconds (Sexing reaction) 30 seconds (*Trp53* reaction, *DsRed-Express* reaction, *Cenpagfp* reaction)	x30 (Sexing reaction) x35 (*Trp53* reaction, *DsRed-Express* reaction, *Cenpagfp* reaction)
60°C (Sexing reaction) 59°C (*Trp53* reaction, *DsRed-Express* reaction) 58°C (*Cenpagfp* reaction)	20 seconds (Sexing reaction) 30 seconds (*Trp53* reaction, *DsRed-Express* reaction, *Cenpagfp* reaction)	
72°C	30 seconds (Sexing reaction) 1 minute (*Trp53* reaction, *DsRed-Express* reaction, *Cenpagfp* reaction)	
72°C	5 minutes	x1
12°C (Sexing reaction) 4°C (*Trp53* reaction, *DsRed-Express* reaction, *Cenpagfp* reaction)	Hold	

1.5 µL of 10x Xylene Cyanol or Bromophenol Blue loading dye was added to each of the

completed reactions, which were then run on a 1% or 1.5% agarose gel containing RedSafe or SYBR Safe DNA dye. Bands on the gel were visualised using a Gel Doc.

2.5.3. Blastocyst DNA Extraction and PCR Genotyping

2.5.3.1. DNA Extraction from Blastocysts

Ddx3y^{mKate2}/*Cenpagfp* blastocysts were collected as outlined in Section 2.4.1 with minimal M2 media (< 2 µL). Embryos were thawed from -20°C to room temperature for DNA extraction using the method described in Scavizzi et al[198]. Briefly, 10 µL of PBND buffer[198] (Table 2.7) plus 0.1 mg/mL of Proteinase K (9.95 µL PBND + 0.05 µL Proteinase K (20 mg/mL)) was added per tube. Tubes were capped, contents pulse-spun to the bottom of the tubes, then samples were incubated in a thermocycler at 56°C for three hours with hourly vortexing to allow digestion of the embryos. The thermocycler temperature was raised to 95°C for 15 minutes to inactivate the Proteinase K. Samples were vortexed at maximum speed for two to three seconds, contents were pulse-spun to the bottom of the tubes and allowed to cool to room temperature. Lysate was used in genotyping reactions (Section 2.5.3.2).

Table 2.7 - PCR Buffer Nonionic Detergents (PBND)

Reagent	Final Concentration
KCl	50 mM
Tris HCl pH 8.3	10 mM
$MgCl_2$	2.5 mM
Gelatin	0.1 mg/mL
Nonidet P40 (NP40)	0.45% v/v
Tween 20	0.45% v/v
dH_2O	To volume

2.5.3.2. Confirmation of DNA Recovery and *Cenpagfp* Genotyping by PCR

2 µL of the blastocyst lysate from Section 2.5.3.1 was used in a PCR to amplify the *mHprt* X chromosome-linked locus using the primers listed in Table 2.3. This was performed as a control to confirm that intact DNA was extracted successfully. Samples that yielded an amplicon band in the *mHprt* reaction were expected to also yield results in the *Cenpagfp* reaction, as this was a test reaction to confirm the presence of usable (amplifiable) DNA. However, it should be noted that DNA is susceptible to shearing, and with such low yields from blastocysts (< 0.5 ng), it is possible that breaks could occur within the regions of interest for amplification in these reactions, resulting in failed PCR reactions despite the presence of otherwise usable DNA.

The *mHprt* PCR was performed using AmpliTaq Gold in a 20 µL reaction volume, which included the AmpliTaq Gold 10x PCR Buffer, combined with UltraPure dH_2O, 10 mM dNTPs, 10 mM $MgCl_2$, 0.5 U of AmpliTaq Gold DNA polymerase, 1 µL of the combined 10 µM forward and reverse primers, and the crude DNA lysate; total reaction volume 20 µL. The reactions were cycled as described in Table 2.6 (Sexing reaction), with the modification that the initial 95°C denaturation step was increased from three to 10 minutes. 2 µL of Xylene Cyanol loading dye was added to each of the completed reactions, which were run on a 1.5-1.75% agarose gel containing SYBR Safe DNA stain and imaged for the presence of the amplicon band on the Gel Doc system.

5 µL of the remaining blastocyst lysate was then used in a 30 µL reaction to amplify the *Cenpa*$^{+}$ and *Cenpa*^{g} alleles using the primers in Table 2.3. This PCR contained AmpliTaq Gold 10x PCR Buffer, combined with Ultra Pure dH_2O, 10 mM dNTPs, 10 mM $MgCl_2$, 1.5 U of AmpliTaq Gold DNA polymerase, 1 µL each of 10 µM forward and reverse primers for both alleles, and the crude DNA lysate; total reaction volume 30 µL. The reactions were cycled in a thermocycler according to the *Cenpagfp* cycling conditions in Table 2.10 with the initial 95°C denaturation step increased to 10 minutes. 3 µL of Xylene Cyanol loading dye was added to each of the completed reactions, which were then run on a 1.5-1.75% agarose gel containing SYBR Safe DNA stain and imaged for the presence of the amplicon bands on a Gel Doc.

2.6. Cell Culture and Cytological Work

2.6.1. Derivation of Thymus-Derived Cells from *Ddx3y*^{mKate2}/*Trp53* Knockout Mice

Thymuses collected from *Ddx3y*^{mKate2}/*Trp53*$^{-/-}$ and *Ddx3y*^{mKate2}/*Trp53*$^{+/+}$ mice (Section 2.3.2) were transferred into a 100 mm tissue culture plate in 10% DMEM media. Two 32G needles were removed from their packaging and bent at approximately 45° angle, and these needles were then used to manually disaggregate the thymuses by repeatedly puncturing the organ to release the cells into suspension. The cell suspension was then removed from the dish using a 10 mL pipette, passed through a cell strainer into a 50 mL Falcon tube, and additional DMEM was added to the dish. The needles were again used to disrupt the tissue to collect the suspension cells as above. This was repeated three to four times, and the plate was rinsed with DMEM to collect any remaining cells in the dish. Harvested cells either proceeded to red blood cell (RBC) lysis (below) and cell sorting, or were incubated for up to one hour in 10% DMEM in a tissue culture incubator (37°C, 5% CO_2), before RBC lysis and sorting.

Once the cells had been collected/following short incubation, the suspensions were pelleted at 350 x g. The supernatant was discarded and the cell pellets were resuspended in 15 mL of Ammonium Chloride RBC lysis buffer (Table 2.8). Cells were incubated with gentle rocking for five

minutes at room temperature to allow for RBC lysis. The remaining cells were pelleted at 350 x g, then resuspended in 300 µL to 500 µL of PBS + 2% FBS. 0.2 µg of DAPI was added per sample immediately before sorting using fluorescence-activated cell sorting (FACS) (Section 2.6.5).

Table 2.8 - Ammonium Chloride Red Blood Cell Lysis Buffer

Reagent	Final Concentration
Ammonium Chloride	154.4 mM
Potassium Bicarbonate	10 mM
EDTA	97.3 µM
dH_2O	To volume
Recipe as per[199].	

2.6.2. Derivation of Primary Mouse Embryonic Fibroblasts (PMEFs)

Primary mouse embryonic fibroblasts (PMEFs) were derived from midgestation Ddx3ymkate3/*Trp53* KO embryos (Section 2.4.2.3). Heads and internal organs of E10.5 to E12.5 Ddx3ymkate3/*Trp53* KO embryo were removed using sharp-tipped forceps. Internal organs were discarded, and heads were retained and frozen without PBS for later DNA extraction Section 2.5.1). The mouse carcass was then transferred into a 15 mL Falcon tube with 1 mL to 2 mL of cold PBS, and the carcass was passed through a 25G or 32G needle attached to a 5 mL syringe approximately five times to manually disaggregate the carcass. The tissue suspension was pelleted in a centrifuge at 350 x g for 5 minutes, and the PBS was carefully aspirated off. The tissue pellets were resuspended in 5 mL of 0.025% trypsin, placed at 37°C for 10 minutes, then mixed by inversion. The samples were then incubated a further 10 minutes at 37°C, followed by addition of 5 mL of 8% DMEM per tube and inversion of samples. Cells were pelleted at 350 x g for 10 minutes, media carefully aspirated off, and cells were resuspended in 10 mL of 8% DMEM. Cell suspensions were divided evenly between two 15 cm tissue culture plates, and were grown in a total volume of 20 mL of 8% DMEM per plate in tissue culture incubators, 37°C, 5% CO_2.

2.6.3. Culturing of PMEFs

Culturing of PMEFs generated in Section 2.6.2 was achieved as follows. Media was aspirated off of adherent cultures once cells approached 80% to 90% confluence. The cells were washed with between 0.5 mL and 5 mL of pre-warmed (37°C) PBS, depending on plate size, to remove any residual media. The plate was gently tilted to allow the PBS to wash over the entire surface of the plate, followed by aspiration of all liquid from the plate. Between 1 mL and 10 mL of room temperature 0.025% trypsin as added per plate depending on plate size, and plates were tilted to ensure even coverage of trypsin across the entire surface. Plates were placed into tissue culture incubator (37°C, 5% CO_2) for approximately five to ten minutes, at which time they were checked

for detachment of cells from the plate surface. This was aided by gently tapping the side of the plate, and if required, further incubation for an additional five to ten minutes in the tissue culture incubator. Plates were again gently tapped to aid in final dislodgement of cells from plate surfaces, and trypsin-cell suspensions were briefly pipetted over the surface of the plate to further aid in detachment and disaggregation of cells from one another. Between 1 mL and 12 mL of 8% or 10% DMEM was added per plate to inactivate the trypsin, and the suspensions were pipetted over the surface of the plate to homogenise the suspensions to single cell. Cells were then either harvested for downstream applications or freezing, or were subcultured into fresh tissue culture plates with fresh media, typically split between 1:3 or 1:4.

PMEFs were frozen in FreezeMix prepared by MCRI tissue culture department, with 1 mL FreezeMix-cell suspension per cryovial. Cryovials were placed into room temperature isopropanol-chamber freezer containers containing 250 mL isopropanol, which were then placed into -80°C freezers. These freezer containers controlled the freezing of the cells at a standard 1°C decrease in temperature per minute to avoid damaging the cells. Once the container and cells had reached -80°C, the cryovials were removed from the container and transferred into cardboard storage boxes in the -80°C freezer. The freezing container was allowed to return to room temperature before being used again.

To thaw cryopreserved cells for culture, the appropriate cryovial was removed from the storage box and placed onto dry ice to prevent premature thawing of the sample. The cryovial was held around the lip of the lid, and partially submerged in a 37°C water bath and gently swirled around in the water until the entire tube had thawed. The contents of the cryovial were then transferred to a 15 mL Falcon tube containing 3 mL of 10% DMEM, which was then mixed by inversion. The cell suspensions were pelleted at 350 x g for 5 minutes and the liquid was carefully aspirated off. The cells were resuspended in prewarmed (37°C) 10% DMEM and plated out as appropriate to cell number. Cells were passaged as above as required.

2.6.4. Mitotic Spindle Poison and/or High Passage Number Challenges of *Ddx3y*^{mKate2}/*Trp53* KO PMEFs

Ddx3y^{mKate2}/*Trp53*$^{-/-}$ and *Ddx3y*^{mKate2}/*Trp53*$^{+/+}$ PMEFs at either passage one to two ('low passage number') or passage 10 ('high passage number', cultured for approximately one month) were grown to confluency in either serum-containing media (DMEM) or serum-free (serum-replacement) media, then harvested as described in Section 2.6.3 and seeded into 24-well plates at 0.1 x 10^6 cells per well in 0.5 mL of 8% DMEM. Plates were placed into a 37°C, 5% CO_2 incubator for approximately 24 hours to allow the cells to adhere to the plate. Media was removed, cells were washed twice with pre-warmed (37°C) PBS, and 0.5 mL of the relevant media containing either 100 ng/mL of Nocodazole, 100 ng/mL of Colcemid, 100 µM of Monastrol (high passage number only) or

no drug (control) was added to plates. The cells were then placed back in the incubator for 24 hours.

Media was removed, cells were washed twice with pre-warmed (37°C) PBS, before 0.5 mL drug-free media was added to each plate. Cells were then placed back at 37°C, 5% CO_2, and allowed to recover from the drug challenge for 48 hours before harvest. Harvested cells were pelleted at 350 x g for five minutes, supernatant was removed and cells were resuspended in 200 µL PBS + 2% FBS. 0.1 µg of DAPI was added to the tube immediately prior to sorting as described in Section 2.6.5.

2.6.5. Fluorescence-Activated Cell Sorting (FACS)

Ddx3y^{mKate2}/*Trp53* KO PMEFs (Sections 2.6.2 and 2.6.4) and thymic cells (Section 2.6.1) were sorted into mKate2-positive and negative populations using fluorescence-activated cell sorting (FACS) on the BD FACSARIA Fusion Cell Sorter or BD Influx Cell Sorter. Cells were sorted by the MCRI Flow Cytometry and Imaging Facility staff, with input from the PhD candidate, gated progressively for "Cells" (separate from debris), "Single Cells", "Live Cells" (DAPI negative), and into "RFP (mKate2) Positive" and "RFP (mKate2) Negative" populations. Refer to Figures 4.2 and 4.4 for example cell sorts for PMEFs and thymus cells, respectively.

2.7. Analysis of Copy Number Variation (CNV) at the *Rbmy* Locus of the Y$^{A/HeJ}$ Chromosome

2.7.1. Preliminary Application of the *Rbmy*/*Ddx3y* CNV Assay Primers using Conventional PCR

Primer pairs were designed to amplify regions of the *Rbmy* and *Ddx3y* genes from the mouse Y chromosome in order to assess *Rbmy* gene copy number using PCR-based assays, specifically the Droplet Digital PCR (ddPCR) system. *Ddx3y* was chosen as a single locus reference gene for the analysis of *Rbmy* copy number, as both genes are Y chromosome-linked. Prior to adapting these assays to the ddPCR system, a preliminary trial of these primers (Table 2.3) was performed using conventional PCR to both (i) confirm that both assays would amplify under the same cycling conditions, and (ii) determine whether there was an indication of an *Rbmy* copy number change in A/HeJ samples relative to A/J samples. This would be indicated by a discernible difference in relative amplification signal intensity between the target (*Rbmy*) and reference (*Ddx3y*) assays between the two strains.

Reactions were run using the AmpliTaq Gold 10x PCR Buffer, combined with UltraPure dH_2O, 10 mM dNTPs, 10 mM $MgCl_2$, 1.25 U of AmpliTaq Gold DNA polymerase, 1 µL each of 10 µM forward and reverse primers for both genes (Table 2.3), and 1 µL of crude DNA lysate (refer to Section

2.5.1.1), total reaction volume of 25 µL. DNA from A/HeJ males, A/J males and a single female control from each strain were used. The *Rbmy* and *Ddx3y* assays were run in the same reaction for each sample to allow for comparison of the amplification of each amplicon. Samples were cycled in a thermocycler according to the conditions in Table 2.9. 2.5 µL of Xylene Cyanol loading dye was added to each of the completed reactions, which were then run on a 2% agarose gel containing SYBR Safe DNA dye.

Table 2.9 - *Rbmy* CNV Conventional PCR Cycling Conditions

Temperature	Duration	Cycles
95°C	10 minutes	x1
95°C	30 seconds	x35
59°C	30 seconds	
72°C	1 minute	
72°C	5 minutes	x1
12°C	Hold	

The agarose gel was imaged using a Gel Doc, and the .tiff file was assessed using the ImageJ FIJI software. Briefly, the image was converted to grey scale, and the Rectangular Selections tool was used to draw a rectangular box around both (*Rbmy* and *Ddx3y*) bands in each well. The command Analyse>Gels>Select First Lane was entered to select the first sample lane, and the command Analyse>Gels>Select Next Lane was used for all subsequent sample lanes. The profile of each of the lanes' intensity was plotted using the command Analyse>Gels>Plot Lanes. This produced the plots in Appendix 8.2. Using the Straight Line tool, the two peaks, representing each of the *Rbmy* and *Ddx3y* bands, were separated and the area of the plots corresponding to each of the bands was measured using the Wand tool. These peaks' values were labelled onto the plots using the Analyse>Gels>Label Peaks command, with their size being expressed as a percentage of the total area of both peaks. From this data, the relative intensity of the *Rbmy* band relative to the *Ddx3y* band was calculated by dividing the *Rbmy* values by the *Ddx3y* values.

2.7.2. Digital Droplet Polymerase Chain Reaction (ddPCR) Copy Number Variation (CNV) Analysis of the *Rbmy* Locus

To assess the number of *Rbmy* repeats, neat DNA extracted from the heads of A/HeJ, A/J and BALB/c embryos (Section 2.5.1.2) was used in a copy number variation (CNV) Droplet Digital Polymerase Chain Reaction (ddPCR) analysis using the same primers trialled in Section 2.7.2 (Table 2.3). The DNA was diluted to 10 ng/µL in TE buffer, and this dilution was confirmed using a Nanodrop. 25 µL ddPCR reactions were made up using the Evagreen© ddPCR 2x Master Mix (Bio-Rad©), with the reference (*Ddx3y*) and target (*Rbmy*) amplicons run in separate reactions. Restriction enzyme *Hin*dIII (NEB, Table 2.10) was included in the reaction mix to a final concentration

of 2 U/reaction, 100 nM of the forward and reverse primers for the respective assay, and 1 µL of the 10 ng/µL DNA was added to each reaction (or UltraPure dH_2O for no template control (NTC) wells). UltraPure dH_2O was used to make up the reactions to the 25 µL volume. Each sample for each amplicon was run in duplicate to account for possible pipetting error.

The reactions were prepared in 96 well ddPCR semi-skirted plates (Bio-Rad©) which were loaded into the Bio-Rad© QX200™ Auto Droplet Generator (AutoDG). The AutoDG combined 20 µL (containing a total of 8 ng of template DNA) of each reaction with 70 µL of Evagreen© oil to generate droplets of approximately 1 nL volume; total approximate number of droplets generated per 20 µL of reaction mix is 20,000 droplets. These droplet reactions were transferred by the AutoDG to a fresh 96 well ddPCR plate, which was sealed with a foil seal using the Bio-Rad© PX1™ PCR Plate Sealer with 180°C heat applied for five seconds. The plate was run on the Bio-Rad© C1000 Touch™ Thermal Cycler with 96-Deep Well Reaction Module according to the conditions in Table 2.11. Following thermocycling, the plate was transferred to the Bio-Rad© Droplet Reader. The acquisition parameters in the QuantaSoft software set to ABS (absolute quantification) for direct quantification (DQ), and the machine was run to collect data on the fluorescence of the droplets of each reaction.

Table 2.10 - *Hind*III Restriction Site

$HindIII = \frac{A\|AGCTT}{TTCGA\|A}$

Table 2.11 - *Rbmy* CNV ddPCR Cycling Conditions

Temperature	Duration	Cycles
95°C	10 minutes	x1
95°C	30 seconds	x35
61°C	1 minute	
4°C	5 minutes	x1
95°C	5 minutes	
4°C	Hold	
Ramp Rate: 2°C per second		

Data were analysed in the QuantaSoft Analysis Pro (AP) software. The concentration of the amplicon in each reaction was calculated by the software in copies per µL, and this value was averaged over duplicate wells. These average values were substituted into the CNV calculation provided by Bio-Rad©[200]:

$$CNV = \frac{Concentration\ of\ Target}{Concentration\ of\ Reference} * (Number\ of\ Reference\ Loci\ per\ Diploid\ Genome)$$

where the "number of reference loci per diploid genome" was assigned as 1, as the Y chromosome is hemizygous, and the reference locus is the single-copy *Ddx3y* gene (2n=1).

The values obtained from these calculations were compared across the three strains using the GraphPad Prism software; refer to Section 2.9 for analysis.

2.8. *Sry* Methylation Analysis

Sections 2.8.1 (extraction from genital ridges without mesonephroi only) and 2.8.2 were performed by Miss Alison Graham. Data analysis of the results from Section 2.8.2 was performed in collaboration with Miss Alison Graham (approximately 50% of analysis, Section 2.9.1). Section 2.8.1 (extraction from genital ridges with mesonephroi only) was performed by the PhD candidate.

2.8.1. DNA Extraction from Mouse Embryonic Genital Ridges for Bisulfite Conversion

DNA was extracted from embryonic genital ridges without mesonephroi, and genital ridges with mesonephoi attached, from A/HeJ, A/J and BALB/c embryos at E11.25, E11.5, E12.0 and E12.5 (Section 2.4.2.4), using the Bioline ISOLATE II Genomic DNA Extraction kit as per the company's 'Bench-Top Protocol" with minor modifications as below. Briefly, the genital ridges were thawed from -20°C and the microfuge tubes were briefly pulse spun to ensure that the tissue was at the bottom of the tube. 205 µL of Lysis Buffer GL and Proteinase K solution (kit provided) (180 µL and 25 µL, respectively) was added per sample, followed by brief vortexing and a three hour incubation with periodic vortexing at 56°C until the tissues were completely lysed.

Following incubation, the samples were briefly vortexed, and 200 µL of Lysis Buffer G3 was added per sample. The samples were vigorously vortexed, incubated at 70°C for 10 minutes, then vortexed again briefly. 210 µL of absolute (96-100%) EtOH was added to each lysate before vigorous vortexing. The spin column was assembled per kit instructions, and the total lysate volume was loaded into the top of the spin column. Samples were centrifuged in a bench top centrifuge at 11,000 x g for one minute to bind the DNA to the column membrane, and flow through was discarded. The membrane was washed sequentially with 500 µL Wash Buffer GW1 and 600 µL Wash Buffer GW2, with the columns centrifuged for one minute at 11,000 x g and flow through discarded after each centrifugation.

The spin column was replaced into the collection tube and centrifuged at 11,000 x g for a further one minute to dry the membrane, and the collection tube and flow through were both discarded. The spin column was transferred to a fresh 1.5 mL Eppendorf tube and 15 µL, 35 µL or 60 µL of preheated 70°C Elution Buffer G was added to the spin column membrane. The elution buffer

incubated on the column at room temperature for five minutes, before the assembly was centrifuged at maximum speed for two minutes. The flow through was placed back onto the spin column membrane and centrifuged again at maximum speed for two minutes to maximise DNA yield. The spin column was discarded, after which DNA concentration was analysed on a Nanodrop, and samples were stored at -30°C until downstream use.

2.8.2. Preliminary Bisulfite Sequencing

2.8.2.1. Bisulfite Conversion of Genital Ridge DNA

In order to assess DNA methylation with bisulfite sequencing, the first step was to bisulfite convert the sample. Bisulfite conversion is the process by which unmethylated cytosines (C) are converted uracil (U) residues, while methylated cytosines (^{m}C) remain unconverted[201,202]. Amplification of the converted DNA (Section 2.8.2.2) results in the U being amplified as a thymine (T) residue[201,202]. The subsequent sequencing of the amplified DNA detects these C to T changes, and hence, detects the methylation status of the C at the individual base level[201,202].

Table 2.12 - Tail Somite Number of Embryos used in Preliminary Bisulfite Sequencing of *Sry*

	Tail Somite Number		
Stage	**A/HeJ**	**A/J**	**BALB/c**
E11.5	15,16,17,17	15+, 17,17,18	16,17,18,18
E12.5	24,24-25,24-25,25	24,24,24-25,25	25,25-26,26,26

Genital ridge DNA from E11.5 and E12.5 embryos (refer to Table 2.12) was subjected to bisulfite conversion using the Zymo Research EZ DNA Methylation-Direct™ Kit. Briefly, 20 µL of DNA from each sample (approximately between 168 ng and 434 ng of DNA) was diluted with 25 µL of dH_2O and 5 µL of M-dilution buffer (total volume 50 µL). The dilution was mixed well by pipetting and was incubated at 42°C for 20 minutes. During this incubation step, three tubes of the CT Conversion Reagent was prepared by adding 210 µL of the M-dilution and 750 µL of dH_2O to each supplied tube of the CT Conversion Reagent, followed by vortexing the tubes at maximum speed for 10 minutes. Once the incubation of the diluted DNA was complete, 100 µL of the CT Conversion Reagent was added per tube. Reactions were mixed well by pipetting, and tubes were covered by foil and placed at 50°C to incubate overnight (approximately 13.5 hours).

The following day, the reactions were removed from 50°C and placed on ice (0°C to 4°C) for 10 minutes. 400 µL of M-Binding Buffer was added to a Zymo-Spin™ IC Column placed inside a collection tube for each sample. Following the ice incubation, the reactions were loaded into the Columns containing M-Binding Buffer and the reactions were mixed by inverting multiple times, followed by centrifugation at maximum speed for 30 seconds. Flow through was discarded, and 100

µL of the M-Wash Buffer was added to each column before another 30 second centrifugation at maximum speed. 200 µL of the M-Desulphonation Buffer was added to each column and allowed to incubate at room temperature for 20 minutes, followed by another maximum speed centrifugation, 30 seconds. The previous wash step with M-Wash buffer was repeated twice using a volume of 200 µL, with centrifugation and discard of flow through between each wash.

Following the final wash, the columns were centrifuged at maximum speed for a further one minute to remove all traces of the wash buffer. The columns sat at room temperature for approximately five minutes before being transferred into fresh brown 1.5 mL Eppendorf tubes. 10 µL of the M-Elution Buffer was added per column directly to the column matrix. The columns were incubated at room temperature for two minutes, before centrifugation at maximum speed for one minute. The eluted samples were then placed onto ice while 5 µL of the DNA was transferred to a separate brown 1.5 mL Eppendorf tube; one aliquot was stored at -20°C and the other aliquot was stored at -80°C.

2.8.2.2. Nested PCR on Bisulfite-Converted DNA

In order to prepare the samples bisulfite-converted in Section 2.8.2.1 for sequencing, the regions of interest needed to be amplified by nested PCR. Each of the bisulfite-converted samples, as well as control methylated and unmethylated DNA and dH_2O, were used in nested PCR reactions run for each region of interest: *Sry* promoter, forward and reverse strand, and *Sry* gene, forward and reverse strand (Table 2.3). The reactions were set up across two 96-well plates: plate 1 contained all reactions amplifying the *Sry* promoter and gene forward strands; plate 2 contained all reactions amplifying the *Sry* promoter and gene reverse strands.

Master mixes for Round 1 of each reaction were prepared using the Qiagen 10x PCR buffer, combined with UltraPure dH_2O, 200 nM 'outer' primer pair (Table 2.3) for each reaction, 10 mM dNTPs, HotStar *Taq*, and 0.8 µL of either bisulfite-converted sample DNA, control DNA or dH_2O, with total reaction volume of 20 µL. Samples were cycled in a thermocycler according to the conditions in Table 2.13. The Round 2 PCR master mixes were prepared and run as above, using 1 µL of Round 1 products as template and using the 'inner' primer pairs (Table 2.3).

Table 2.13 - Nested *Sry* PCR Cycling Conditions

Temperature	Duration	Cycles
95°C	15 minutes	x1
95°C	30 seconds	x31
56°C (Plate 1) 54°C (Plate 2)	1 minute	
72°C	1 minute	
72°C	3 minutes	x1
4°C	Hold	

Following thermocycling, 5 µL of each Round 2 reaction was added to 1 µL of Promega 6x loading buffer and run on a 1.5% agarose gel containing RedSafe DNA dye to confirm amplifications were successful.

2.8.2.3. Mass Cleavage

The Epityper Mass Cleave Reagents were used to prepare the amplified samples for methylation analysis on the Epityper. Briefly, the samples were treated with the Shrimp Alkaline Phosphatase (SAP) treatment as below. A master stock was created by combining 1.7 µL of nuclease-free dH_2O and 0.3 µL of SAP per sample (420 samples, total master stock volume = 840 µL) and mixed well. Using a multichannel pipette, 2 µL of the above solution was aliquotted into each well of a 387 well plate. 5 µL of the Round 2 PCR for each reaction from plates 1 and 2 was added to the 384-well plate. The plate was sealed with sealing film and spun at 560 x g for one minute to collect all liquid in the bottom of the wells. The plate was then incubated in a 384-well PCR machine as follows: 37°C for 20 minutes, 85°C for 5 minutes, final dwell temperature 4°C. The plate was removed from the thermocycler and immediately frozen at -20°C.

For the Mass T Cleavage Assay, the following master mix was made up according to Table 2.14. Using a multichannel pipette, 5 µL of the master mix was added per well to a 384-well plate. The SAP reaction plate was thawed and 2 µL of each well's reaction was transferred to the 384-well containing the Mass T Cleavage Assay master mix. The plate was sealed with sealing film and spun down to collect all liquid at the bottom of the wells. The plate was incubated at 37°C in a 384-well thermocycler, then removed and frozen at -20°C until clean up.

Table 2.14 - Mass T Cleavage Assay Master Mix

Reagent	Volume per Well
RNase-free dH_2O	3.21 µL
5x T7 polymerase buffer	0.89 µL
T Cleavage mix	0.22 µL
100mM DAT	0.22 µL
T7 RNA and DNA polymerase	0.40 µL
RNase A	0.06 µL
Total volume	5 µL

For clean up, 20 µL of dH_2O was added per well in the 384-well resin plate using a multichannel pipette, and the plate was pulse spun down to collect the liquid at the bottom of the wells. Resin was added to the plate and the plate was sealed with sealing film. The plate was incubated at room temperature with rocking for 20 minutes before being frozen at -20°C overnight. The plate was then thawed and given to staff from the MCRI Sequenom Platform Facility along with

the SpectroCHIP® to be run on the Sequenom®.

2.8.3. Digital Droplet Polymerase Chain Reaction (ddPCR) CpG Methylation Analysis of the *Sry* Promoter

2.8.3.1. Restriction Digest of Genital Ridge DNA

To prepare the DNA for the assay, 50 ng of DNA from each genital ridge sample was digested in three separate reactions: *Nla*III only (recognition site not at CpG site; "Unlink Only") and *Nla*III + *Msp*JI ("Methylation-Dependent"), as outlined in Table 2.15. *Msp*JI is a methylation-dependent restriction enzyme that can only cut DNA if the cytosine of its recognition sequence is methylated. Refer to Table 2.16 for restriction enzyme recognition and cut sites. Note that *Msp*JI does not cut at its recognition site; instead it makes a staggered cut at nine base pairs (top strand) and 13 bases (bottom strand) away from the recognition site.

The inclusion of *Nla*III in these digestion reactions was essential to unlink the two CpG loci targeted in this experiment due to their close proximity (refer to Figure 6.10). This would allow the template for each amplicon to be randomly assorted into different droplets in the ddPCR reaction to allow for quantification. All reactions were incubated at 37°C for 18 hours, then heat inactivated at 65°C for 20 minutes. Digests were stored at -20°C until use in the ddPCR reaction (Section 2.8.3.2). Final DNA concentration following digestion was 1 ng/µL.

Table 2.15 - Restriction Enzyme Digestion Conditions

	"Unlink Only"	**"Methylation-Dependent"**
dH_2O	To volume	To volume
10x CutSmart buffer	5 µL	5 µL
***Nla*III (10 U/µL)**	0.5 µL (5 U)	0.5 µL (5 U)
***Msp*JI (5 U/µL)**	-	1 µL (5 U)
30x Enzyme Activator Solution	-	1.67 µL
DNA	50 ng	50 ng
Total Volume	**50 µL**	**50 µL**

Table 2.16 - Restriction Enzyme Recognition and Cut Sites

$MspJI = \frac{^{m}CNNR(N)_9}{GNNY(N)_{13}} = \frac{mCNNRNNNNNNNNN\|\_\_\_\_\_}{GNNYNNNNNNNNNNNNN\|}$
$NlaIII = \frac{CAGT\|}{\|GTAC}$

2.8.3.2. ddPCR Amplification of CpG Loci in the *Sry* Promoter

25 µL ddPCR reactions were made up using the Evagreen© ddPCR 2x Master Mix (Bio-Rad©). Forward and reverse primers for each amplicon were added to their relevant reactions at final concentrations: 200 nM for CpG -537 and 150 nM for CpG -300. 10 ng of digested DNA of each condition (Section 2.8.3.2.1, Table 2.15) was added to the relevant wells (or UltraPure dH_2O for NTC wells). UltraPure dH_2O was used to make up the reactions to the 25 µL volume. Each sample for each digestion condition was run in duplicate to account for possible pipetting error. Additionally, *Nla*III-digested head DNA from male A/HeJ, A/J and BALB/c embryos, a female BALB/c embryo and genital ridge DNA from female embryos of all three strains at 18 ts, were all included as controls.

The reactions were prepared in 96-well ddPCR semi-skirted plates (Bio-Rad©) that were then loaded into the Bio-Rad© QX200™ Auto Droplet Generator (AutoDG), which combined 20 µL of each reaction (equalling 8 ng of template DNA) with 70 µL of Evagreen© oil to generate droplets of approximately 1 nL volume; total approximate number of droplets generated per 20 µL of reaction mix is 20,000 droplets. These droplet reactions were transferred by the AutoDG to a fresh 96-well ddPCR plate, which was then sealed with a foil seal using the Bio-Rad© PX1 ™ PCR Plate Sealer with 180°C heat applied for 5 seconds. The plate was run on the Bio-Rad© C1000 Touch ™ Thermal Cycler with 96-Deep Well Reaction Module according to Table 2.17. Following cycling, the plate was transferred to the Bio-Rad© Droplet Reader, and the acquisition parameters in the QuantaSoft software set to ABS (absolute quantification) for direct quantification (DQ). The machine was run to collect data on the fluorescence of the droplets contained within the reaction.

Table 2.17 - *Sry* CpG ddPCR Cycling Conditions

Temperature	Duration	Cycles
95°C	10 minutes	x1
95°C	30 seconds	x40
58°C	1 minute	
4°C	5 minutes	x1
95°C	5 minutes	
4°C	Hold	
Ramp Rate: 2°C per second		

2.8.4. Bisulfite Sequencing of the Sry Promoter

Genital ridge DNA samples assessed by the Methylation-Dependent ddPCR analysis (Section 2.8.3) were also assessed by bisulfite sequencing. Approximately 500 ng of DNA from each sample was aliquotted into a 96-well plate, and the DNA was dried by incubation in a thermocycler at 65°C with the lid open until all liquid had evaporated (approximately 1.5 hours to 2 hours). The plate was

then sealed with film and mailed to the Australian Genomic Research Facility (AGRF), where the DNA was bisulfite converted and sequenced.

2.9. Statistics

For all statistical analyses in this project, the significance level was set at $p < 0.05$. Any p-values that were at or exceeded 0.05 were deemed not significant. Analyses were performed in GraphPad Prism software (Section 2.1.6.2). All averages in this project are expressed as mean ± standard deviation (SD), except where noted otherwise, such as mean ± standard error of the mean (SEM).

Comparisons between genotypes and sex ratios of mice and embryos were analysed by unpaired two-tailed t-tests with Welch's correction to not assume equal standard deviations, or Analysis of Variance (ANOVA) with multiple comparisons. Comparisons between cell culture conditions and drug conditions were tested using two-way ordinary ANOVA with multiple comparisons, to assess the impact of the various factors on the results (genotype, culture conditions, drugs), as well as compare each condition combination to all others. For each of the multiple analyses, the mean difference and standard deviation was calculated, and an adjusted p-value was produced for each pairing. For studies that involve a change over time, such as change with age (Section 5.2.2), the trend lines were the linear regressions of the appropriate data subsets, and the slope of each trend line was compared with others in its relevant set, as well as to zero.

For assessment of overall productivity of A/HeJ and A/J males, a mean litter size per male was calculated by dividing [the total number of pups born from all matings] by [the number of litters produced/fathered by a male over his reproductive lifespan]. These mean litter sizes were combined in datasets for each strain and the mean for each was calculated. This averaging was performed to compensate between stud males that fathered several litters and males that fathered few litters. Non-productive males, which fathered no litters, or litters from productive males that were unable to be counted due to cannibalism of pups, were excluded from this analysis. In order to assess the effect of paternal age on litter size, the number of pups born per litter was plotted against the age of the father in days at time of birth of the pups minus 20 days to estimate the age of the father at conception of the litter. This was performed due to the majority of litters being produced through standard matings, rather than timed matings, and as such the exact date of conception was unknown.

Graphical representations of data were generated to display mean ± standard deviation or the linear regression trend line as appropriate to the dataset in question.

2.9.1. Data Analysis of Preliminary Bisulfite Sequencing of *Sry*

The raw data obtained from the Sequenom® from Section 2.8.2 was reorganised such that technical replicates for each sample/amplicon combination were clustered together by Miss Alison Graham. The mean for each CpG site's methylation state was calculated across the three technical replicates to give a methylation state at each CpG site for each sample. These sample means were then used to calculate mean methylation at individual CpG sites between different strain/stage combinations (i.e., the mean of the biological replicates of a single CpG was calculated), and to calculate the difference in overall strand/amplicon methylation between strain/age combinations (methylation of all CpGs within each amplicon was averaged for each biological sample, then these means were averaged across biological replicates of the same stage/strain). This analysis was performed in collaboration with Miss Alison Graham in Microsoft Excel and GraphPad Prism (refer to Section 2.1.6.2).

To assess this data, two-way ANOVA analyses were performed for the forward and reverse strands of the gene and promoter, including multiple comparisons between each strain/stage/CpG site configuration. The statistical software calculated the comparison and significance for all configurations present in each amplicon.

2.9.2. Data Analysis of *Sry* CpG Methylation ddPCR

Following data acquisition in Section 2.8.3.2, the QuantaSoft software produced plots of the fluorescence amplitude of each droplet in a given reaction. Broadly, there were three bands of droplets present: CpG -537-positive droplets, with an amplitude of approximately 15000; CpG -300-positive droplets, with an amplitude of approximately 12000, and double negative droplets, with an amplitude of approximately 6000 (refer to Figure 6.10B). However, between reactions, typically varying with the digestion condition, these amplitudes changed, oftentimes occurring at greater amplitudes. However, the band with the highest amplitude was always considered to be the CpG -537 band, while the middle band was always considered to be the CpG -300 band. The band with the lowest amplitude in ddPCR analyses was always the negative droplets.

Due to the variation in droplet band amplitudes, each well was manually thresholded in the QuantaSoft AP software, with thresholding performed on the group of reactions assessing a single biological sample (i.e. all six wells assessing the DNA of a single embryo's genital ridges were assessed as a batch). Where possible, when wells in the same sample group had a similar amplitude range, thresholds were set to the same level in multiple wells. In certain wells, there was a significant amount of 'rain' between the respective bands. In these cases, all attempts were made to approximate an appropriate division between bands for thresholding, and this approximation was consistently maintained as much as possible between samples.

Manual thresholding was performed to assess the amount of amplification of both CpG sites' amplicons ('Both CpGs'), followed by manual thresholding to assess the amount of amplification of CpG -537 only (top band). The CpG -300 value was calculated by subtracting the CpG -537 value from the Both CpGs value. All values were recorded as "Copies/µL", as this assessment was easily comparable between reactions, by accounting for reactions with fewer droplets formed by the Auto DG.

As each sample/digest condition was run in the ddPCR analysis in duplicate, duplicate wells were averaged to give a value for the Unlink Only (*Nla*III-only) and Methylation-Dependent (*Nla*III + *Msp*JI) reactions, respectively. Using these means, the percentage change from the Unlink Only digest for the Methylation-Dependent digests were calculated for each sample. The percentage change for each digest condition was transferred into GraphPad Prism (Section 2.1.6.2), and was graphed by stage (embryonic day). A two-way ANOVA, including multiple comparisons, was also performed on the data entered by stage groupings using the GraphPad Prism software, to compare the methylation of genital ridges of the three strains at the different stages of development.

2.9.3. Data Analysis of Bisulfite Sequencing of *Sry* Promoter

The results of the bisulfite sequencing by AGRF (Section 2.8.4) were reported as a value between 0.0 (0% methylation) and 1.0 (100% methylation) for each CpG site within the promoter. These values were entered into GraphPad Prism, plotted according to stage, and analysed by a two-way ANOVA with multiple comparisons. The values reported were differences between strain/stage combinations, although values were also calculated as strain/stage/CpG site comparisons. The statistical software calculated the comparisons and the significance for all comparisons.

Chapter 3: Characterisation of the *Ddx3y*^{mKate2} and *Hprt*$^{DsRed\text{-}Express}$ Reporter Mouse Strains

3.1. Introduction

The *Ddx3y*^{mKate2} reporter Y chromosome, and the mouse strain carrying it, were created to be used as tools for chromosome instability research. This chapter details the finalisation of this mouse strain's characterisation, so as to inform on the features of this reporter Y chromosome that are pertinent to its utility in such research. Additionally, another fluorescent reporter mouse strain, carrying the *Hprt*$^{DsRed\text{-}Express}$ X chromosome, was characterised in order to provide a comparison for the *Ddx3y*^{mKate2} model to highlight the reporter Y chromosome's strengths and weaknesses.

The *Ddx3y*^{mKate2} mouse strain has previously[5] been assessed in this laboratory to determine when in the mouse's development the signal from the fluorescent reporter protein, mKate2, was detectable, as well as differences between adult tissues. This previous work[5] found that the onset of fluorescence occurred during preimplantation embryonic development[5], and that this fluorescence persisted through to sexual maturity in the male mouse in a tissue-dependent manner[5] (refer to Section 3.1.1.2).

In order to extend upon the previous characterisation[5] of the *Ddx3y*^{mKate2} mouse, this study assessed the changes in the fluorescent reporter signal in adult tissues several hours post-mortem, and in adult tissues from a mouse of advanced age. The mKate2 signal in different cell and tissue types was also examined by immunohistochemistry (IHC) performed on sections of late embryonic tissue. These experiments were performed in order to finalise characterisation of the *Ddx3y*^{mKate2} fluorescent reporter Y chromosome on a chromosomally stable background.

Additionally, the *Hprt*$^{DsRed\text{-}Express}$ reporter X chromosome (refer to Section 3.1.2) mouse strain was also characterised in this study. This reporter X chromosome was selected for characterisation as there are many similarities between it and the *Ddx3y*^{mKate2} reporter Y chromosome. By characterising the *Hprt*$^{DsRed\text{-}Express}$ mouse strain, it was possible to tailor the characterisation of this model such that it closely paralleled the characterisation performed for the *Ddx3y*^{mKate2} strain. This enabled effective comparison of these two fluorescent reporter mouse strains (Section 3.3.2).

Overall, the aims of this chapter were to complete the characterisation of the *Ddx3y*^{mKate2} mouse strain on a stable background, and to characterise the *Hprt*$^{DsRed\text{-}Express}$ mouse strain in order

to compare and contrast the two fluorescent reporter mouse strains.

3.1.1. *Ddx3y*^{mKate2} Reporter Background

3.1.1.1. Creation of the *Ddx3y*^{mKate2} Reporter Y Chromosome and the *Ddx3y*^{mKate2} Mouse Strain

The *Ddx3y*^{mKate2} reporter Y chromosome was created by Drs Paul Kalitsis and Jeff Mann (Murdoch Children's Research Institute, MCRI), by targeted insertion of a gene cassette adjacent to the *Ddx3y* locus on the short arm of the mouse Y chromosome in 129S1/SvImJ (refer to Section 2.2.1) embryonic stem (ES) cells. The transgene cassette contained a neomycin resistance gene (*Neo*^{R}) under the control of the phosphoglycerate kinase (PGK) promoter, and a far-red fluorescent protein gene, *mKate2*, under the control of the strong synthetic cytomegalovirus chicken beta actin (CMV-CAG) promoter[174] (Figure 3.1). The neomycin resistance gene was included in the gene cassette to be used for selection of successfully targeted ES cells.

Figure 3.1 outlines the targeting strategy; briefly, the gene cassette was flanked by homology arms containing sequence homologous to exons 8 to 12 and 13 to 17 of the *Ddx3y* gene to allow specific targeting of this locus. This targeting construct was introduced into the ES cells by electroporation, and via homologous recombination, the transgene cassette was inserted into the Y chromosome such that the coding sequence of the *Ddx3y* gene was not interrupted. This was essential, as *Ddx3y* is not only needed for male sexual function, playing a role in early gonocyte development[85,86] in gestation, but is also essential for early division in the male embryo[87].

The *Ddx3y* gene codes for an ATP-dependent DEAD (Asparganine-Glutamine-Alanine-Asparganine)-box RNA helicase (Y chromosome-linked) that plays a role in RNA metabolism. This locus was selected for targeted insertion of the transgene cassette as the gene shows broad expression across many different tissues in both embryonic and adult mice (Figure 3.2). This makes *Ddx3y* unique amongst other genes on the mouse Y chromosome, which have their expression restricted to the male reproductive system. The broad expression of *Ddx3y* throughout the mouse indicated that this region of the Y chromosome was unlikely to be repressed across different tissues. This was advantageous for insertion of a reporter gene, as the permissive chromatin environment of the target locus indicated a low risk of repression of the reporter gene.

Successfully targeted ES cells were screened for using neomycin selection, the presence of mKate2 fluorescence, gel electrophoresis and Southern blot hybridisation. These ES cells were then injected into recipient 129S1/SvImJ blastocysts according to standard methods[68] to create chimeric embryos. These chimeras were then implanted into pseudo-pregnant females, and the resulting male offspring were mated to 129S1/SvImJ females for germline transmission.

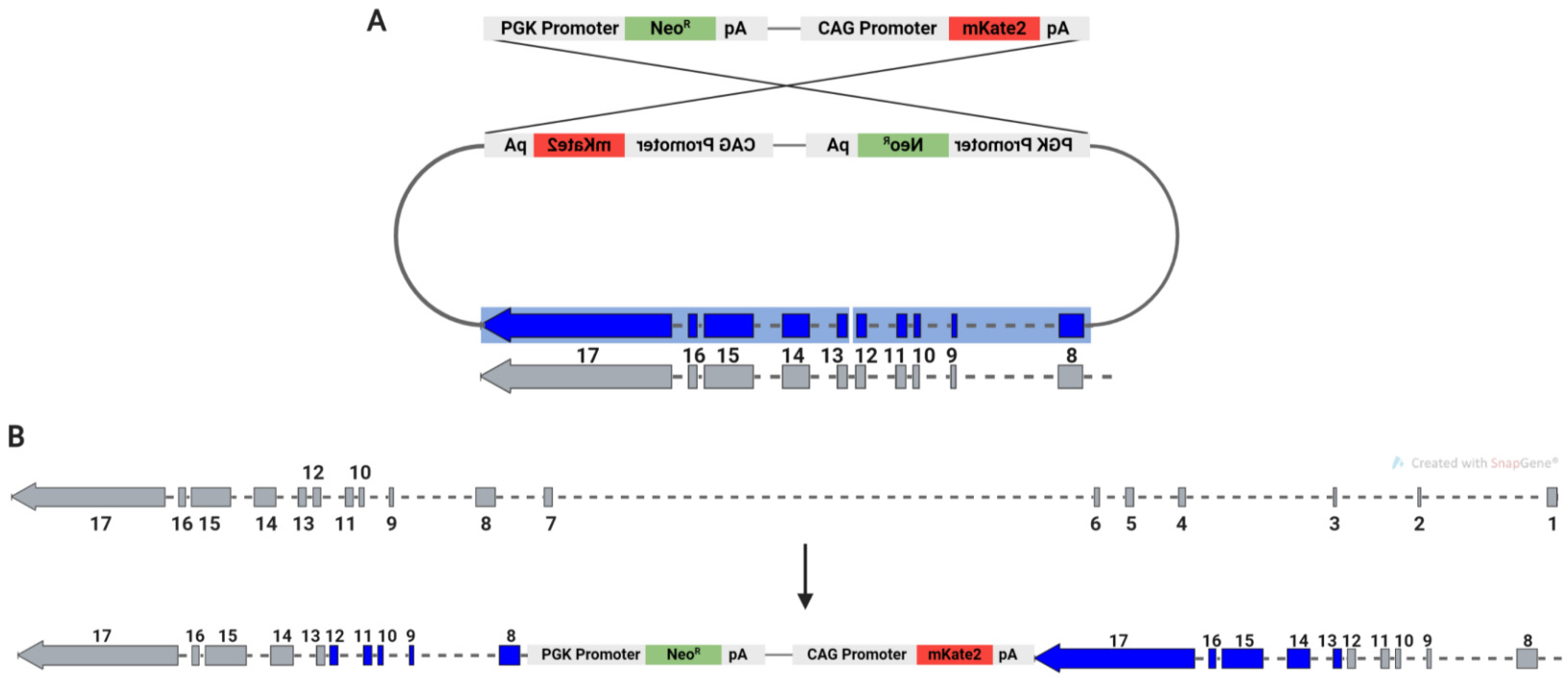

Figure 3.1 – Creation of the *Ddx3y*^{mKate2} Y Chromosome

Schematic of the gene targeting strategy to insert the mKate2 reporter gene cassette into the mouse Y chromosome to generate the *Ddx3y*^{mKate2} mouse strain. Briefly, a gene cassette was synthesised containing a neomycin resistance gene (*Neo*^{R}) under a phosphoglycerate kinase (PGK) promoter, and a gene for a red fluorescent protein called mKate2 under the control of a cytomegalovirus chicken β-actin (CMV-CAG) promoter. This targeting construct's arms contained regions of homology to exons 8 to 17 of the *Ddx3y* gene. The targeting construct was assembled using standard recombinant DNA technology, and was linearised between exons 12 and 13. This construct was electroporated into mouse embryonic stem (ES) cells, and the targeting arms' complementarity facilitated insertion of the gene cassette adjacent to the *Ddx3y* gene locus via homologous recombination. This targeting strategy was designed to leave the *Ddx3y* gene locus intact. Successfully targeted ES cells were selected for using neomycin and Southern blot hybridisation, before then being injected into recipient blastocysts to generate chimeric embryos, which were transferred into pseudopregnant female mice to gestate to term, yielding male mice carrying the *Ddx3y*^{mKate2} reporter Y chromosome.

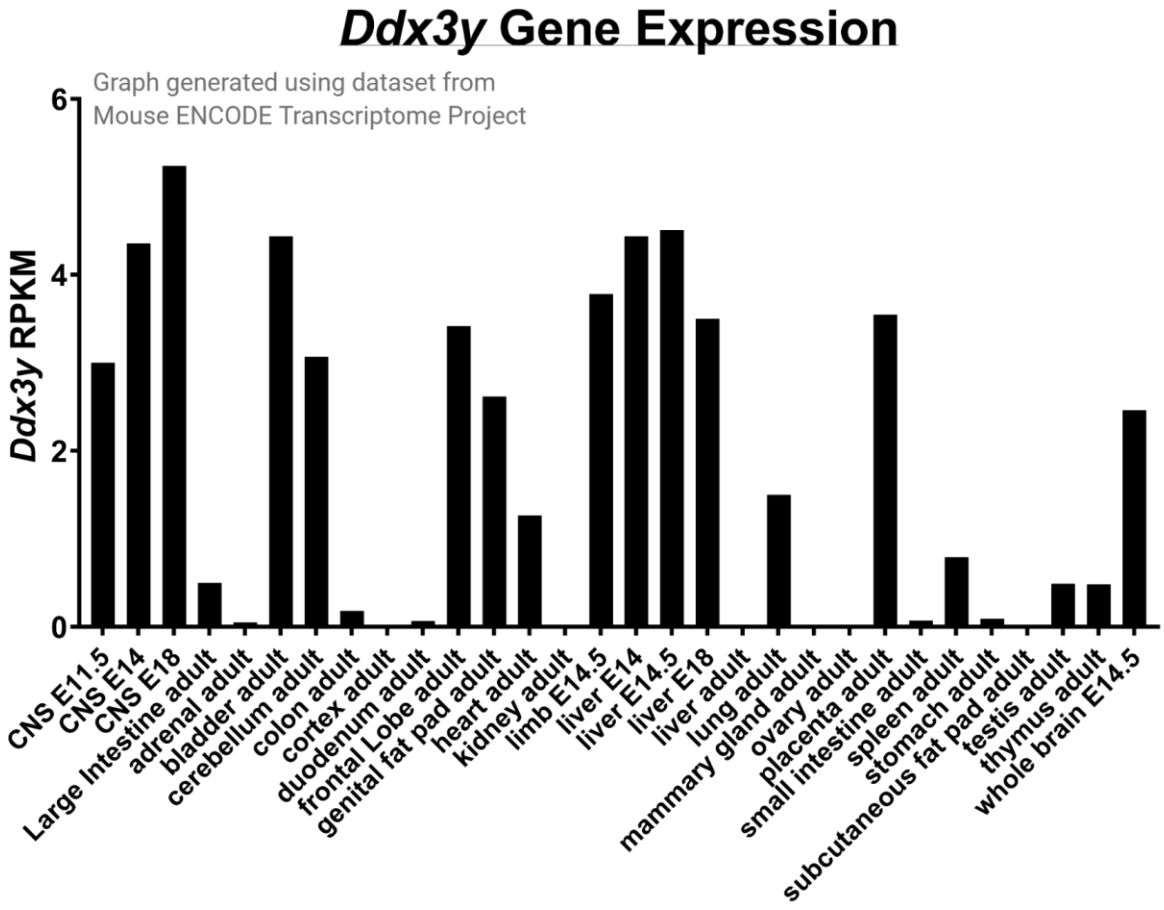

Figure 3.2 – Tissue Expression of the *Ddx3y* Gene in Mouse

Plot of *Ddx3y* gene expression data from the RNA Profiling Datasets generated by the Mouse ENCODE Project[3]. This gene is broadly expressed in many of the tissue types assessed, including the central nervous system and embryonic structures.

Germline-competent transgenic *Ddx3y*^{mKate2} males were used for breeding to establish the *Ddx3y*^{mKate2} mouse strain on the 129S1/SvImJ background at MCRI. In the *Ddx3y*^{mKate2} reporter strain, all males were carriers of this reporter Y chromosome, and passed it on to all their male offspring.

3.1.1.2. Previous Characterisation of mKate2 Reporter Signal in the *Ddx3y*^{mKate2} Mouse

Previous work[5] in this laboratory had been performed in order to characterise the mKate2 fluorescence observable in the *Ddx3y*^{mKate2} mouse strain. This work[5] examined the onset of mKate2 fluorescence in *Ddx3y*^{mKate2} male embryos[5], and how the fluorescence presented in male tissues at sexual maturity[5]. The key findings of this previous characterisation are outlined in Figure 3.3.

By examining preimplantation *Ddx3y*^{mKate2} embryos from the two-cell stage through to the late blastocyst stage prior to implantation, it was found that the mKate2 fluorescence was detectable by fluorescence microscopy from the beginning of cavitation of a compacted morula into a blastocyst (occurring at approximately E3.25[203], Figure 3.3A). This fluorescence occurred across all lineages in the preimplantation embryo (trophectoderm and ICM[68], Section 1.1.4), as seen in the blastocyst image[5] (Figure 3.3A). Preimplantation *Ddx3y*^{mKate2} embryos from the cavitation stage through to the end of preimplantation development (fully expanded blastocysts) were observed to maintain this mKate2 fluorescence across all cells of the embryo[5].

Ddx3y^{mKate2} midgestation embryos were also examined at E9.5 (Figure 3.3B), to determine the degree of mKate2 fluorescence present in the male embryos at this stage. This revealed that the broad fluorescence across lineages observed in the blastocyst was still observable in midgestation embryos[5], with male embryos exhibiting mKate2 fluorescence across the entire body[5]. Figure 3.3B shows a male *Ddx3y*^{mKate2} E9.5 embryo alongside a female littermate embryo, illustrating that it is only the males that are fluorescent, with no autofluorescence present in the female's tissues[5]. While there appeared to be some variation in mKate2 fluorescence intensity across different regions of the male embryo, it was likely due to differences in tissue density[5].

The *Ddx3y*^{mKate2} male mouse was also examined for mKate2 fluorescence at six weeks of age[5], the age of sexual maturity in most strains of laboratory mouse[68,204]. In order to perform this examination, several of the major organs were removed from the mouse and examined for mKate2 fluorescence by fluorescence stereomicroscopy[5] (Figure 3.3D). Briefly, the heart exhibited the greatest fluorescence intensity, followed closely by the testis, liver and eye, all of which were highly fluorescent[5]. In the case of the eye, fluorescence was observed in the pupil and at the perimeter of the iris, as well as along the optic nerve[5]. The brain, kidney and lungs each exhibited a moderate to low level of mKate2 fluorescence, and the spleen was non-fluorescent[5]. However, the fat attached to the spleen was moderately fluorescent[5].

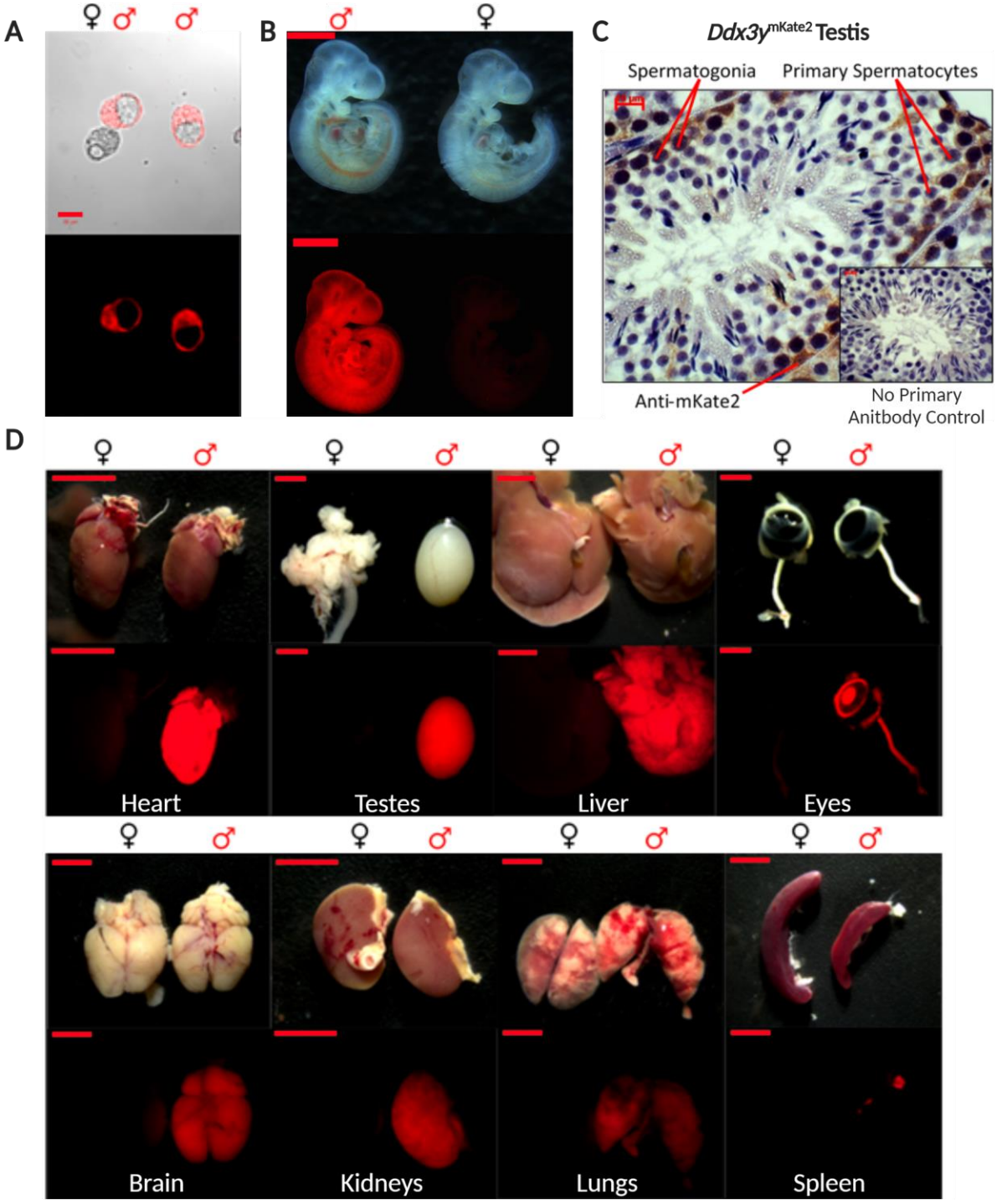
A
B
C
Ddx3y^mKate2 Testis
Spermatogonia
Primary Spermatocytes
Anti-mKate2
No Primary
Anitbody Control
D
Heart
Testes
Liver
Eyes
Brain
Kidneys
Lungs
Spleen

Figure 3.3 – Preliminary Characterisation of mKate2 Signal in the *Ddx3y*^{mKate2} Mouse

Previous examination of mKate2 fluorescence in the *Ddx3y*^{mKate2} mouse across the lifespan[5]. (A) mKate2 fluorescence in *Ddx3y*^{mKate2} preimplantation embryos activated at the blastocyst stage, from approximately E3.25 onwards. Non-fluorescent embryo (left) is a female littermate. (B) mKate2 fluorescence persisted at midgestation in *Ddx3y*^{mKate2} embryos. This image has a fluorescent male (left) and a non-fluorescent female (right) E9.5 embryo. (C) Shut down of mKate2 expression throughout the spermatogenic process. 6 µm testis sections from *Ddx3y*^{mKate2} (main image) and wild type (inset image) males were stained for mKate2 signal using the DAB IHC system; brown precipitate indicates mKate2. This signal occurs in cells lining the perimeter of the seminiferous tubules: spermatogonia and pre-pachytene primary spermatocytes. Purple counterstain was haematoxylin. (D) Whole organ images of mKate2 fluorescence from a six-week-old *Ddx3y*^{mKate2} male and an age-matched non-fluorescent female. The organs decreased in fluorescence intensity from the heart (brightest, saturated fluorescence) and testis and liver (next brightest) to the eye (strong fluorescence of certain regions), brain and kidney (moderate fluorescence). The lungs had low mKate2 fluorescence, and the spleen was completely non-fluorescent, with the exception of the fluorescent fat attached to the spleen. Scale bars are 50 µm (A), 1 mm (B), 10 µm (C), 5 mm (D: heart, gonad, liver, brain, kidney, lungs, spleen) and 2 mm (D: eye).

Additionally, testis sections from a *Ddx3y*^{mKate2} mouse and a wild type mouse (Figure 3.3C) were stained for mKate2 signal using immunohistochemistry (IHC)[5]. This was performed because the sex chromosomes are known to become inactivated through meiotic sex chromosome inactivation (MSCI) during the first meiotic division of spermatogenesis (refer to Section 1.1.5.2.1). The seminiferous tubules of the *Ddx3y*^{mKate2} testis were examined to determine whether there was cessation of mKate2 signal (brown precipitate in Figure 3.3C) in spermatogenic cells following the onset of MSCI. Staining for mKate2 was present in the cells lining the perimeter of the seminiferous tubules[5]: the spermatogonia and the early primary spermatocytes. As cells progressed through spermatogenesis towards the lumen of the tubule, they became negative for mKate2 signal, correlating with the maintenance of MSCI in which the Y (and X) chromosome is transcriptionally silenced. The absence of mKate2 signal persisted throughout the subsequent spermatogenic cells[5], as would be expected due to the maintenance of Y chromosome inactivation in these cells.

3.1.2. Creation of the *Hprt*$^{DsRed\text{-}Express}$ Reporter X Chromosome

The *Hprt*$^{DsRed\text{-}Express}$ reporter X chromosome mouse model was another fluorescent reporter transgenic mouse strain that bore many similarities to the *Ddx3y*^{mKate2} strain. For this reason, the characterisation of the *Hprt*$^{DsRed\text{-}Express}$ mouse strain has been included in this study in order to provide a comparison to the *Ddx3y*^{mKate2} model to highlight its strengths and limitations.

The *Hprt*$^{DsRed\text{-}Express}$ reporter X chromosome was created by Dr Jeff Mann (MCRI), and employed an orange/red fluorescent protein reporter (DsRed-Express) inserted into a sex chromosome; in this case, the X chromosome. This reporter X chromosome was created by targeted insertion of a transgene cassette into the *Hprt* locus on the mouse X chromosome, employing the same strategy as outlined in Tang et al (2002)[179], with two major changes. First, the *DsRed-Express* coding sequence (under the control of the CAG promoter) replaced the *Cre* coding sequence; and second, the neomycin resistance gene (*Neo*^{R}, under the control of the PGK promoter) was flanked by *loxP* sites.

As a brief overview, the gene cassette described above, including the fluorescent protein gene *DsRed-Express* (also known as DsRedT1[178], Clontech Inc.), was flanked by homology arms to exons 2 and 3 of the *Hprt* gene. The resulting targeting vector was introduced into 129S1/SvImJ ES cells by electroporation, and the transgene cassette was inserted into the X chromosome via homologous recombination. Successful recombinants were screened for using neomycin selection and Southern blot hybridisation. These recombinant ES cells were injected into recipient 129S1/SvImJ blastocysts according to standard methods[68] to create chimeric embryos.

These chimeras were then implanted into pseudo-pregnant females, and resulting male offspring were mated to 129S1/SvImJ females for germline transmission. Offspring crosses which carried the knock-in allele were mated with *Cre*-deleter[179] mice. This breeding facilitated removal of

the *Neo*^{R} gene to generate the final knock-in line, termed *Hprt*$^{DsRed\text{-}Express}$. Like *Ddx3y*^{mKate2}, the *Hprt*$^{DsRed\text{-}Express}$ mouse line was maintained on a 129S1/SvImJ background at MCRI.

The *Hprt* gene on the X chromosome encodes the Hypoxanthine-guanine phosphoribosyltransferase enzyme, which plays a key role in purine nucleotide generation through the purine salvage pathway[205,206]. This gene is considered a housekeeping gene, as it is constitutively active[207], as indicated in the tissue expression data in Figure 3.4. This expression profile indicated a lack of repression at this locus, suggesting a low likelihood of repression of the gene cassette inserted into the X chromosome in this region. Indeed, the *Hprt* locus has been shown to be a permissive region for the insertion of transgenes[208-210].

The X chromosome is unique target for creation of a reporter chromosome, as it is able to exist in a homologous pair in females (XX), similar to autosomes, but is present in a single copy (hemizygous) in males (XY). This results in different gene expression patterns for a given X chromosome-linked gene between male and female carriers, as X chromosome gene dosage must be balanced between the two sexes. This is achieved through silencing of additional X chromosome/s within a cell such that only a single X chromosome is active. This process is known as X chromosome inactivation (XCI, refer to Section 1.1.2.1), and, in somatic tissues, randomly affects any given X chromosome in a cell. This is essential to ensure that females (XX) and males (XY) both only have a single active X chromosome per cell, to ensure that the dose of active metabolic X chromosome-linked genes is the same in both sexes[211].

The process of XCI in XX females is an important factor for consideration of using the X chromosome to develop a transgenic reporter chromosome. In females, homozygous carriers of a transgenic X chromosome would show ubiquitous expression of the transgene, subject to its tissue expression profile. Heterozygotes, however, would exhibit a variable expression of the reporter transgene across tissues it is expressed in, with approximately 50% of cells within a given tissue expressing from the reporter X chromosome, while the remaining 50% of cells would have transcriptionally inactivated the reporter X chromosome through XCI. In males, as the X chromosome is present in only a single copy, it would not be transcriptionally inactivated in any cells. This would result in ubiquitous expression of the reporter in cell types which actively express the transgene. In this way, transgene expression in males would align with the expression that would be observed in a homozygous female.

This chapter will describe further characterisation of the *Ddx3y*^{mKate2} mouse model, including age-related changes to mKate2 fluorescence in a one-year-old *Ddx3y*^{mKate2} mouse, followed by characterisation of the *Hprt*$^{DsRed\text{-}Express}$ mouse model from preimplantation development through to sexual maturity. These two transgenic mouse strains and the characteristics of their reporter fluorescence will be compared to highlight the strengths and limitations of each.

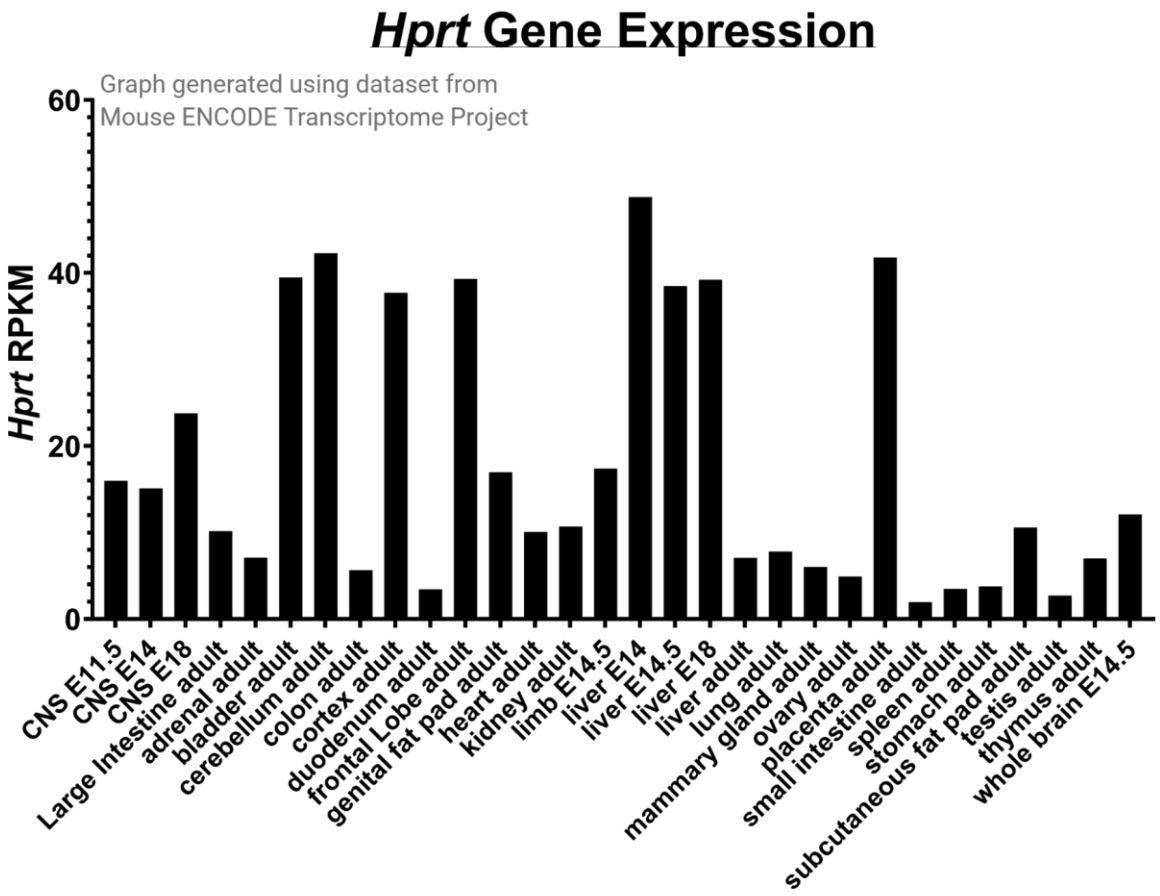

Figure 3.4 – Tissue Expression of the *Hprt* Gene in Mouse

Plot of *Hprt* gene expression data from the RNA Profiling Datasets generated by the Mouse ENCODE Project[3]. This gene has been observed to exhibit expression of varying levels in all tissue types assessed, with high expression in the embryonic liver, adult bladder, central nervous system and placenta.

3.2. Results

3.2.1. Characterisation of mKate2 Signal in the *Ddx3y*^{mKate2} Mouse across the Lifespan

Characterisation of the *Ddx3y*^{mKate2} mouse performed prior[5] to this project focused on examining mKate2 signal from preimplantation embryonic development, through midgestation, to males at sexual maturity (Figure 3.3). In order to finalise characterisation of this model, examination of tissues from embryos later in gestation (Section 3.2.1.1), as well as in organs collected in advanced age (Section 3.2.1.3), was performed. Additionally, the persistence of the mKate2 fluorescent reporter in adult organs many hours post-mortem was examined (Section 3.2.1.2). For each assessment of whole, unfixed tissues, fluorescence was qualitatively classified as high intensity (strong red fluorescent signal), low intensity (weak red fluorescent signal) and medium intensity (intermediate red fluorescent signal between high and low intensity), by comparing different tissues' images from fluorescence stereomicroscopy imaging. This was due to difficulties in standardising between different tissue types, and was to serve as an indication of potential advantageous tissues for future research.

3.2.1.1. Tissue-Specific Variation in mKate2 Within Embryonic Structures

Previous assessment of *Ddx3y*^{mKate2} midgestation embryos and adult organs was performed by examination of mKate2 fluorescence by microscopy at either the whole embryo or whole organ level[5] (Figure 3.3). However, this broad examination did not reflect the potential for variation in reporter signal within a single structure, as organs and embryos are composed of a variety of cells which may regulate the mKate2 transgene differently.

In order to assess mKate2 signal in different tissues within a structure, the head, forelimbs, heart and testis of an E17.5 *Ddx3y*^{mKate2} male embryo were collected, fixed and sectioned. These tissue sections were then subjected to anti-mKate2 immunohistochemistry (IHC, Figure 3.5). This process allowed for detection of the mKate2 protein (brown precipitate[212]) in different cell types within each structure examined.

The forelimbs and head of the embryo exhibited the greatest tissue variation of the structures assessed, as expected, due to the variety of cells that comprise these structures. The forelimbs (Figure 3.5C) contained bone in the limb and paw, and these regions showed low to no mKate2 signal. Conversely, the musculature of the limb and paw surrounding the bone showed relatively high levels of anti-mKate2 staining. In the embryonic head (Figure 3.5A), the brain and eye, as well as musculature in the neck and jaw regions, exhibited high levels of mKate2 signal. The tissues towards the nasal region of the embryo, however, showed less signal, again highlighting variation within a single structure.

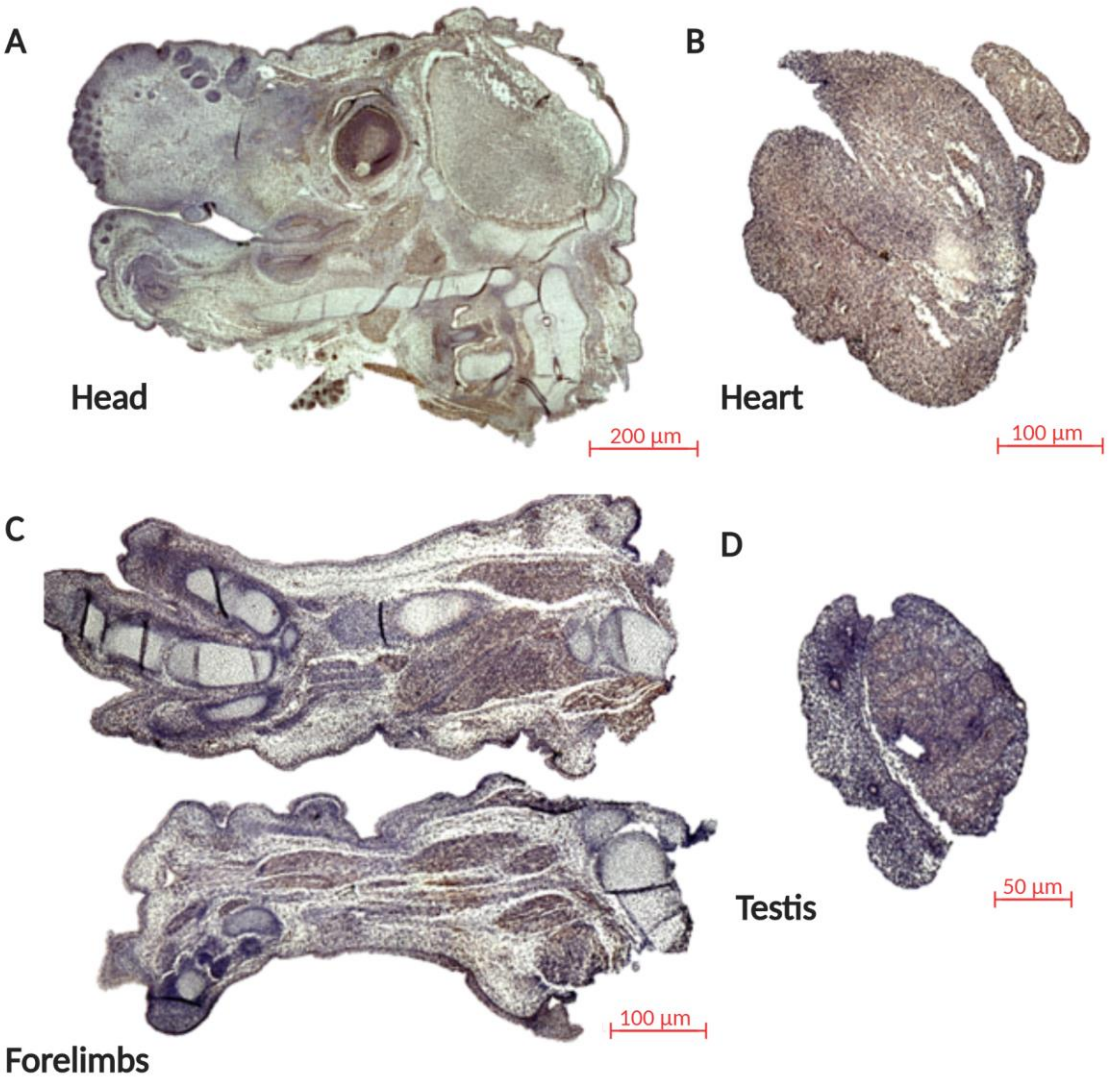

Figure 3.5 – Immunohistochemistry staining for mKate2 in *Ddx3y*^{mKate2} Embryo Tissues

DAB immunohistochemistry (IHC) staining of mKate2 in *Ddx3y*^{mKate2} E17.5 embryo tissues. 6 µm sections of the head (A), heart (B), forelimbs (C) and testis (D) were stained for mKate2 signal by IHC, visualised by brown precipitate[201]. Purple counterstain was haematoxylin. The intensity of mKate2 signal varied in intensity between each of the structures examined, and between different tissues within a section (except for the heart). (A) The brain, eye and muscles of the head stained most strongly for mKate2. (B) Anti-mKate2 staining occurred intensely and consistently across the entire heart. (C) The muscle groups within the forelimbs stained most intensely of this tissue, while the rest of the limbs have moderate staining, except for the interior of the bones, which were mKate2-negative. (D) The testis had strong mKate2 staining across the tissue. However, the strongest of this staining occurred within the testis cords.
Images are composites of multiple images per tissue (except testis) as sections were too large to image in a single view. Scale bars are 50 µM (D, testis), 100 µm (C, forelimbs; B, heart) and 200 µm (A, head).

The heart and testis, in comparison to the above, exhibited less variation between regions of the structures, as these organs are comprised of fewer cell types compared to the forelimbs and head. The E17.5 testis (Figure 3.5D) returned a consistent pattern of anti-mKate2 staining across the organ, with the cells within the testis cords (germ cells, Sertoli cells and peritubular myoid cells[119]) yielding high mKate2 signal. In contrast, the cells in the interstitium, including the androgenic Leydig cells[119], did not stain strongly for mKate2 signal.

The presence of high mKate2 signal in the testis cords of the E17.5 testis, which will give rise to the seminiferous tubules, was contrary to what was observed in the sectioning and staining of the adult *Ddx3y*^{mKate2} testis (Figure 3.5D). The adult testis section contained a seminiferous tubule, which only had anti-mKate2 staining around its perimeter of the tubule, as the *Ddx3y*^{mKate2} Y chromosome was inactivated as the spermatogenic cells progressed through meiosis. The contrast between the adult testis section and the results seen in the E17.5 testis were the result of differences in the composition of this organ at these two time points. In the adult testis, the germ cells have differentiated into the stem cells, spermatogonia, which feed into the spermatogenesis process. Meanwhile, in the E17.5 testis, the germ cells have yet to differentiate into spermatogonia[68,119], as the type A spermatogonia appear three to seven days after birth[68]. As a result, all of the meiotic daughter cells which would have inactivated the reporter Y chromosome do not exist, only the stem cell population (at this stage, prospermatogonia) which was shown to be mKate2-positive in the adult testis.

In the heart (Figure 3.5B), all cells in this organ uniformly expressed a high level of mKate2 across the entire organ. This uniformity would be expected from the known structure of the heart, being an organ composed nearly entirely of a single cell type (cardiomyocytes), with this cell type comprising the majority of the mass of the heart[213]. The remaining mass of the heart predominantly consists of endothelial cells[213]. As cardiomyocytes are a type of muscle cell, the staining of this tissue in the heart, in addition to the musculature of the head and forelimbs, suggests that muscle cells in *Ddx3y*^{mKate2} mice tend to express the fluorescent reporter at high levels. This would also account for the high mKate2 fluorescence observed in the six-week-old heart (Figure 3.3D).

This sectioning and staining of tissues from a late-gestation *Ddx3y*^{mKate2} embryo demonstrated that mKate2 signal can vary between cell types within a structure which appears to be uniformly fluorescent at the whole organ level. These findings highlight the need for precise selection of cell type to be used in experiments with the *Ddx3y*^{mKate2} mouse model, to ensure that the target population are indeed mKate2-positive.

3.2.1.2. mKate2 Fluorescence of Adult *Ddx3y*^{mKate2} Organs Persists at a Low Level for Several Hours Post-Mortem in a Tissue-Dependent Manner

The previous examination of adult *Ddx3y*^{mKate2} organ fluorescence (refer to Figure 3.3D) was

performed immediately following euthanasia and tissue collection. However, when performing tissue collection experiments with a large number of animals, there can be significant time delays between euthanasia/tissue collection, and downstream assessment of the tissue. This can be a particularly pertinent factor to consider in experiments involving fluorescent reporter animals such as the *Ddx3y*^{mKate2} mouse, as the fluorescence intensity may decline as the fluorescent protein degrades within cells and is not replaced by newly expressed protein. In order to assess the *Ddx3y*^{mKate2} model's utility, it was prudent to assess the persistence of mKate2 fluorescence post-mortem in *Ddx3y*^{mKate2} tissues to better inform on future experimental designs. Due to the reported stability of the mKate2 protein[214], combined with strong fluorescence observed in the freshly collected tissues, it was hypothesised that the organ fluorescence would show persistence for hours post-mortem. To examine this, it was decided that assessment of fluorescence persistence in whole *Ddx3y*^{mKate2} organs was to be conducted between five and 10 hours after euthanasia.

Five *Ddx3y*^{mKate2} males between 53 and 125 days of age were culled, and their organs were collected and imaged during the following intervals: 5.5 to 6 hours, 6 to 6.75 hours, 6.75 to 7.25 hours, 8 to 8.5 hours and 8.5 to 9 hours post-mortem. Following both euthanasia, the mouse carcasses were stored in chilled conditions (at 4°C), and following collection, organs were stored on ice in PBS when not being imaged. Chilled conditions were employed to slow degradation of the mKate2 protein in the tissues post-mortem. These intervals represent the time taken to image all eight organs from each individual mouse.

Table 3.1 - Relative mKate2 Fluorescence Intensity in *Ddx3y*^{mKate2} Organs Several Hours Post-Mortem

	Heart	**Testis**	**Liver**	**Eyes**	**Kidneys**	**Brain**	**Lungs**	**Spleen**
5.5 - 6 Hours Post-Mortem	Moderate	Low	Very Low	Absent	Absent	Very Low	Absent	Absent
	Change from 5.5-6 Hours Post-Mortem							
6 - 6.75 Hours Post-Mortem	None							
6.75 - 7.25 Hours Post-Mortem	None							
8 - 8.5 Hours Post-Mortem	None							
8.5 - 9 Hours Post-Mortem	None							

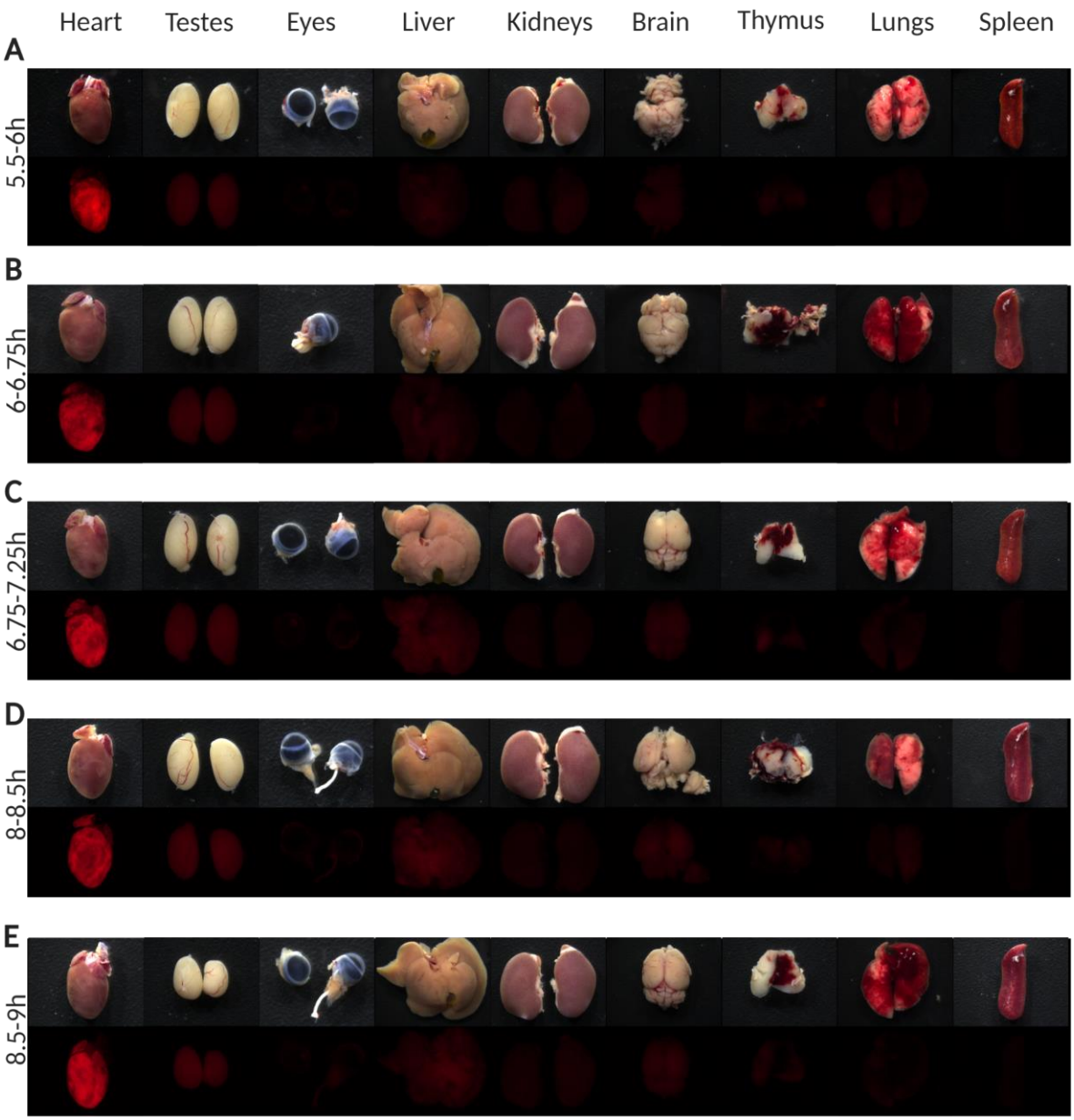

Figure 3. 6 – Fluorescence of *Ddx3y*^{mKate2} Organs Collected Many Hours Post-Mortem

Fluorescence and bright-field images of whole organs from adult *Ddx3y*^{mKate2} males imaged at (A) 5.5 to 6 hours, (B) 6 to 6.75 hours, (C) 6.75 to 7.25 hours, (D) 8 to 8.5 hours and (E) 8.5 to 9 hours post-mortem. Fluorescence of all organs declined relative to freshly-imaged six-week-old organs (Figure 3.3D). The heart retained the greatest florescence intensity, and the testis and liver retained a very low level of fluorescence. All other organs have no detectable licence. There was no discernible difference between the fluorescence intensity of a given organ between each of the time points.

The fluorescence intensities of organs imaged at each time point can be seen in Figure 3.6. As would be expected, the longer the time between death and imaging, the more fluorescence intensity declined, as the cells are no longer producing new mKate2 protein and existing protein begins to be degraded. Table 3.1 outlines the comparison of organ fluorescence between individuals/over time. Briefly, between 5.5 to 6 hours post-mortem (Figure 3.6A), the mKate2 fluorescence was clearly still detectable in the heart, but was starkly reduced in intensity relative to freshly collected organs. Fluorescence was faintly detectable in the testis, liver and brain. This pattern was sustained in the organs imaged between each of the listed intervals. This indicates that there is the same pattern of fluorescence intensity reduction for each organ at these time points, with no further substantial decline between 5.5 and 9 hours post-mortem.

These results indicate that the mKate2 signal experiences sharp decline in intensity by five hours post-mortem, with all other organs except the heart exhibiting either very low fluorescence or were non-fluorescent. It is likely that the persistence of mKate2 fluorescence in the heart was due to the high intensity of fluorescence observed in the heart when immediately imaged (Figure 3.3D). While the heart remained moderately fluorescent through to nine hours post-mortem, for all organs and tissues, it would be highly recommended to either use fresh *Ddx3y*^{mKate2} tissue shortly after collection, or to promptly fix the tissue in some way if the mKate2 signal requires preservation for an extended period of time.

3.2.1.3. mKate2 Fluorescence Declines with Advanced Age in the *Ddx3y*^{mKate2} Male

In the *Ddx3y*^{mKate2} mouse, mKate2 fluorescence was present in a tissue-dependent manner out to sexual maturity, approximately six weeks of age (Figure 3.3D). As Y chromosome-linked genes can change in expression with increased age in humans as a result of increased methylation (repression) on the Y chromosome[215], organs from a one-year-old *Ddx3y*^{mKate2} male were collected and imaged for mKate2 fluorescence. This was performed to conclude the characterisation of mKate2 fluorescence in the *Ddx3y*^{mKate2} mouse strain.

The brain, eyes, heart, lungs, kidneys, spleen, liver and testes were harvested from a 52-week-(one year)-old *Ddx3y*^{mKate2} male, and imaged for mKate2 fluorescence (Figure 3.7). The differences in mKate2 fluorescence intensity between the organs generally followed the same pattern as observed in the six-week-old male (refer to Figure 3.3D), albeit with drastically reduced overall mKate2 fluorescence. Table 3.2 compares the relative fluorescence intensities between organs from the six-week-old and one-year-old *Ddx3y*^{mKate2} males.

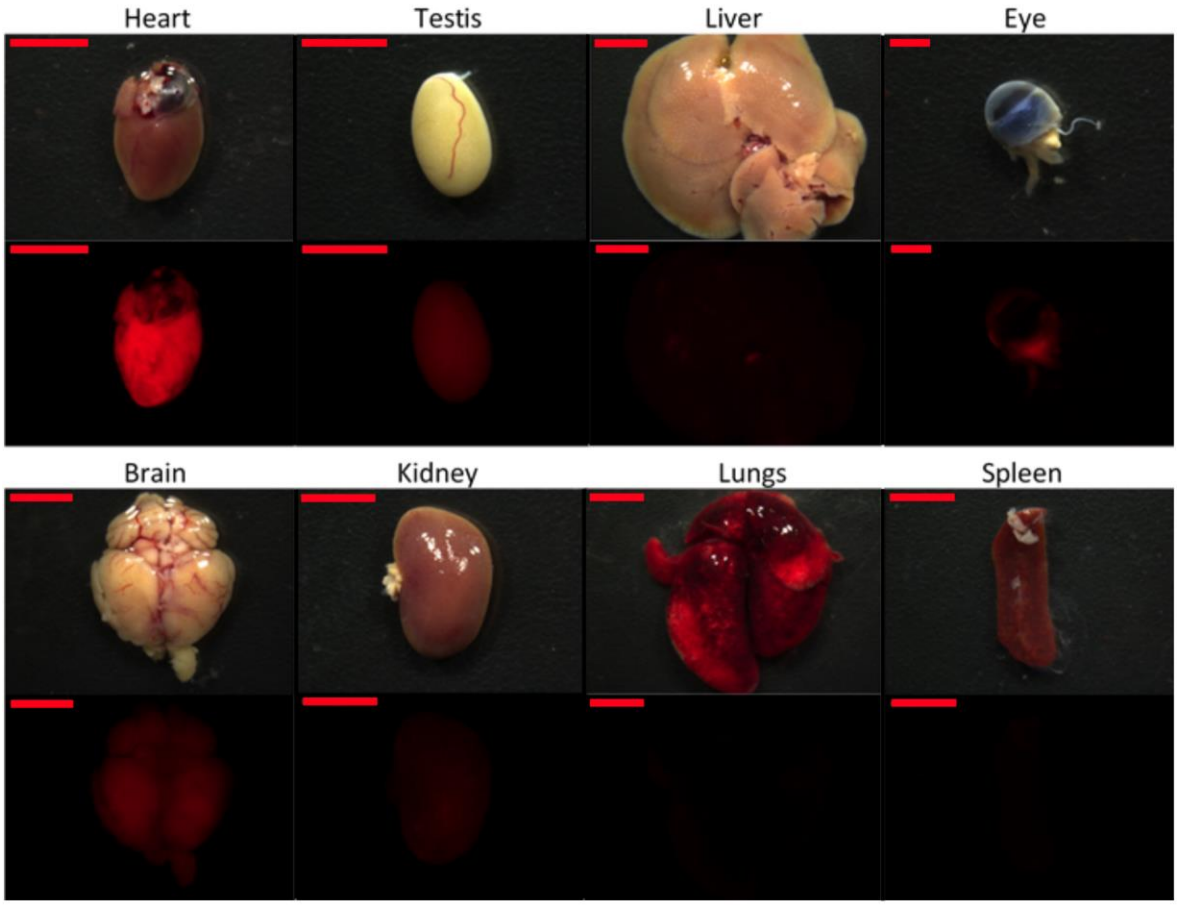

Figure 3.7 – Fluorescence of Organs Collected from Aged *Ddx3y*^{mKate2} Mouse

mKate2 fluorescence (bottom) and bright-field (top) images of whole organ images from a one-year-old *Ddx3y*^{mKate2} male mouse. Relative to the six-week-old *Ddx3y*^{mKate2} male (refer to Figure 3.3D), all aged organs were less fluorescent. The heart remained the most strongly fluorescent of all organs examined. However, the next most fluorescent organs in the six-week-old male (testis, liver and eye) exhibited a stark decline in fluorescence; the liver was non-fluorescent, and the eye and testis are only dimly fluorescent. The brain also declined in fluorescence with age, and, along with the kidney, were now of similar intensity to the aged testis. The lungs were non-fluorescent at one-year-old, and the spleen remained non-fluorescent. Scale bars are 5 mm (heart, gonad, liver, brain, kidney, lungs, spleen) and 2 mm (eye).

Table 3.2 - Comparison of mKate2 Fluorescence Intensity in *Ddx3y*^{mKate2} Organs between Six-Week-Old and a One-Year-Old Male

	Six-week-old *Ddx3y*^{mKate2} Male	One-year-old *Ddx3y*^{mKate2} Male
Heart	Very High	Moderate
Testes	High	Low
Liver	High	Absent
Eyes	High	Low
Brain	Moderate	Low
Kidney	Moderate	Low
Lungs	Low-Moderate	Absent
Spleen	Absent	Absent

The heart remained the most intensely fluorescent organ in the one-year-old male, as was the case in the six-week-old male; however, the fluorescence intensity in the one-year-old heart was greatly diminished, retaining only moderate intensity. Despite this decline, the heart was the organ that best maintained mKate2 signal, with the other examined organs' fluorescence declining far more starkly. The testes, eye, brain and kidney retained a low level of mKate2 fluorescence, a substantial decrease for the testes and eyes particularly, as, in the six-week-old male, these two organs exhibited high mKate2 fluorescence. The brain and kidney's fluorescence at six weeks of age, meanwhile, was more moderate, and thus this relative decline was less severe than that of the testes and eyes. The greatest decline with age, however, was observed in the liver, which was one of the most intensely fluorescent organs in the six-week-old male. In the one-year-old male, however, the liver was non-fluorescent, as were the lungs (reduced from low-moderate fluorescence in the six-week-old lungs), joining the spleen, which was non-fluorescent at both ages.

This sharp decline in mKate2 fluorescence intensity in the organs of the one-year-old *Ddx3y*^{mKate2} male indicates that the expression of mKate2 changes over the lifespan of the mouse, decreasing across all organs. This age-related decline in the fluorescent reporter signal is an important characteristic of this mouse model when designing experiments, as it suggests that the optimal time to use the *Ddx3y*^{mKate2} mouse is early in its lifespan, before the stark decline observed at one year of age.

3.2.2. Characterisation of the *Hprt*$^{DsRed\text{-}Express}$ Mouse

The *Hprt*$^{DsRed\text{-}Express}$ reporter mouse strain bore many similarities to the *Ddx3y*^{mKate2} reporter strain, including similar reporter chromosome generation strategies (refer to Sections 3.1.2 and 3.1.1.1, respectively), and were maintained on the same inbred strain background (129S1/SvImJ) at MCRI, and the *Hprt*$^{DsRed\text{-}Express}$ mouse not been previously characterised. Therefore, due to these similarities, the *Hprt*$^{DsRed\text{-}Express}$ mouse strain was selected characterisation in order to serve as a

comparison to the *Ddx3y*^{mKate2} strain.

This comparison serves two purposes: first, to contrast the utility of a reporter Y chromosome to that of a reporter X chromosome, and second, to compare how the *Ddx3y*^{mKate2} and *Hprt*$^{DsRed\text{-}Express}$ fluorescent reporter mouse strains specifically may be of use in research. This study characterised the *Hprt*$^{DsRed\text{-}Express}$ mouse strain, assessing the DsRed-Express fluorescence from preimplantation development through to adulthood, in the same manner in which the *Ddx3y*^{mKate2} strain was previously assessed for mKate2 fluorescence[5], with similar assessment of high/medium/low intensity as *Ddx3y*^{mKate2} tissues (Section 3.2.1). Conducting the characterisation of the *Hprt*$^{DsRed\text{-}Express}$ mouse in the same manner as that performed for the *Ddx3y*^{mKate2} mouse enabled ease of direct comparisons between these two strains.

This section details the characterisation of the *Hprt*$^{DsRed\text{-}Express}$ mouse, and the characteristics of this mouse model are compared to those of *Ddx3y*^{mKate2} mouse in Section 3.3.2.

3.2.2.1. DsRed-Express Fluorescence was Detectable in Preimplantation Development When the *Hprt*$^{DsRed\text{-}Express}$ Reporter X Chromosome was Maternally-inherited

As the paternal X chromosome is preferentially inactivated for the majority of preimplantation development (refer to Section 1.1.2.1), it was essential to assess whether this affected the activation of the DsRed-Express transgene on the *Hprt*$^{DsRed\text{-}Express}$ X chromosome in the early embryo. The paternal X chromosome in XX embryos is specifically silenced by imprinted X chromosome inactivation (XCI) in the embryo until post-implantation (refer to Section 1.1.2.1). It has previously been observed that approximately 3% of mouse X chromosome genes escape XCI[216], being expressed from both the active and inactive X chromosome. Regarding the *Hprt*$^{DsRed\text{-}Express}$ reporter chromosome, it was essential to confirm whether the DsRed-Express fluorescent reporter transgene was subject to the imprinted XCI of the paternal X chromosome in the early embryo. To assess this, preimplantation *Hprt*$^{DsRed\text{-}Express}$ embryos were examined by confocal microscopy, with the reporter X chromosome either maternally- or paternally-inherited.

Embryos from E1.5 to E3.75 were collected from matings of X$^{Hprt\ DsRed\text{-}Express}$X (carrier) females with XY (wild type) males, and of XX (wild type) females with X$^{Hprt\ DsRed\text{-}Express}$Y (carrier) males (Figures 3.8A and B, respectively). This was performed, both to examine the effect of parental inheritance on DsRed-Express expression as detailed above, and also with the aim to examine the intensity of DsRed-Express fluorescence in both male and female embryos. This was because males pass their X chromosome onto all female offspring only, whereas females pass either of their X chromosomes onto offspring of both sexes equally. By assessing litters of X$^{Hprt\ DsRed\text{-}Express}$X females, it could be determined whether there were sex differences in DsRed-Express fluorescence intensity in preimplantation development, as all preimplantation embryos should be actively expressing from the maternally-inherited *Hprt*$^{DsRed\text{-}Express}$ X chromosome.

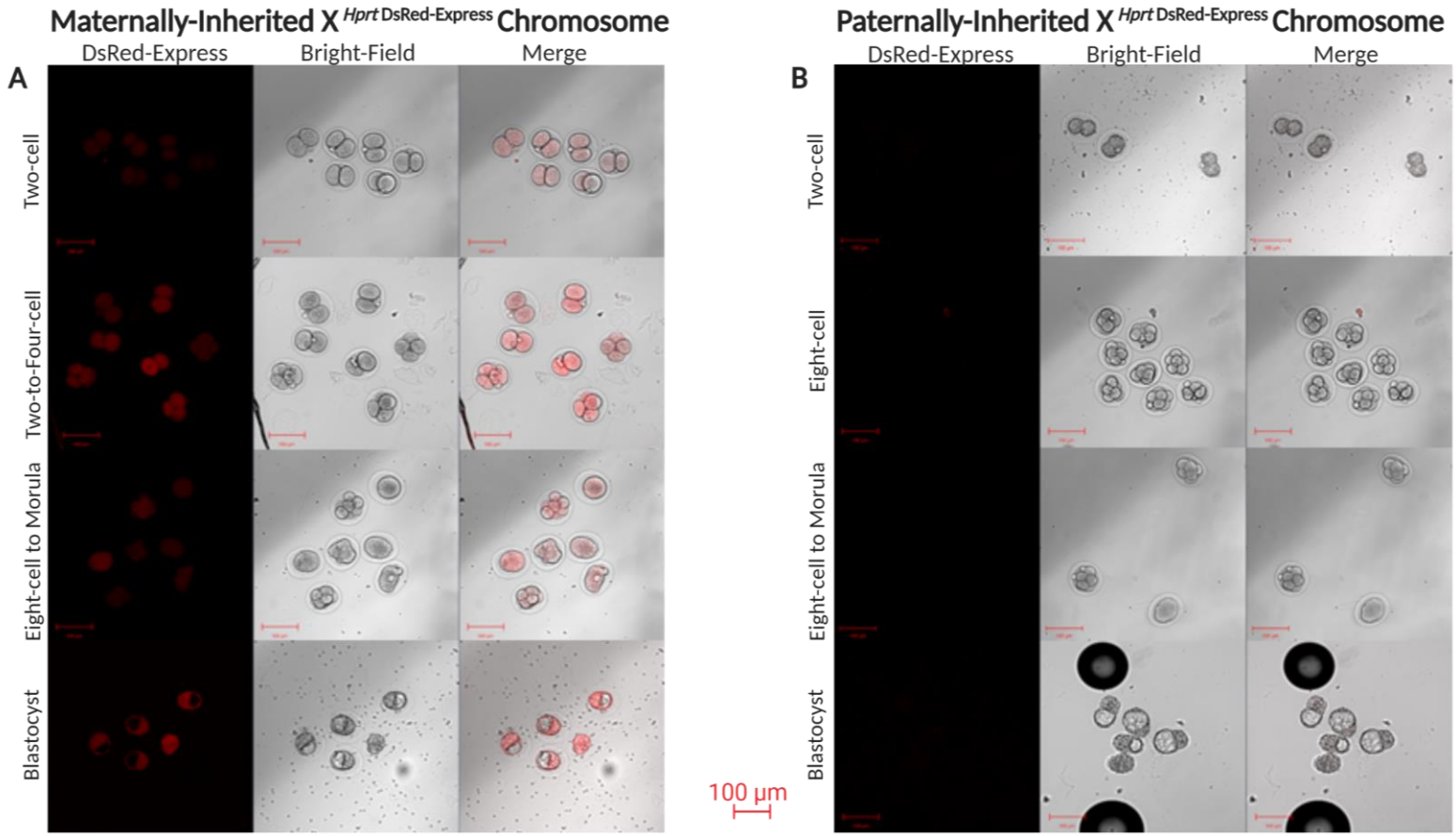

Figure 3.8 - Preimplantation Embryos Carrying Either a Paternally-Derived or a Maternally-Derived *Hprt*$^{DsRed-Express}$ Reporter X Chromosome

Preimplantation embryos from *Hprt*$^{DsRed-Express}$ matings were collected between E0.5 and E4.0. Representative images of embryos: carrying maternally-derived (A) or paternally-derived (B) reporter X chromosome. Representative images: DsRed-Express fluorescence (left), bright-field (centre) and merge (right) images of (A and B top) two-cell, (A upper middle) two-to-four-cell, (B upper middle) eight-cell, (A and B lower middle) eight-cell-to-compacting-morula or (A and B bottom) blastocysts. DsRed-Express fluorescence was detectable only in embryos with a maternally-derived reporter chromosome (A) from the late two-cell stage (A upper middle) to the blastocyst (A bottom), in which there was a mix of embryos exhibiting either high or low DsRed-Express fluorescence intensity. No embryos in (B) exhibited fluorescence. Scale bars are 100 µm.

Matings of X$^{Hprt\ \text{DsRed-Express}}$Y males with X$^{Hprt\ \text{DsRed-Express}}$X females were not performed, as X$^{Hprt\ \text{DsRed-Express}}X^{Hprt\ \text{DsRed-Express}}$ female embryos (homozygous for the *Hprt*$^{\text{DsRed-Express}}$ X chromosome) were not desired. This was due to the likelihood that they would be indistinguishable from male embryos in the event of sex differences in fluorescence. Additionally, X$^{Hprt\ \text{DsRed-Express}}X^{Hprt\ \text{DsRed-Express}}$ female embryos would not be informative as to whether there was a sex difference in activation of the fluorescent reporter, as potential transgene activation due to paternal X chromosome escape would be masked by the maternally-inherited *Hprt*$^{\text{DsRed-Express}}$ X chromosome.

Examination of preimplantation embryos carrying either a paternally or maternally-inherited *Hprt*$^{\text{DsRed-Express}}$ reporter X chromosome (Figure 3.8) revealed a distinct difference in activation of the DsRed-Express fluorescent reporter. When the *Hprt*$^{\text{DsRed-Express}}$ reporter X chromosome was paternally-inherited (Figure 3.8B), there was no detectable fluorescence from the fluorescent reporter, with all embryos remaining staunchly non-fluorescent from two-cell onwards. While the absence of fluorescence in the later preimplantation stages (four-cell to blastocyst) was not unexpected, as the paternal X chromosome is preferentially inactive in XX embryos from the four-stage onwards[67] (refer to Section 1.1.2.1), the lack of any detectable fluorescence in two-cell embryos was somewhat surprising. Genes from both the maternal and paternal X chromosomes are briefly active at the two-cell stage[67]; therefore, it is possible that the paternal *DsRed-Express* allele was active prior to the preferential inactivation of the paternal X chromosome at the four-cell stage. The non-fluorescence of all two-cell embryos suggests that, while the gene may have been briefly active, this did not result in sufficient DsRed-Express protein being expressed to produce fluorescence visible by microscopy.

For embryos collected from X$^{Hprt\ \text{DsRed-Express}}$X females (maternal inheritance), however, there was an unexpected finding: there is a very low level in DsRed-Express fluorescence present in all embryos at the early two-cell stage (Figure 3.8A). At this stage, the embryonic genome has yet to activate, with the embryo replacing maternal transcripts with its own, embryo-derived transcripts in late two-cell (refer to Section 1.1.4). However, following embryonic genome activation (EGA) at the late two-cell stage, there was a combination of two-cell embryos which maintained this low level of fluorescence, and two-cell embryos which exhibited a distinctly higher level of fluorescence. This is likely the result of EGA occurring throughout the two-cell stage, with the embryos carrying the *Hprt*$^{\text{DsRed-Express}}$ X chromosome activating transcription from their own (maternally-inherited) X chromosome, including the DsRed-Express transgene.

Beyond the two-cell stage, litters of embryos at subsequent stages were consistently a combination of low and high fluorescence embryos, with no non-fluorescent embryos present as would have been expected from this mating. From these observations, it was predicted that the low level of fluorescence present in all embryos at early two-cell may be maternally-derived DsRed-Express protein that was retained in the oocyte that had yet to degrade, as many maternal proteins from the oocyte are known to persist beyond EGA[68]. Therefore, it can be predicted that the low

fluorescence embryos present from late two-cell and beyond were, in fact, wild type embryos (XX or XY) that did not carry the *Hprt*$^{DsRed\text{-}Express}$ reporter X chromosome.

As described above, the paternal X chromosome is preferentially inactivated throughout most of preimplantation development, with the exception of a brief window of activity at the two-cell stage[67]. Of embryos carrying a maternally-derived *Hprt*$^{DsRed\text{-}Express}$ X chromosome, male embryos would be expressing the transgene due to the absence of XCI in their XY cells. Meanwhile, female embryos would preferentially express the transgene from the active maternal *Hprt*$^{DsRed\text{-}Express}$ X chromosome from the four-cell stage onwards, with this maternal allele having become active at EGA (two-cell). This accounts for the absence of preimplantation embryos exhibiting mosaic fluorescence/non-fluorescence between their cells, as would be expected in the presence of random XCI. Therefore, X$^{Hprt\ DsRed\text{-}Express}$Y male and X$^{Hprt\ DsRed\text{-}Express}$X female embryos could not be visually distinguished from one another at this stage of development, as both sexes exhibited fluorescence in all cells. Likewise, the sex of wild-type embryos could not be determined by microscopy at this stage, as both XY males and XX females were wholly non-fluorescent. Ideally, genotyping for sex would be performed on these embryos prior to downstream work. In this study, sex genotyping was not performed as the Y chromosome *Sry* gene was unable to be amplified by PCR on limited blastocyst DNA, despite troubleshooting efforts.

From these results, the *Hprt*$^{DsRed\text{-}Express}$ X chromosome has been shown to be subject to the imprinted XCI that affects the paternal X chromosome, with the transgene unable to escape this inactivation in preimplantation development. When the *Hprt*$^{DsRed\text{-}Express}$ X chromosome was maternally-inherited, and therefore active in all cells of male and female preimplantation embryos, fluorescence from the *DsRed-Express* transgene has been observed from the late two-cell stage onwards, coinciding with activation of the embryonic genome and subsequent production of embryo-derived transcripts and proteins.

3.2.2.2. DsRed-Express Fluorescence was Present at Midgestation Embryonic Development in Both Sexes of *Hprt*$^{DsRed\text{-}Express}$ Mice

While it was determined that DsRed-Express fluorescence was only present in preimplantation embryos carrying a maternally-inherited *Hprt*$^{DsRed\text{-}Express}$ X chromosome (Section 3.2.2.1), due to preferential inactivation of the paternal X chromosome, this imprinted XCI is known to be reversed in the post-implantation embryo[62] (refer to Section 1.1.2.1). Imprinted paternal XCI is replaced with random XCI in the embryo following implantation, resulting in the paternal and maternal X chromosomes each being equally likely to be inactivated in a given cell[62]. Therefore, in order to assess the sex differences in DsRed-Express fluorescence due to the action random XCI in the females, *Hprt*$^{DsRed\text{-}Express}$ embryos were examined at midgestation using fluorescence stereomicroscopy.

Embryos were collected at E9.5 from matings between X$^{Hprt\ DsRed\text{-}Express}$X females with XY males, and between XX females with X$^{Hprt\ DsRed\text{-}Express}$Y males (Figure 3.9). Again, no embryos were derived from matings of X$^{Hprt\ DsRed\text{-}Express}$Y males with X$^{Hprt\ DsRed\text{-}Express}$X females to avoid the undesired X$^{Hprt\ DsRed\text{-}Express}X^{Hprt\ DsRed\text{-}Express}$ female embryos, which were predicted to be visually indistinguishable from X$^{Hprt\ DsRed\text{-}Express}$Y male embryos fluorescence.

The litter of four E9.5 embryos carrying a paternally-derived *Hprt*$^{DsRed\text{-}Express}$ X chromosome (Figure 3.9A) was observed to have equal numbers of fluorescent and non-fluorescent embryos (two embryos each). From the inheritance pattern of paternal X chromosome, it was expected that all fluorescent embryos would be female, and all non-fluorescent embryos would be male. This prediction was confirmed by genotyping. The occurrence of these fluorescent embryos at E9.5, having inherited their *Hprt*$^{DsRed\text{-}Express}$ X chromosome paternally, demonstrates that the preferential inactivation of the paternal X$^{Hprt\ DsRed\text{-}Express}$ chromosome in preimplantation development was indeed reversed in post-implantation development as expected, thereby allowing expression from the paternal *DsRed-Express* allele.

Of embryos carrying a maternally derived *Hprt*$^{DsRed\text{-}Express}$ X chromosome (Figure 3.9B), a mix of fluorescent and non-fluorescent embryos was recovered. In the sample collected here, there was a slight bias towards fluorescent embryos, accounting for six of the nine (66.6%) embryos in this litter. However, this was likely the effect of small sample size, as only one litter was examined, and the maintenance colony of these mice showed no sex or genotype skew in litters of X$^{Hprt\ DsRed\text{-}Express}$X females. It would therefore be expected that, with a sufficiently large embryo sample size, 50% of embryos would be fluorescent, with 25% of these being male and the other 25% being female.

The three non-fluorescent embryos from this litter were identified by genotyping to be two females and a male. As shown in Figure 3.9B(i) and (ii), the wild type female and male embryos, respectively, were found to exhibit no fluorescence at E9.5. This differed from the observed low level of fluorescence in all preimplantation embryos from an X$^{Hprt\ DsRed\text{-}Express}$X female (Figure 3.9A), and was most likely due to the degradation of the maternal DsRed-Express protein as the embryos progressed through post-implantation development.

Two of these six fluorescent embryos were observed to exhibit markedly reduced fluorescence compared to the other four fluorescent embryos. The less intensely fluorescent embryos were predicted to be female, as approximately half of their cells would have randomly inactivated the *Hprt*$^{DsRed\text{-}Express}$ X chromosome and hence become non-fluorescent, resulting in mosaic fluorescence. Meanwhile, the more intensely fluorescent embryos were predicted to be male, with the *Hprt*$^{DsRed\text{-}Express}$ X chromosome active in every cell due to the lack of XCI. These predictions were confirmed through genotyping, indicating that male and female *Hprt*$^{DsRed\text{-}Express}$ embryos can be sexed visually based on fluorescence alone at E9.5

When fluorescent embryos from the paternally-inherited and maternally-inherited *Hprt*$^{DsRed\text{-}Express}$ litters (Figure 3.9A and B, respectively) were compared, it was apparent that the fluorescent female embryos from both litters exhibited a similar level of fluorescence intensity. Therefore, the paternal origin of the *Hprt*$^{DsRed\text{-}Express}$ X chromosome in females did not affect the overall DsRed-Express fluorescence of the embryo at midgestation.

Additionally, in both the female and male fluorescent embryos, there was some variation in DsRed-Express fluorescent intensity across the embryo body, which, like in E9.5 *Ddx3y*^{mKate2} embryos (Figure 3.3B), appeared to be a function of tissue density, with more dense regions of the embryo being more intensely fluorescent.

3.2.2.3. DsRed-Express Fluorescence Varied Between Tissues and Organs in the Adult *Hprt*$^{DsRed\text{-}Express}$ Mouse, and Between Sexes

Examination of E9.5 *Hprt*$^{DsRed\text{-}Express}$ embryos identified that there was a difference in fluorescence intensity between male and female embryos, due to random XCI in the female embryos, with female embryos exhibiting a lower fluorescence intensity relative to male embryos (Figure 3.9). In both sexes, however, there were no apparent differences between fluorescence intensity in different tissues of the body at E9.5, with the entire embryo being fluorescent. As many structures are either not present or under-developed at this early stage of gestation, it was essential to examine adult tissues in *Hprt*$^{DsRed\text{-}Express}$ male and female mice to determine whether the broad fluorescence observed at midgestation would be maintained through to adulthood.

The brain, eyes, thymus, heart, lungs, kidneys, spleen, liver, gonads, visceral fat and abdominal fat (from the abdominal fat pad) were collected from six-week-old male and female *Hprt*$^{DsRed\text{-}Express}$ mice, as well as from age-matched male and female controls. These organs were then imaged for DsRed-Express fluorescence at various exposures (refer to legend of Figure 3.10 for exposures used) using fluorescence stereomicroscopy alongside organs from wild type male and female littermates (Figure 3.10).

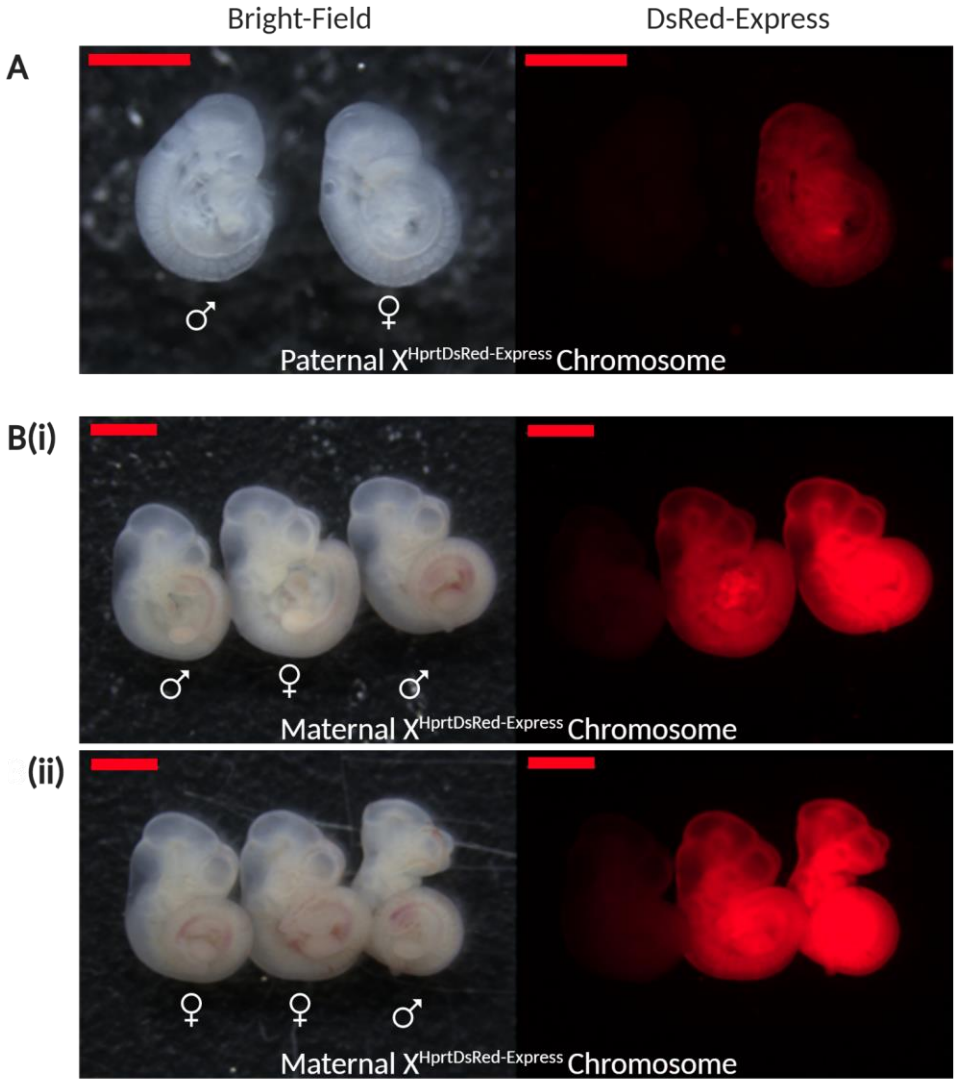

Figure 3.9 – Midgestation Embryos Carrying Either a Paternally-Derived or a Maternally-Derived *Hprt*$^{DsRed\text{-}Express}$ Reporter X Chromosome

Embryos carrying a (A) paternally- or (B) maternally-inherited *Hprt*$^{DsRed\text{-}Express}$ X chromosome. Female embryos that inherited a reporter chromosome ((A) right, (B(i)) and (ii) centre) exhibited a low level of DsRed-Express fluorescence due to random inactivation of the *Hprt*$^{DsRed\text{-}Express}$ reporter X chromosome. Male and female embryos that did not inherit the reporter X chromosome were non-fluorescent (males: (A) left, (B(ii)) left; female: (B(i)) left). Male embryos that did inherit the *Hprt*$^{DsRed\text{-}Express}$ X chromosome exhibited a higher level of DsRed-Express fluorescence ((B(i)) left and (ii) left) than female carriers. Scale bars are 1 mm.

Table 3.3 - Comparison of DsRed-Express Fluorescence Intensity in Adult *Hprt*$^{DsRed\text{-}Express}$ Organs between the Sexes

	Hprt$^{DsRed\text{-}Express}$ Male	*Hprt*$^{DsRed\text{-}Express}$ Female
Heart	High-Moderate	Moderate, non-uniform
Gonads	Testes - very high	Ovaries - high
Liver	High	Moderate, mottled
Eyes	Moderate	Moderate, non-uniform
Brain	Low	Very low
Kidney	Moderate	Low-Moderate, slightly mottled
Lungs	Low-Moderate	Low, mottled
Spleen	Very low	Extremely low, mottled
Abdominal Fat	Low-Moderate	Low
Visceral Fat	Very high	Very high, mottled fluorescent/non-fluorescent
Fluorescence in male and female organs was uniform across the organ unless otherwise stated		

All organs from the *Hprt*$^{DsRed\text{-}Express}$ mice exhibited at least some level of fluorescence, with clear differences in fluorescence intensity between both the different organs, and between the sexes. Table 3.3 outlines comparative fluorescence intensities between male and female *Hprt*$^{DsRed\text{-}Express}$ organs. In all organs, the male *Hprt*$^{DsRed\text{-}Express}$ tissues were more intensely fluorescent than the female *Hprt*$^{DsRed\text{-}Express}$ organs. Additionally, in multiple female organs, the fluorescence was not simply of lower intensity, but had a non-uniform or 'mottled' pattern, highlighting regions of non-fluorescence within the organ. This was likely due to clonal inheritance of XCI, as it there is evidence that descendants of a cell are likely to inactivate the same X chromosome as their progenitor, depending on cell type[211,217].

The most intense DsRed-Express fluorescence observed in both sexes was in visceral fat (Figure 3.10l), with the tissue rapidly becoming over-exposed during imaging, needing to be imaged at the lowest exposure to ensure accurate visualisation of the fluorescence pattern. In addition to the highly fluorescent nature of this tissue, the DsRed-Express protein in the tissue resulted in a colour change to the visceral fat when viewed in white light (bright-field). The wild-type fat was pale beige in colour, while the *Hprt*$^{DsRed\text{-}Express}$ fat was bright pink. This colour change also enabled clear visualisation of the effect of XCI in the female tissue: while the *Hprt*$^{DsRed\text{-}Express}$ male visceral fat was entirely pink, the *Hprt*$^{DsRed\text{-}Express}$ female fat was a mix of pink and pale beige fat. From this appearance, it was clear that a subset of cells in the female visceral fat had randomly inactivated either the wild-type X chromosome (pink tissue, DsRed-Express-positive, *Hprt*$^{DsRed\text{-}Express}$ X chromosome active) or the *Hprt*$^{DsRed\text{-}Express}$ X chromosome (pale tissue, DsRed-Express-negative, wild-type X chromosome active).

The abdominal fat, in comparison, was white-coloured in both *Hprt*$^{DsRed\text{-}Express}$ and wild type

mice of both sexes when viewed in white light, and exhibited a far lower level of fluorescence than the visceral fat (Figure 3.10J). In male abdominal fat, the tissue was low-moderately fluorescent, with the female fat being only lowly fluorescent. When examined as a whole, the female tissue appeared to be uniformly lower in fluorescence, rather than exhibiting a mottled appearance of fluorescent and non-fluorescent regions, as was observed in the visceral fat.

Of the remaining organs, the most intensely fluorescent organ was the gonads, with the testes (male) observed to exhibit a very high level of uniform fluorescence, and the ovaries (female) also being highly fluorescent (Figure 3.10B). While the ovaries were slightly lower in fluorescence intensity relative to the testes, the fluorescence of the ovary appeared largely uniform, with the only variations across the organ appearing to be due to the structure of the ovary, with this organ not exhibiting a mottled mix of fluorescent and non-fluorescent regions. While this observation of the $X^{Hprt\ DsRed\text{-}Express}X$ ovary indicated that there is an overall reduction in fluorescence intensity relative to the $X^{Hprt\ DsRed\text{-}Express}Y$ testis, comparing these two different organs can pose potential complications. It would be advisable in future to compare a $X^{Hprt\ DsRed\text{-}Express}X$ ovary and a $X^{Hprt\ DsRed\text{-}Express}X^{Hprt\ DsRed\text{-}Express}$ ovary, to remove any potential differences in the fluorescence being due to the structure of the organ, as opposed to being due to random XCI resulting in mosaic fluorescence.

The heart was the next most intensely fluorescent organ (Figure 3.10A), with the HprtDsRed-Express male heart exhibiting a high-moderate fluorescence intensity across the organ. The HprtDsRed-Express female heart, meanwhile, showed slightly reduced moderate florescence, with a non-uniform florescence pattern. This non-uniform fluorescence in the female heart appeared result in regions of non-fluorescence. The kidney (Figure 3.10F) was the next most intensely fluorescent organ, with moderate fluorescence present in the male kidney, and low-moderate fluorescence with a slight mottled appearance in the female kidney.

The HprtDsRed-Express male lungs exhibited low-moderate fluorescence, while the female lungs were lowly fluorescent, and were observed to have a mottled fluorescence pattern (Figure 3.10G). The eyes were moderately fluorescent in both sexes (Figure 3.10D), with the main distinction between the sexes being the non-uniformity of fluorescence across the female eyes. The brain, meanwhile, was lowly fluorescent in the male, and extremely lowly but uniformly fluorescent in the female (Figure 3.10E). The least fluorescent organ in both sexes was the spleen (Figure 3.10H), with very low fluorescence observable in the male spleen. The fluorescence of the female spleen was reduced relative to that of the male spleen, exhibiting extremely low florescence in the female, with this organ also presenting with a mottled fluorescent pattern.

In all tissues examined, the male and female wild-type tissues remained non-fluorescent as expected, with no autofluorescence observed. However, in some of the organs which were highly fluorescent in the HprtDsRed-Express samples, such as the visceral fat, the fluorescence from these organs was reflected onto the wild-type organs.

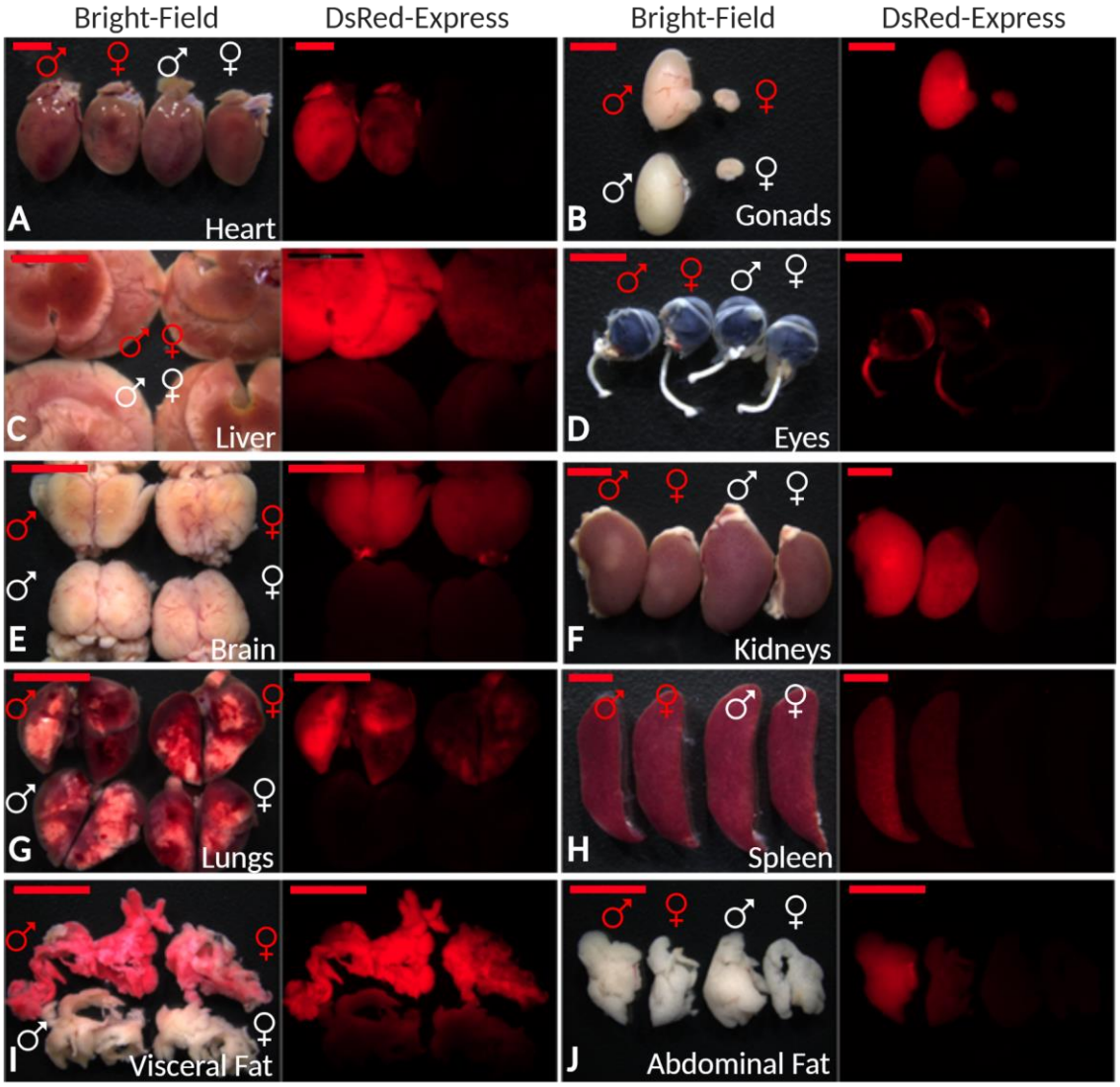

Figure 3.10 - Fluorescence Differences between Male and Female *Hprt*$^{DsRed\text{-}Express}$ Organs

Organs harvested from *Hprt*$^{DsRed\text{-}Express}$ male and female and wild type littermate controls imaged for bright-field (left) and DsRed-Express fluorescence (right). The organs imaged are the (A) heart, (B) gonads, (C) liver, (D) eyes, (E) brain, (F) kidney, (G) lungs, (H) spleen, (I) visceral fat and (J) abdominal fat. Different DsRed-Express exposures selected to avoid over-saturation of the fluorescence and to demonstrate difference between male and female HprtDsRed-Express organs.

Exposures: 50 ms (I), 250 ms (B), 500 ms (C), 750 ms (A), 1 sec (G) and 1.5 sec (D), (E), (F), (H), (J).

Scale bars: 2 mm (A), (B), (D), (F), (H) and 5 mm (C), (E), (G), (I), (J).

For all *Hprt*$^{DsRed\text{-}Express}$ organs, the male tissue had greater fluorescence intensity than the corresponding female tissue. The most intensely fluorescent tissue was the visceral fat, while the eye and spleen both had the lowest fluorescence. For (A), (D), (F), (H) and (J), order is (left to right) *Hprt*$^{DsRed\text{-}Express}$ male, *Hprt*$^{DsRed\text{-}Express}$ female, wild type male and wild type female. For (B), (C), (E), (G), (I), order is (top row, left to right) *Hprt*$^{DsRed\text{-}Express}$ male, *Hprt*$^{DsRed\text{-}Express}$ female and (bottom row, left to right) wild type male, wild type female.

The next most fluorescent organ was the liver (Figure 3.10C), which was highly fluorescent in the male, exhibiting moderate fluorescence in the female. The fluorescence in the *Hprt*$^{DsRed\text{-}Express}$ male liver was uniform, contrasting the *Hprt*$^{DsRed\text{-}Express}$ female liver which exhibited a clear mottled fluorescence pattern, more in line with that observed in the pattern in the visceral fat. This was hypothesised to also be a clonal effect.

Overall, there is a clear difference in DsRed-Express fluorescence between the *Hprt*$^{DsRed\text{-}Express}$ sexes in adulthood, due to the presence of random XCI in the tissues of the female. This results in female tissues being less intensely fluorescent relative to male organs. This reduction due to XCI of the reporter chromosome can present as a uniform reduction in fluorescence in the female tissues, or in a non-uniform or mottled appearance involving distinction between fluorescent and non-fluorescent regions of the tissue. These non-uniform presentations are hypothesised to be due to clonal inheritance of XCI.

3.3. Discussion

This chapter described work characterising two mouse strains carrying reporter chromosomes with fluorescent protein transgenes. Firstly, the primary focus of this study, the *Ddx3y*^{mKate2} reporter strain, required further characterisation to fully define the utility of this model. To achieve this, the mKate2 fluorescence of the *Ddx3y*^{mKate2} mouse was assessed in three ways: in a tissue-specific manner in late embryonic structures, in adult tissues many hours post-mortem, and finally, in organs from a *Ddx3y*^{mKate2} male of advanced age.

The second characterisation performed in this chapter was of the *Hprt*$^{DsRed\text{-}Express}$ mouse, carrying a reporter X chromosome. As this mouse strain bore many similarities to the *Ddx3y*^{mkate2} mouse, the fluorescence in *Hprt*$^{DsRed\text{-}Express}$ mice was assessed to parallel the work performed on the *Ddx3y*^{mKate2} mouse previously[5]. This included assessing the onset of DsRed-Express fluorescence in embryogenesis, as well as the fluorescence in adult organs. This was performed examining both sexes of the *Hprt*$^{DsRed\text{-}Express}$ mouse to account for the effect of X chromosome inactivation (XCI). The characteristics of these two mouse models are compared in Section 3.3.2 in order to highlight their strengths and limitations.

3.3.1. The Persistence of mKate2 Fluorescence Across the Lifespan of the *Ddx3y*^{mKate2} Mouse

The *Ddx3y*^{mKate2} reporter Y chromosome was created to be used as a tool for chromosome instability, due to the non-essential nature of the Y chromosome in regards to viability. This non-essential nature is due to the function of its genes being restricted solely to the male reproductive system. Loss of this chromosome *in vitro* or *in vivo* in the mouse does not result in lethality, an ideal

feature for a reporter chromosome in research involving chromosome instability.

As the *Ddx3y*^{mKate2} Y chromosome and its resulting mouse strain were created with the intention of generating a resource for researchers, it was necessary to characterise the conditions under which the signal from the fluorescent protein reporter, mKate2, was detectable. This characterisation was aimed at generating a baseline of the time points and tissues which would likely be amenable for experiments using the *Ddx3y*^{mKate2} model.

Initial characterisation of the *Ddx3y*^{mKate2} mouse was previously performed[5] (Section 3.1.1.2), and identified that mKate2 fluorescence was detectable in the latter part of preimplantation development, and persisted through midgestation into adulthood, with fluorescence present at varying degrees in a tissue-dependent manner at six weeks of age (Figure 3.3). These findings indicated promise for this model, due to the high level of mKate2 fluorescence broadly present across male embryos, beginning in the blastocyst and persisting through to midgestation[5]. In the adult, multiple organs were examined to reveal a high level of mKate2 signal in most organs[5].

From these previous observations, two gaps in the characterisation of the *Ddx3y*^{mKate2} mouse were identified. Firstly, the lack of examining mKate2 signal at the cell level within complex structures. And second, the lack of assessment of age-related changes to mKate2 fluorescence in the mouse, as it has been observed that Y chromosome aneuploidy increases with advanced age in the mouse[218]. This chapter outlined the work performed to address these gaps, and hence complete the characterisation of the *Ddx3y*^{mKate2} mouse.

While the previous examination of midgestation *Ddx3y*^{mKate2} embryos appeared to indicate that mKate2 fluorescence was ubiquitous during gestation[2], the observation in adult organs that mKate2 fluorescence varied between organs suggested that there was tissue differences in this fluorescence. Further to that, structures from a male E17.5 *Ddx3y*^{mKate2} embryo, one to two days prior to birth, were examined using immunohistochemistry (IHC) to identify differences in mKate2 signal between cells of complex structures, such as the head, limbs, and the internal organs, the heart and testis.

This staining revealed that, within a single structure, there can indeed be cell- and tissue-specific variation in mKate2 signal. This analysis indicated that structures, including whole embryos, which appear to be uniformly fluorescent when imaged as a whole, likely possesses both mKate2-positive and negative cell populations. This would likely affect how the *Ddx3y*^{mKate2} model may be used in experiments, depending on the details of the work to be conducted, particularly when working with whole organs or whole animals. It would be necessary to carefully select the tissue and/or cells to be targeted for use in order to be assured that they are uniformly mKate2-positive. This would be particularly relevant in structures which are composed of a variety of cell types.

However, when examining a structure composed of a limited number of cell types, such as the heart, primarily comprised of cardiomyocytes, this process may be streamlined, as the staining of the embryonic heart demonstrated that there was indeed uniform mKate2 signal in this organ.

Additionally, these IHC findings from the E17.5 tissues demonstrated that, at the cell level, the incidence of mKate2 signal can change over development. This was clear in the staining of the embryonic testis. As this organ was collected from an embryo, the cells within the testis cords (primordial germ cells) had not yet begun spermatogenesis, which occurs post-natally (refer to Section 1.1.5.2.1). As these germ cells had not yet differentiated into spermatogonia, nor entered the spermatogenic pathway, their Y chromosome had not yet been silenced, which was reflected in the high mKate2 signal observed in the testis cords. In contrast, IHC staining of a *Ddx3y*^{mKate2} testis performed during the previous characterisation[5] of the model identified mKate2 signal was absent from most cells in the seminiferous tubule[5], the successor to the testis cords. This absence was due to the inactivation of the *Ddx3y*^{mKate2} Y chromosome as the cells progressed through meiosis, and hence restricted mKate2 to the spermatogonia and primary spermatocytes, the only cells carrying an active Y chromosome[5]. This demonstrates that a change in the cell population of an organ can change the proportion of mKate2-positive cells within that organ, an important consideration if planning to use *Ddx3y*^{mKate2} organs or tissues in research.

It was necessary to understand how the mKate2 fluorescence of *Ddx3y*^{mKate2} organs changed with advanced age required assessment, as the reporter chromosome in this mouse model was the Y chromosome. In the XY individual, the Y chromosome is the non-essential sex chromosome, and has been previously shown to be prone to aneuploidy in advanced age. In humans, it has been observed that men over 40 years old are prone to losing the Y chromosome from cells from their bone marrow, increasing from approximately 10% loss in men in their 40s and 50s, to approximately 75% loss in men in their 80s and 90s[219]. Likewise, in mice, Y chromosome aneuploidy had been observed in cortical nuclei, with a statistically significant increase in aneuploid nuclei between mice at four months of age and at 28 months (2.3 years) of age[218]. However, despite the noted propensity of the Y chromosome to be unstable in old age[218], this effect was not observed in the spleen[218]. This indicates that age-related effects on the stability of the Y chromosome can vary between different cell types.

Additionally, studies in humans have discovered that there are age-related effects on Y chromosome gene regulation. A recent study by Lund et al (2019)[215] examined Y chromosome CpG methylation (a marker of gene repression) in four cohorts of men, three Danish cohorts and one Scottish cohort, assessing blood-based methylation data[215] . This study identified that over 82% of Y chromosome CpG sites assessed became hypermethylated with age[215], indicating increased repression with age.

These findings bolstered the need to assess the persistence of mKate2 fluorescence in

advanced age in the *Ddx3y*^{mKate2} mouse, as there was potential for fluorescence to decline with age, either due to Y chromosome aneuploidy, or age-related repression. Further to this, organs from a one-year-old *Ddx3y*^{mKate2} mouse were examined using fluorescence stereomicroscopy. This examination revealed that there was a decline in mKate2 intensity with advanced age in all organs examined, with two organs (liver and lungs) becoming wholly non-fluorescent.

While Y chromosome aneuploidy may play a factor in this decline in mKate2 fluorescence, it is unlikely to be the sole cause, as the reported rates of age-related Y chromosome aneuploidy does not affect a large percentage of cells. For example, Faggioli et al[218] identified a rate of approximately 2% Y chromosome aneuploidy in mouse cortical nuclei at 28 months, 16 months older than the mouse assessed in this study. One potential cause of this decline may be due to changes to the organs' structure in old age, as multiple mouse organs, including the spleen[220], liver[221], kidney[222,223], and lungs[224] have been observed to undergo age-related structural changes and/or increased risk of fibrosis[221,224]. Another cause may be changes to the regulation of Y chromosome genes in advanced age, such as an age-related increase in Y chromosome repression affecting expression of the mKate2 transgene. The precise mechanism of this decline in fluorescence will be a subject for future study. It would be prudent to assess this in target cells and tissues if planning to use the *Ddx3y*^{mKate2} mouse in an age-related chromosome instability study, as this work identified that the degree of fluorescence decline varied between organs. Additionally, it would be advisable to perform an age series examining the degree of mKate2 fluorescence in organs of mice at increasing ages; for example, in one month increments.

3.3.2. Comparison of the *Ddx3y*^{mKate2} and the *Hprt*$^{DsRed\text{-}Express}$ Mouse Strains

The *Hprt*$^{DsRed\text{-}Express}$ mouse model was selected to be characterised in this study in order to serve as a comparison to the *Ddx3y*^{mKate2} strain, the main focus of this project. The aim of this comparison was to highlight the strengths and weaknesses of each model, with a focus on the *Ddx3y*^{mKate2} mouse. This section discusses the characteristics of the *Hprt*$^{DsRed\text{-}Express}$ mouse as they compare to those of the *Ddx3y*^{mKate2} mouse.

The *Hprt*$^{DsRed\text{-}Express}$ was generated by targeted insertion of a transgene cassette into a known locus on the X chromosome with the aim to maximise expression of the reporter gene, *DsRed-Express*. This gene codes for the DsRed-Express fluorescent protein, and the gene cassette carrying this gene was inserted into the mouse X chromosome at the *Hprt* locus, as the chromosomal region of this housekeeping gene was unlikely to result in repression of the *DsRed-Express* gene.

The *Hprt*$^{DsRed\text{-}Express}$ mouse was an ideal model to compare with the *Ddx3y*^{mKate2} mouse for several reasons. Firstly, a similar method of construction was employed to generate both mouse models, by targeted insertion of the transgene into a broadly-expressed single copy gene. Second, DsRed-Express and mKate2 have somewhat overlapping excitation/emission spectra (554/586 and 588/633 for DsRed-Express and mKate2, respectively, Figure 3.11). Third, both fluorescent proteins

are constitutively fluorescent basic proteins that are fast maturing[178,214]. Fourth, both fluorescent reporter chromosomes were maintained on a 129S1/SvImJ background at MCRI, indicating that expression and resulting fluorescence from either transgene would be subject to the same genetic effects.

In addition to the similarities in the reporter chromosomes' creation and strain maintenance, characterisation of these two mouse models revealed commonalities in their fluorescence patterns (summarised in Table 3.4). Both strains' fluorescent reporter transgenes were observed to activate during preimplantation embryo development, with the DsRed-Express fluorescence appearing earlier in development than mKate2 fluorescence. However, the presence of DsRed-Express fluorescence in preimplantation embryos was dependent on the parental origin of the reporter X chromosome. Fluorescence in embryos carrying a maternally-inherited *Hprt*$^{\text{DsRed-Express}}$ X chromosome was detectable by microscopy in late two-cell embryos, while mKate2 fluorescence was observed from the late morula/very early blastocyst stage (beginning of cavitation, Figure 3.3A).

Onset of fluorescence by at least the later stages of preimplantation development in both strains is advantageous, as it allows for easy screening for embryos carrying the reporter chromosome. This could be of use in selecting embryos for implantation into pseudopregnant females if a researcher wanted to ensure all pups born carried the reporter chromosome, or if wanting to generate ES cells for *in vitro* work with these models. The only limitation for the *Hprt*$^{\text{DsRed-Express}}$ mouse in regards to this is that this screening is only possible for embryos with a maternally-inherited *Hprt*$^{\text{DsRed-Express}}$ X chromosome, as the paternal X chromosome is specifically silenced during preimplantation development as discussed in Section 1.1.4. However, sex selection of preimplantation *Hprt*$^{\text{DsRed-Express}}$ embryos cannot be performed based on fluorescence, as male and female transgenic embryos are indistinguishable at this stage. This represents an advantage that the *Ddx3y*$^{\text{mKate2}}$ mouse has over the *Hprt*$^{\text{DsRed-Express}}$ strain.

While it was observed that the fluorescent reporter in the *Hprt*$^{\text{DsRed-Express}}$ mouse was detectable approximately three days earlier than that in the *Ddx3y*$^{\text{mKate2}}$ mouse, by E9.5, embryos carrying their respective fluorescent reporter chromosome from both strains were fluorescent. Both strains' male embryos exhibited a similar level of fluorescence across the entire embryo. Additionally, neither strain's E9.5 male embryo displayed variation in fluorescence across the various tissues present in the midgestation embryo, other than due to tissue density, which was similar between both strains' embryos. As predicted due to the presence of random XCI, female *Hprt*$^{\text{DsRed-Express}}$ embryos exhibited fluorescence at approximately half the intensity of the male embryos, also subject to tissue density. From these results, there was no apparent difference between the *Hprt*$^{\text{DsRed-Express}}$ and *Ddx3y*$^{\text{mKate2}}$ strains at E9.5, with the exception of XCI in fluorescent females in the *Hprt*$^{\text{DsRed-Express}}$ strain.

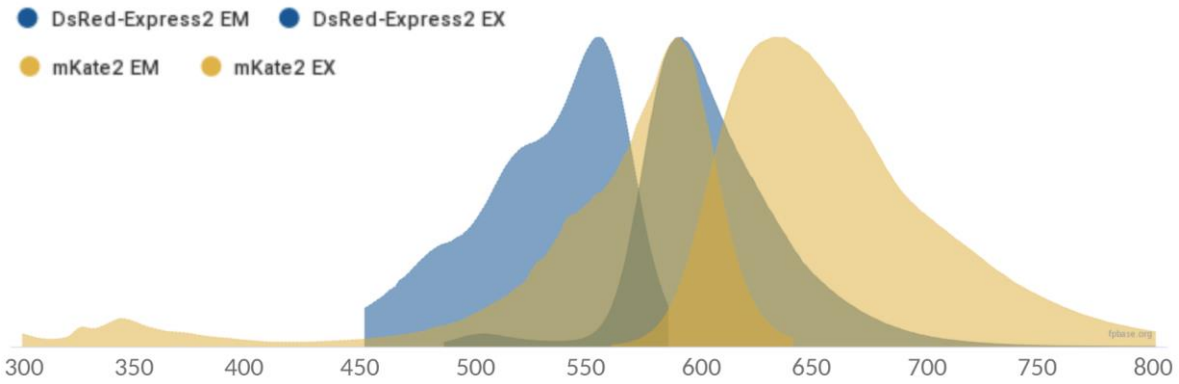

Figure 3.11 - Comparison of mKate2 and DsRed-Express Excitation/Emission Spectra
Image of overlaid mKate2 (blue) and DsRed-Express (yellow) excitation/emission spectra. Modified from imaged generated using FPBase[6] on 13/01/2020. This plot illustrates the different fluorescence emission spectra of these two different fluorescent proteins.

For both strains, screening for embryos carrying the reporter chromosome can be easily accomplished on the basis of fluorescence. In the case of the *Hprt*$^{DsRed\text{-}Express}$ strain, male and female embryos are clearly distinguishable from one another due to the difference in fluorescence intensity, while in the *Ddx3y*^{mKate2} strain, all fluorescent embryos are known to be male. This is advantageous, as removal of the need to screen for transgenic embryos and sex reduces the workload associated with experiments involving both the *Ddx3y*^{mKate2} and *Hprt*$^{DsRed\text{-}Express}$ mouse strains.

Table 3.4 - Comparison of *Ddx3y*^{mKate2} and *Hprt*$^{DsRed\text{-}Express}$ Mouse Strains

	***Ddx3y*^{mKate2}**		***Hprt*$^{DsRed\text{-}Express}$**	
Fluorescence in preimplantation development	Yes - beginning of cavitation (Figure 3.3A)		Yes - from late 2-cell (maternally-inherited only) *note, persistence of DsRed-Express fluorescence in wild type embryos from oocyte* (Figure 3.8A)	
Fluorescence at midgestation	Yes - across whole embryo (Figure 3.3B)		Yes - across whole embryo in both sexes, males more fluorescent than females (Figure 3.9)	
	Six-Week-Old (Figure 3.3D)	**One-Year-Old** (Figure 3.7)	**Six-Week-Old Male** (Figure 3.10)	**Six-Week-Old Female** (Figure 3.10)
Heart	Very High	Moderate	High-Moderate	Moderate, Non-Uniform
Gonads	High	Low	(Testes) Very High	(Ovaries) High
Liver	High	Absent	High	Moderate, Mottled
Eyes	High	Low	Moderate	Moderate, Non-Uniform
Brain	Moderate	Low	Low	Very Low
Kidney	Moderate	Low	Moderate	Low-Moderate, Slightly Mottled
Lungs	Moderate	Absent	Low-Moderate	Low, Mottled
Spleen	Absent	Absent	Very Low	Extremely Low, Mottled
Abdominal Fat	Moderate	N/A	Low-Moderate	Low
Visceral Fat	N/A	N/A	Extremely High	Very High, Mottled
Fluorescence was uniform across organ unless otherwise stated				

One major difference between the creation of the *Hprt*$^{DsRed\text{-}Express}$ and *Ddx3y*^{mKate2} strains was the chromosome selected to generate each reporter chromosome. While both of these models were created by transgene cassette insertion into a sex chromosome, the X and Y chromosomes are different (Section 1.1.2). Most notably is the effect on inheritance, with the Y chromosome only able to be transmitted father to son, while the X chromosome can be transmitted by either parent and inherited by both sexes (father to daughter, mother to both son and daughter).

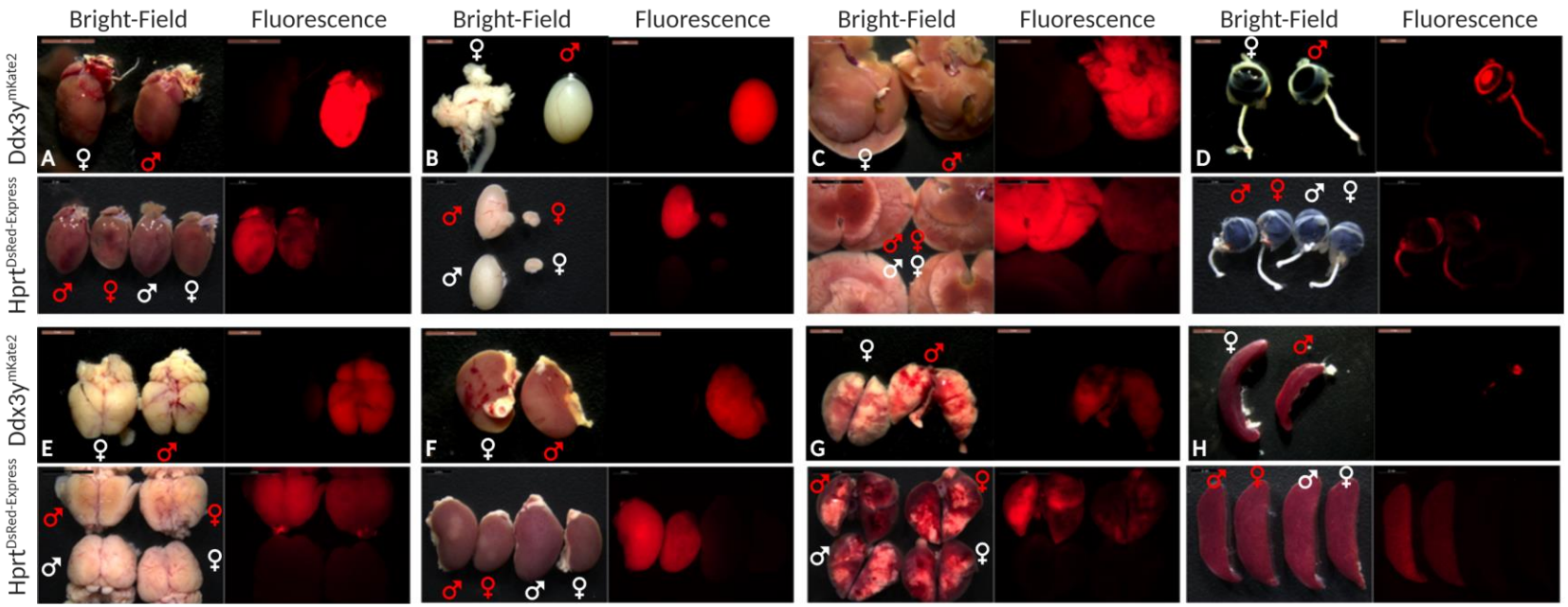

Figure 3.12 - Comparison of *Hprt*$^{\text{DsRed-Express}}$ and *Ddx3y*$^{\text{mKate2}}$ Organ Fluorescence at Six Weeks of Age

Side-by-side comparison of the fluorescence of *Ddx3y*$^{\text{mKate2}}$ (top images, from Figure 3.3D) and *Hprt*$^{\text{DsRed-Express}}$ mice at six weeks of age (bright-field left, fluorescence right, from Figure 3.10). Organs examined were the heart (A), the gonads (B), the liver (C), the eyes (D), the brain (E), the kidneys (F), the lungs (G) and the spleen (H). In the *Hprt*$^{\text{DsRed-Express}}$ strain, female organs exhibited approximately half the fluorescence intensity as male tissues. The *Ddx3y*$^{\text{mKate2}}$ heart was more intensely fluorescent than the heart of either sex of *Hprt*$^{\text{DsRed-Express}}$ mice, while the liver of males from both sexes exhibited similarly high fluorescence. The fluorescence observed in male tissues of both strain was similar in the gonads, brain and kidney. The spleen from both sexes of the *Hprt*$^{\text{DsRed-Express}}$ strain were both fluorescent, in comparison to the non-fluorescent spleen of the *Ddx3y*$^{\text{mKate2}}$ male.

As noted in the *Hprt*$^{DsRed\text{-}Express}$ results (Section 3.2.2), the post-implantation and adult X*Hprt*$^{DsRed\text{-}Express}$X (heterozygous carrier) female *Hprt*$^{DsRed\text{-}Express}$ mouse undergoes random XCI in all cells, transcriptionally silencing one of the X chromosomes. This had clear effects on the fluorescence intensity in female *Hprt*$^{DsRed\text{-}Express}$ tissues. Males, conversely, do not experience XCI, due to only carrying a single X chromosome; instead their single X chromosome is active in every cell. In the *Hprt*$^{DsRed\text{-}Express}$ strain, despite the difference in fluorescence intensity between the sexes, the relative differences between the organs of each sex followed the same trend

As males of both strains were hemizygous for their respective reporter chromosome, male *Hprt*$^{DsRed\text{-}Express}$ mice were considered the most appropriate comparison for the *Ddx3y*^{mKate2} mouse. This removed the impact of non-uniform fluorescence observed in the female *Hprt*$^{DsRed\text{-}Express}$ samples in the comparison, as this was due to XCI rather than a feature of the DsRed-Express transgene expression. Therefore, the following comparison discusses the differences between the *Hprt*$^{DsRed\text{-}Express}$ and *Ddx3y*^{mKate2} male organs. The fluorescence of the *Hprt*$^{DsRed\text{-}Express}$ female organs relative to the male *Hprt*$^{DsRed\text{-}Express}$ organs is summarised in Table 3.3 and Figure 3.12.

In both the *Ddx3y*^{mKate2} and *Hprt*$^{DsRed\text{-}Express}$ males, the fluorescence from the relevant reporter chromosome was moderate to high in the majority of organs (Figure 3.12). With the exception of the *Ddx3y*^{mKate2} spleen, all organs examined exhibited some degree of fluorescence. While there was not a complete correlation between the expression profile of the endogenous genes (*Hprt*, refer to Figure 3.4; *Ddx3y*, refer to Figure 3.2). This finding reinforced the choice of insertion loci for each reporter mouse strain. The loci chosen for each were selected due to the genes' broad expression profiles, as these were predicted to be unlikely to cause repression of the fluorescent reporter.

Despite the broad fluorescence present in nearly all of the *Hprt*$^{DsRed\text{-}Express}$ and *Ddx3y*^{mKate2} organs examined, there were differences in the fluorescence intensity of the same organ between the strains, as well as differences in the relative intensities between the organs of each strain (Figure 3.12).

In the six-week-old *Ddx3y*^{mKate2} mouse, there was a moderately high level of fluorescence intensity across many organs. The heart, testis, eyes and liver were highly fluorescent, while the brain, kidney and lungs exhibited moderate fluorescence intensity (Figure 3.12). The *Ddx3y*^{mKate2} heart (Figure 3.12A), in particular, had extremely high fluorescence, far more intense than any other organ in either the *Ddx3y*^{mKate2} or *Hprt*$^{DsRed\text{-}Express}$ strains, with the possible exception of the *Hprt*$^{DsRed\text{-}Express}$ visceral fat. However, as this tissue was not assessed in the original assessment of the *Ddx3y*^{mKate2} mouse, the fluorescence of this cannot be meaningfully compared between the strains.

Of the whole organs, the liver in both strains (Figure 3.12C) exhibited a similarly high level of fluorescence intensity, as did the testes (Figure 3.12B). The *Hprt*$^{DsRed\text{-}Express}$ brain and eye exhibited

a slightly lower fluorescence intensity relative to their *Ddx3y*^{mKate2} counterparts (Figures 3.12E and D, respectively). The difference in fluorescence intensity between the *Ddx3y*^{mKate2} and *Hprt*$^{DsRed\text{-}Express}$ heart (Figure 3.12A), however, was the most stark, with the *Hprt*$^{DsRed\text{-}Express}$ being substantially less fluorescent. The *Ddx3y*^{mKate2} lungs, however, were noticeably dimmer than the *Hprt*$^{DsRed\text{-}Express}$ lungs (Figure 3.12G). Another significant difference observed between the organs of these two strains was in the fluorescence of the spleen (Figure 3.12H). The *Ddx3y*^{mKate2} spleen was wholly non-fluorescent, while the spleen of both *Hprt*$^{DsRed\text{-}Express}$ sexes exhibited fluorescence, even in the presence of XCI in the female.

These differences in the fluorescence of adult organs between the *Ddx3y*^{mKate2} and *Hprt*$^{DsRed\text{-}Express}$ mouse strains demonstrated that, although both insertion loci were selected for their broad expression, there were indeed differences in the fluorescence from the transgene in each model. Interestingly, these differences did not necessarily correlate with the gene expression of the endogenous locus. For example, the *Ddx3y*^{mKate2} liver was highly fluorescent (Figure 3.3D), but *Ddx3y* gene expression data (refer to Figure 3.2) shows little to no expression in this organ. Likewise, the data on *Hprt* expression (Figure 3.4) indicates low to moderate expression of the gene in the liver, but this organ was the most intensely fluorescent organ examined in the *Hprt*$^{DsRed\text{-}Express}$ mouse (Figure 3.10).

As the fluorescent reporter gene in each strain was inserted under control of the strong synthetic CAG promoter[174], it would be reasonable to predict that the difference in the expression of the transgene (here, assessed indirectly by fluorescence intensity) was due to the locus of the reporter gene. This encompasses both the chromosome carrying the gene, X chromosome compared to Y chromosome, as well as the chromatin environment of the endogenous gene locus, *Hprt* versus *Ddx3y*. In order to further explore this, it would be advisable to perform gene expression analysis specific to the *DsRed-Express* and *mKate2* transgenes in each specific tissue to better determine the effect of the loci on the expression of these reporter genes.

An advantage of the *Ddx3y*^{mKate2} mouse strain over the *Hprt*$^{DsRed\text{-}Express}$ strain was not requiring genotyping of animals, as the reporter Y chromosome was known to be carried by all males (and no females) in the strain. The *Hprt*$^{DsRed\text{-}Express}$ mouse, on the other hand, carried its transgene on an X chromosome that can be inherited in both sexes, so all offspring of a carrier parent must be genotyped to identify transgenic carriers. This is an increased workload in the *Hprt*$^{DsRed\text{-}Express}$ strain relative to the *Ddx3y*^{mKate2} strain.

The characterisation of the *Hprt*$^{DsRed\text{-}Express}$ mouse performed in this study did not assess changes in fluorescence in advanced age, as was performed for the *Ddx3y*^{mKate2} characterisation. It is recommended that such an assessment be performed in order to fill this gap in the stand-alone characterisation of the *Hprt*$^{DsRed\text{-}Express}$ mouse, and hence inform on the utility of this mouse model as a tool for researchers. As was recommended in Section 3.3.1 for the *Ddx3y*^{mKate2} strain characterisation, this would be best performed in an age series of increasing mouse ages, in order

to determine if and when the fluorescence changes with age.

This lack of assessing the change in fluorescence with in the *Hprt*$^{DsRed\text{-}Express}$ mouse also resulted in an inability to compare the decline in mKate2 fluorescence intensity at one year of age to another fluorescent reporter, particularly one on the same strain background. As was speculated in Section 3.3.1, it is reasonable to hypothesise that the decline in mKate2 fluorescence in the aged *Ddx3y*^{mKate2} organs was the result of age-related repression of the Y chromosome. The X chromosome carries genes with metabolic and housekeeping functions, and therefore would not be likely to become repressed with age. This was a notable difference in selection of the X chromosome as opposed to the Y chromosome for generating a reporter chromosome, particularly when considering use in longevity experiments.

However, despite this age-related effect on the Y chromosome, the primary advantage of the *Ddx3y*^{mKate2} mouse over the *Hprt*$^{DsRed\text{-}Express}$ mouse was, in fact, the selection of the Y chromosome. The Y chromosome is not essential to viability in a cell or an animal, contrasting to the X chromosome. As such, the Y chromosome can be lost from cells, or from the entire mouse, without compromising survival. Additionally, the hemizygous nature of the Y chromosome in males was advantageous, as this chromosome may therefore be assayed for in a presence/absence manner, rather than needing to determine chromosome copy number. These make the *Ddx3y*^{mKate2} Y chromosome a superior choice for use in chromosome instability experiments.

When considering reporter X chromosomes such as *Hprt*$^{DsRed\text{-}Express}$, however, more variables must be accounted for. In males, as the X chromosome is also hemizygous, it may also be assayed for in a presence/absence fashion, like the Y chromosome. However, due to the essential nature of the X chromosome for viability, a reporter X chromosome in a male would not be able to be lost from a cell or organism without resulting in lethality. This is a significant difficulty in using the *Hprt*$^{DsRed\text{-}Express}$ X chromosome in chromosome instability research.

This issue may be avoided through use of female mice and samples, as they carry two X chromosomes, and loss of one X chromosome due to instability would not result in lethality. However, the use of females in this regard poses new difficulties. The primary complication is the effect of XCI in female cells. As only one X chromosome is active in a given cell, loss of the reporter X chromosome cannot easily be assayed for in a presence/absence fashion based on mKate2 fluorescence, as the reporter chromosome may simply be inactivated, not lost. Assaying for chromosome loss on the basis of lack of fluorescence would still be possible, by sorting for non-fluorescent cells, then examining their karyotype to determine whether the reporter X chromosome had been lost or merely inactivated. However, this laborious method is contrary to the desired function of a reporter such as the *Ddx3y*^{mKate2} Y chromosome. This again highlights the strength of using a reporter Y chromosome as a tool for chromosome instability research.

The *Hprt*$^{DsRed\text{-}Express}$ mouse line could be of use in a double reporter line, in which both options for an X chromosome carry a fluorescent reporter, for instance, the *DsRed-Express* gene of the *Hprt*$^{DsRed\text{-}Express}$ X chromosome, and a *Green Fluorescent Protein* (*GFP*) gene on the alternate chromosome. This would result in males that fluoresced either red or green, depending on which X chromosome was inherited, and females which would exhibit mosaic fluorescence, with approximately 50% of cells fluorescing red and the other 50% fluorescing green. This may be of use when assessing the state of stem cells to determine whether they are pluripotent stem cells (PS cells) distinct from epiblast stem cells (EpiS cells), or appropriately reprogrammed induced PS cells (iPS cells), as both PS cells and iPS cells show X chromosome reactivation such that both X chromosomes are active in a given cell[225]. In a double reporter system such as the one described above, X$^{Hprt\ DsRed\text{-}Express}$X^{GFP} PS cells would simultaneously fluoresce both red and green, indicating that both X chromosomes are active. This has been shown to be a marker of these cells being naive[225,226], needed for these stem cells to be used in chimera generation[225]. In Kobayashi et al (2016)[225], this was demonstrated using X chromosomes carrying an *mCherry* and *mGFP* gene, respectively.

Overall, while both the *Hprt*$^{DsRed\text{-}Express}$ mouse strain and the *Ddx3y*^{mKate2} mouse strain have great potential to be used in a variety of research applications, the *Ddx3y*^{mKate2} strain is most applicable to chromosome instability research, the purpose for which it was created.

3.3.3. The *Ddx3y*^{mKate2} Strain as a Tool for Chromosome Instability Research

The *Ddx3y*^{mKate2} reporter Y chromosome was created to be a tool for use in chromosome instability research. The choice to target the Y chromosome for insertion of the fluorescent reporter transgene, *mKate2*, was due to the Y chromosome being hemizygous. This resulted in the reporter Y chromosome being able to be assayed for in a presence/absence fashion, rather than quantifying the dose of the reporter, as would be the case with autosomes, and in females, the X chromosome (discussed in Section 3.3.2). Additionally, the mouse Y chromosome is small and not essential for viability in either cells or in the mice themselves. Therefore, its loss due to chromosome instability would not adversely affect the model being used, and instead may be used as an indicator of the presence of chromosome instability.

As the reporter gene codes for the fluorescent protein mKate2, the *Ddx3y*^{mKate2} mouse strain has been assessed in terms of detectable mKate2 fluorescence, as fluorescence was intended to provide an easy method of assessing whether the reporter Y chromosome had been lost due to instability. This mouse strain was generated as a tool to provide cells and tissues of various types for research. Further to this, the characteristics of the fluorescence in this mouse model was assessed to create a baseline to inform researchers selecting a models for use.

Previous characterisation on the *Ddx3y*^{mKate2} mouse strain had identified the onset of mKate2 fluorescence in early development, and persistence of this fluorescence into sexual

maturity. This study has extended this characterisation to show that the presence and intensity of mKate2 fluorescence is dependent on cell type, and the overall intensity of fluorescence in whole organs declines in advanced age. While this age-related decline is less than ideal for a reporter chromosome for use in assessing changes in chromosome instability with age, the broad fluorescence observed earlier in life, including during embryogenesis, remains a strength of this mouse strain.

Additionally, the examination of *Ddx3y*^{mKate2} organs several hours post-mortem revealed that the fluorescence from the mKate2 protein can persist for an extended period of time under chilled conditions in a tissue-dependent manner. The heart, in particular, exhibited persistence of fluorescence, still being clearly mKate2-positive out to 8.5 to 9 hours post-mortem. However, all organs examined experienced a marked decline in fluorescence intensity as rapidly as within five hours. This limits the time frame within which the desired tissues may be harvested from the *Ddx3y*^{mKate2} mouse, potentially having bearing on the planning of experiments involving this strain.

In particular, the high intensity of fluorescence in the embryonic stages and in many organs of the young adult mouse are highly promising for use of the *Ddx3y*^{mKate2} mouse strain in research. The mKate2 fluorescence in the blastocyst is advantageous when needing to screen for sex in preimplantation embryos, a stage in which the sexes are indistinguishable. This can be of use when aiming to derive embryonic stems (ES) cells. These *Ddx3y*^{mKate2} ES cells could then be used in *in vitro* chromosome instability assays, in which the loss of the *Ddx3y*^{mKate2} reporter Y chromosome could be assayed for based on fluorescence, such as with flow cytometry. This could also be applied to cells derived from fluorescent midgestation *Ddx3y*^{mKate2} embryos, such as primary mouse embryonic fibroblasts (PMEFs). These cells have also been shown to be mKate2-positive[5], and as such would also be amenable to *in vitro* assays and fluorescence-based cell sorting.

The early onset of fluorescence in male *Ddx3y*^{mKate2} embryo may also be of use as a tool for generating new genetically modified mouse strains. As only male (XY) blastocysts in this strain are fluorescent, female (XX) embryos are easily screened for, and these XX embryos may then be injected with XY ES cells to generate chimeras. As XX spermatogenic cells fail to complete meiosis[227], the XX blastocyst-derived cells would be unable to contribute to the male germline, of the chimeric mouse, while the (genetically modified) XY ES cell-derived cells would be able to generate functional sperm. This is vital in the generation of a new mouse line, as using XY (mKate2-positive) blastocysts, would result in chimeric offspring in which both the ES cell-derived cells and blastocyst-derived cells would be able to contribute to the germline; an undesirable outcome when generating a new strain.

Beyond the embryonic stage, the *Ddx3y*^{mKate2} mouse holds other advantages for use in research. Several of the organs examined exhibited moderate to high levels of mKate2 fluorescence at six weeks of age, and, as demonstrated in the IHC staining of different tissues, complex structures can contain cell populations with high mKate2 signal. These organs and cells may be of use in

assessments of *in vivo* chromosome instability, such as use of carcinogens. In such an experiment, a highly fluorescent organ or cell type could be tracked for loss of the *Ddx3y*^{mKate2} restorer Y chromosome following treatment of the animal with a substance suspected to induce cancer through causing chromosome segregation defects. This kind of experiment could also be replicated *in vitro* with cells derived from highly fluorescent organs, for example cultured cardiomyocytes derived from the highly mKate2-positive heart.

Another *in vivo* chromosome instability experiment with the *Ddx3y*^{mKate2} mouse could be through the combination of the *Ddx3y*^{mKate2} reporter Y chromosome with an inducible mutation or conditional knockout. For example, it is possible to genetically engineer a mouse in which a certain cell type removes or 'knocks out' a gene from its genome in response to the developmental program of the cell. This can be achieved by flanking the gene of interest with *loxP* sites ('floxing' the allele) in a mouse line, and crossing that mouse line with a line in which *Cre* recombinase is expressed only within a specific cell type upon treatment of the mouse with a particular substance such as doxycycline[228]. The Cre recombinase will then excise the sequences between the *loxP* sites, removing the floxed allele and knocking out the gene. If this strategy were applied to, for example, a gene involved in the spindle assembly checkpoint[229], administering doxycycline would result in an increase in chromosomal missegregation events only in cells in which *Cre* was active[229]. Combining the *Ddx3y*^{mKate2} reporter Y chromosome with such a model which targeted a cell type known to be highly mKate2 fluorescent would allow for an easy method of assaying chromosome instability in the given cell population.

Chromosome instability is highly associated with tumours[229]. Inducing chromosome instability in highly fluorescent *Ddx3y*^{mKate2} cells, such as with a carcinogen or through knocking out a gene essential for mitosis, can result in cells capable of metastasis. Metastasis is the ability of tumour cells to migrate from their tissue of origin to invade other areas of the body[230]. Metastatic cells positive for mKate2 fluorescence could be transplanted into an immunosuppressed mouse such as a nude mouse[231], in which all cells from the host mouse are non-fluorescent. The mKate2-positive metastatic cells could then be easily identified following metastasis, thus tracing the course of the chromosomally unstable cells through the host body. This would be highly informative as to the effect of the given mutation/s on disease course.

A characteristic of the *Ddx3y*^{mKate2} strain which is both advantageous and disadvantageous is that this reporter chromosome is a Y chromosome. There are two main advantages of using a Y chromosome as a reporter chromosome: the first is that it may be assayed for in a presence/absence manner due to its hemizygosity. Second, its non-essential nature is beneficial as its loss from cells or organisms will not result in lethality. However, the main disadvantage of a reporter Y chromosome is that this mouse model is restricted to only male mice and their cells/tissues. As there is a growing body of evidence of sex differences in cancer development and features[232], which may arise from differences in the presence of instability, it is inadvisable to exclude XX individuals from

chromosome instability research.

Additionally, a limitation of the current characterisation of the *Ddx3y*^{mKate2} mouse is the lack of proteomic and gene expression data. Instead, fluorescence was examined here as an indicator of expression. It would be advisable to assess these parameters in future work, in order to better compare the level of the reporter transgene within different cell types. These analyses were not performed in this study, as it aimed to characterise the pattern of fluorescence in the *Ddx3y*^{mKate2} mouse as a baseline for the strain, and to highlight tissues which may of be of further interest for researchers.

Overall, the *Ddx3y*^{mKate2} reporter strain has many strengths which result in this model being highly useful to chromosome instability research. The characterisation of this mouse strain, both previously[2] and in this study, form a solid foundation of strengths upon which future researchers can build with specific chromosome instability experiments.

Chapter 4: Modelling the *Ddx3y*^{mKate2} Reporter Y Chromosome on Known Instability Backgrounds

4.1. Introduction

Completion of the characterisation of the *Ddx3y*^{mKate2} mouse (Chapter 3) indicated that this strain is highly amenable for use as a tool in chromosome instability research. However, this study aimed to not only finalise the characterisation of this model, but to demonstrate how it may be used in such research.

Further to this, two known chromosome instability genetic backgrounds were selected, the *Trp53* knockout[4] background (refer to Section 4.1.1) and *Cenpagfp*[29] fusion knock-in background (refer to Section 4.1.2), upon which to model the use of the *Ddx3y*^{mKate2} reporter Y chromosome. To achieve this, the *Ddx3y*^{mKate2} reporter Y chromosome was crossed onto each of these backgrounds. The resulting intercrossed strains were assessed for loss of fluorescence in experiments designed to maximise chromosome instability.

This chapter describes the experiments using the *Ddx3y*^{mKate2}/*Trp53* knockout and *Ddx3y*^{mKate2}/*Cenpagfp* knock-in intercrossed strains to examine the *Ddx3y*^{mKate2} reporter Y chromosome in the context of chromosome instability. This was performed to demonstrate the utility of mKate2 fluorescence from the *Ddx3y*^{mKate2} Y chromosome as a reporter for chromosome loss from instability.

4.1.1. *Trp53* Knockout Background

The tumour suppressor gene *Trp53* (Transformation Related Protein 53[192]) is often referred to as the 'guardian of the genome'[233,234], due to its vital role in preventing proliferation of abnormal cells. It achieves this by inducing growth and cell cycle arrest, DNA repair, senescence and/or apoptosis in affected cells[235,236].

Absence of Trp53 has been shown to increase aneuploidy and genome instability[237,238], with a strong association with cancer development. Indeed, it has been reported that the *TRP53* gene is mutated in approximately half of all human cancers[233,235,238]. It has been indicated that cells which carry two null *Trp53* mutations (*Trp53*$^{-/-}$), and hence do not produce Trp53 protein, experience a disruption to the tetraploidy G1/S (Gap phase 1/Synthesis phase) checkpoint[237], leading to

aneuploidy[237,238].

A targeted knockout of the *Trp53* gene in mice was generated by Jacks and colleagues, reported in a 1994 paper: "Tumor spectrum analysis in *Trp53*-mutant mice"[4]. Briefly, exons 2 to 6 of the coding sequence of the *Trp53* gene were replaced by targeted insertion of a neomycin resistance gene[4], replacing approximately 40% of the coding sequence[4]. The resulting allele was shown to result in the absence of functional Trp53 protein, confirming it to be a null allele[4], henceforth referred to in this project as *Trp53*$^{-}$ (the wild-type *Trp53* allele to be referred to as *Trp53*$^{+}$).

This null allele resulted in a greatly increased propensity for mice to develop a spectrum of tumours[4], with the types and proportions of tumours differing between heterozygous (*Trp53*$^{+/-}$) and homozygous (*Trp53*$^{-/-}$) knockout mice. *Trp53*$^{+/-}$ mice developed a variety of tumours from the approximately nine to 10 months of age, primarily due to loss of heterozygosity in the tumours[4], in which the wild-type allele was lost, resulting in those tumour tissues being null for *Trp53*[4].

In *Trp53*$^{-/-}$ mice, however, tumours developed much earlier, from approximately three months of age onwards[4]. These tumours were predominantly lymphomas (71%), usually of the thymus[4]. Despite being initially healthy, the majority of *Trp53*$^{-/-}$ mice died within the first six months of life, with 100% either having died or been euthanised by nine months of age[4].

As *Trp53*$^{-/-}$ mice experience karyotypic anomalies[233,237,239], the *Ddx3y*^{mKate2} chromosome was crossed onto the *Trp53* knockout (KO) background to generate the *Ddx3y*^{mKate2}/*Trp53* KO strain. This intercrossed strain was then used for assessing the utility of this reporter chromosome on a chromosomally unstable background in embryogenesis (Section 4.2.1.1.1), primary mouse embryonic fibroblast (PMEF) cell culture (Section 4.2.1.1.2), and in the cells derived from the tumour-prone thymus in adult mice on this background (Section 4.2.1.2), with a focus on the *Ddx3y*^{mKate2}/*Trp53*$^{-/-}$ mice.

4.1.2. *Cenpagfp* Background

To provide another model demonstrating that the *Ddx3y*^{mKate2} reporter Y chromosome may be of use as a tool in chromosome instability research, the reporter chromosome was crossed onto the *Cenpagfp* background.

The *Cenpagfp* transgene and resulting carrier strain were developed by Kalitsis and colleagues, described in a 2003 paper: "Partially functional Cenpa-GFP fusion protein causes increased chromosome missegregation and apoptosis during mouse embryogenesis"[29]. To create the *Cenpagfp* allele, the stop codon of the *Cenpa* (Centromere Protein A, Section 1.1.1.1) gene was replaced with the coding sequence for green fluorescent protein (GFP), generating a fusion protein in which GFP is attached to the C-terminus of the essential centromere protein, Cenpa[29]. In this

project, the wild-type *Cenpa* allele was designated as *Cenpa*$^{+}$, and the *Cenpagfp* fusion allele as *Cenpa*^{g}.

This fusion protein was found to not exert a deleterious effect in heterozygous (*Cenpa*$^{+/g}$) animals, which were observed to be healthy and fertile[29]. However, *Cenpagfp* homozygotes (*Cenpa*$^{g/g}$) experienced embryonic lethality[29]. At midgestation, *Cenpa*$^{g/g}$ embryos were present in Mendelian proportions (25%) up until E9.5, at which point they were observed to be smaller and highly malformed relative to their heterozygous and wildtype littermates[29]. Beyond E9.5, *Cenpa*$^{g/g}$ embryos then decline rapidly in proportion from E10.5, becoming completely absent by E12.5[29].

Cytological examination of cells from *Cenpa*$^{g/g}$ embryos identified massive chromosome segregation errors and high rates of apoptosis[29]. These segregation errors included lagging chromosomes, resulting in a 61% rate of aneuploidy, primarily due to chromosome loss, with 34% of *Cenpa*$^{g/g}$ cells having lost one chromosome, as well as the generation of micronuclei[29].

It was predicted that the large Cenpagfp fusion protein (43.2 kDa compared to native mouse Cenpa protein, 17 kDa[29]) experiences steric hindrance when attempting to bind to centromeres[29]. However, due to the lack of adverse effect in homozygotes, it was hypothesised that this steric hindrance was compensated for in the *Cenpa*$^{+/g}$ embryos and mice, suggesting that the defects in the *Cenpa*$^{g/g}$ embryos was due to absence of wild-type Cenpa[29].

As *Cenpa*$^{g/g}$ embryos have been shown to be highly chromosomally unstable, being particularly prone to chromosome loss due to segregation errors[29], this background was selected for use in modelling the utility of the *Ddx3y*^{mKate2} chromosome. To achieve this, the *Ddx3y*^{mKate2} reporter Y chromosome was crossed onto the *Cenpagfp* background, generating the intercrossed *Ddx3y*^{mKate2}/*Cenpagfp* strain. The aim of this intercross was to obtain male *Ddx3y*^{mKate2}/*Cenpa*$^{g/g}$ embryos, from which cells could be derived for use in *in vitro* chromosome instability assays.

4.2. Results

4.2.1. Modelling the *Ddx3y*^{mKate2} Chromosome on the *Trp53* Knockout Background

The *Trp53* knockout (KO) background was selected for modelling the *Ddx3y*^{mKate2} reporter chromosome because of its reported high incidence of aneuploidy due to chromosome instability[237]. *In vitro* culture of *Trp53*$^{-/-}$ primary mouse fibroblasts with serum-containing media has been shown previously to result in massive changes to the ploidy of these cells[238]. Interestingly, culturing these cells with serum-free chemically-defined culture media was observed to not only preserve their karyotype, but also their mitotic potential, with these primary cells becoming functionally immortal

in culture[238].

In the *Trp53* KO mouse strain[4], a high incidence of tumours has been reported in the *Trp53*$^{-/-}$ mice due to the instability present in this genotype[4]. In the context of *Trp53*$^{-/-}$ mice, the target *Trp53* genotype for this study, these tumours were predominantly lymphomas affecting the thymus[4]. Collection of the tumour-prone thymus from *Ddx3y*^{mKate2}/*Trp53*$^{-/-}$ mice (Section 4.2.1.2), as well as *Ddx3y*^{mKate2}/*Trp53*$^{-/-}$ embryos and PMEFs (Sections 4.2.1.1.1 and 4.2.1.1.2, respectively), were anticipated to yield mosaic cell populations, containing a variety of different karyotypes, particularly affecting the *Ddx3y*^{mKate2} Y chromosome.

It was predicted that the small, non-essential nature of the *Ddx3y*^{mKate2} Y chromosome would result in its loss from these unstable cells, and consequently, there would be a loss of mKate2 fluorescence. This could then be detected by fluorescence activated cell sorting (FACS), for example.

4.2.1.1. Modelling the *Ddx3y*^{mKate2} Chromosome in *Trp53*$^{-/-}$ Embryos and Embryo-Derived Cells

As absence of Trp53 has been associated with karyotypic abnormalities[237], it was essential to confirm whether the *Ddx3y*^{mKate2} reporter Y chromosome was stable through embryogenesis, and not lost before birth. PMEFs derived from *Ddx3y*^{mKate2}/*Trp53* KO embryos were also used for *in vitro* modelling on this background.

4.2.1.1.1. The *Ddx3y*^{mKate2} Reporter Chromosome is Stable in Embryogenesis in the Absence of Trp53

In order to confirm that the *Ddx3y*^{mKate2} reporter chromosome was not prone to loss in embryogenesis in the absence of Trp53, midgestation embryos between E10.5 and E12.5 were collected from *Ddx3y*^{mKate2}/*Trp53* heterozygous crosses. Figure 4.1A contains representative images of embryos from each sex/genotype combination. All male embryos exhibited mKate2 fluorescence, with no apparent difference in fluorescence intensity between the three *Trp53* genotypes. This demonstrated that sex could be determined by fluorescence stereomicroscopy in *Ddx3y*^{mKate2}/*Trp53* KO embryos. However, as there were no discernible morphological differences between the three *Trp53* genotypes, PCR genotyping was required to ascertain *Trp53* genotype for all embryos.

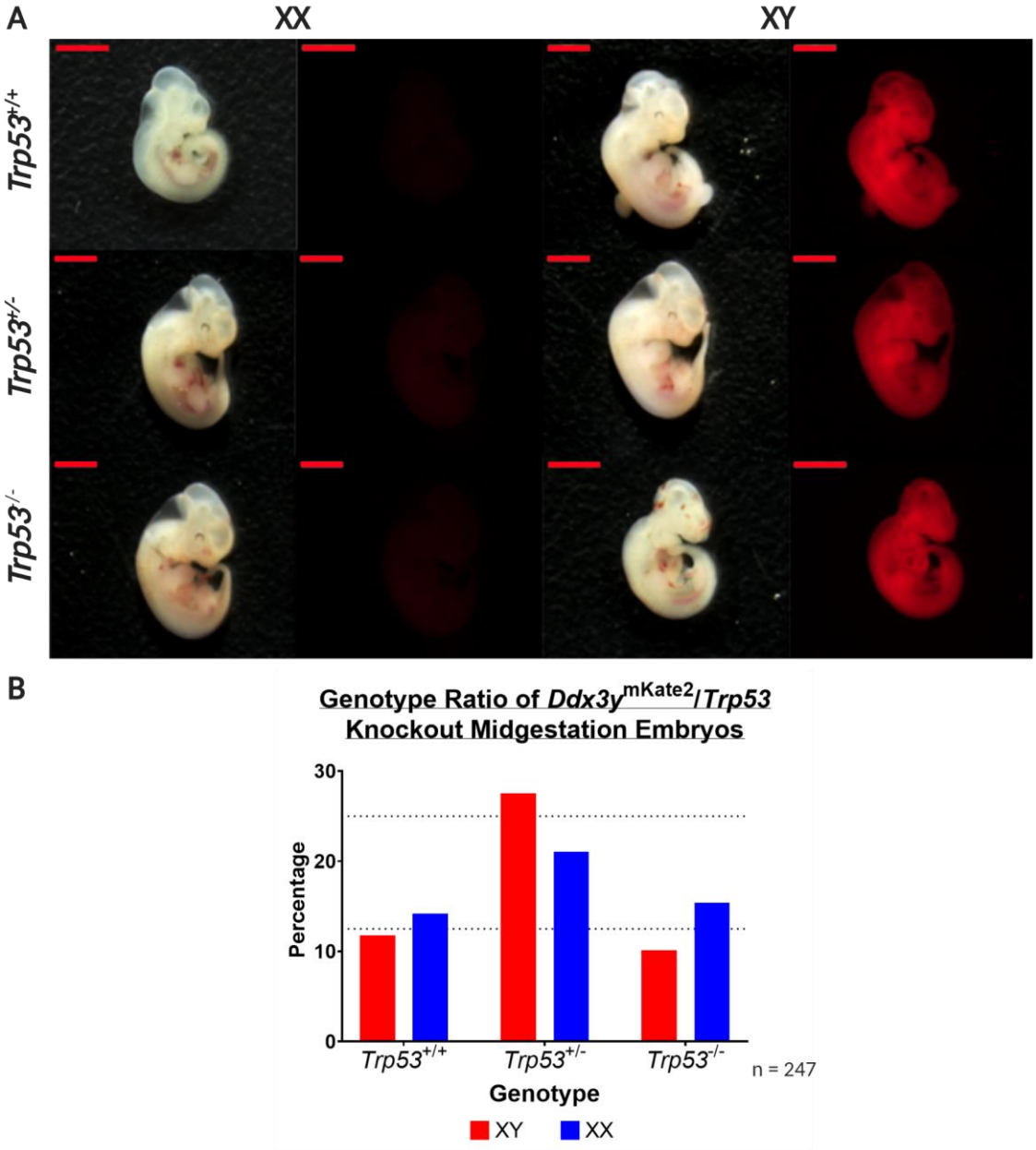

Figure 4.1 - Examination of mKate2 Fluorescence in *Ddx3y*^{mKate2}/*Trp53* KO Embryos

Embryos from heterozygous *Ddx3y*^{mKate2}/*Trp53* KO matings were collected between E10.5 and E12.5. (A) Representative mKate2 fluorescence (right) and bright-field (left) images of each of the sex/genotype combinations recovered from these litters. All male (XY) embryos were fluorescent, with no apparent difference in intensity between the genotypes, and all female (XX) embryos were non-fluorescent. (B) Distribution of sex/genotype combinations of embryos collected at midgestation. Dotted lines are 12.5% (expected percentage for *Trp53*$^{+/+}$ and *Trp53*$^{-/-}$ males and females, individually) and 25% (expected percentage for *Trp53*$^{+/-}$ males and females, individually). Scale bars are 2 mm (A).

As shown in Figure 4.1B, embryos of all sex/genotype combinations were present at approximately expected Mendelian proportions, with a 1:2:1 ratio of *Trp53*$^{+/+}$:*Trp53*$^{+/-}$:*Trp53*$^{-/-}$ in both sexes, with no sex bias. There was a slight sex skew in the *Ddx3y*^{mKate2}/*Trp53*$^{+/-}$ embryos, with a slight enrichment of females (27.5% compared to 21.1% male); however, this is likely a sampling effect, as the difference between the sexes was non-significant at $p > 0.9999$. As the focus of using the *Ddx3y*^{mKate2}/*Trp53* KO intercrossed strain was to model the use of the *Ddx3y*^{mKate2} reporter Y chromosome on a known instability background, all following work focused on mKate2-positive male (XY) embryos and PMEFs.

To determine whether there was a difference in the proportion of mKate2-positive cells between embryos of different *Trp53* genotypes that was not visually detectable by fluorescence stereomicroscopy, the cells from male *Ddx3y*^{mKate2}/*Trp53* KO embryos were assessed. The carcases of male embryos (n = 20 embryos) from heterozygous crosses were manually disaggregated and sorted by FACS into mKate2-positive and -negative populations (a representative sample sort plot is presented in Figure 4.2A). Again, there was a clear following of the 1:2:1 Mendelian ratio of the genotypes of this subset of embryos (4 *Trp53*$^{+/+}$ (20%) : 11 *Trp53*$^{+/-}$ (55%): 5 *Trp53*$^{-/-}$ (25%)).

It was found that there was no significant difference between the proportion of mKate2-positive cells obtained from male *Ddx3y*^{mKate2}/*Trp53* KO embryos of each of the three genotypes (Figure 4.2B), with the mean mKate2-positive proportion of each genotype lying between 50% and 65% (*Trp53*$^{+/+}$: 51.33 ± 17.96%, *Trp53*$^{+/-}$: 54.36 ± 7.33%, *Trp53*$^{-/-}$: 64.76 ± 14.20%, mean ± standard deviation (SD)). However, the range of values returned for individual embryos in the *Trp53*$^{+/+}$ and *Trp53*$^{-/-}$ genotypes (Figure 4.2B) showed more variation, as reflected in the SD of each cohort. In the *Trp53*$^{+/+}$ samples, the range of values was [24.40%, 61.30%], with the value of 24.40% being an outlier from the remaining samples. Removal of this outlier would result in the *Trp53*$^{+/+}$ samples' mean mKate2-positive proportion increasing to 60.30 ± 0.87%, [59.80%, 61.30%], a value with extremely low variation. The *Trp53*$^{+/-}$ embryos had no obvious outliers, with all values falling within the range [40.30%, 64.90%].

The *Trp53*$^{-/-}$ embryo samples, however, had a large range of values [44.10%, 78.70%], with no apparent outliers. This wide range of values was reflected in the large SD, 14.20%. While this does suggest greater variation in the proportion of cells that are mKate2-positive between individual *Trp53*$^{-/-}$ embryos, there was no significant difference between the *Trp53*$^{-/-}$ embryos' values and those from the other two genotypes. Therefore, it can be concluded that the *Ddx3y*^{mKate2} Y chromosome was stable in embryogenesis in the absence of Trp53.

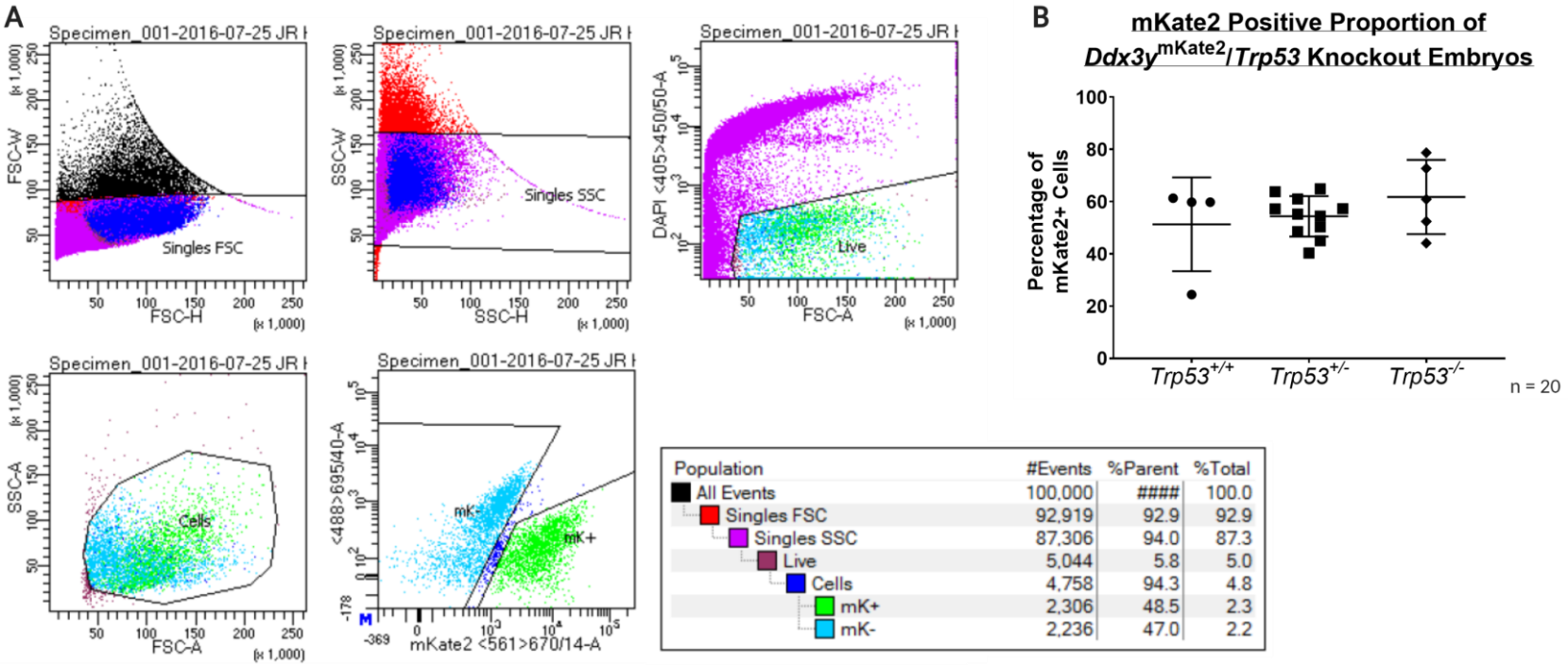

Figure 4.2 - Fluorescence-Activated Cell Sorting (FACS) of Male *Ddx3y*^{mKate2}/*Trp53* KO Embryos

(A) Example sort plot of male *Ddx3y*^{mKate2}/*Trp53* KO embryos, showing the gating strategy. Progressively gating for: "Cells" (separate from debris), "Single Cells", "Live Cells" (DAPI-negative), and into "mK+" and "mK-" (mKate2-positive and -negative, respectively). Percentages used in (B) and quoted in the text were derived from the "% Parent" column. (B) Graph depicting percentage of mKate2-positive cells derived from disaggregated midgestation male embryos. Each data point represents one embryo; data generated through fluorescence-activated cell sorting (FACS) analysis. There was no significant difference in mean proportion of mKate2-positive cells between each of the three *Trp53* genotypes.

4.2.1.1.2. *Ddx3y*^{mKate2}/*Trp53*$^{-/-}$ Primary Mouse Embryonic Fibroblasts Do Not Experience a Decline in mKate2-Positive Population Under Genotoxic Stress

As it was observed that there was no significant decline in mKate2-positive cells in *Ddx3y*^{mKate2}/*Trp53*$^{-/-}$ embryos compared to the *Ddx3y*^{mKate2}/*Trp53*$^{+/+}$ and *Ddx3y*^{mKate2}/*Trp53*$^{+/-}$ littermates, and hence no loss of the *Ddx3y*^{mKate2} Y chromosome, PMEFs were derived from XY (fluorescent) midgestation embryos of all three *Trp53* genotypes for use *in vitro*. These *in vitro* experiments were designed to increase the instability associated with the *Trp53*$^{-/-}$ background. It was anticipated that this increased instability may result in loss of the *Ddx3y*^{mKate2} reporter Y chromosome, due to its small size and non-essential nature, and that this loss could then be assayed for using FACS to detect a decrease in mKate2-positive PMEFs.

Trp53$^{-/-}$ PMEFs have been shown to be chromosomally unstable in long term culture when serum, such as foetal bovine serum (FBS), is included in the culture media[238], with karyotypic abnormalities appearing within three population doublings[238]. By the thirtieth population doubling, nearly all cells examined were found to have deviated from the normal diploid karyotype[238]. Of cells with abnormal chromosome numbers, at both the third and thirtieth population doubling, the predominant change from the diploid number was to approximately 80 chromosomes, and in some cases, as high as 100 chromosomes[238]. As the mouse diploid (2n) genome is spread amongst 40 chromosomes, a karyotype of 80 chromosomes represents tetraploidy (4n).

This was not unexpected, as mouse *Trp53*$^{-/-}$ fibroblasts have been observed previously to become aneuploid in culture[240], including tetraploid or even octoploid (8n)[240]. However, it has been shown that growing *Trp53*$^{-/-}$ PMEFs in chemically-defined serum replacement (serum-free conditions, 'SR') maintained a diploid karyotype far beyond 30 population doublings, with this observed up to the sixtieth population doubling[238]. The incidence of aneuploidy from *in vitro* culture in *Trp53*$^{-/-}$ PMEFs has been attributed to genotoxic stress, with the cells unprotected from these effects due to the absence of Trp53 protein[238].

In addition to the aneuploidy resulting from culture conditions, *Trp53*$^{-/-}$ mouse fibroblasts have also been demonstrated to be highly susceptible to aneuploidy induction by exposure to mitotic spindle poisons (MSPs), such as Colcemid or Nocodazole, for one or more days becoming 4n or greater[240-242]. Wild type fibroblasts exposed to such MSPs were occasionally observed to have a small population of octoploid cells[240]; however, this was significantly different from the large increase observed in polyploid *Trp53*$^{-/-}$ cells[240].

However, it is interesting to note that when *Trp53*$^{-/-}$ PMEFs under genotoxic stress were subjected to chromosome counts, there were often a variety of different chromosome numbers returned other than the more common 40 (low population doubling) or 80 (both low and high population doubling) chromosomes[238]. While these different counts tended to cluster around these

values, representing changes in ploidy resulting from failures in genome division, there were cells which had gained or lost one or more individual chromosomes[238]. A useful observation from this was observed in the low population doubling *Trp53*$^{-/-}$ PMEFs was that, at the third population doubling, approximately one fifth of metaphases had a chromosome count less than 40[238].

This indicates that, at least in the early stage of responding to genotoxic stress, while *Trp53*$^{-/-}$ PMEFs tend to accumulate chromosomes, including a second diploid genome to become 4n, these cells can also be prone to losing chromosomes. This was considered to be highly advantageous to the work modelling the *Ddx3y*^{mKate2} reporter Y chromosome on the *Trp53* KO background, as this suggested potential for this reporter Y chromosome to be lost from *Ddx3y*^{mKate2}/*Trp53*$^{-/-}$ PMEFs *in vitro*.

It was hypothesised that the *Ddx3y*^{mKate2} reporter Y chromosome may be lost, either at a low passage or a high passage, in *Ddx3y*^{mKate2}/*Trp53*$^{-/-}$ PMEFs cultured with FBS-containing media. To maximise the likelihood that loss of the reporter Y chromosome had occurred, high passage number *Ddx3y*^{mKate2}/*Trp53*$^{-/-}$ PMEFs were assessed for loss of mKate2 fluorescence. This was because these cells were predicted to not be selected against, due to the Y chromosome not being required for cell viability. This was anticipated to result in a larger proportion of mKate2-negative cells than what may be observable at a low passage number, as these cells would be expected to persist in culture. *Ddx3y*^{mKate2}/*Trp53*$^{-/-}$ PMEFs at both low and high passages were also treated with MSPs, in order to increase the stress on the cells, with the aim to increase the likelihood of a loss event.

Figure 4.3 plots the mKate2-positive proportion of PMEFs from each of the three experiments in this section: *Ddx3y*^{mKate2}/*Trp53*$^{-/-}$ PMEFs kept in extended culture (high passage number) with FBS-containing media ("Serum Culture"), compared with those cultured in chemically-defined serum replacement ("SR Culture", Figure 4.3A) to maintain karyotypic stability; low passage number *Ddx3y*^{mKate2}/*Trp53*$^{-/-}$ PMEFs treated with MSPs (Figure 4.3B); and a preliminary trial of high passage number *Ddx3y*^{mKate2}/*Trp53*$^{-/-}$ PMEFs treated with MSPs (Figure 4.3C).

In order to first establish whether extended serum culture alone was capable of inducing loss of the *Ddx3y*^{mKate2} reporter Y chromosome in *Ddx3y*^{mKate2}/*Trp53*$^{-/-}$ PMEFs, *Ddx3y*^{mKate2}/*Trp53*$^{+/-}$ and *Ddx3y*^{mKate2}/*Trp53*$^{-/-}$ PMEFs were cultured for 10 passages in either Serum Culture or SR Culture. *Ddx3y*^{mKate2}/*Trp53*$^{+/-}$ PMEFs were included in this study due to the tendency of *Trp53*$^{+/-}$ mice to develop tumours due to loss of heterozygosity. The dotted line in Figure 4.3A represents the proportion of mKate2-positive cells in wild-type (*Trp53*$^{+/+}$) *Ddx3y*^{mKate2} PMEFs.

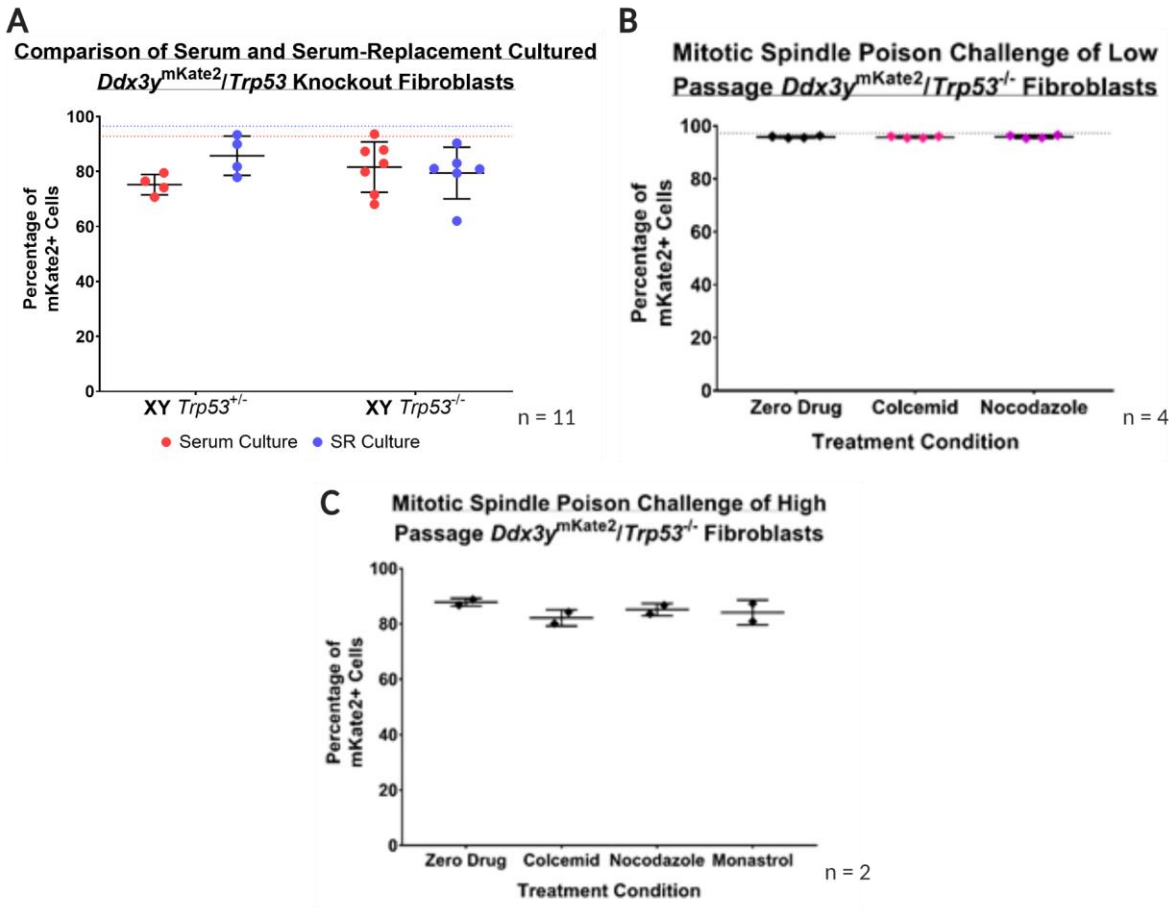

Figure 4.3 - mKate2-Positive Proportions of Challenged *Ddx3y*^{mKate2}/*Trp53* KO PMEFs

Primary mouse embryonic fibroblasts (PMEFs) were derived from male *Ddx3y*^{mKate2}/*Trp53*$^{+/+}$, *Ddx3y*^{mKate2}/*Trp53*$^{+/-}$ and *Ddx3y*^{mKate2}/*Trp53*$^{-/-}$ midgestation embryos and subjected to conditions to induce genotoxic stress. (A) to (C) are plots depicting percentage of mKate2-positive cells following different challenge conditions. Each data point represents one biological replicate; data generated through FACS analysis (sorted as per Figure 4.2A). (A) *Ddx3y*^{mKate2}/*Trp53*$^{+/-}$ and *Ddx3y*^{mKate2}/*Trp53*$^{-/-}$ PMEFs were cultured for 10 passages in either serum-containing media ('Serum Culture') or chemically-defined-serum-replacement (SR)-containing media ('SR Culture'). (B) Early passage *Ddx3y*^{mKate2}/*Trp53*$^{-/-}$ PMEFs were treated with 100 ng/mL of either Colcemid or Nocodazole for 24 hours, then released into drug-free media for 24 hours prior to sorting. (C) *Ddx3y*^{mKate2}/Trp53-/- PMEFs were cultured for 10 passages in either serum-containing media or chemically-defined-serum-replacement (SR)-containing media, then 100 ng/mL of either Colcemid or Nocodazole, or 100 µM of Monastrol, for 24 hours, then released into drug-free media for 24 hours prior to sorting.

Following sorting with FACS, the difference in the percentage of mKate2-positive cells between Serum Cultured (81.60 ± 9.16%, [68.07%, 93.60%]) and SR Cultured (79.45 ± 9.38%, [62.00%, 90.30%]) populations was not significant ($p = 0.946$), with both population returning a high percentage of mKate2-positive cells. While these values did vary between the treatment conditions (Serum and SR Culture) and between the genotypes, there was no significant difference between any of these samples (all $p > 0.05$). Therefore, the genotoxic stress from extended culture with serum was insufficient to induce loss of the *Ddx3y*^{mKate2} reporter Y chromosome in *Ddx3y*^{mKate2}/*Trp53*$^{-/-}$ PMEFs.

Due to this observation, the addition of 24 hours of MSP treatment to serum cultured *Ddx3y*^{mKate2}/*Trp53*$^{-/-}$ PMEFs was performed, both at low passage (Figure 4.3B) and at high passage (Figure 4.3C). This was done in order to increase the stress on the cells to attempt to increase the likelihood of the *Ddx3y*^{mKate2} reporter Y chromosome being lost. The MSP challenge was only performed on two biological replicates in the high passage number experiment as a trial (Figure 4.3C), as work by Woo and Poon[238] showed that the greatest incidence of chromosome loss due to genotoxic stress in *Trp53*$^{-/-}$ PMEFs occurred in the early passages[238]. For both the low passage and high passage PMEFs, the MSPs employed were Colcemid and Nocodazole. For the trial on high passage number PMEFs, the MSP Monastrol was also added (Figure 4.3C).

Following the MSP challenge of low passage number *Ddx3y*^{mKate2}/*Trp53*$^{-/-}$ PMEFs (Figure 4.3B), the mKate2-positive proportions of the two treatment conditions (Colcemid and Nocodazole) were compared to that of cells cultured without MSP treatment ("Zero Drug"). Unfortunately, there was no significant difference between the three conditions, with the mean fluorescent population at approximately 96% for each condition (Zero Drug: 95.85 ± 0.37%, Colcemid: 95.73 ± 0.38%, Nocodazole: 95.90 ± 0.59%). Additionally, there was extremely low variance between the individual data points in each condition, and between three conditions, with all values falling between 95.30% and 96.50%. Therefore, there was no loss of the *Ddx3y*^{mKate2} reporter Y chromosome from early passage *Ddx3y*^{mKate2}/*Trp53*$^{-/-}$ PMEFs under the stress of serum culture combined with MSP treatment.

The above experiment was trialled with high passage number *Ddx3y*^{mKate2}/*Trp53*$^{-/-}$ PMEFs, with the addition of another MSP, Monastrol, to attempt to increase the likelihood of losing the *Ddx3y*^{mKate2} Y chromosome. Unfortunately, the results of this trial (Figure 4.3C) returned similar results as the previous two results. There was no difference between each of the treatment conditions, with each of the values similar to those obtained in the extended culture only trial, all falling between 80% and 90% mKate2-positive proportion. Due to the lack of encouraging results in this trial, this experiment was not repeated on a significant number of biological repeats.

These three experiments demonstrated that *Ddx3y*^{mKate2}/*Trp53*$^{-/-}$ PMEFs were not likely to lose the *Ddx3y*^{mKate2} reporter Y chromosome when experiencing genotoxic stress from serum culture

or mitotic disruption due to MSP treatment. As the aim of the *Ddx3y*^{mKate2}/*Trp53* KO intercrossed strain was to model loss of the reporter Y chromosome and demonstrate how this loss may be assayed for, these results indicate that PMEFs were not the ideal system for demonstrating this. Instead, another tissue known to be unstable in the absence of Trp53 would be preferable for this modelling (Section 4.2.1.2).

4.2.1.2. *Ddx3y*^{mKate2}/*Trp53*$^{-/-}$ Thymuses had Highly Variable Proportions of mKate2-Positive Cells

Trp53$^{-/-}$ mice are known to develop tumours from approximately three months of age onwards[4]. The majority of these tumours were lymphomas affecting the thymus (thymic lymphoma)[4]. All *Trp53*$^{-/-}$ mice were found to either have died or needed to be euthanised by six months of age[4]. This demonstrates the high rate of abnormality in the thymus of *Trp53*$^{-/-}$ mice, making this organ a good candidate for assessing potential loss of the *Ddx3y*^{mKate2} reporter Y chromosome in the intercrossed *Ddx3y*^{mKate2}/*Trp53* KO strain.

In order to take advantage of these abnormal cells, without compromising animal welfare, the thymuses of *Ddx3y*^{mKate2}/*Trp53*$^{-/-}$ and *Ddx3y*^{mKate2}/*Trp53*$^{+/+}$ male mice were collected at approximately four months of age. By this age, either (a) the animal would have developed an overt thymic lymphoma, or (b) the cells in the tumour-prone thymus would be abnormal, without the thymus appearing morphologically abnormal. Ageing the mice beyond this point was unethical, due to the high likelihood of compromising animal welfare from tumour presence. Additionally, some *Ddx3y*^{mKate2}/*Trp53*$^{-/-}$ mice developed tumours earlier due to random chance, and as a result were collected before reaching four months of age, as the presence of observable tumours was not compatible with animal welfare. Cells were then isolated from the thymus of each mouse and sorted on the basis of mKate2 fluorescence (Figure 4.4).

While some *Ddx3y*^{mKate2}/*Trp53*$^{-/-}$ mice occasionally also developed non-thymus tumours, consistent with what had previously been described for the *Trp53*$^{-/-}$ genotype[4], these samples were not included in analysis. Due to the differing origins of these non-thymus tumours, these heterogeneous origins would not be amenable to comparisons between individuals, since not all mice developed additional tumours, and those that did, tended to have the tumours occur in a variety of body regions.

The thymus is a specialised lymphoid organ of the immune system residing in the chest cavity, which is responsible for maturation of T lymphocytes[243,244]. As such, it contains both T lymphocytes at various stages of maturity, as well as the cells that support the developing lymphocytes[243,244]. The thymus was selected for analysis in the *Ddx3y*^{mKate2}/*Trp53* KO intercrossed strain for two reasons. Firstly, as stated above, there is a high propensity for *Trp53*$^{-/-}$ mice to develop thymic lymphomas[4] (refer to Section 4.1.1). Second, the *Ddx3y* tissue expression data (Figure 3.2)

showed that there is a moderately low level of *Ddx3y* gene expression in the thymus, suggesting that this organ would be permissive to expression of the *mKate2* reporter transgene.

The sorting of cells from the *Ddx3y*^{mKate2}/*Trp53*$^{-/-}$ and *Ddx3y*^{mKate2}/*Trp53*$^{+/+}$ thymuses (including potential thymic lymphomas) allowed for a meaningful comparison in mKate2-positive population changes in the *Trp53*$^{-/-}$ samples. Figure 4.4 illustrates representative gating of *Ddx3y*^{mKate2}/*Trp53*$^{+/+}$ and *Ddx3y*^{mKate2}/*Trp53*$^{-/-}$ thymus cell sorts (Figure 4.4A and B, respectively). Figure 4.5C shows the mKate2-positive proportions of cells from the *Ddx3y*^{mKate2}/*Trp53*$^{+/+}$ and *Ddx3y*^{mKate2}/*Trp53*$^{-/-}$ thymuses, as well as representative fluorescence stereomicroscopy images of thymuses from each genotype (Figure 4.5A and B, respectively).

As seen in the representative FACS plots in Figure 4.4, the range of mKate2 intensity values in the mKate2-positive population was greater in the *Ddx3y*^{mKate2}/*Trp53*$^{-/-}$ sample (Figure 4.4B) than in the *Ddx3y*^{mKate2}/*Trp53*$^{+/+}$ sample (Figure 4.4A). This suggests that there were *Ddx3y*^{mKate2}/*Trp53*$^{-/-}$ cells with increased mKate2 fluorescence intensity relative to the *Ddx3y*^{mKate2}/*Trp53*$^{+/+}$ cells. As the *Trp53*$^{-/-}$ genotype has been shown to be associated with gain of chromosomes (discussed in Section 4.2.1.1.2), it was hypothesised that this increase in mKate2 fluorescence intensity was due to the presence of additional *Ddx3y*^{mKate2} reporter Y chromosome/s present in these cells. However, this was not confirmed.

The *Ddx3y*^{mKate2}/*Trp53*$^{+/+}$ thymus cell populations were almost entirely non-fluorescent, with the percentage of mKate2-positive cells between 0.94% and 1.81% (Figure 4.5C). There was, however, a single outlier in these samples, which had an mKate2-positive proportion of 11.30% (not shown). Inclusion of this outlier resulted in a mean mKate2-positive proportion of 3.92 ± 4.93% (n = 4) in the *Ddx3y*^{mKate2}/*Trp53*$^{+/+}$ thymuses. However, due to the low variation between the remaining three *Ddx3y*^{mKate2}/*Trp53*$^{+/+}$ samples, this outlier was excluded from further analysis. Therefore, the mean mKate2-positive proportion of the *Ddx3y*^{mKate2}/*Trp53*$^{+/+}$ thymus-derived cells was 1.46 ± 0.46% (n = 3). This reflected the fluorescence stereomicroscopy image of the *Ddx3y*^{mKate2}/*Trp53*$^{+/+}$ thymus (Figure 4.5A), which exhibited no visible fluorescence.

In contrast, the *Ddx3y*^{mKate2}/*Trp53*$^{-/-}$ thymus samples varied widely in their mKate2-positive proportion, [4.59%, 49.36%], with a mean of 24.86 ± 14.79% (n = 7) (Figure 4.5C). The difference in mKate2-positive populations between *Ddx3y*^{mKate2}/*Trp53*$^{+/+}$ and *Ddx3y*^{mKate2}/*Trp53*$^{-/-}$ samples was highly significant, p = 0.0057. When compared to the *Ddx3y*^{mKate2}/*Trp53*$^{+/+}$ thymus populations, there was a dramatic increase in the mKate2-positive population in the *Ddx3y*^{mKate2}/*Trp53*$^{-/-}$ thymuses, as the lowest value in those samples was more than double that of the greatest *Ddx3y*^{mKate2}/*Trp53*$^{+/+}$ sample (4.59% compared to 1.81%, a two-and-a-half time relative increase). This was also seen in the image of the *Ddx3y*^{mKate2}/*Trp53*$^{-/-}$ thymus (Figure 4.5B), showing a low level of mKate2 fluorescence, another a stark difference from the non-fluorescent *Ddx3y*^{mKate2}/*Trp53*$^{+/+}$ thymus (Figure 4.5A).

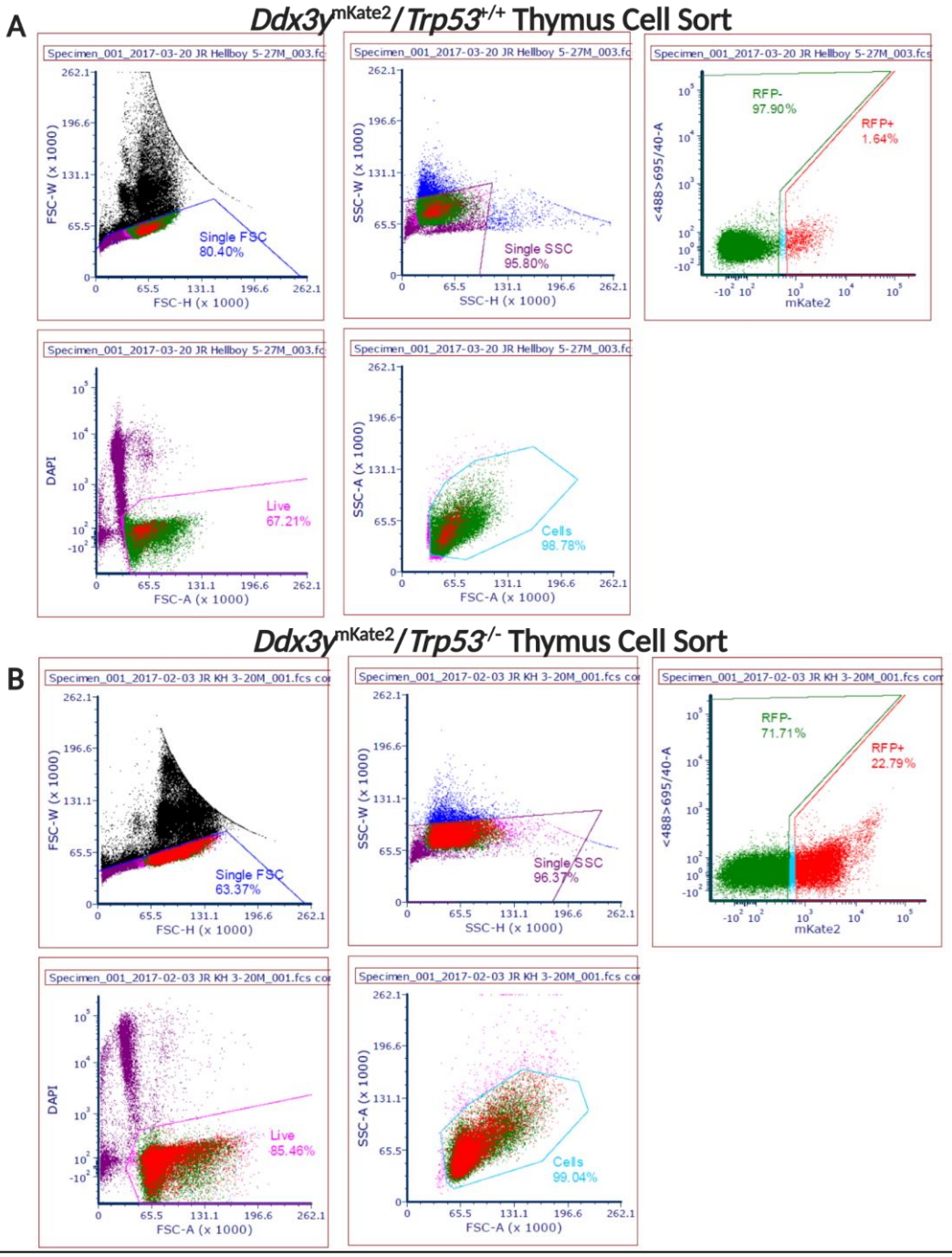

Figure 4.4 - Example Fluorescence-Activated Cell Sorting (FACS) Plots of *Ddx3y*^{mKate2}/*Trp53*$^{+/+}$ and *Ddx3y*^{mKate2}/*Trp53*$^{-/-}$ Thymus Cells

Example sort plots of *Ddx3y*^{mKate2}/*Trp53*$^{+/+}$ (A) and *Ddx3y*^{mKate2}/*Trp53*$^{-/-}$ (B) thymus cells, showing the gating strategy. Progressive gating for: "Cells" (separate from debris), "Single Cells", "Live Cells" (DAPI negative), and into "RFP+" and "RFP-" (mKate2-positive and -negative, respectively). The spread of mKate2-positive cells in the *Ddx3y*^{mKate2}/*Trp53*$^{-/-}$ sample (B) along the mKate2 fluorescence intensity (x) axis was greater than that seen in the *Ddx3y*^{mKate2}/*Trp53*$^{+/+}$ sample (A).

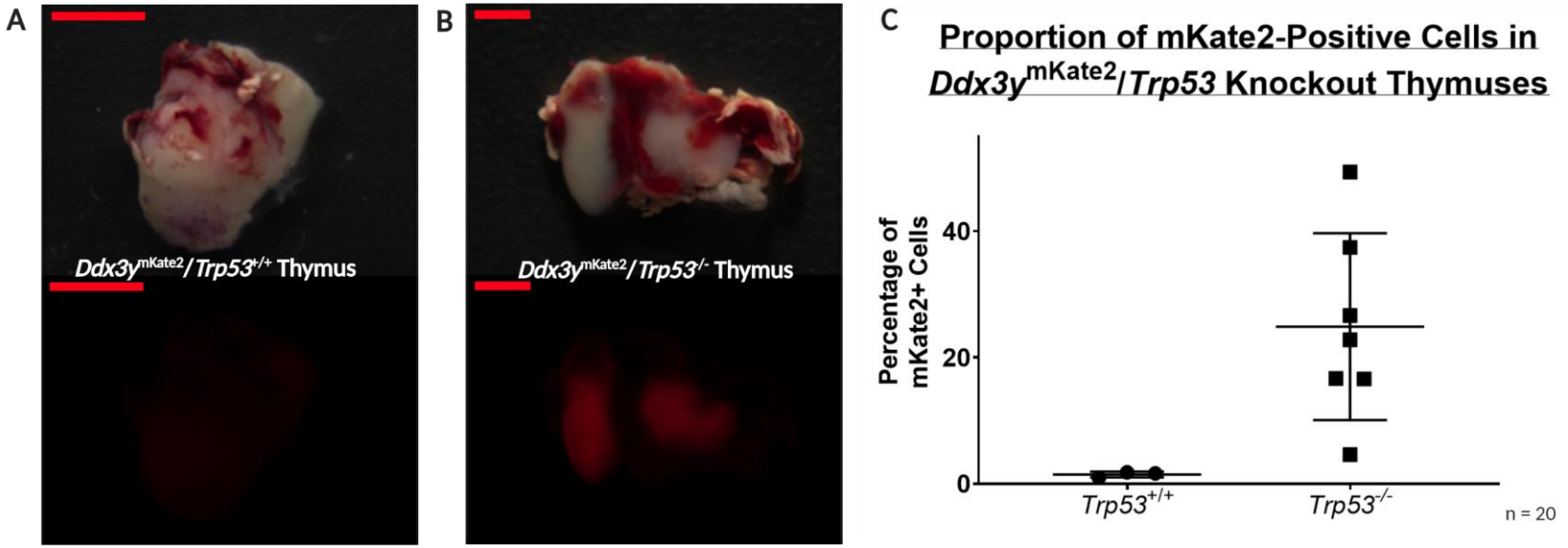

Figure 4.5 - mKate2 Fluorescence in *Ddx3y*^{mKate2}/*Trp53*$^{-/-}$ Thymuses

Trp53$^{-/-}$ mice develop tumours from approximately three months of age, with high incidence of lymphomas[4]. Therefore, in order to examine unstable cells from this genotype, thymuses of *Ddx3y*^{mKate2}/*Trp53*$^{-/-}$ mice were harvested for analysis at approximately four months old. Bright-field (top) and mKate2 fluorescence (bottom) images of whole *Ddx3y*^{mKate2}/*Trp53*$^{+/+}$ (A) and *Ddx3y*^{mKate2}/*Trp53*$^{-/-}$ (B) thymuses. These images illustrate the variation in fluorescence of the thymus between the two genotypes, from no fluorescence (A) to high fluorescence (B). (C) Suspension cells were harvested from thymuses of four-month-old *Ddx3y*^{mKate2}/*Trp53*$^{+/+}$ and *Ddx3y*^{mKate2}/*Trp53*$^{-/-}$ mice and sorted based on mKate2 fluorescence. The percentage of cells that were mKate2-positive were plotted. *Ddx3y*^{mKate2}/*Trp53*$^{+/+}$ samples (n = 3) contained very few mKate2-positive cells (24.86 ± 14.79%, [4.59, 49.36]), whereas the samples from *Ddx3y*^{mKate2}/*Trp53*$^{-/-}$ mice (n = 7) showed high variation in mKate2-positive (1.46 ± 0.461%, [0.94, 1.81]). The difference between the *Ddx3y*^{mKate2}/*Trp53*$^{+/+}$ and *Ddx3y*^{mKate2}/*Trp53*$^{-/-}$ samples was highly significant, p = 0.0057.

Additionally, the wide range of mKate2-positive values in the *Ddx3y*^{mKate2}/*Trp53*$^{-/-}$ samples likely reflected these individual organs being in various stages of malignancy, especially considering that four months of age is well within the reported range for thymic lymphoma development[4]. This experiment aimed to both ascertain whether the *Ddx3y*^{mKate2} thymus was fluorescent, and, should it be mKate2-positive, whether loss of the *Ddx3y*^{mKate2} reporter Y chromosome could be detected by a decline in the mKate2-positive cell population of a *Ddx3y*^{mKate2}/*Trp53*$^{-/-}$ thymus. Unfortunately, it was revealed that the wild-type *Ddx3y*^{mKate2} (*Ddx3y*^{mKate2}/*Trp53*$^{+/+}$) thymus was non-fluorescent at the whole organ level, with an extremely low proportion of mKate2-positive cells (< 2%).

However, an unexpected finding of this experiment was that there was an increase in the mKate2-positive population of the *Ddx3y*^{mKate2}/*Trp53*$^{-/-}$ thymus cells. While this work was performed with the expectation of finding a reduction in the fluorescent cell population, in light of the low proportion of fluorescent cells in the *Ddx3y*^{mKate2}/*Trp53*$^{+/+}$ thymus, this finding of increased mKate2-positive cells was still informative. Previous assessment of the *Trp53*$^{-/-}$ mouse[4] revealed that cells from the thymic lymphomas were double positive for the T cell markers CD-4 and CD-8 (CD4^{+}CD8^{+}), indicating that the origin of the tumours were from relatively immature thymocytes[4].

Based on this, it is predicted that the large population of mKate2-positive cells was comprised predominantly of immature thymocytes. While it has been shown that CD4^{+}CD8^{+} cells account for approximately 6.07 ± 1.19% of thymocytes at six to eight weeks of age[245], triple the level of mKate2-positive cells observed in the *Ddx3y*^{mKate2}/*Trp53*$^{+/+}$ thymus, it is also known that the thymus degenerates with age, declining in size and function[246]. This decline affects the cellularity of the thymus; in mice, at four months of age the cellularity has declined to approximately half of the value observed in newborn mice[247]. Therefore, it would not be unexpected for the immature thymocytes population to be lower in four month old mice relative to six to eight week mice. This also supports the hypothesis that the mKate2-positive cells in the *Ddx3y*^{mKate2}/*Trp53*$^{+/+}$ samples were indeed immature thymocytes. However, repeating this experiment on *Ddx3y*^{mKate2}/*Trp53*$^{+/+}$ and *Ddx3y*^{mKate2}/*Trp53*$^{-/-}$ thymus samples stained for the CD-4 and CD-8 T cell markers would be recommended.

If it is presumed that the mKate2-positive cells were the same cell type in both the *Ddx3y*^{mKate2}/*Trp53*$^{+/+}$ and *Ddx3y*^{mKate2}/*Trp53*$^{-/-}$ thymuses, specifically immature thymocytes, the results of this experiment appear to show lineage expansion in the *Ddx3y*^{mKate2}/*Trp53*$^{-/-}$ thymus. While not the intended function of the *Ddx3y*^{mKate2} reporter Y chromosome, this would be a highly useful feature, as the ability to trace malignant cells' migration following metastasis is valuable to cancer research.

Overall, the aim of the *Ddx3y*^{mKate2}/*Trp53* knockout intercrossed strain work was to obtain cells which lost the *Ddx3y*^{mKate2} reporter Y chromosome due to chromosome instability. This would illustrate how the loss of the *Ddx3y*^{mKate2} reporter Y chromosome could be assayed for based on

mKate2 fluorescence, in order to demonstrate its utility on a known chromosome instability background; however, there was no observed loss of mKate2 fluorescence in the absence of *Trp53*. This indicated that the *Trp53* KO background was not an ideal choice for modelling loss of the *Ddx3y*^{mKate2} reporter Y chromosome due to instability. However, the malignancy of the *Ddx3y*^{mKate2}/*Trp53*$^{-/-}$ thymus indicated potential for the *Ddx3y*^{mKate2} reporter chromosome to be employed as a lineage marker.

4.2.2. Modelling the *Ddx3y*^{mKate2} Reporter Y Chromosome on the *Cenpagfp* Knock-In Instability Background

The *Cenpagfp* mouse background was selected as model onto which to cross the *Ddx3y*^{mKate2} Y chromosome due the documented high rate of aneuploidy observed[29] in homozygous knock-in (*Cenpa*$^{g/g}$) embryos and cells. In particular, the demonstrated tendency for cells of this genotype to lose chromosomes[29] was highly preferential for this work, as there was a high likelihood that the *Ddx3y*^{mKate2} chromosome would be lost from cells on this highly unstable background. By assaying for loss of mKate2 fluorescence following loss of the *Ddx3y*^{mKate2} reporter Y chromosome, this intercrossed strain model would be a proof of principle for the utility of the *Ddx3y*^{mKate2} reporter Y chromosome as a tool for chromosome instability research.

The initial aim for this study was that *Ddx3y*^{mKate2}/*Cenpa*$^{g/g}$ embryos which were mosaics for loss of the *Ddx3y*^{mKate2} Y chromosome would be recovered prior to the onset of embryonic lethality after E9.5. These embryos' cells would then be sorted based on mKate2 fluorescence. The sorted mKate2-positive and negative populations would then be probed for the presence or absence of the *Ddx3y*^{mKate2} Y chromosome, to confirm that the loss of mKate2 fluorescence was due to loss of the reporter Y chromosome.

4.2.2.1. Male *Ddx3y*^{mKate2}/*Cenpa*$^{g/g}$ Embryos were Absent at E9.5

The original *Cenpagfp* mouse strain was observed to have a 1:2:1 ratio of genotypes in E9.5 embryos resulting from heterozygous crosses[29], before the proportion of *Cenpa*$^{g/g}$ declines to be completely absent by E12.5[29]. However, this original paper did not quantify the sex ratio present in these embryos[29]. Previous work in this laboratory examining another fluorescent reporter Y chromosome on the *Cenpagfp* background[5] identified a reduction in XY *Cenpa*$^{g/g}$ embryos at E9.5 from the expected Mendelian proportion (4.08% compared to the expected 12.5%)[5], while XX *Cenpa*$^{g/g}$ embryos occurred at approximately the expected frequency (14.29%, total n = 49 E9.5 embryos)[5].

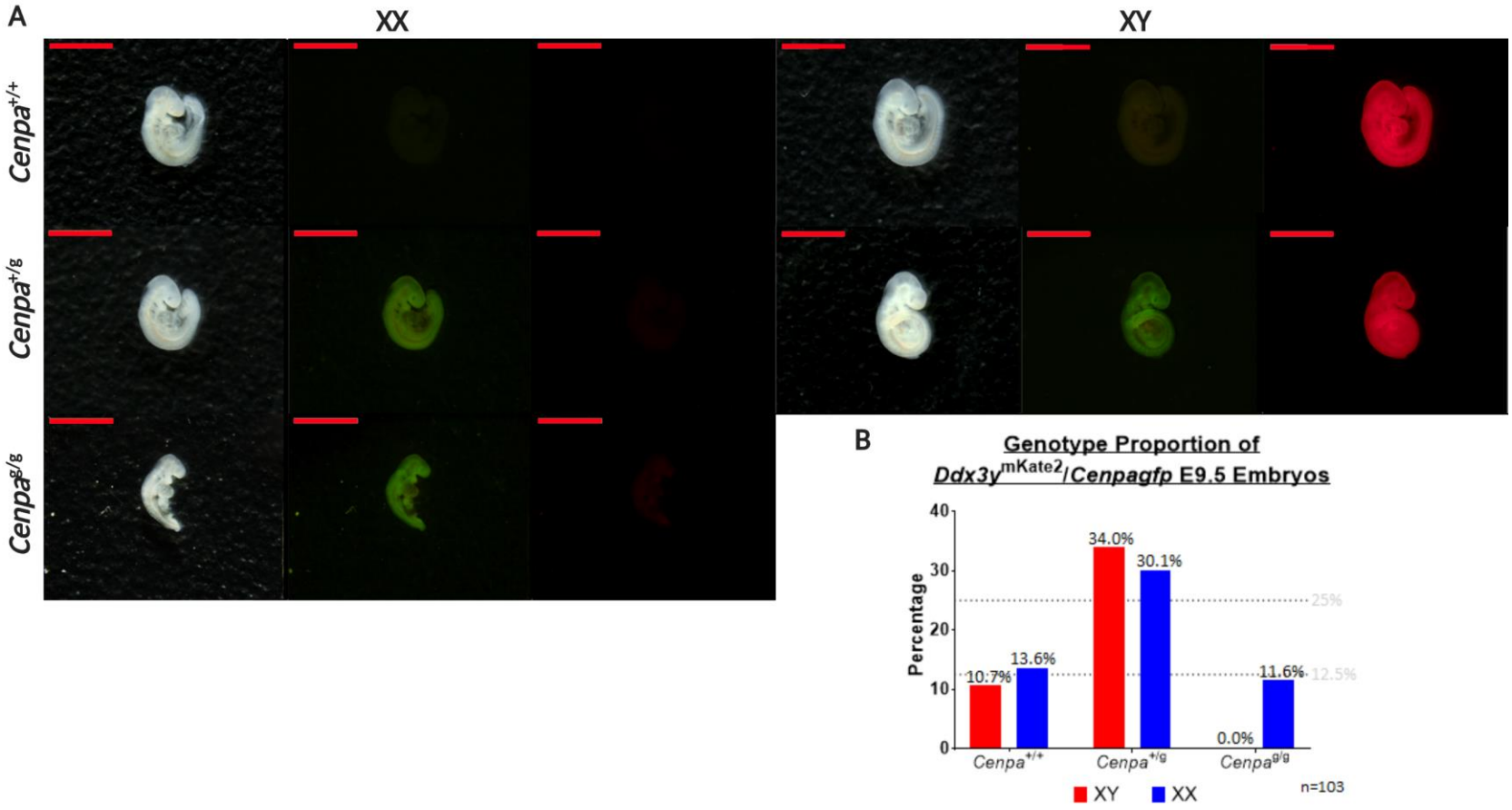

Figure 4.6 - Examination of mKate2 in E9.5 *Ddx3y*^{mKate2}/*Cenpagfp* Embryos

Embryos from *Ddx3y*^{mKate2}/*Cenpagfp* heterozygous matings were collected at E9.5. (A) Representative mKate2 fluorescence (right), GFP fluorescence (centre) and bright-field (left) images of each of the sex/genotype combinations recovered from these litters. All male (XY) embryos were mKate2 fluorescent, with no apparent difference in intensity between the *Cenpa* genotypes recovered, and all female (XX) embryos were mKate2-negative. However, no male *Ddx3y*^{mKate2}/*Cenpa*$^{g/g}$ embryos were recovered. All embryos carrying one (*Cenpa*$^{+/g}$) or two (*Cenpa*$^{g/g}$) copies of the *Cenpagfp* allele exhibited a low level of GFP fluorescence. (B) Distribution of sex/genotype combinations of *Ddx3y*^{mKate2}/*Cenpagfp* embryos collected at E9.5. Dotted lines are 12.5% (expected percentage for *Cenpa*$^{+/+}$ and *Cenpa*$^{g/g}$ males and females, respectively) and 25% (expected percentage for *Cenpa*$^{+/g}$ males and females, respectively). Scale bars are 1 mm (A).

Following generation of the *Ddx3y*^{mKate2}/*Cenpagfp* intercrossed strain, embryos were collected from heterozygous matings at E9.5, prior to the onset of lethality[29]. Embryos were preliminarily sexed visually based on mKate2 fluorescence, and were classified as *Cenpa*$^{+/+}$ (GFP-negative) or either *Cenpa*$^{+/g}$ or *Cenpa*$^{g/g}$ (GFP-positive). The *Cenpa*$^{+/g}$ and *Cenpa*$^{g/g}$ genotypes were unable to be distinguished on the basis of fluorescence; however, abnormal morphology and small size (Figure 4.6A) typically indicated a *Cenpa*$^{g/g}$ embryo[29]. Both sex and *Cenpa* genotype were confirmed by PCR.

While it was expected that there may be a reduction in the proportion of XY *Ddx3y*^{mKate2}/*Cenpa*$^{g/g}$ embryos at E9.5 based on previous results[5], collection of litters of *Ddx3y*^{mKate2}/*Cenpagfp* embryos at this stage (n = 103) revealed that the target embryo, XY *Ddx3y*^{mKate2}/*Cenpa*$^{g/g}$, was completely absent (Figure 4.6). This was despite XX *Ddx3y*^{mKate2}/*Cenpa*$^{g/g}$ embryos again occurring at the expected Mendelian proportion of 1 in 8 embryos (12/103 embryos, 11.65%) (Figure 4.6B).

The absence of XY *Ddx3y*^{mKate2}/*Cenpa*$^{g/g}$ embryos resulted in an overall sex skewing of the embryos, with male XY embryos reduced to 44.66% (46/103 embryos, Figure 4.6B). Additionally, there appeared to be an enrichment in *Ddx3y*^{mKate2}/*Cenpa*$^{+/g}$ embryos of both sexes at this stage (33.98% (35/103) male and 30.10% (31/103) female; expected 25% (26/103), Figure 4.6B). However, this sex skew was likely due to the deficit of XY *Ddx3y*^{mKate2}/*Cenpa*$^{g/g}$ embryos, skewing the percentage, rather than an absolute increase in *Ddx3y*^{mKate2}/*Cenpa*$^{+/g}$ embryos conceived.

Figure 4.6A illustrates representative images of the various sex and genotype combinations of *Ddx3y*^{mKate2}/*Cenpagfp* embryos recovered at E9.5. As expected, all male (XY-*Ddx3y*^{mKate2}) embryos exhibited mKate2 fluorescence, and embryos carrying the *Cenpagfp* allele (*Cenpa*$^{+/g}$ and *Cenpa*$^{g/g}$ embryos) exhibited a low level of GFP fluorescence. The XX *Ddx3y*^{mKate2}/*Cenpa*$^{g/g}$ embryos recovered were small and malformed relative to the other E9.5 embryos present in these litters, as expected[18].

Interestingly, throughout the embryo collection process, it was noticed that there were a number of implantation sites in the uterine horns which contained no embryo, only the degraded remains of extra-embryonic tissues (termed resorption sites[248]). Unfortunately, these degraded tissues within the resorption sites were unable to be separated from maternal tissues, and therefore were not amenable to *Cenpagfp* genotyping. While these embryos would likely have been able to be genotyped for the presence of Y chromosome material (sex genotyping), as the maternal tissue would not carry the Y chromosome, this was not performed due to the inability to determine *Cenpa* genotype. Without confirmed *Cenpa*$^{g/g}$ embryos, the knowledge of the sex of the resorptions would not confirm the speculation that these were the remnants of XY *Cenpa*$^{g/g}$ embryos. Additionally, given the degraded state of the resorptions, there was a strong possibility of incorrectly determining the sex of the embryo; if the DNA recovered from the embryo was sufficiently degraded, affecting the Y chromosome genes used for sex genotyping, a resorption may be incorrectly designated as XX.

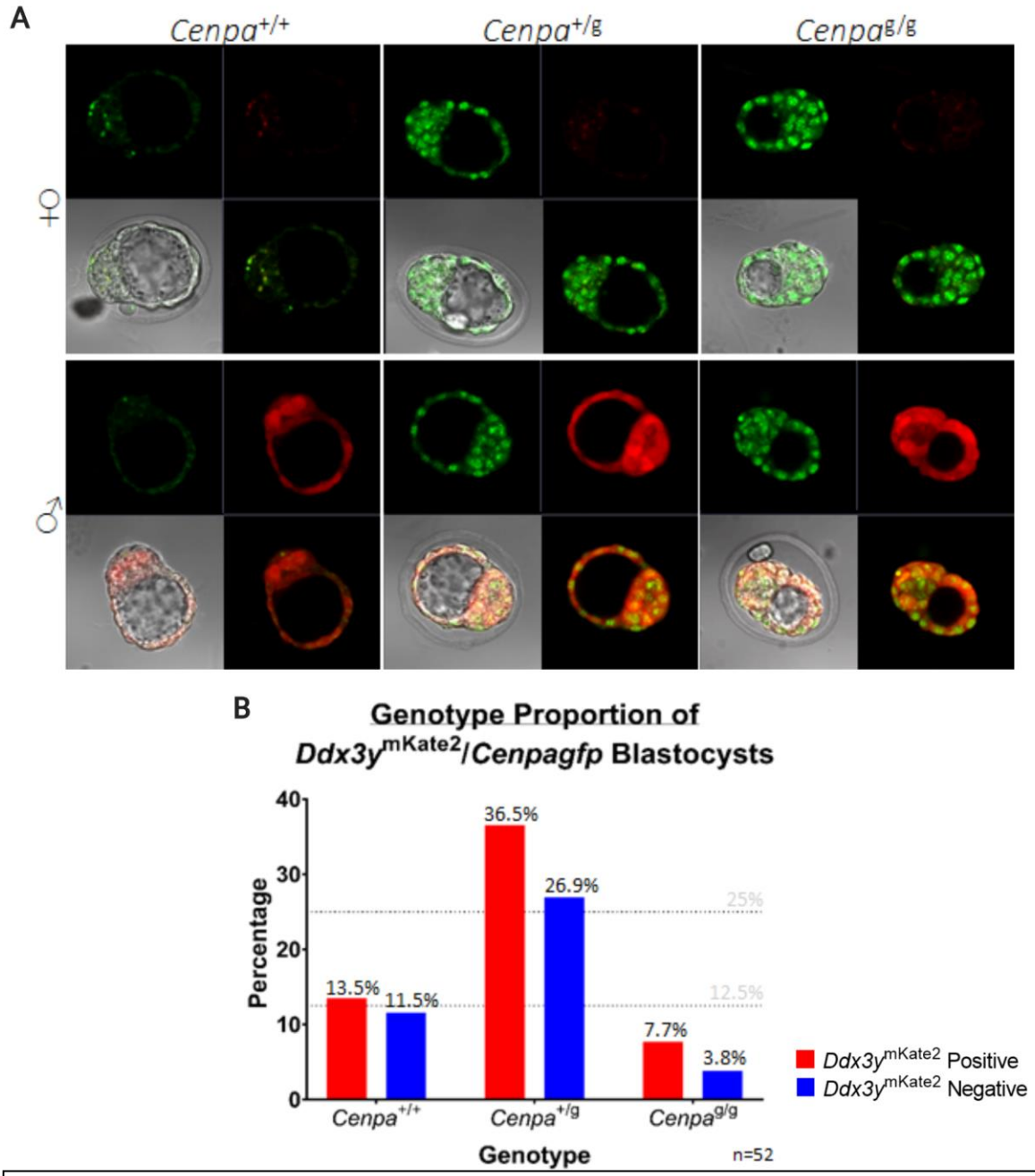

Figure 4.7 - Examination of mKate2 Fluorescence in *Ddx3y*^{mKate2}/*Cenpagfp* Blastocysts

Blastocyst stage embryos from *Ddx3y*^{mKate2}/*Cenpagfp* heterozygous matings were collected at E3.5. (A) Representative GFP fluorescence (top left), mKate2 fluorescence (top right), bright-field + fluorescence merge (bottom left) and fluorescence merge only (bottom right) images of each of the sex/genotype combinations recovered from these litters. All mKate2-positive embryos were considered to be XY, with all mKate2-negative embryos considered to be female. All GFP-positive embryos were considered to be either *Cenpa*$^{+/g}$ or *Cenpa*$^{g/g}$, with GFP-negative embryos considered *Cenpa*$^{+/+}$. (B) Distribution of mKate2 fluorescence (sex)/*Cenpa* genotype combinations of *Ddx3y*^{mKate2}/*Cenpagfp* blastocysts that were genotyped. Dotted lines are 12.5% (expected percentage for *Cenpa*$^{+/+}$ and *Cenpa*$^{g/g}$ males and females, respectively) and 25% (expected percentage for *Cenpa*$^{+/g}$ males and females, respectively).

Across all collections, 13 resorption sites were observed, indicating that there was a substantial loss of embryos after implantation but prior to the collection time point of E9.5. As the number of these implantation sites is similar to the number of XX *Ddx3y*^{mKate2}/*Cenpa*$^{g/g}$ embryos recovered, it was hypothesised that these resorption sites may be the remnants of premature lethality in the XY *Ddx3y*^{mKate2}/*Cenpa*$^{g/g}$ embryos. Therefore, collection of preimplantation *Ddx3y*^{mKate2}/*Cenpagfp* embryos was conducted to confirm whether XY *Ddx3y*^{mKate2}/*Cenpa*$^{g/g}$ embryos were present at Mendelian proportions prior to implantation.

4.2.2.2. Male *Ddx3y*^{mKate2}/*Cenpa*$^{g/g}$ Embryos were Reduced, but Present, at the Blastocyst Stage

It was hypothesised that the resorption sites containing only degraded tissue were the remains of XY *Ddx3y*^{mKate2}/*Cenpa*$^{g/g}$ embryos which were able to develop to implantation, but experienced premature lethality shortly thereafter. Therefore, it was predicted that collecting embryos at an earlier stage of development would result in recovery of XY *Ddx3y*^{mKate2}/*Cenpa*$^{g/g}$ embryos.

Ddx3y^{mKate2}/*Cenpagfp* embryos were collected at E3.5-E3.75, the blastocyst stage, as it is after the onset of mKate2 fluorescence in the male *Ddx3y*^{mKate2} embryos (refer to Section 3.1.1.2). This would allow for determination of blastocyst sex based on the presence or absence of mKate2 fluorescence. This removed the need to genotype the blastocysts for sex chromosome genes, streamlining this experiment. Additionally, as the blastocyst stage directly precedes implantation into the uterus (Section 1.1.4), assessing the presence of *Ddx3y*^{mKate2}/*Cenpa*$^{g/g}$ embryos at this stage would give the best indication of whether these embryos were indeed surviving up until implantation.

Ddx3y^{mKate2}/*Cenpagfp* blastocysts were collected and imaged using fluorescence confocal microscopy, and were classified as male (mKate2-positive) or female (mKate2-negative), and as either GFP-positive (*Cenpa*$^{+/g}$ or *Cenpa*$^{g/g}$) or GFP-negative (*Cenpa*$^{+/+}$). Representative images of each of the sex and genotype combinations are presented in Figure 4.7A. Again, as detailed in Section 4.2.2.1, *Ddx3y*^{mKate2}/*Cenpa*$^{+/g}$ and *Ddx3y*^{mKate2}/*Cenpa*$^{g/g}$ embryos were not clearly distinguishable on the basis of GFP fluorescence. However, there was no morphological differences between the *Cenpa*$^{+/g}$ and *Cenpa*$^{g/g}$ embryos at this stage (Figure 4.7A). Blastocysts were then frozen until DNA extraction, and the resulting lysate was used in a *Cenpa* genotyping PCR assay.

Blastocyst collections recovered 68 embryos, 48 of which were GFP-positive (70.6%), approximating the expected combined rate of *Cenpa*$^{+/g}$ and *Cenpa*$^{g/g}$ embryos (expected: 50% and 25% respectively; combined expected: 75%). Of the 68 recovered blastocysts, 36 blastocysts were mKate2-positive (male; 52.9%), with 27 of these also being positive for *Cenpagfp* signal (39.7% of total collected blastocysts, 75.0% of male blastocysts; expected: 37.5% of total, 75% of male).

However, only 56 of the 68 recovered *Ddx3y*^{mKate2}/*Cenpagfp* blastocysts were able to be genotyped by PCR (82.3%), with the remaining 12 embryos not returning a PCR result, likely due to insufficient DNA having been recovered. An additional four blastocysts which had returned a PCR result were excluded from further analysis, as the determined genotype did not match the observed phenotype, such as a wild type genotype returned for an embryo that was GFP-positive by microscopy. This was attributed to contamination of the DNA, and hence the true genotypes of these embryos were undetermined.

Of the 52 blastocysts that appeared to genotype correctly, there was a slight bias towards male embryos, accounting for 57.7% of the cohort (30/52 embryos, Figure 4.7B). *Ddx3y*^{mKate2}/*Cenpa*$^{+/+}$ blastocysts were present at expected levels (25.0%, 13/52 embryos), with male *Ddx3y*^{mKate2}/*Cenpa*$^{+/+}$ embryos (13.46%, 7/52 embryos) and female *Ddx3y*^{mKate2}/*Cenpa*$^{+/+}$ embryos (11.54%, 6/52 embryos) occurring at similar rates. Of *Ddx3y*^{mKate2}/*Cenpa*$^{+/g}$ and *Ddx3y*^{mKate2}/*Cenpa*$^{g/g}$ blastocysts, however, there was again a shift from Mendelian proportions. Female *Ddx3y*^{mKate2}/*Cenpa*$^{+/g}$ embryos occurred at approximately expected rates (26.9%, 14/52 embryos), whereas male *Ddx3y*^{mKate2}/*Cenpa*$^{+/g}$ embryos appeared to be enriched to 36.5% (19/52 embryos). Additionally, *Ddx3y*^{mKate2}/*Cenpa*$^{g/g}$ embryos of both sexes were reduced: male *Ddx3y*^{mKate2}/*Cenpa*$^{g/g}$ embryos accounted for only 7.7% (4/52 embryos) of collections, a 38.4% relative decrease from the expected level of 12.5%. Female *Ddx3y*^{mKate2}/*Cenpa*$^{g/g}$ embryos were reduced further, only accounting for 3.8% of the cohort, representing two blastocysts, a 69.6% relative decrease from the expected rate.

An unexpected finding of this blastocyst collection was an unexpected bias against female *Ddx3y*^{mKate2}/*Cenpa*$^{g/g}$ embryos that was not observed in the E9.5 collections. It is likely that this apparent bias against female *Ddx3y*^{mKate2}/*Cenpa*$^{g/g}$ embryos is the result of a sampling effect, due to the small number of female *Ddx3y*^{mKate2}/*Cenpa*$^{g/g}$ embryos that would be predicted from a cohort of 52 embryos (six or seven embryos). It is probable that collection of a larger number of blastocysts would result in the relative proportion of female *Ddx3y*^{mKate2}/*Cenpa*$^{g/g}$ embryos increasing to expected rates, as these embryos occurred at Mendelian proportions at E9.5 (Section 4.2.2.1).

This collection of *Ddx3y*^{mKate2}/*Cenpagfp* preimplantation embryos also indicated a bias against male *Ddx3y*^{mKate2}/*Cenpa*$^{g/g}$ embryos similar to that observed in collections of E9.5 embryos (Section 4.2.2.1). However the primary difference between collections at these two time points was that male *Ddx3y*^{mKate2}/*Cenpa*$^{g/g}$ embryos were indeed present prior to implantation, and did not have any apparent abnormalities that would indicate imminent lethality. Indeed, the *Ddx3y*^{mKate2}/*Cenpa*$^{g/g}$ and *Ddx3y*^{mKate2}/*Cenpa*$^{+/g}$ embryos were unable to be differentiated based on morphology in either sex.

The ability to recover male *Ddx3y*^{mKate2}/*Cenpa*$^{g/g}$ embryos at this stage confirmed that the deficiency in these embryos at midgestation was not due to the absence of male

Ddx3y^{mKate2}/*Cenpa*$^{g/g}$ embryos conceptions. Also, as these blastocysts were collected at approximately one day from hatching and implantation into the uterine wall (Section 1.1.4), and had normal morphology, it is reasonable to assume that the male *Ddx3y*^{mKate2}/*Cenpa*$^{g/g}$ embryos were indeed implanting into the uterine wall before the onset of lethality. This would account for the lack of E9.5 male *Ddx3y*^{mKate2}/*Cenpa*$^{g/g}$ embryos and the presence of resorption sites observed in midgestation collections.

The confirmation that male *Ddx3y*^{mKate2}/*Cenpa*$^{g/g}$ embryos were present at the blastocyst stage was encouraging for the use of the *Cenpagfp* background to model the utility of the *Ddx3y*^{mKate2} reporter Y chromosome. At this early stage of development, no mKate2-positive (male) blastocysts exhibited any apparent mosaic mKate2 fluorescence, indicating that there was no loss of the *Ddx3y*^{mKate2} reporter chromosome between conception and E3.75. Therefore, this time point would be an ideal target for collecting male *Ddx3y*^{mKate2}/*Cenpa*$^{g/g}$ embryos for *in vitro* culture, as it is likely that all cells derived from these blastocysts (ES cells) would carry the *Ddx3y*^{mKate2} Y chromosome. Instability could then be induced in these ES cells in culture by subjecting the cells to genotoxic stress, with the aim to increase the likelihood of losing the *Ddx3y*^{mKate2} Y chromosome. This loss could then be assayed for using FACS, and would be an ideal method of demonstrating how the *Ddx3y*^{mKate2} reporter Y chromosome could be of use in assessing the incidence of chromosome loss.

4.3. Discussion

This chapter detailed the two intercrossed mouse strains carrying the *Ddx3y*^{mKate2} reporter Y chromosome on known chromosome instability backgrounds. These two intercrossed strains, *Ddx3y*^{mKate2}/*Trp53* knockout (KO) and *Ddx3y*^{mKate2}/*Cenpagfp*, were generated with the aim to model how the *Ddx3y*^{mKate2} reporter Y chromosome could be of use as a tool in chromosome instability research. In both intercrossed strains, the aim was to induce chromosome loss that would ideally affect the *Ddx3y*^{mKate2} reporter Y chromosome, and that the resulting loss of mKate2 fluorescence would then be able to be detected using methods such as FACS.

The first intercrossed strain was created by crossing the *Ddx3y*^{mKate2} reporter Y chromosome onto the tumour-prone *Trp53* KO[180] background. This genetic background had previously been shown to experience aneuploidy *in vitro* and *in vivo*[4,238], and it was predicted that this aneuploidy would affect the *Ddx3y*^{mKate2} reporter Y chromosome such that it would be lost. The *Ddx3y*^{mKate2}/*Trp53*$^{-/-}$ genotype was examined for this by assessing the mKate2-positive cell proportion in the tumour-prone thymus and in cells cultured under stress. This proportion was compared to determine how it differed from that observed in the control *Ddx3y*^{mKate2}/*Trp53*$^{+/+}$ genotype.

The second intercrossed strain employed in this chapter resulted from crossing the

Ddx3y^{mKate2} reporter Y chromosome on to the *Cenpagfp* fusion knock-in[29] background. This transgenic strain has a high propensity for chromosome loss in cells of *Cenpa*$^{g/g}$ embryos[29], such that embryos of this genotype experience embryonic lethality[29]. Embryos from the *Ddx3y*^{mKate2}/*Cenpagfp* intercrossed strain were collected, in order to obtain *Ddx3y*^{mKate2}/*Cenpa*$^{g/g}$ embryos whose cells would then be used in *in vitro* chromosome instability assays.

4.3.1. The *Ddx3y*^{mKate2} Chromosome on a *Trp53* Knockout Background

The *Trp53* KO background[4] was selected for modelling the utility of the *Ddx3y*^{mKate2} reporter Y chromosome, as this genetic background results in a high incidence of tumours in homozygous KO (*Trp53*$^{-/-}$) mice[4]. The aneuploidy associated with tumour development indicated that this background would be a good model of chromosome instability upon which the *Ddx3y*^{mKate2} Y chromosome could be assessed.

The initial aim of crossing the *Ddx3y*^{mKate2} reporter Y chromosome onto the *Trp53* KO background was to attempt to induce a random chromosome loss event under conditions that increased instability in the absence of Trp53. The intention was that such a loss event would affect the *Ddx3y*^{mKate2} reporter Y chromosome due to its small size, which would then be able to be assayed for based on loss of mKate2 fluorescence. It was hypothesised that the non-essential nature of the *Ddx3y*^{mKate2} Y chromosome would result in preferential persistence of cells that had lost the *Ddx3y*^{mKate2} Y chromosome relative to cells that lost the X chromosome or an autosome/s. Therefore, it was predicted that there would be an enrichment of mKate2-negative cells due to loss of the *Ddx3y*^{mKate2} reporter Y chromosome, particularly in the presence of genotoxic stress.

Due to the incidence of tumours in *Trp53*$^{-/-}$ mice[4] and the noted karyotype changes in *Trp53*$^{-/-}$ cells under stress conditions[238,240-242], screening for loss of the *Ddx3y*^{mKate2} reporter chromosome in the *Ddx3y*^{mKate2}/*Trp53*$^{-/-}$ intercross was performed both *in vivo*, in the tumour-prone thymus, and *in vitro*, in primary mouse embryonic fibroblasts (PMEFs) under genotoxic stress.

Once it was confirmed that there was no loss of the *Ddx3y*^{mKate2} reporter Y chromosome in midgestation *Ddx3y*^{mKate2}/*Trp53*$^{-/-}$ embryos, these embryos were used to derive *Ddx3y*^{mKate2}/*Trp53*$^{-/-}$ PMEFs. These cells were then cultured under conditions to increase genotoxic stress, in order to exacerbate the instability associated with their *Trp53* genotype. However, none of these *in vitro* experiments yielded a decrease in the mKate2-positive population, indicating that the chromosome instability associated with stressed *Trp53*$^{-/-}$ cells did not result in the loss of the *Ddx3y*^{mKate2} Y chromosome. This was not unexpected, as *Trp53*$^{-/-}$ PMEFs under stress, such as when cultured with serum-containing media[238] or treated with mitotic spindle poisons (MSPs)[240-242], tend to gain chromosomes, up to and including doubling of the diploid number[240].

However, it had been previously observed that aneuploidy resulting in a reduction from the

diploid number occurred in approximately 20% of *Trp53*$^{-/-}$ PMEFs within three population doublings in serum-containing media[238], and that even low rates of chromosome loss could be induced in as little as 48 hours under this culture condition[238]. Therefore, it had been speculated that the small size and non-essential nature of the *Ddx3y*^{mKate2} Y chromosome would increase the likelihood of its loss in these aneuploidy events. Unfortunately, it was determined that the instability of the *Ddx3y*^{mKate2}/*Trp53*$^{-/-}$ PMEFs did not result in 39,XO cells, as the *Ddx3y*^{mKate2} Y chromosome was not lost.

Interestingly, this series of cell culture experiments instead demonstrated that, regardless of *Trp53* genotype, the proportion of mKate2-positive cells increased in culture in *Ddx3y*^{mKate2} PMEFs relative to the proportion present in the freshly sorted *Ddx3y*^{mKate2}/*Trp53* KO embryos. Additionally, *Ddx3y*^{mKate2}/*Trp53* KO PMEFs of all genotypes showed no change in the percentage of fluorescent cells with drug (MSP) treatment. This presented interesting implications for use of the *Ddx3y*^{mKate2} model in an *in vitro* compared to an *in vivo* study, as these differing values indicates that either experimental system would require careful establishment of baseline values for mKate2-positive and -negative populations. It would be valuable to explore this further with different cell types, by comparing the proportion of mKate2-positive cells in freshly collected tissues and in cells kept in culture for various lengths of time.

In addition to the *in vitro* work, the cells of the tumour-prone thymus of *Ddx3y*^{mKate2}/*Trp53*$^{-/-}$ males were assessed for changes to the proportion of mKate2-positive cells. As with the *Ddx3y*^{mKate2}/*Trp53*$^{-/-}$ PMEFs, this was performed with the aim to obtain cells which lost the *Ddx3y*^{mKate2} reporter Y chromosome and, subsequently, their mKate2 fluorescence. However, as the *Ddx3y*^{mKate2} thymus had not previously been assessed for mKate2 fluorescence, either as a whole organ, nor in cells derived from the organ, this was also examined. Unfortunately, the *Ddx3y*^{mKate2}/*Trp53*$^{+/+}$ thymus was not mKate2 fluorescent, nor were the vast majority of immune cells derived from it. This was discouraging for further use of this tumour-prone tissue in the *Trp53* KO intercross, as any loss of the *Ddx3y*^{mKate2} reporter chromosome and its resulting fluorescence in the *Ddx3y*^{mKate2}/*Trp53*$^{-/-}$ thymus would likely be undetectable.

However, upon sorting the cells derived from the *Ddx3y*^{mKate2}/*Trp53*$^{-/-}$ thymus, it was found that the mKate2-positive population differed significantly from the proportion observed in the *Ddx3y*^{mKate2}/*Trp53*$^{+/+}$ thymus. This suggested an additional use for the *Ddx3y*^{mKate2} reporter Y chromosome: lineage marking. As the thymic lymphomas of the *Trp53*$^{-/-}$ mice were reported to originate from expansion of immature thymocytes[4], it is hypothesised that the mKate2-positive cells in both the *Ddx3y*^{mKate2}/*Trp53*$^{+/+}$ and *Ddx3y*^{mKate2}/*Trp53*$^{-/-}$ thymuses were also immature thymocytes, with this cell population expanded in the latter genotype. By staining with T cell markers, it would be ideal to determine the identity of these fluorescent cells, and identify whether the mKate2-positive cells were a single cell type or a heterogeneous mix of different cell types. Unfortunately, this was unable to be performed in this study.

However, the significant difference in the percentage of mKate2-positive thymus-derived cells between the *Ddx3y*^{mKate2}/*Trp53*$^{+/+}$ and *Ddx3y*^{mKate2}/*Trp53*$^{-/-}$ samples, and the tendency for malignancy in the thymus of *Ddx3y*^{mKate2}/*Trp53*$^{-/-}$ mice, suggests that these mKate2-positive cells likely had similar cellular identities, and that the increase in their proportion in the *Ddx3y*^{mKate2}/*Trp53*$^{-/-}$ thymus was likely the result of expansion of this lineage. Therefore, the florescence of the mKate2 reporter highlighted this lineage expansion in the *Ddx3y*^{mKate2}/*Trp53*$^{-/-}$ thymus. While this may not be applicable to all cell types, as evidenced by the high mKate2-negative cell population in the *Ddx3y*^{mKate2}/*Trp53*$^{+/+}$ thymus, for cell types that are known to be mKate2-positive, the presence of the *Ddx3y*^{mKate2} reporter chromosome has great potential to mark cell types as their numbers increase, and potentially, whether they metastasise throughout the body for *in vivo* experiments. This is a previously unconsidered function of the *Ddx3y*^{mKate2} Y chromosome, and hence extends its utility.

In light the propensity for *Trp53*$^{-/-}$ cells to gain chromosomes, combined with the noted increased mKate2 fluorescence intensity in the *Ddx3y*^{mKate2}/*Trp53*$^{-/-}$ cells detected by FACS (refer to Figure 4.4B), it is hypothesised that in both the *in vitro* experiments and in the *Ddx3y*^{mKate2}/*Trp53*$^{-/-}$ thymuses there were cells which had gained additional copies of the *Ddx3y*^{mKate2} reporter Y chromosome. As the Y chromosome does not undergo inactivation in cells with multiple Y chromosomes (unlike the X chromosome), it would be reasonable to assume that all copies of the *Ddx3y*^{mKate2} reporter Y chromosome in a cell would express the *mKate2* transgene. This increased expression of the transgene would be expected to result in greater mKate2 fluorescence, such as what was observed in the chromosomally unstable *Ddx3y*^{mKate2}/*Trp53*$^{-/-}$ thymus cells (Figure 4.4B).

Ideally, this would be assessed by sorting *Ddx3y*^{mKate2}/*Trp53*$^{-/-}$ thymus cell populations by FACS into non-fluorescent, normal mKate2 fluorescence intensity (based off of values from *Ddx3y*^{mKate2}/*Trp53*$^{+/+}$ control cells, Figure 4.4A), and high mKate2 fluorescence intensity (Figure 4.4B). These three subpopulations could then be examined for presence or absence of the *Ddx3y*^{mKate2} reporter Y chromosome, and potentially, additional *Ddx3y*^{mKate2} Y chromosomes. This could be performed by assessing metaphase spreads and chromosome counting, or through fluorescence *in situ* hybridisation (FISH), in which a probe to the Y chromosome is applied to fixed cells. This would confirm whether there was a gain of additional *Ddx3y*^{mKate2} Y chromosome/s in the high mKate2 fluorescence cells, and whether there was a correlation between gain of the *Ddx3y*^{mKate2} reporter Y chromosome and increased mKate2 fluorescence intensity. Also, such assessment would reveal whether all mKate2-negative cells lack the *Ddx3y*^{mKate2} reporter chromosome, or if there is a subpopulation of cells which retain the chromosome but are merely non-fluorescent.

As the stated aim of this work was to model the *Ddx3y*^{mKate2} reporter Y chromosome in the context of chromosome instability resulting in loss, the *Ddx3y*^{mKate2}/*Trp53* KO intercrossed strain was overall not the ideal instability background for this purpose. The intention of creating the *Ddx3y*^{mKate2}

reporter chromosome was to generate a tool for use in chromosome instability, primarily to aid researchers in identifying incidences of chromosome loss, as this hemizygous chromosome can be assayed for in a presence/absence fashion. However, the propensity of the *Trp53*$^{-/-}$ genotype to accumulate chromosomes[4,238] was not consistent with this goal. Particularly, as the *Ddx3y*^{mKate2} Y chromosome is not amenable for easy assaying for in a dose-dependent manner, gain of additional *Ddx3y*^{mKate2} reporter chromosomes would require additional examination to detect, undermining the intended ease of this tool. Therefore, for the stated aim of this work, the *Trp53* KO background was not suitable for modelling the utility of the *Ddx3y*^{mKate2} reporter Y chromosome in the context of chromosome loss.

However, the *in vivo* work in this chapter demonstrated that the *Ddx3y*^{mKate2} reporter Y chromosome could be amenable to other reporter functions, such as lineage tracing. This was an unexpected benefit of generating the *Ddx3y*^{mKate2}/*Trp53* KO intercross strain.

4.3.2. The *Ddx3y*^{mKate2} Reporter Y Chromosome on the *Cenpagfp* Instability Background

The transgenic *Cenpagfp* knock-in background[29] was selected for modelling the utility of the *Ddx3y*^{mKate2} reporter Y chromosome due to the high rate of chromosome instability, with a particular propensity for chromosome loss, observed in the homozygotes (*Cenpa*$^{g/g}$)[29]. As the *Ddx3y*^{mKate2} reporter Y chromosome was designed for use in chromosome instability research, specifically the ability to assay for its loss based on the presence or absence of mKate2 fluorescence, the *Cenpagfp* background was highly advantageous for demonstrating this utility.

The gross missegregation events observed in *Cenpa*$^{g/g}$ embryos cause premature lethality of the embryos, with their numbers reducing beyond E9.5, becoming completely absent by E12.5[29]. Therefore, collection of *Ddx3y*^{mKate2}/*Cenpagfp* embryos at E9.5, prior to the onset of embryonic lethality of the *Ddx3y*^{mKate2}/*Cenpa*$^{g/g}$ embryos was performed, with the target embryos being the XY *Ddx3y*^{mKate2}/*Cenpa*$^{g/g}$ embryos. As previous work had shown that *Ddx3y*^{mKate2} embryos were mKate2-positive at E9.5 (Section 3.1.1.2)[5], any loss of the *Ddx3y*^{mKate2} reporter Y chromosome from cells in the *Ddx3y*^{mKate2}/*Cenpa*$^{g/g}$ embryos would be detectable by cell sorting for mKate2 fluorescence.

It was predicted that cells in the *Ddx3y*^{mKate2}/*Cenpa*$^{g/g}$ embryos which had lost the *Ddx3y*^{mKate2} Y chromosome would be able to persist in the embryo until E9.5, as loss of the Y chromosome does not affect cell viability. Therefore, it was predicted that XY *Ddx3y*^{mKate2}/*Cenpa*$^{g/g}$ embryos would likely be mosaics of regions with and without mKate2 fluorescence, due to loss of the *Ddx3y*^{mKate2} reporter Y chromosome from a subset of cells. This would ideally be assessed by FACS performed on disaggregated embryos, followed by FISH on the sorted cells.

While the original publication on the *Cenpagfp* knock-in mouse only assessed *Cenpa* genotype ratios without also accounting for the sex of the embryos[29], previous work in this laboratory observed that another intercrossed strain with the *Cenpagfp* mouse resulted in a reduced proportion of XY *Cenpa*$^{g/g}$ embryos at E9.5[5], likely due to premature lethality. Therefore, it was expected that there would also be a reduction in XY *Ddx3y*^{mKate2}/*Cenpa*$^{g/g}$ embryos at this stage.

However, despite the high number of E9.5 *Ddx3y*^{mKate2}/*Cenpagfp* embryos collected, none were XY *Ddx3y*^{mKate2}/*Cenpa*$^{g/g}$. Instead, there were resorption sites throughout the uteri of the female mice, indicating that there was a high rate of premature lethality. Given that these resorption sites occurred at a similar rate to the XX *Ddx3y*^{mKate2}/*Cenpa*$^{g/g}$ embryos, it was predicted that these resorption sites were the remains of XY *Ddx3y*^{mKate2}/*Cenpa*$^{g/g}$ embryos, which appeared to be experiencing a 100% rate of premature lethality in this particular intercross. The presence of resorption sites, combined with the absence of XY *Ddx3y*^{mKate2}/*Cenpa*$^{g/g}$ embryos, lead to the hypothesis that the XY *Ddx3y*^{mKate2}/*Cenpa*$^{g/g}$ embryos were surviving preimplantation development, well enough that they were implantation competent before lethality occurred.

To test this, *Ddx3y*^{mKate2}/*Cenpagfp* blastocysts were collected, as XY embryos would have become mKate2 fluorescent and therefore be detectable by fluorescence microscopy. From these collections, it was determined that the XY *Ddx3y*^{mKate2}/*Cenpa*$^{g/g}$ embryos were indeed surviving preimplantation development, albeit at a lower rate than expected, with no gross abnormalities observed in the blastocysts that would suggest lethality onset before implantation.

One unusual observation from these blastocyst collections was that there was a reduction in the relative proportion of XX *Ddx3y*^{mKate2}/*Cenpa*$^{g/g}$ embryos at this stage. However, as this reduction was absent at E9.5, this was likely a function of a small sample size. It is predicted that collection of a larger number of blastocysts would return the proportion of the XX *Ddx3y*^{mKate2}/*Cenpa*$^{g/g}$ embryos to Mendelian proportions. Such a collection may also see a rise in the proportion of XY *Ddx3y*^{mKate2}/*Cenpa*$^{g/g}$ blastocysts, as the rate of resorption sites observed at E9.5 was the same as the rate of XX *Ddx3y*^{mKate2}/*Cenpa*$^{g/g}$ embryos. This suggests that XX *Ddx3y*^{mKate2}/*Cenpa*$^{g/g}$ and XY *Ddx3y*^{mKate2}/*Cenpa*$^{g/g}$ embryos were both conceived and implanted at similar rates.

While it was initially expected that loss of the *Ddx3y*^{mKate2} reporter Y chromosome in XY *Ddx3y*^{mKate2}/*Cenpa*$^{g/g}$ embryos would be able to be assayed for directly from embryos, it was also an intention of this work that cells from the XY *Ddx3y*^{mKate2}/*Cenpa*$^{g/g}$ embryos would then be used in chromosome instability induction experiments. These experiments would likely parallel those performed on the *Ddx3y*^{mKate2}/*Trp53*$^{-/-}$ PMEFs (Section 4.2.1.1.2), with the XY *Ddx3y*^{mKate2}/*Cenpa*$^{g/g}$ cells subjected to mitotic spindle poison (MSP) treatment. This was planned to be performed with XY *Ddx3y*^{mKate2}/*Cenpa*$^{g/g}$ PMEFs derived from E9.5 embryos; however, these embryos were not present at this time point.

Following confirmation of the presence of XY *Ddx3y*^{mKate2}/*Cenpa*$^{g/g}$ embryos at the blastocyst stage, it was intended that embryonic stem (ES) cells would be derived from these blastocysts, particularly since there was no indication of mosaic loss of mKate2 fluorescence in the XY *Ddx3y*^{mKate2}/*Cenpa*$^{g/g}$ blastocysts. These *Ddx3y*^{mKate2}/*Cenpa*$^{g/g}$ ES cells would then be treated with MSPs to attempt to exacerbate the chromosome segregation errors associated with the *Cenpa*$^{g/g}$ genotype. These ES cells could then be sorted with FACS into mKate2-positive and -negative populations, and be probed with FISH for the presence or absence of the *Ddx3y*^{mKate2} Y chromosome. Unfortunately, due to time constraints resulting from lengthy optimisation of the blastocyst genotyping PCR, this was unable to be performed.

Despite the difficulties encountered with the *Ddx3y*^{mKate2}/*Cenpagfp* strain, there is still substantial potential for this intercrossed strain for modelling the utility of the *Ddx3y*^{mKate2} reporter Y chromosome. The presence of XY *Ddx3y*^{mKate2}/*Cenpa*$^{g/g}$ blastocysts is encouraging for this aim, as these embryos can be used to derive ES cells for instability induction as described above. This experiment would neatly demonstrate how the *Ddx3y*^{mKate2} reporter Y chromosome could be used as a tool in chromosome instability research.

Chapter 5: Characterisation of the A/HeJ Sex Determination Phenotype

5.1. Introduction

The A/HeJ mouse strain has previously been described to have an abnormal testis phenotype, in which a proportion of males develop either small testes or ovotestes (gonads composed of ovarian and testicular tissue)[2]. This defect was causally linked to the Y chromosome ($Y^{A/HeJ}$) of this strain[2]. Prior to assessing the molecular cause of this phenotype, it was prudent to first confirm the presence of the described phenotype in the A/HeJ colony at the Murdoch Children's Research Institute (MCRI).

This chapter details the assessment of the A/HeJ male phenotype in the MCRI colony. This assessment was performed to address two aims. Firstly, to confirm that the A/HeJ male phenotype in the MCRI colony aligned with the previously reported phenotype, including sex skewing and examination of gonadal and genital phenotypes. Second, this work aimed to generate additional data on the A/HeJ male phenotype, with a focus on the adult mouse, in order to better characterise the effect of this defect, such as the impact on fertility.

5.1.1. Initial Phenotypic Characterisation of the A/HeJ Mouse Phenotype By Hunt et al (2008)

The A/HeJ mouse strain has been reported to have an abnormal gonadal phenotype observed in a proportion of males[2]. This defect was initially characterised in the colony maintained at the Jackson Laboratory by Hunt and colleagues in a 2008 paper titled 'The A/HeJ Y Chromosome: Another Good Y Gone Bad'[2]. The A/HeJ strain was found to exhibit sex skewing, manifesting in a colony-wide reduction in males to 46.8%[2]. Additionally, it was noted that many males in this colony were non-productive (unable to produce pups)[2]. Of the non-productive males examined, 4% were identified as overt hermaphrodites due to possessing gonads of mixed testicular and ovarian tissue (an ovotestis), with a further 17% found to have small testes that produced no epididymal sperm[2].

As the Y chromosome contains genes related to testis determination and function (refer to Sections 1.1.2.2 and 1.1.5.2), the A/HeJ Y chromosome ($Y^{A/HeJ}$) was crossed onto the C57BL/6J background to create a consomic strain (C57BL/6J-$Y^{A/HeJ}$)[2]. Examination of this consomic strain confirmed that the abnormal gonadal phenotype was solely due to the Y chromosome of the A/HeJ mouse, rather than being due to other genes in the A/HeJ genome[2].

Once the A/HeJ defect was causally linked to the presence of the $Y^{A/HeJ}$ chromosome, it was initially predicted[2] that this Y chromosome was being lost from a subset of cells in the bipotential gonad, and that the resulting 39,XO cells were the cause of ovarian tissue development in the ovotestes[2]. This prediction was based upon other mouse strains with ovotestis development, in which the abnormality was causally linked to the Y chromosome[2].

One such strain was the WtEiJ mouse strain[24,103,104], in which the Y chromosome (Y^{WtEiJ}) was highly prone to missegregation in early development, specifically within the first few cleavage divisions following fertilisation[103] (Section 1.1.4). This lead to the resulting mouse being a mosaic for the sex chromosomes (XO/XY/XYY)[104]. In particular, the proportion of 39,XO cells in the genital ridge (refer to Section 1.1.5.1) which had lost the Y^{WtEiJ} chromosome resulted in either ovotestis or ovary development[249]. The development of ovarian tissue was due to the absence of the Y^{WtEiJ} chromosome in these 39,XO cells, as the Y chromosome carries the molecular trigger for testis determination, the *Sry* gene. This instability of the Y^{WtEiJ} chromosome was shown to be due to a reduction in its centromere, leading to impaired division of this Y chromosome during early embryonic cleavages[24].

As it had been confirmed that the ovarian development in the ovotestes of the WtEiJ strain were due to loss of the Y^{WtEiJ} chromosome from cells in the gonad, Hunt et al (2008)[2] assessed the ovarian and testicular portions of E13.5 to E15.5 embryonic ovotestes[2]. This analysis was performed to determine whether the $Y^{A/HeJ}$ chromosome had been lost from the ovarian portions of these C57BL/6J-$Y^{A/HeJ}$ embryonic gonads[2]. However, it was determined that the $Y^{A/HeJ}$ chromosome was retained at the same rate in both the ovarian and testicular tissues of the ovotestes[2], indicating that the cause of the phenotype was not due to loss of the A/HeJ Y chromosome[2].

This chapter describes the observed phenotype in A/HeJ males of the MCRI colony, and as well as that of control strain (A/J and BALB/c) males. This work aimed to both confirm that the A/HeJ phenotype occurs in the MCRI colony as previously reported[2], and to generate additional data on the A/HeJ adult phenotype to extend the characterisation of this defect.

5.2. Results

5.2.1. Confirmation of the Reported A/HeJ Male Phenotype in the MCRI A/HeJ Colony

Prior to assessing the $Y^{A/HeJ}$ chromosome for molecular changes (Chapter 6), it was essential to confirm that males in the MCRI A/HeJ colony produced the expected phenotype. Examination of embryos and adult mice revealed that gonadal abnormalities consistent with the reported A/HeJ phenotype[2] were present in male mice of the MCRI A/HeJ colony, and not in the MCRI control A/J

colony. The A/J colony was used as a control, as the A/J mouse strain is the closest related strain to the A/HeJ strain[182] (Section 2.2.1).

5.2.1.1. Males were Reduced in the A/HeJ Colony, but not in the Control A/J Colony

The original characterisation of the A/HeJ male mouse reported a reduction in males in the Jackson Laboratory colony to 46.8% of the population[2]. In order to assess whether a comparable reduction in males was present in the MCRI A/HeJ colony, breeding data was assessed from both the A/HeJ strain and the closely related control strain, A/J, from the time of the strains' respective arrivals at MCRI (1st July 2014 and 1st January 2014, respectively), until the end of 2018, in which the final litters born in 2018 were the last included in all further analyses.

Over the four years the A/HeJ strain was maintained at MCRI, 16 generations of mice were born into the A/HeJ colony, totalling 442 individuals. Analysis of this data revealed that there had been a statistically significant reduction in males to 45.9% of the population across these 16 generations, $p = 0.0258$ (Figure 5.1A), in line with the previously reported sex skew in this strain[2]. In contrast, the closely related A/J strain colony at MCRI bred for 15 generations, producing 560 individuals, in which there was no statistically significant difference between the numbers of males and females born ($p = 0.8007$) (Figure 5.1B). Notably, in both the A/HeJ and A/J colonies, there was some variation in the sex ratio between individual generations, as shown in the range of data points in Figure 5.1; however, tabulating all individuals born to their respective colony accounted for this generation-to-generation variance.

The original publication[2] speculated that mice carrying ovotestes that were primarily composed of ovarian tissue may develop externally as females[2], resulting in XY sex reversal. In order to ensure that there were no XY sex reversed female mice in the A/HeJ colony that may be missed in screening for gonadal abnormalities, a subset of A/HeJ male and female mice were routinely genotyped for the presence of the *Sry* gene. As it had been previously confirmed that the $Y^{A/HeJ}$ chromosome retained the *Sry* gene[2], any mice positive for *Sry* could be concluded to be XY. Through this genotyping, it was confirmed that there were no *Sry*-positive female A/HeJ mice ($n = 45$), and all male mice ($n = 74$) were positive for *Sry*. Therefore, it can be concluded that there was no sex reversal in the MCRI A/HeJ colony, and therefore, by examining mice classified as males at weaning, no XY mice would be inadvertently excluded from analysis.

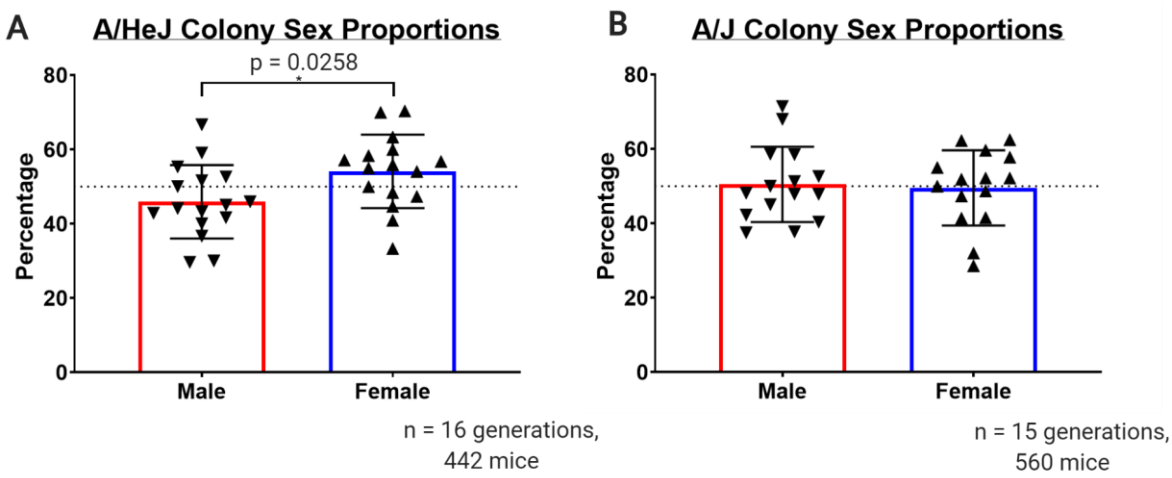

Figure 5.1 - Sex Ratios in the A/HeJ and A/J MCRI Colonies

The percentage of males and females in each of 16 generations of A/HeJ mice (n = 442 mice) and 15 generations of A/J mice (n = 560 mice) breeding at MCRI from 2014 to the end of 2018 was calculated. The mean of these percentages was taken and plotted to give an overall sex ratio of the colony. Individual data points are the percentage of each sex per generation. (A) Male A/HeJ mice were significantly reduced relative to females, accounting for 45.9% of the colony, p = 0.0258. (B) There was no sex skew observed in the A/J colony. Dotted line equals 50% of the population, the expected percentage for each of the sexes.

5.2.1.2. Abnormal Gonad Development Observed in A/HeJ E14.5 Embryos

The previous characterisation of the A/HeJ male phenotype focused primarily on the presentation of abnormal embryonic gonads[2]. Therefore, while confirming that the MCRI A/HeJ colony replicated the A/HeJ phenotype, A/HeJ embryos were assessed for the presence of abnormal XY gonads. To accomplish this, gonads were collected from A/HeJ embryos, as well as embryos from the control strain BALB/c, at E14.5 and examined for morphology on a dissection stereomicroscope. Gonads from BALB/c embryos were collected as controls, as this strain has no reported abnormalities in its testis determination or development, and therefore the gonads from these embryos would develop as normal ovaries or testes.

Embryos were collected at E14.5, as this time point occurred after the window of testis determination (E10.5 to E12.5, Section 1.1.5.2), with sufficient time for the gonads to undergo morphological changes associated with ovarian or testicular development. Also, this time point fell within the time points assessed in the original characterisation of A/HeJ (E13.5 to E15.5)[2], as at these ages, testes and ovaries are morphologically distinct. At E14.5, testes have begun to round up and develop testis cords, and were close to double the size of the ovaries, enabling differentiation between the gonads based on visual inspection during dissection.

At collection, pairs of gonads from E14.5 A/HeJ (n = 61) and BALB/c (n = 8) embryos were assessed visually for size and morphology. Each embryo was classified as having normal ovaries (Figure 5.2A), normal testes (Figure 5.2B), or abnormal gonads that were "testis-like" (Figure 5.2C). BALB/c gonad pairs were all categorised into either normal ovaries or normal testes, and all embryos deemed to have normal testes were confirmed to be XY by genotyping.

Of A/HeJ embryos, 29 of the 61 embryos were XY, representing 47.54% of the collected embryos (Figure 5.2D). This replicated the A/HeJ sex skew observed in the MCRI A/HeJ colony (45.9%) and in the original characterisation (46.8%)[2]. The majority of embryos collected were classified as having either normal testes or normal ovaries (24 embryos, 39.34% of collections, and 32 embryos, 52.46% of collections, respectively), with all embryos with testes being XY, and those with ovaries being XX.

The remaining five A/HeJ embryos (8.20%, Figure 5.2E) possessed gonads that appeared to be of an intermediate or poorly formed appearance, with all five of these embryos being XY. These abnormal gonads had the presence of striations indicating testis cords, and were often larger than normal ovaries; however, their morphology was markedly different from the normal testes (Figure 5.2C), typically being flatter than the rounded up testes. This resulted in these gonads being classified as "testis-like". Normal testes occurred in 24 of the 29 XY embryos, accounting for 82.76% of XY embryos (39.34% of all embryos), while the remaining five embryos carrying testis-like gonads accounted for 17.24% of the XY embryos (8.20% of all embryos).

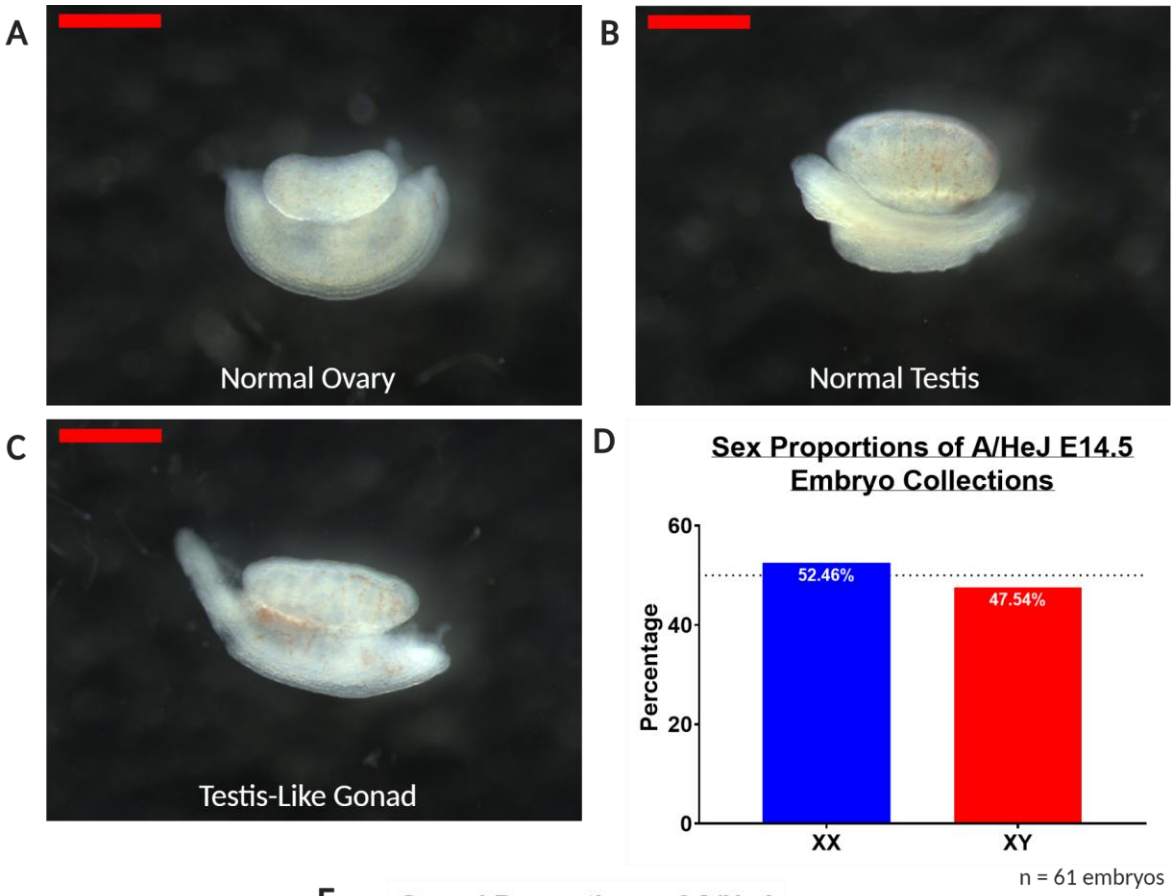
A
Normal Ovary
B
Normal Testis
C
Testis-Like Gonad
D
Sex Proportions of A/HeJ E14.5 Embryo Collections
Percentage
60
40
20
0
52.46%
47.54%
XX
XY
n = 61 embryos
E
Gonad Proportions of A/HeJ E14.5 Embryos
52.46% Ovaries
39.34% Testes
8.20% Testis-Like

Figure 5.2 - Abnormal Gonads Identified in A/HeJ E14.5 Male Embryos

Embryonic gonads were examined from A/HeJ embryos at E14.5, after the window of testis determination. (A) to (C) illustrate the three observed gonadal phenotypes: ovary (A), testis (B), and testis-like (C). There was a sex skew (D) present in these collections, with males being reduced relative to females, accounting for 47.54% of the cohort (n = 61 embryos). The collected gonads were examined for overall morphology and each pair were classified into three categories: testes, ovaries, or testis-like (E). These classifications were determined visually based on the size and shape of the gonads, as well as the presence or absence of testis cords. The majority of gonads were either ovaries (52.46%) or testes (39.34%), with the remaining 8.20% classified as testis-like (n = 61 gonads pairs). There was 100% concordance between an embryo having testes or testis-like gonads and being XY. Scale bars are 500 µm.

The incidence of abnormal gonads observed in embryonic XY A/HeJ gonads in this study (17.24%) deviated from the previous reported value for abnormal embryonic gonads in this strain. The original characterisation of C57BL/6J-$Y^{A/HeJ}$ embryonic gonads identified a rate of gonadal abnormality of 26.0% of 23 XY embryos examined (one embryo (4.3%) with attenuated cord growth, and five embryos (21.7%) with at least one ovotestis)[2], a difference of approximately 9% from the value found in this study. The cause of this discrepancy between this study and the previous study[2] is unclear; it may simply be due to a sampling effect in either of the studies, and hence may be rectified by examining a larger number of embryos.

Despite this discrepancy, the occurrence of abnormal gonads in XY A/HeJ embryos at E14.5 in the MCRI A/HeJ colony indicated that the reported A/HeJ embryonic male gonadal phenotype was indeed present in the MCRI colony. Therefore, it can be expected that abnormal gonads will also be present in A/HeJ adults (Section 5.2.1.3), and that the $Y^{A/HeJ}$ chromosome present in the A/HeJ males of the MCRI colony will carry the defect that causes this phenotype (Chapter 6).

5.2.1.3. Presence of Abnormal Gonads in Male A/HeJ Mice of the MCRI Colony

The original characterisation[2] of the A/HeJ mouse strain identified that 4% of non-productive males were hermaphrodites, carrying ovotestes[2], with an additional 17% of non-productive males possessing small testes which produced no epididymal sperm[2]. This yielded a total of 21% of non-productive males having some form of gonadal abnormality. However, this figure was speculated to be an underestimate of the total rate of gonadal abnormalities[2], as the analysis only assessed non-productive males[2]. It was predicted that mice carrying ovotestes with a large enough proportion of testicular tissue would likely retain some fertility, and hence be excluded from this analysis due to being productive[2]. Therefore, it was predicted that the incidence of gonadal abnormalities amongst A/HeJ males would increase were productive males also examined[2].

Adult A/HeJ males were assessed in this study for two reasons. First, to confirm the presence of abnormal gonads in adult A/HeJ males in the MCRI colony. Second, to determine whether expanding the assessment beyond non-productive males would result in replication of, or deviance from, the reported 21% rate of abnormal gonad development in the A/HeJ strain[2]. To achieve this, gonads were collected from A/HeJ males in an opportunistic manner as these males were culled for routine colony maintenance. Gonads were also collected from A/J males in a similar manner to serve as controls.

This strategy was selected for two reasons: firstly, it removed any bias between productive versus non-productive males, as both successful and unsuccessful breeders, as well as males never mated, were all equally likely to be selected as samples. Second, this enabled collection of gonads from males at various stages of the lifespan. This was advantageous, as the original study did not indicate the ages at which affected mice were identified.

For all collections, the body of the euthanised mouse was weighed prior to dissection, and following dissection, masses were obtained for the gonads individually and as a pair. Gonads were then imaged on a stereomicroscope.

Through the opportunistic collection of adult gonads, 39 A/HeJ and 38 A/J males were assessed at a variety of ages, with all collections falling within the range [49 days of age (d), 276 d]. All A/J gonads were found to have developed as normal testes, whereas five of the A/HeJ males were identified to have abnormal gonads (Figure 5.3), representing 12.8% of the A/HeJ males examined. For these five abnormal A/HeJ gonads, a pair of gonads from an age-matched A/J control male are shown in Figure 5.3. Table 5.1 lists the masses of these A/HeJ and age-matched A/J gonads, with the gonads listed as either left or right based on their location within the mouse, and also details the change in mass of the abnormal A/HeJ gonads from the A/J control gonads. Appendix Table A2 compares the abnormal A/HeJ gonads' mass and volume to that of their normal partners.

Table 5.1 - Comparison of Abnormal A/HeJ Gonad Pairs with Age-Matched A/J Control Gonad Pairs

Age (days, (A/HeJ)/ (A/J))	A/HeJ (Mass in mg) *(Volume in mm^3)		A/J (Mass in mg) *(Volume in mm^3)		A/HeJ Change from A/J (Mass, Percentage Mass) *(Volume, Percentage Volume)	
	Left	Right	Left	Right	Left	Right
* 56 d/ 48 d	25.2 mm^3	71.0 mm^3	65.8 mm^3	63.4 mm^3	-40.6 mm^3, -61.7%	+7.6 mm^3, +12.0%
74 d/ 78 d	33.0 mg	53.4 mg	70.0 mg	76.1 mg	-37.0 mg, -52.1%	-22.7 mg, -29.8%
173 d **/ 173 d	24.8 mg	22.2 mg	70.6 mg	69.6 mg	-45.8 mg, -64.9%	-47.4 mg, -68.1%
190 d **/ 196 d	14.0 mg	65.4 mg	77.1 mg	75.6 mg	-63.1 mg, -81.8%	-10.2 mg, -13.5%
216 d/ 209 d	50.8 mg	32.6 mg	78.2 mg	74.3 mg	-27.4 mg, -35.0%	-41.7 mg, -56.1%

For each entry, the abnormal gonad/s are highlighted in yellow, as are the calculations regarding the abnormal gonad/s in the final column.

*For the 56d A/HeJ and 48d A/J collections, no masses were available. Approximate volumes were calculated from images of the gonads as described in Appendix 8.1.

**Failed breeders (non-productive males).

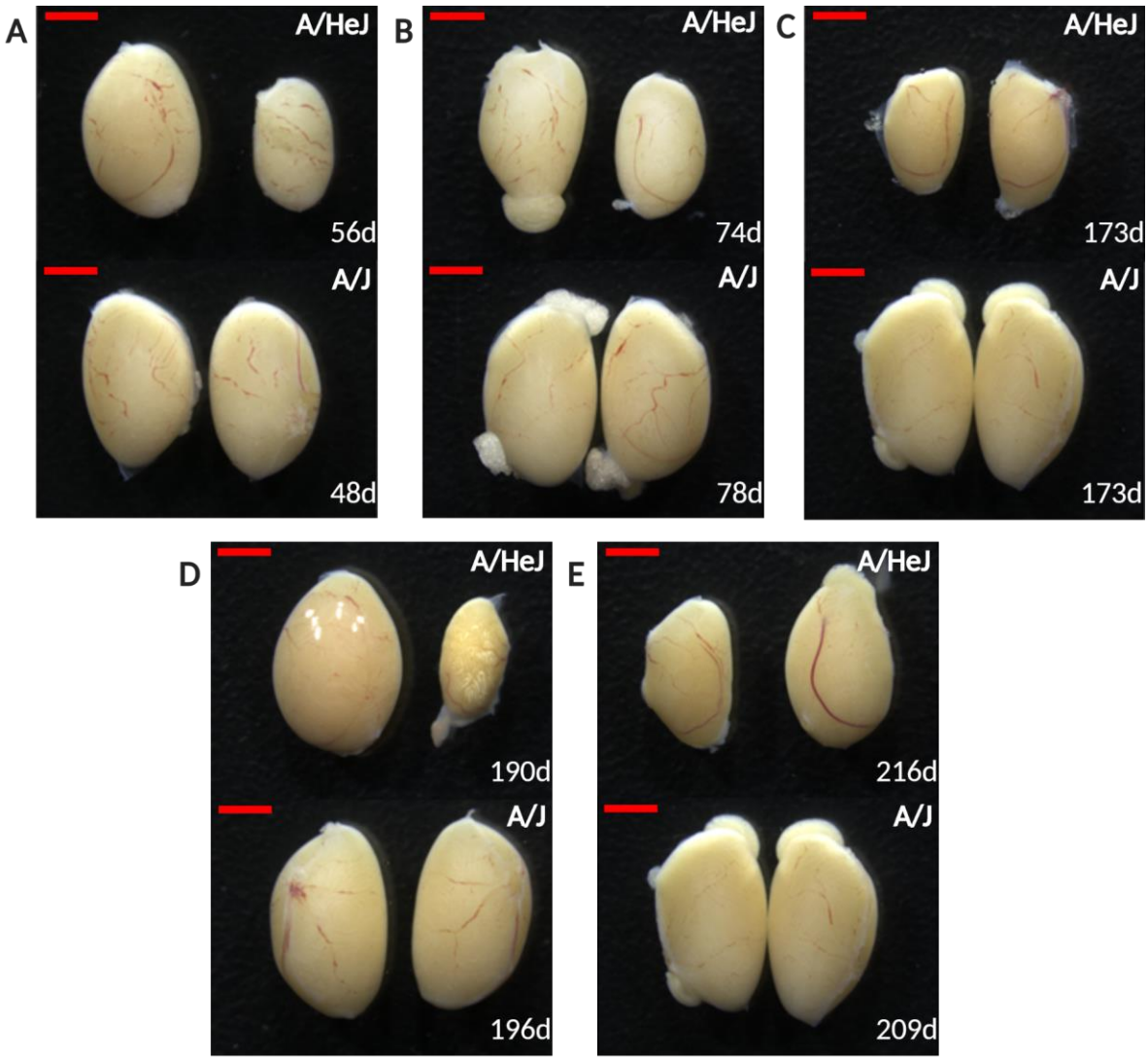

Figure 5.3 - Abnormal A/HeJ Gonads and Age-Matched Control A/J Gonads

Abnormal gonads recovered from A/HeJ male mice at different ages (A to E, top images) and age-matched A/J control male gonads (A to E, bottom images). The ages of the mice at collection increased from approximately six weeks of age (A) to approximately seven months of age (E), with the age increasing with subsequent samples (A to E). One abnormal gonad and one normal gonad were recovered from a 56 day old (d, A) and 74 d (B) A/HeJ male, with the abnormal gonad approximately one-third the mass of its counterpart. Normal A/J gonads (48 d, A; 78 d, B) below. Two abnormal gonads recovered from a 173 d (C) A/HeJ male; normal A/J gonads (173 d) below. One significantly small abnormal gonad recovered in the abdominal cavity of a 190 d (D) A/HeJ male, and one normal gonad recovered from the scrotum. Normal A/J (196 d) gonads below. One abnormally small A/HeJ gonad (216 d) and one normal gonad recovered. Normal A/J gonads (209 d) below. Scale bars are 2 mm.

Four of the five A/HeJ males carrying abnormal gonads (56 d (Figure 5.3A top), 74 d (Figure 5.3B top), 190 d (Figure 5.3D top), and 216 d (Figure 5.3E top)) were found to have only a single abnormal gonad, with the other gonad in the pair being of normal size and morphology. While not unexpected, as the testis determination pathway acts within each gonad autonomously, this was a feature not noted in the original characterisation. The remaining A/HeJ male identified to have abnormal gonads (173 d, Figure 5.3C top) was found to have both gonads be equally reduced in mass with similar morphology to one another.

In all abnormal A/HeJ gonads, the mass of the gonad was reduced relative to the A/J control gonad by at least one-third (Table 5.1), with seminiferous tubules visible in each abnormal gonad (Figure 5.3). Three of the four abnormal gonads which occurred with a normal partner were observed to occur on the left side of the animal (Figures 5.3A top, B top and D top), with the remaining gonad occurring on the right side (Figure 5.3E top). This was likely due to random chance, again due to the autonomous nature of gonads undergoing testis determination. However, as there were differences between the characteristics of each gonad pair, each will be discussed individually below.

The A/HeJ male which possessed two abnormal gonads (Figure 5.3C top) was aged 173 d at the time of collection, and was a failed breeder (non-productive male). Both gonads were located in the pelvic region, as expected for testes, and appeared to have reasonably ordered seminiferous tubules and vasculature similar to normal testes, albeit of a reduced size relative to the normal control A/J testes (Figure 5.3C bottom). Additionally, both of these abnormal A/HeJ gonads were of similar mass: 24.8 mg (left) and 22.2 mg (right), and therefore were similarly reduced relative to the A/J controls (left: 70.6 mg, right: 69.6 mg).

The gonads recovered from the 74 d A/HeJ male were an abnormal gonad and a normal partner (Figure 5.3B top), both of which were collected from the pelvic region. The morphology of the abnormal gonad was similar to that observed in the 173 d male (above), retaining vasculature and seminiferous tubules of a similar appearance to the control testes. However, the mass of the 74 d abnormal gonad was greater than that of the 173 d abnormal gonads, being reduced to approximately half the mass of the corresponding A/J gonad (33.0 mg and 70.0 mg, respectively (Figure 5.3B bottom), a 52.1% decrease).

The mass of the abnormal gonad assessed in the oldest of these A/HeJ males (216 d, Figure 5.3E top) was also reduced by approximately half of the corresponding A/J gonad (Figure 5.3E bottom), weighing 32.6 mg compared to the 74.3 mg mass of the control gonad (56.1% reduction). This abnormal gonad had a similar appearance to the 74 d and 173 d abnormal gonads, although was slightly smaller and less rounded. In contrast, the youngest A/HeJ mouse from which an abnormal gonad was recovered was 56 d at collection (Figure 5.3A top). Unfortunately, only calculated volumes were available for this gonad pair, as well as for its age-matched A/J control pair

(Figure 5.3A bottom, Table 5.1). This abnormal gonad was also recovered from the pelvic region, and was calculated to have a volume of 25.2 mm^3, approximately one third of the volume calculated for A/J control gonad (65.8 mm^3, a 61.7% reduction). This abnormal gonad was vascular, but appeared to have less densely-packed seminiferous tubules relative to the control testes.

The remaining abnormal A/HeJ gonad was the most divergent of all those recovered (Figure 5.3D top). Collected from a failed breeder male at 190 d of age, this gonad was located within the abdominal cavity, instead of in the pelvic region with its normal sized partner. This was in the region in which ovaries are typically located, and hence this gonad was classified as 'undescended'. Additionally, this abnormal gonad had the most reduced mass relative to the corresponding A/J control gonad of all the abnormal gonads recovered, weighing only 14.0 mg. This represented a 78.6% reduction relative to the A/J control gonad (65.4 mg, Figure 5.3D bottom). This abnormal gonad was also far smaller in size and less rounded relative to both its normal sized partner and both of the A/J controls, and was more yellow in colour. Seminiferous tubules were observable in this gonad; however, relative to normal testes, these tubules appeared to be somewhat less organised relative to controls.

These abnormal gonads recovered from the MCRI A/HeJ colony confirmed the presence of the A/HeJ phenotype in adult mice of this colony. However, these were recovered at a different rate than that observed in the original publication, accounting for 12.8% of A/HeJ males examined. This was likely due to the assessment of males regardless of productivity; however, the two failed breeders (non-productive males) which were found to have gonadal abnormalities had the two stand-out examples of the A/HeJ phenotype. The first (173 d, Figure 5.3C top) had abnormalities in both gonads, with both reduced to a similar degree. The second male (190 d, Figure 5.3D top) was identified to have an undescended gonad of substantially different morphology relative to controls. These differed from the remaining three males identified, which carried only a single reduced gonad, and this was likely the cause of the non-productive nature of these two males.

Additionally, the data collected in this section has added to the characterisation of the A/HeJ male phenotype. Here, representative images and masses for abnormal gonads and normal control testes have been provided. This data was not included in the original publication[2], due to its focus on the embryonic phenotype.

Overall, these results confirm the incidence of abnormal male gonads in the MCRI A/HeJ colony. Therefore, it can be reasonably assumed that the molecular cause of this phenotype is also present on the $Y^{A/HeJ}$ chromosome in this colony, and therefore this $Y^{A/HeJ}$ chromosome was amenable to further analysis to determine this cause (Chapter 6).

5.2.1.4. Genital Abnormalities Present in A/HeJ Mice Reported to be Hermaphrodites

The initial indication that there was a defect in the A/HeJ males reported in the original characterisation[2] was identified in a mouse with abnormal external genitalia sent to the Eicher laboratory in 1993[2]. There, that mouse was determined to be a true hermaphrodite due to the presence of both ovarian and testicular tissue within the gonads[2]. However, this single A/HeJ mouse was the only mouse reported in the original publication to exhibit genital abnormalities, and the nature of the abnormality was not described[2].

Incidentally, three A/HeJ males in the MCRI colony were detected by Animal Facility staff as being "hermaphrodites", having been observed to possess atypical external male genitalia. These three A/HeJ males, along with a normal A/HeJ male control and a normal A/J male control (all 14 to 16 weeks of age) were euthanised, and their genitalia imaged (Figure 5.4). The length of the protruded genitalia and the anogenital distance (AGD) were also measured for each mouse and are reported in Table 5.2.

Table 5.2 - Length of Genitalia and Anogenital Distance of Abnormal and Control A/HeJ and A/J Males

Mouse	Length of Protruded Genitalia	Anogenital Distance
Control A/J Male (Figure 5.4A)	5.0 mm	9.0 mm
Control A/HeJ Male (Figure 5.4B)	5.9 mm	10.0 mm
Abnormal A/HeJ Male (Figure 5.4C)	4.7 mm	10.0 mm
Abnormal A/HeJ Male (Figure 5.4D)	2.4 mm	11.0 mm
Abnormal A/HeJ Male (Figure 5.4E)	N/A	11.0 mm

The control A/J and A/HeJ males' genitalia (Figure 5.4A and B, respectively) were well-formed and able to be protruded from the abdomen. Both control genitalia were of similar lengths, 5.0 mm and 5.9 mm for the A/J and A/HeJ males, respectively. Of the three A/HeJ mice with abnormal genitalia, each had a unique presentation when protruded. Two of the A/HeJ mice (Figures 5.4C and D) had external genitalia that, relative to the control genitalia, were malformed and diminished in size. One A/HeJ male's genitalia were more substantially reduced in length, measuring 2.4 mm (Figure 5.4D), whereas the remaining genitalia were 4.7 mm in length (Figure 5.4C), similar to the control A/J male's genitalia. Both of the abnormal A/HeJ genitalia appeared to be slightly discoloured relative to the control genitalia, being yellow-toned rather than the beige/pink tone observed in the control A/J and A/HeJ genitalia.

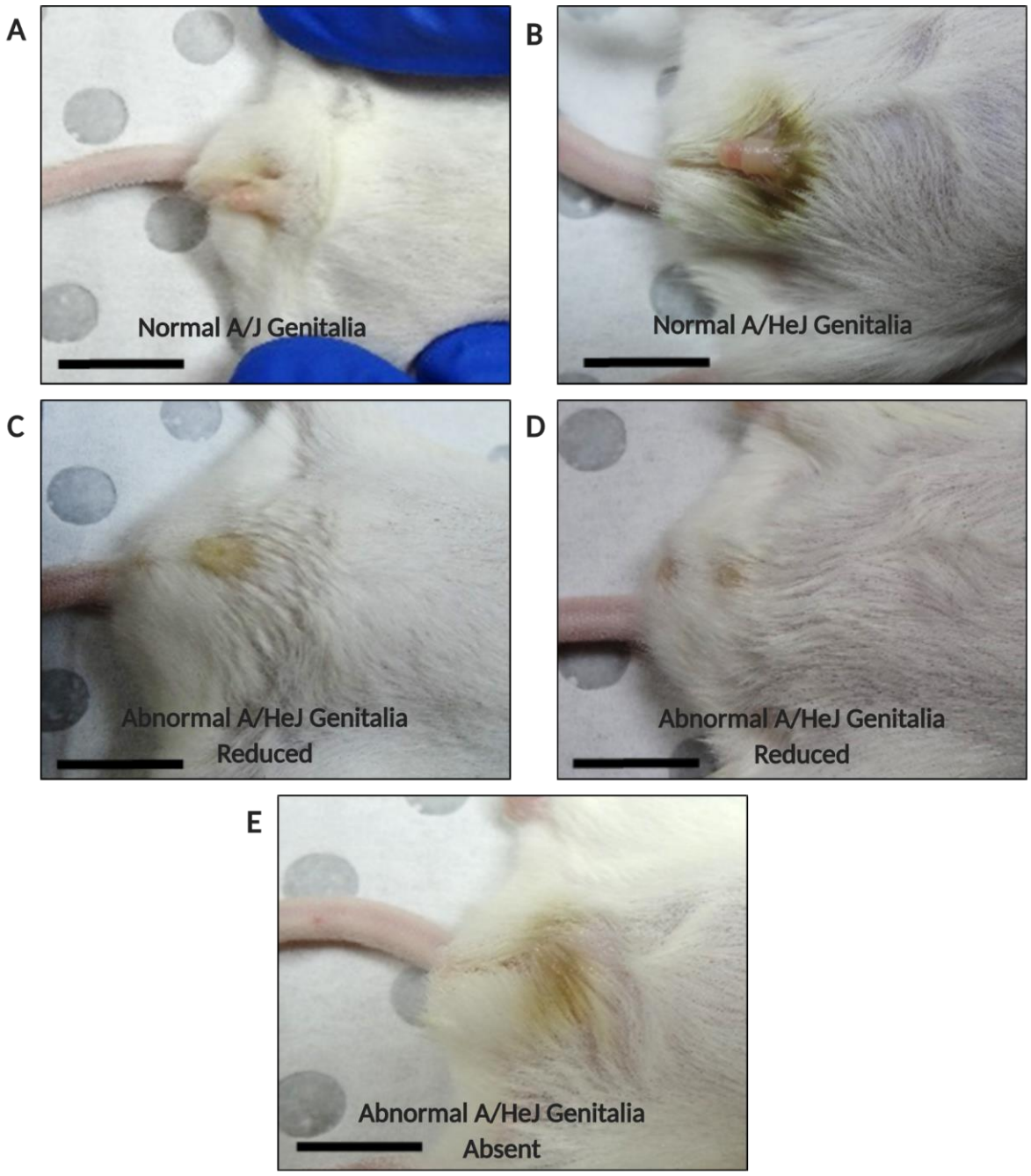

Figure 5.4 - Abnormal A/HeJ Genitalia

Three A/HeJ mice were identified as having abnormal genitalia by MCRI Animal Facility staff. The above images show an age-matched normal A/J (A) and A/HeJ (B) male genitalia, while (C) through to (E) show images of the abnormal A/HeJ genitalia. (C) Abnormal malformed genitalia of similar length as the control genitalia (4.7 mm compared to 5.0 mm (A) and 5.9 mm (B)). (D) Abnormal malformed genitalia length was reduced by approximately half compared to normal control genitalia (2.4 mm). (E) External genitalia absent, instead a mound structure was present with a slit-like structure. Scale bars are 1 cm.

The remaining A/HeJ mouse identified as a "hermaphrodite" differed from both the control genitalia and the other abnormal A/HeJ genitalia. This mouse (Figure 5.4E) did not have any external genitals, with no structure able to be protruded from the abdomen. Upon closer inspection of the lower abdominal region, it was found that there was no external prepuce (skin flap which protected the retracted genitalia (penis)[250,251]) through which genitalia could protrude. Instead, examination of this region revealed a small "slit"-like structure, likely to serve as a urinary opening, with the vicinity around this structure slightly raised in a mound.

The absence of external genitalia in this mouse was initially suspected to indicate that it had undergone sex reversal. However, upon dissection, testes were observed in the pelvic region, indicating that testis determination had occurred during embryogenesis. Therefore, it was speculated that there was an unknown defect in the development of the genitalia following testis determination.

In addition to assessing the genitalia of the abnormal A/HeJ mice, the anogenital distance (the distance between the genitalia and the anus, AGD) was also measured. AGD is sexually dimorphic in mice, with the distance in males being approximately double that observed in females[252]. It was predicted that if the abnormal A/HeJ mice had incomplete sex determination or sex reversal, that the AGD in these mice would be reduced compared to the AGD in the control mice. However, this was not observed, with all three abnormal A/HeJ mice having the same or greater AGD as both of the control mice (Table 5.2), with all five measurements being within 2 mm of each other (range [9 mm, 11 mm]). Therefore, it can be concluded that the cause of the abnormal genitalia in these three A/HeJ mice did not adversely affect the development of a sufficient AGD.

The presence of the abnormal and absent genitalia in these A/HeJ mice served as another confirmation of the A/HeJ phenotype in the MCRI colony, despite this not being reported in the original publication beyond being the first indication of a defect in A/HeJ males. In addition to this confirmation, this work has also provided quantitative (genitalia and AGD measurements) and qualitative (images, Figure 5.4) data regarding the A/HeJ phenotype as it manifests externally.

5.2.2. Further Characterisation of the A/HeJ Male Phenotype in Adults

The presence of gonadal and genital defects in males of the MCRI A/HeJ colony like those reported in the previous characterisation[2] of this strain's phenotype was confirmed in Section 5.2.1.This ensured that the A/HeJ phenotype was presenting in the MCRI colony before beginning investigations into its cause. In addition to this confirmation, however, this study also identified novel features of the A/HeJ male phenotype, which aimed to add detail to the characterisation of the adult A/HeJ phenotype. This was achieved by assessing gonads collected from adult A/HeJ males in pursuit of abnormal gonads (Section 5.2.1.3), as well assessing data on the productivity of the males in this strain.

5.2.2.1. Gonad Mass in A/HeJ Males is Reduced Overall and Declines with Age

As gonads were collected from A/HeJ (n = 39 mice) and A/J (n = 38 mice) males in Section 5.2.1.3 in order to confirm the incidence of abnormal A/HeJ gonads, measurements of the gonads' mass, both individually and as a pair, were taken in order to provide quantitative data on these abnormal gonads. Throughout this process, the mass of normal A/HeJ and normal control A/J gonads were also recorded as they were collected. The A/HeJ and A/J males whose gonads were collected were differing ages at the time of sample collection, due to the opportunistic sampling method employed. This resulted in samples from a wide range of ages, from sexual maturity through to nine months (276 d) of age (range [49 d, 276 d]). Table 5.3 compares the gonad masses of old and young A/HeJ and age-matched A/J males in Figure 5.5D and C, respectively.

Table 5.3 - Comparison of Old and Young A/HeJ and A/J Gonad Dimensions and Paired Gonad Mass

Mouse (Figure ID)	Age in Days	Left Gonad *		Right Gonad *		Paired Gonad Mass (mg)
		Length (mm)	Width (mm)	Length (mm)	Width (mm)	
Young A/J (Figure 5.5C top)	78 d	6.74 mm	4.37 mm	6.89 mm	4.19 mm	146.1 mg
Young A/HeJ (Figure 5.5C bottom)	74 d	6.58 mm (-2.3%)	4.38 mm (+0.23%)	6.86 mm (-0.44%)	4.39 mm (+4.77%)	141.3 mg (-3.29%)
Old A/J (Figure 5.5D top)	276 d	6.97 mm	4.38 mm	7.04 mm	4.20 mm	157.6 mg
Old A/HeJ (Figure 5.5D bottom)	263 d	6.11 mm (-12.34%)	3.87 mm (-11.64%)	6.35 mm (-9.80%)	3.56 mm (-15.24%)	94.7 mg (-39.91%)
*Length and width values measured from images as described in Section 2.1.6.1. Percentages in A/HeJ rows represent percentage change relative to the corresponding A/J gonad.						

This allowed for the assessment of gonad mass over the lifespan in both A/HeJ mice and in the control strain, A/J, and was assessed as change in paired gonad mass over time for all gonads collected (including abnormal gonads) (Figure 5.5A). As gonad collections were conducted as opportunistically, there were few mice that are age-matched to the day between the two strains, necessitating that the data be viewed in terms of the overall trend.

The first fact noted about the plot of paired gonad mass and age at collection (Figure 5.5A) was that, over the entire collection age range, A/HeJ males' paired gonad mass was less than that of A/J males' of similar age. This was observed in the youngest A/HeJ and A/J mice (Figure 5.5C), with the discrepancy in paired gonad mass increasing as the mice advanced in age, leading to the second notable fact about this data.

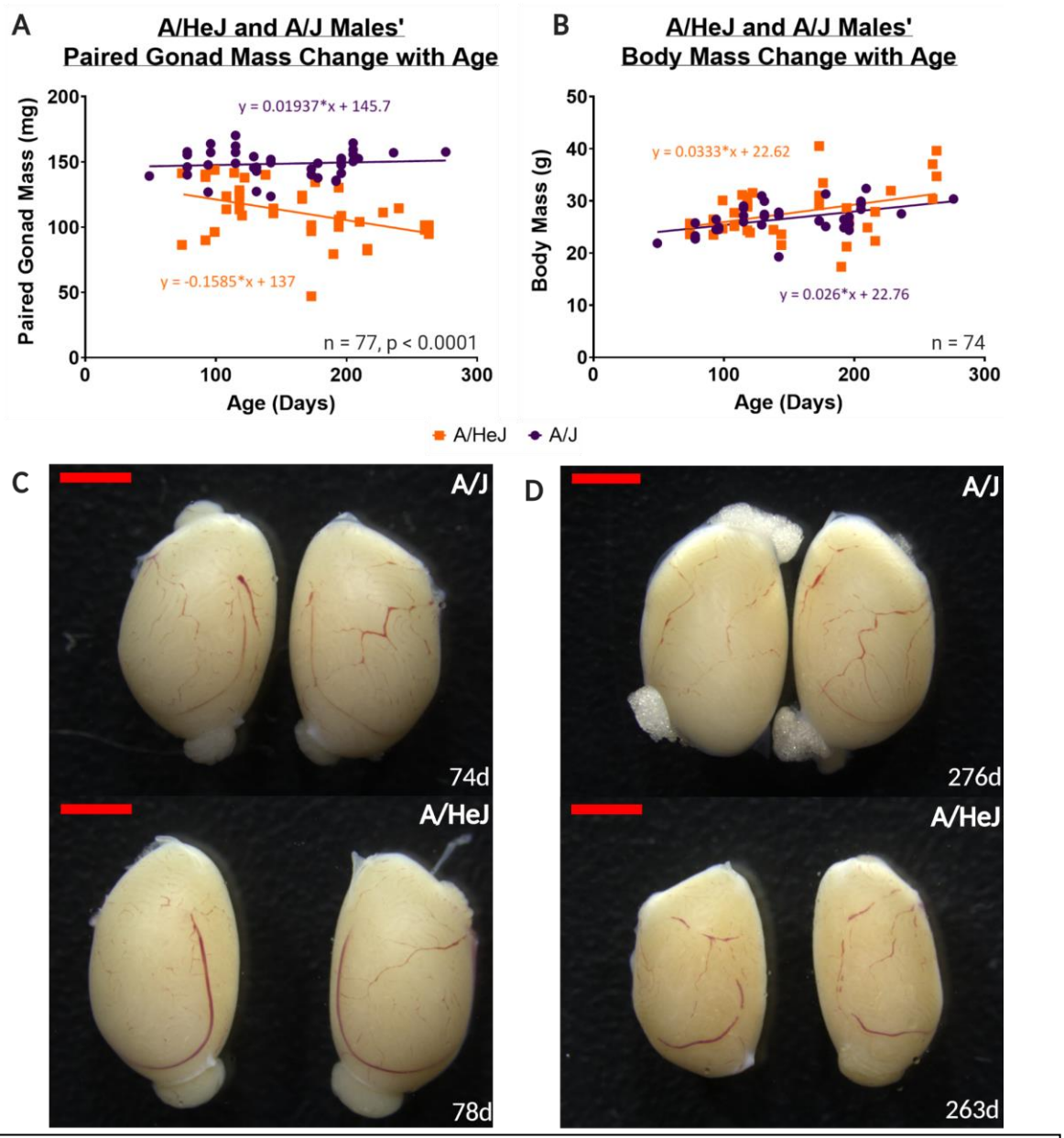

Figure 5.5 - Change in A/HeJ Gonad Mass Over Time

(A) Plot of paired gonad mass against age of mouse at collection for A/HeJ (orange) and A/J (purple) male mice. A/J paired gonad mass remained constant over the age range assessed. A/HeJ paired gonad mass, however, significantly declined with increased age ($p < 0.0001$). (B) Body mass of A/HeJ and A/J males collected for gonads. Both strains' body mass increased slightly with age, with no decline in A/HeJ mice that would correspond to the decline in A/HeJ paired gonad mass in (A). (C) Age-matched young A/HeJ and A/J gonads (74 d (bottom) and 78 d (top), respectively). At this age, the gonads of both strains appeared similar in size. (D) Age-matched old A/HeJ and A/J gonads (263 d (bottom) and 276 d (top), respectively). The A/HeJ gonads at this age were reduced in mass relative to the A/J gonads (paired mass = 94.7 mg and 157.6 mg, respectively), as well as appearing smaller visually. Scale bars for (C) and (D) are 2 mm.

While A/J males' paired gonad mass remained relatively constant across all ages, A/HeJ males' paired gonad mass significantly declined as the A/HeJ males increased in age at time of collection. A linear regression trend line fitted to both the A/HeJ (orange) and A/J (purple) data in Figure 5.5A highlights the overall decline in A/HeJ paired gonad mass, with the A/HeJ paired gonad mass data being significantly different from the A/J data ($p = 0.0095$). The correlation between paired gonad mass and age for the A/HeJ cohort was also significant at $p = 0.0073$ ($R^2 = 0.1789$), while there was no correlation for the A/J paired gonad masses. This indicates that there was an age-related effect on paired gonad mass in the A/HeJ males only.

This decline in gonad mass in the A/HeJ males can also be observed visually; as seen in Figure 5.5D, the oldest collected A/HeJ gonads (Figure 5.5D bottom, 263 d) appeared smaller than the oldest collected A/J gonads (Figure 5.5D top, 276 d), with the A/HeJ gonads being reduced in length and width relative to the A/J gonads (Table 5.3). This represented a decline in the overall volume of the A/HeJ gonads, which was also reflected in the 62.9 mg reduction in mass from that of the A/J gonad pair. Conversely, the young A/HeJ and A/J gonads (Figure 5.5C bottom, 74 d, and Figure 5.5C top, 78 d, respectively) were of similar lengths, widths and masses (Table 5.3), indicating that the A/HeJ gonads begin at a similar size to the A/J gonads before the onset of mass (and volume) decline with age in the A/HeJ males.

As seen in Figure 5.5A, in both the A/HeJ and A/J cohorts, there was variance in the paired gonad mass collected at a given age, such as in the younger mice, in which many A/HeJ gonad pairs had a mass similar to or greater than some of the A/J control pairs. However, the overall trend of declining A/HeJ paired gonad mass can be illustrated by comparing the masses of gonads collected at the earliest (74 d) and latest (263 d) time points at which there were samples in both strains. There were two A/HeJ mice at each of these respective ages in this dataset, with the 74 d males having a mean paired gonad mass of 113.85 mg, while the 263 d males' mean paired gonad mass was 98.10 mg, a 13.83% decrease over 189 days.

It was speculated that the decline in paired gonad mass with age observed in the A/HeJ males may be due to an overall decline in these mice. Therefore, the body mass prior to collection of the gonads was plotted against age at collection for the A/HeJ and A/J males (Figure 5.5B). Males of both strains were found to increase in body mass at a similar rate ($p = 0.6517$), with A/HeJ males tending to increase slightly more than A/J males. The ranges of body mass values were similar for both the A/HeJ [17.36 g, 40.51 g] and A/J [19.28 g, 32.38 g] males. The mean body mass of each strain was also similar (A/HeJ: 27.87 g, A/J: 26.65 g); however, there was more variation in A/HeJ body masses, as reflected in the standard deviation, 5.079 as compared to 2.788 for the A/J data.

Therefore, it can be concluded that there was an age-related decline in A/HeJ gonads that was not the result of an overall decline in the mass of these mice. This trend of age-related change to the mass of A/HeJ gonads was not reported in the original characterisation[2] of this strain's

phenotype, and was therefore a novel finding of this study.

5.2.2.2. A/HeJ Males Father Smaller Litters than A/J Males

In light of the reduced mass of A/HeJ gonads at all ages determined in Section 5.2.2.1, it was speculated that this gonadal phenotype may exert an effect on the fertility of A/HeJ males. To assess this, productivity of A/HeJ breeder males was compared to A/J breeder males using breeder data from each colony, from the first generations born in the MCRI Animal Facility (1st of July, 2014 and 1st of January, 2014, respectively), through to the last litters born in 2018. For each breeder male, productivity was calculated as the mean number of pups produced per litter (Figure 5.6A).

The mean number of pups produced by a single male in each strain fell within similar ranges, between one and seven pups for A/HeJ males, and between one and eight pups for A/J males. Overall, however, A/HeJ males produced fewer pups per litter on average, with a mean litter size of 4.02 ± 1.50 pups (n = 46 males), compared with A/J males, which produced an average of 4.87 ± 1.70 pups per litter (n= 48 males) (Figure 5.6A). When comparing these means, the decline of 0.85 ± 0.33 (mean ± SEM) pups per litter in the A/HeJ males relative to A/J males was statistically significant at p = 0.0122. This indicated that there was a slight but significant reduction in A/HeJ male productivity compared to the closely related control strain, likely as a result of the phenotype in the A/HeJ males.

Following this finding, breeder data was then assessed as a function of male age at time of conception, due to the age-related decline in A/HeJ gonad mass identified in Section 5.2.2.1. This was performed as the reduction in gonadal mass in A/HeJ males with age was predicted to adversely affect litter size, and an insufficient number of breeder males' gonads were collected over a sufficient age range to assess the relationship between paired gonad mass and litter size directly. Therefore, the number of pups born per litter was plotted against the approximate age of the male at conception (calculated as per Section 2.9) (Figure 5.6B).

Over the approximately four years of breeding in the A/HeJ and A/J colonies, 118 and 130 litters were born, respectively. The maximum number of pups in a litter were 11 pups for the A/J colony, and nine pups for the A/HeJ colony, with the mean number of pups per litter overall being significantly different between the two strains (5.29 ± 2.03 pups/litter and 4.69 ± 1.86 pups/litter, respectively, p = 0.0147). This value differs from the mean of the mean number of pups per litter calculated per male described above, as that was an assessment of the overall productivity of a male over its lifespan, whereas the mean number of pups (reported in this Section) assessed the variation between individual litters.

Figure 5.6 - A/HeJ and A/J Male Productivity

(A) Comparison of mean number of pups produced per litter for all breeder A/HeJ (orange) and A/J (purple) breeder males from the start of their respective colonies in 2014 to the end of 2018. There was a statistically significant reduction in mean number of pups produced by A/HeJ males relative to males from the closely related A/J strain: 4.02 ± 1.50 pups (n= 46 males) and 4.87 ± 1.70 pups (n = 48 males) per litter, respectively; p = 0.0122. (B) Plot of individual litter size against approximate age of male at conception (litter date of birth minus 20 d) for A/HeJ and A/J breeder males. There was no significant change in litter size with increased age, nor was there a significant difference between the two strains.

The aim of this comparison was to determine whether A/HeJ litter size declined with age, as this would indicate an effect of decreasing gonad mass on male productivity. However, the difference in litter size over time between A/HeJ and A/J was not significantly different ($p = 0.5574$), as suggested by the trend lines in Figure 5.6B.

Taken together, the above assessments of breeder data indicates that, while there was a age-related decline in A/HeJ male gonad mass, this reduced mass did not significantly reduce litter size with increased age relative to the A/J control strain, despite the fact that A/HeJ males father smaller litters overall.

5.3. Discussion

In this chapter, the phenotype of the A/HeJ male mice was assessed for two reasons. Firstly, to confirm that the MCRI A/HeJ colony replicated the abnormal male phenotype reported in the original characterisation[2]. This was necessary, as four years (2014 to 2018) and 16 generations had intervened between the arrival of the strain at MCRI from the Jackson Laboratory and the conclusion of this study. This assessment was to ensure that the phenotype had not been lost due to genetic drift through breeding within MCRI.

Additionally, the second aim of this chapter was to extend the characterisation of the A/HeJ phenotype from what was initially reported[2]. The focus in this study was on the adult phenotype, as the original characterisation focused primarily on embryonic phenotype[2]. This study aimed to supplement the original publication[2] by providing quantitative and qualitative data of the adult A/HeJ phenotype, with the goal to better assess the effect of the $Y^{A/HeJ}$ chromosome on male gonadal phenotype.

5.3.1. Confirmation of the A/HeJ Male Phenotype in the MCRI A/HeJ Colony

Prior to assessing the $Y^{A/HeJ}$ chromosome to determine the molecular aetiology of the A/HeJ male sex determination defect, it was essential to confirm that the reported phenotype was also present in the MCRI colony. This was to ensure that the $Y^{A/HeJ}$ chromosome present in the MCRI A/HeJ colony also elicited these gonadal abnormalities, and was therefore carried the same defect as the $Y^{A/HeJ}$ chromosome in the original characterisation[3]. This was a necessary step, as the Y chromosome is more susceptible to genetic drift than the X chromosome or the autosomes[21,61] (Section 1.1.2.2). As the MCRI A/HeJ colony was 16 generations removed from the source stock, confirmation of the phenotype was required to confirm that the causative element on the $Y^{A/HeJ}$ chromosome hadn't been lost due to genetic drift throughout breeding.

The most readily available assessment of the A/HeJ phenotype was the incidence of sex

skewing, reducing the proportion of males. The reduction in males in the MCRI colony closely matched that reported in the original publication (45.9% and 46.8%[2], respectively), giving the first indication that the MCRI A/HeJ colony was replicating the phenotype. However, the original indications of abnormality in the A/HeJ strain reported in the original characterisation was assessment of a male with abnormal genitalia sent to the Eicher laboratory in 1993[2]. This appears to have been the precipitating event for monitoring and examining the A/HeJ strain over the 12 years reported in the original characterisation publication[2].

Following detection of three A/HeJ mice classified as "hermaphrodites" by Animal Facility staff due to the presence of abnormal external genitalia, genital abnormalities in the A/HeJ strain were also able to be examined in the MCRI colony. This examination identified two males with abnormal genitalia, both which were malformed and reduced in size, and an additional male that did not have any external genitalia. While the presence of abnormal genitalia was not represented to be a defining characteristic of the phenotype in A/HeJ mice with males, their occurrence did bolster the confirmation of the reported phenotype in the MCRI A/HeJ colony.

The primary component of the A/HeJ phenotype, however, was the incidence of male mice possessing ovotestes and small testes[2], which had been identified at a rate of 21% amongst non-productive males[2]. The limitation of this value in the original characterisation[2] was the assessment of only non-productive males, leading the authors to suggest that inclusion of productive males would alter the reported rate of gonadal abnormalities[2].

The authors'[2] original prediction for including productive A/HeJ males in assessment of gonadal phenotype was that the rate of gonadal abnormality would rise, as some males' abnormal gonads may retain partial function and fertility[2]. However, upon non-biased collection of A/HeJ males regardless of breeder status in this study, the inverse was found to be the case. Instead, the rate of mice carrying overtly abnormal gonads was markedly reduced relative to that previously identified in non-productive A/HeJ males (12.8% reduced from 21%[2]).

The reduction in the percentage of A/HeJ mice with gonadal abnormalities with inclusion of productive/non-breeder males in this study suggests that there were no males with abnormal gonads being missed by assessing only non-productive males in the original characterisation[2]. Of the five males identified with abnormal gonads in this study, three were never mated, and hence their fertility not assessed, with the remaining two having been mated to either one or two females, yielding no pups. Of successful A/HeJ breeder males whose gonads were collected, none possessed abnormal gonads. Based on the results from this study combined with that from the previous study[2], it is likely that overtly abnormal gonads (ovotestes and small testes) occur only within non-productive A/HeJ males, with none of these abnormal gonads retaining sufficient function to result in a productive male.

The original characterisation primarily focused on the defects in embryonic gonads resulting from the presence of the $Y^{A/HeJ}$ chromosome in a consomic strain (C57BL/6J-$Y^{A/HeJ}$)[2]. Unlike the adult phenotype, the description of the embryonic phenotype was detailed and representative images were provided in the publication[2]. As the embryonic gonadal phenotype was a major focus of that characterisation[2], in order for this study to accurately compare the MCRI A/HeJ colony to the previous report, A/HeJ embryonic gonads were examined. This was to ensure that similar defects in embryonic gonads also appeared in the MCRI colony, as another method to confirm the presence of the A/HeJ male phenotype.

Analysis of the A/HeJ E14.5 embryonic gonads in this study yielded a different proportion of abnormal gonads from that found previously[2], despite both collections showing a reduced proportion of males (47.54%, 29/61 embryos, and 43.40%, 23/53 embryos[2], respectively). In this study, 17.24% of male A/HeJ embryos (8.20% of total collections, 5/61 embryos) had gonads that were classified as abnormal or 'testis-like'. This is a reduction from the reported rate of approximately 26% (6/23 male embryos) gonadal abnormalities in A/HeJ male embryos[2], despite a similar number of male (XY) embryos being examined in both assessments. The discrepancy between the studies may be due to sample size, and may decline with collection of a larger number of embryos. Despite this, the prescience of abnormal 'testis-like' gonads in XY A/HeJ embryos from the MCRI colony confirmed that the A/HeJ male phenotype was indeed detectable in embryonic gonads.

Despite some discrepancies between the results obtained in this study and that from the original characterisation[2], such as the incidence rates of abnormalities in A/HeJ males, this work has served to confirm that the A/HeJ male phenotype was indeed replicated in this colony. Therefore, it can be concluded that the $Y^{A/HeJ}$ chromosome of these males carried the defect identified in the original A/HeJ colony assessed[2].

5.3.2. Novel Characteristics of the A/HeJ Male Phenotype

Following the confirmation that the reported phenotype was present in the MCRI A/HeJ colony, the second aim of this chapter was to better describe the presentation of the A/HeJ male phenotype in adults, as there was a paucity of data on the adult phenotype in the original characterisation[2]. The majority of the previous characterisation focused primarily on the A/HeJ embryonic gonadal phenotype, providing qualitative data in the form of representative images of embryonic gonads[2]. The work performed in this study regarding the adult A/HeJ phenotype, meanwhile, generated both qualitative (representative images) and quantitative (masses, productivity) data.

One aspect of the A/HeJ male phenotype that was not previously described in detail was the classification criteria for abnormal gonads (ovotestes and small testes) as opposed to normal

gonads/testes. To address this, masses were recorded for the gonads collected from A/HeJ males and control A/J males in order to generate data illustrating the defining characteristics of the abnormal gonads in the A/HeJ males, and how these gonads compared to normal A/HeJ and A/J gonads. From these measurements, it was observed that abnormal A/HeJ gonads were reduced in mass by 40% to 80% from the age-matched control A/J gonads, with the mass of the abnormal gonads ranging from 14.0 mg to 33.0 mg, compared to the 70 mg to 80 mg masses of the A/J gonads.

In addition to recording masses, the imaging of the abnormal A/HeJ gonads and normal gonads served to provide specifics regarding the A/HeJ male phenotype. The original characterisation did not provide representative images for the abnormalities obsessed in the A/HeJ adult, only doing so for the embryonic gonads[2]. In order to better describe the adult phenotype, this study presented images of all abnormal gonads collected. In the majority of the abnormal gonads, the affected gonad was similar in appearance to a normal testis, merely reduced in size. These gonads likely represented the small testes described in the original publication[2]. One abnormal gonad, however, was located within the abdominal cavity, being undescended (190 d male, Figure 5.3D). Its appearance was starkly diverged from that of both normal testes and the other abnormal gonads identified, being substantially reduced, differently coloured and having an abnormal appearance to its seminiferous tubules. This appearance, combined with its location in the abdominal cavity, suggest that this gonad was likely an ovotestis. Further collection of abnormal A/HeJ gonads combined with sectioning and staining would be recommended to confirm the presence of ovarian tissue within this type of gonad.

Another interesting observation regarding the incidence of abnormal gonads in A/HeJ males was that, in all bar one mouse, only one of the pair of gonads had developed abnormally, with the partner being of comparable size to the age-matched A/J control gonads. While this was not unexpected, as the cells of each gonad (and hence the gonads themselves) complete sex determination autonomously[91], this was not a fact previously reported[2], representing a novel finding of this study. Additionally, while the original publication predicted that the rate of gonadal abnormalities would rise if productive A/HeJ males were also assessed[2], the findings of this study indicate that abnormal gonads only occur in non-productive males. This was concluded based on the absence of abnormal gonads in any of the successful A/HeJ breeder males collected.

The opportunistic collection strategy employed in this study allowed for collection of gonad pairs from males of both the A/HeJ and A/J strains across a variety of ages within the first nine months of life. The initial report[2] did not describe the ages at which A/HeJ males with abnormal gonads were identified, but as males were examined after they failed to father litters, it is likely these mice were a few months of age at gonad examination. However, the advantage of this study is that the age at collection was recorded for all A/HeJ and A/J males, and from this, it was possible to examine and compare the change in gonad mass with age in both strains. This revealed the previously unknown decline in paired gonad mass with age in A/HeJ males. Prior to this novel

finding, it was presumed that A/HeJ males possessed either abnormal gonads, in the form of ovotestes or small testes, or normal testes. However, as was illustrated in Figure 5.5D (bottom), the gonads of an A/HeJ male at several months of age were smaller than that of control males (Figure 5.5D top), although this decline may not have reached the threshold of classification as a small testis in the original characterisation[2]. However, the appearance of reduced gonads in older A/HeJ males suggests that there is an abnormality associated with the $Y^{A/HeJ}$ chromosome in male gonads which visually appear to have developed normally.

As the information regarding the adult A/HeJ phenotype in the original characterisation tended to be from non-productive males[2], it was speculated that the A/HeJ phenotype, as suggested by the age-related decline above, may negatively affect the productivity of fertile A/HeJ males. Assessment of breeding data for the A/HeJ and control A/J colonies revealed that the mean litter size over the entire reproductive life of the male was slightly but significantly reduced in A/HeJ males relative to A/J males. However, despite the observed age-related decline in the paired gonad mass in the A/HeJ males, there was no significant decline in litter size with increased age, suggesting that the paired gonad mass decline does not have a cumulative negative effect on fertility over time. However, it is possible that the cause of the paired gonad mass decline may also result in the overall reduction in litter size over the total life of the male.

A potential confounder of these results, however, was that productivity was assessed on the two strains' respective genetic backgrounds, as A/HeJ and A/J are separate inbred strains. This allows for the possibility that the difference in litter size was due to other genomic elements, rather than solely due to the effect of the $Y^{A/HeJ}$ chromosome on male fertility. Ideally, both the $Y^{A/HeJ}$ chromosome and $Y^{A/J}$ chromosome would be backcrossed onto the same inbred background, such as onto the C57BL/6J background, to create a consomic strain. Breeding within the consomic strains could then be compared to assess the effect of the different Y chromosomes. Despite this limitation, due to the gonadal phenotype observed in A/HeJ males, it is still likely that the $Y^{A/HeJ}$ chromosome contributes to this decrease in fertility relative to control males.

The novel findings identified in this study have added needed detail to the A/HeJ adult male phenotype, and have suggested that all A/HeJ male gonads are likely affected by the $Y^{A/HeJ}$ chromosome, regardless of an otherwise normal morphology. This indicates that the effects of the $Y^{A/HeJ}$ chromosome on the gonads may be more far reaching than merely causing the development of ovotestes and small testes.

Chapter 6: Structural and Regulatory Changes on the A/HeJ Y ($Y^{A/HeJ}$) Chromosome

6.1. Introduction

The gonadal abnormalities in A/HeJ male mice were causally linked to the $Y^{A/HeJ}$ chromosome through examination of the C57BL/6J-$Y^{A/HeJ}$ consomic strain[2]. In addition to this phenotype, the $Y^{A/HeJ}$ chromosome was observed to exhibit cytological abnormalities[2]. From these observations, the original characterisation[3] predicted that both the A/HeJ male phenotype and the morphological abnormalities were both the result of a structural change at or near the $Y^{A/HeJ}$ centromere[2].

The hypothesis of this study was that this structural change was a deletion within the *Rbmy* tandem repeat array, reducing the copy number of this gene on the $Y^{A/HeJ}$ chromosome. It was predicted that such a deletion in this region would adversely affect regulation of the testis-triggering gene *Sry*, due to increased proximity to the repressive heterochromatin of the centromere. This would alter its expression during the window of testis determination in the genital ridge.

In order to address this hypothesis, two aspects of the $Y^{A/HeJ}$ chromosome were assessed: copy number of the *Rbmy* gene, and methylation (regulation) of the *Sry* gene. Firstly, the $Y^{A/HeJ}$ chromosome *Rbmy* copy number was ascertained, and compared to the *Rbmy* copy number on the Y chromosome from the two control strains, A/J and BALB/c. Secondly, the *Sry* locus was assessed for changes to its methylation state in the genital ridges of A/HeJ and control embryos at various time points throughout testis determination. This was assessed as methylation is a repressor of gene expression[253], and an increased level of *Sry* methylation during testis determination would indicate a delayed or reduced level of *Sry* expression. As the window for testis determination in mouse genital ridges is tightly controlled (Section 1.1.5.2), with the genital ridge unable to commit to testis development beyond E12.5, the timing of *Sry* expression is crucial.

The experiments described in this chapter aimed to assess the *Rbmy* and *Sry* loci on the $Y^{A/HeJ}$ chromosome. To determine the copy number of *Rbmy*, a copy number variation (CNV) Droplet Digital PCR (ddPCR) assay was designed. The methylation of *Sry*, meanwhile, was examined in genital ridges using two methods: a novel methylation-dependent ddPCR assay, and bisulfite sequencing.

Figure 6.1 - Gene Map of the Mouse Y Chromosome Short Arm

Schematic illustrating the genes on the short arm of the mouse Y chromosome, from the telomere (left end of map) to the centromere (right end of map, purple). The genes of interest have been highlighted in red: *Ddx3y*, *Sry* and the *Rbmy* tandem repeat array. The centromere (purple) is also of interest to this project. Map not to scale.

6.1.1. Genes of Interest on the Short Arm of the Y Chromosome

The mouse Y chromosome (described in Section 1.1.2.2) is acrocentric, comprised of a long (q) arm and a very short (p) arm. Of interest to this study is the short arm (Yp), illustrated in Figure 6.1 with relevant loci highlighted, on which the majority of Y chromosome coding genes reside. The primary loci of interest are *Sry*, contained within an inverted repeat, and the large region adjacent to the centromere containing multiple repeats of the gene *Rbmy*. The *Ddx3y* gene, discussed in Section 3.1.1.1, was also used in this study as a reference gene.

6.1.1.1. *Rbmy*

Rbmy is an RNA-binding motif protein encoded on the Y chromosome, and is expressed almost entirely in the testis (Figure 6.2)[92,170,254]. Rbmy is involved in processing of microRNAs (miRNAs), and has been implicated to function in spermatogenesis, as deletions of *Rbmy* copies has been shown to be associated with sperm abnormalities[170]. This gene is present in multiple copies on the mouse Y chromosome, lying adjacent to the centromere on the short arm of the chromosome (Figure 6.1). Previous attempts to determine an exact copy number of *Rbmy* in the tandem repeat array on the mouse Y chromosome via sequencing have encountered difficulty, due to the highly repetitive nature of the region.

Soh et al (2014)[76] set out to sequence the mouse Y chromosome, which until that point had had many gaps in its sequence assembly. To achieve this, the group sequenced several bacterial artificial chromosomes (BACs) containing mouse Y chromosome sequences from the reference genome (C57BL/6J)[76]. These sequences were then assembled into a map of the Y chromosome[76]. However, the entire *Rbmy* gene array was not able to be directly quantified, with only 10 complete gene units containing a copy of the *Rbmy* gene open reading frame (ORF), identified in 370 kb of sequence, able to be accurately sequenced from the BACs[76].

In order to better annotate this region of the Y chromosome, Soh et al estimated the size of the *Rbmy* array to be approximately 1.1 Mb, from identification of 38 *Rbmy*-positive BACs, accounting for average BAC clone size and Y chromosome coverage (155 kb and 5.4X, respectively)[76]. This array size was then divided by the assumed average size of the *Rbmy* gene repeat unit (37 kb) to yield an estimate of approximately 30 copies of *Rbmy* on the $Y^{C57BL/6J}$ chromosome[76]. Subsequent assessments of the size of the *Rbmy* repeat across different mouse strains' Y chromosomes have used this estimate of 30 *Rbmy* copies as the baseline for estimating *Rbmy* copy number on non-$Y^{C57BL/6J}$ chromosomes[255]. Of relevance to this study, it has been found that the $Y^{A/J}$ chromosome has a similar number of *Rbmy* repeats as the reference genome, calculated to be 31 ± 1 repeats[255].

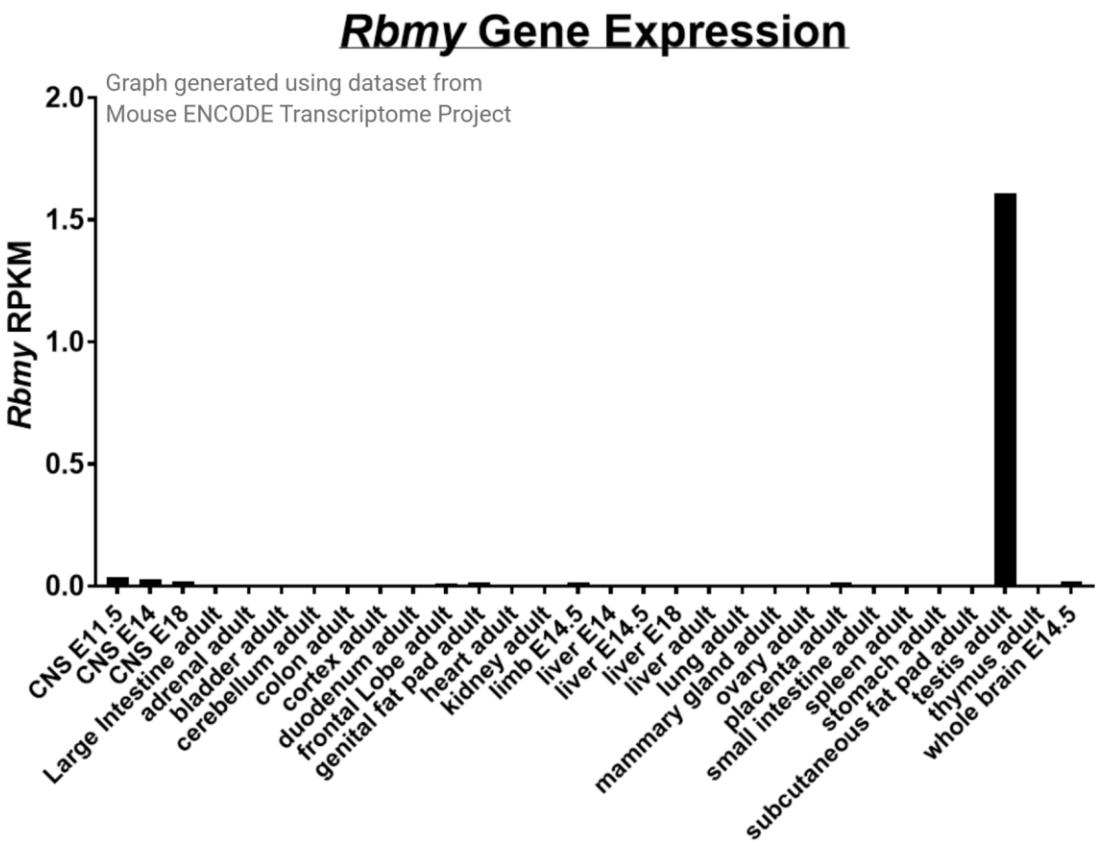

Figure 6.2 - Tissue Expression of the *Rbmy* Gene in Mouse

Plot of *Rbmy* gene expression data from the RNA Profiling Datasets generated by the Mouse ENCODE Project[3]. *Rbmy* is expressed almost exclusively in the adult mouse testis, with some very low expression observed in the embryonic central nervous system.

6.1.1.2. *Sry*

Expression of *Sry* (Sex determining Region of the Y chromosome) is the molecular trigger for a bipotential genital ridge to commit to developing into a testis[91]. Expression of this gene occurs in a subset of the somatic cells of the genital ridge, the pre-Sertoli cells[91]. Following expression of *Sry*, these cells develop into Sertoli cells, the supporting cell lineage of the testis[119,256], and orchestrate the reorganisation of the genital ridge into the highly organised structure of seminiferous tubules in the testis[119,256]. Beyond testis determination, Sertoli cells also function to support the germ cells of the testis as they undergo spermatogenesis[257] (refer to Section 1.1.5.2.1).

The *Sry* gene is encoded on the short arm of the mouse Y chromosome, flanked within an inverted repeat of the H2A histone family member L2B (*H2al2b*) gene, and codes for a transcription factor which possesses a high mobility group (HMG) box[91]. The Sry protein binds to DNA in the minor groove at the sequence (A/T)ACAA(T/A)[91,258] and bends the DNA to an angle between 60° and 85°[91,130]. In pre-Sertoli cells, Sry activates the gene *Sox9* (*Sry*-related HMG box 9) approximately four hours following onset *Sry* expression in the cell[130], with Sry activity persisting for approximately eight hours in a given pre-Sertoli cell[130]. Once activated in the Sertoli cells, *Sox9* is then able to self-activate, as well as activate its own downstream targets[259], with its expression persisting beyond that of *Sry* at E12.5[91,259].

The expression pattern of *Sry* in mice is tightly spatiotemporally regulated[91,119,122-124,130]. Expression begins in the centre of the bipotential genital ridge at approximately E10.5, and the expression moves out in a wave from the centre towards each of the poles of the genital ridge[91,119,130]. *Sry* gene expression peaks at E11.5 and is completely ceased by E12.5[119,130]. The cessation of *Sry* expression follows the same wave pattern as its activation: extinguishing in the centre, before its extinction moves out towards the poles[91,130]. Beyond E12.5, *Sry* is no longer able to induce testis determination[91,118,123,130,260], making the precise timing of the onset of *Sry* expression in the mouse genital ridge highly significant[91,122-124,130].

Mouse *Sry* has two promoters, as the gene produces two transcripts[131,132,261]. It generates a linear transcript, using the most proximal promoter to the coding sequence[131,132], which is translated into Sry protein and acts as a transcription factor as described above. However, there is a second promoter further upstream of the linear promoter, which produces a circular transcript in the genital ridge[132,261] and adult brain[132]. This transcript is not translated into protein, and as yet has no known function[262-265]. It is the linear promoter that is of interest to this work, as this is the transcript translated into Sry protein, triggering testis development. Henceforth, the term "the promoter" and variations thereupon will be referring solely to the linear transcript promoter.

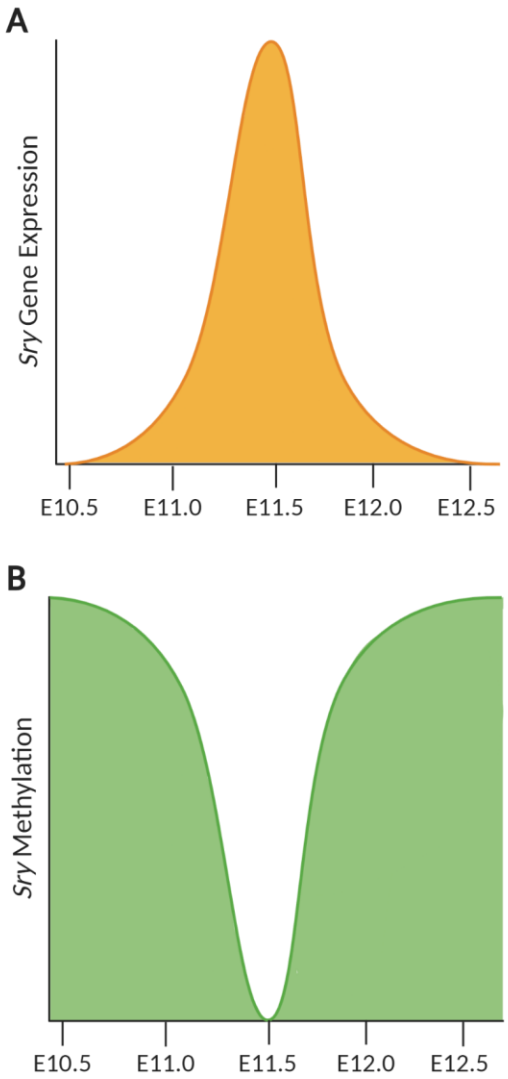

Figure 6.3 - Schematic of the Relationship between *Sry* Gene Expression and *Sry* Methylation
Schematics illustrating the changes in *Sry* gene expression (A) and *Sry* methylation (B) in the mouse genital ridge during testis determination. (A) *Sry* gene expression begins at approximately E10.5, increasing rapidly to peak at E11.5, before declining to be completely absent by E12.5. (B) As *Sry* gene expression rises from E10.5, the methylation of the locus declines rapidly, to reach peak demethylation (minimum methylation) at approximately E11.5 as gene expression peaks. As *Sry* expression declines, the region remethylates to return to the pre-testis determination levels.

The mouse *Sry* gene has been previously shown to be regulated by methylation in the gene promoter[132], with demethylation corresponding to onset of gene expression[132,266]. Methylation is an epigenetic mark that is applied by the cell to the cytosine of CG (CpG) dinucleotides to convert it to 5-methylcytosine[253]. The function of methylation is to repress gene transcription[253], silencing the gene. *Sry* gene expression is tightly regulated by methylation of the five CpGs in the promoter[132]. It has been shown that all five CpGs in the promoter are completely methylated in non-testicular tissues[132], and in the testis outside the window of sex determination during embryogenesis. During testis determination, E10.5 to E12.5, the *Sry* promoter is rapidly demethylated to become near-completely unmethylated at approximately E11.5[132], coinciding with the peak in gene expression at this stage. Following this, the promoter rapidly re-methylates, completing this process by approximately E12.5[132], correlating with cessation of *Sry* expression. Figure 6.3 illustrates the relationship between methylation of the *Sry* promoter and the level of *Sry* gene expression.

It was hypothesised that there has been an increase in the base methylation state at the *Sry* promoter $Y^{A/HeJ}$ chromosome, and that this increase has resulted in the locus requiring longer to demethylate during testis determination. This was predicted to shift the peak in *Sry* gene expression to after the canonical time point of E11.5, and may account for the gonadal abnormalities present in these mice.

6.1.2. Abnormalities of the $Y^{A/HeJ}$ Chromosome Have Been Reported Previously

In the original characterisation of the A/HeJ strain, the $Y^{A/HeJ}$ chromosome was examined cytologically[2]. Initially, this was performed to determine whether the $Y^{A/HeJ}$ chromosome was lost from a subset of cells within the gonads, leading to ovarian tissue development[2]. This was due to the hypothesis that regions which developed ovarian tissue in the A/HeJ ovotestes would have lost the Y chromosome to become 39,XO, as this had been observed in other mouse strains found to develop ovotestes[2,103] (Sections 1.1.4 and 5.1.1). It was determined, however, that the $Y^{A/HeJ}$ chromosome was not being lost from the cells of the gonad, even in the instances of incomplete testis determination, with ovarian regions retaining the $Y^{A/HeJ}$ chromosome at the same rate as the testicular regions (> 95%)[2].

While examining gonadal and somatic C57BL/6J-$Y^{A/HeJ}$ tissues for $Y^{A/HeJ}$ chromosome loss[2], it was observed that the $Y^{A/HeJ}$ chromosome exhibited a slight cytological defect that the authors speculated to be the result of a "weakened" centromere[2]. This manifested in two ways: an increased sister chromatid intracentromeric distance, and premature sister chromatid separation[2]. The increased intracentromeric distance (distance between the centromeres of condensed duplicated sister chromatids of a chromosome) observed on the $Y^{A/HeJ}$ chromosome in metaphase spreads appeared as a noticeable gap between the sister chromatids[2], such as in Figure 6.4A (centre panel,

Y chromosome is green), which contrasted to the normal Y chromosome in Figure 6.4A (left panel) in which the chromatids connect at the centromere. The rate of these gaps between $Y^{A/HeJ}$ chromatids varied between cell type, with 48.0% to 66.2% liver cells and 3.4% to 7.4% of fibroblasts possessing a $Y^{A/HeJ}$ chromosome with a noticeably increased intracentromeric distance[2]. For comparison, the rate of a gap between sister chromatids for the $Y^{C57BL/6J}$ chromosome was observed to be 5.3% and 0.2%, respectively[2], indicating that the intracentromeric distance increase was a function of the $Y^{A/HeJ}$ chromosome. However, the frequency of gaps associated with the $Y^{A/HeJ}$ chromosome did not correlate with the gonadal phenotype[2].

The second defect observed in the $Y^{A/HeJ}$ chromosome was premature sister chromatid separation, in which the sister chromatids of the $Y^{A/HeJ}$ chromosome were observed to separate from one another prematurely relative to the other chromosomes in the cell[2] (Figure 6.4A, right panel). This observation, combined with the increased intracentromeric distance, suggested that there was a structural change at or near the centromere of the $Y^{A/HeJ}$ chromosome[2], and that this change was responsible for both the cytological defects, and the abnormal gonads in A/HeJ males[2].

It was also confirmed that the testis-determining gene *Sry* had not been deleted from the A/ $Y^{A/HeJ}$ chromosome[2]. Embryonic ovotestes in C57BL/6J-$Y^{A/HeJ}$ male embryos were characterised by a central region composed of testicular tissue, with one or both poles consisting of ovarian tissue[2] (Figure 6.4B, right panel ovotestis, left panel normal testis). As the expression of *Sry* begins in the centre of the bipotential gonad and moves outwards to the poles (refer to Section 6.1.1.2), it was suggested that the predicted structural change to the $Y^{A/HeJ}$ chromosome would affect the expression profile of *Sry* in the genital ridge during testis determination, producing abnormal gonads[2].

From the observations of the $Y^{A/HeJ}$ chromosome from the original characterisation[2] of the A/HeJ mouse, it was speculated that a single change, at or near the centromere of the $Y^{A/HeJ}$ chromosome, was responsible for both the cytological and gonadal abnormalities[2]. From this, the hypothesis of this study was that the structural change to the $Y^{A/HeJ}$ chromosome was at the *Rbmy* array locus, and that it resulted in an alteration to regulation of the *Sry* gene during testis determination in A/HeJ embryos.

This chapter describes the assessment of the *Rbmy* and *Sry* loci in A/HeJ and control strain (A/J and BALB/c) males. Firstly, quantification of the *Rbmy* copy number was performed using Droplet Digital (dd)PCR, followed by assessment of *Sry* methylation in genital ridges from various time points across the testis determination window. Methylation was assessed using bisulfite sequencing, as well as a novel ddPCR assay designed in this study.

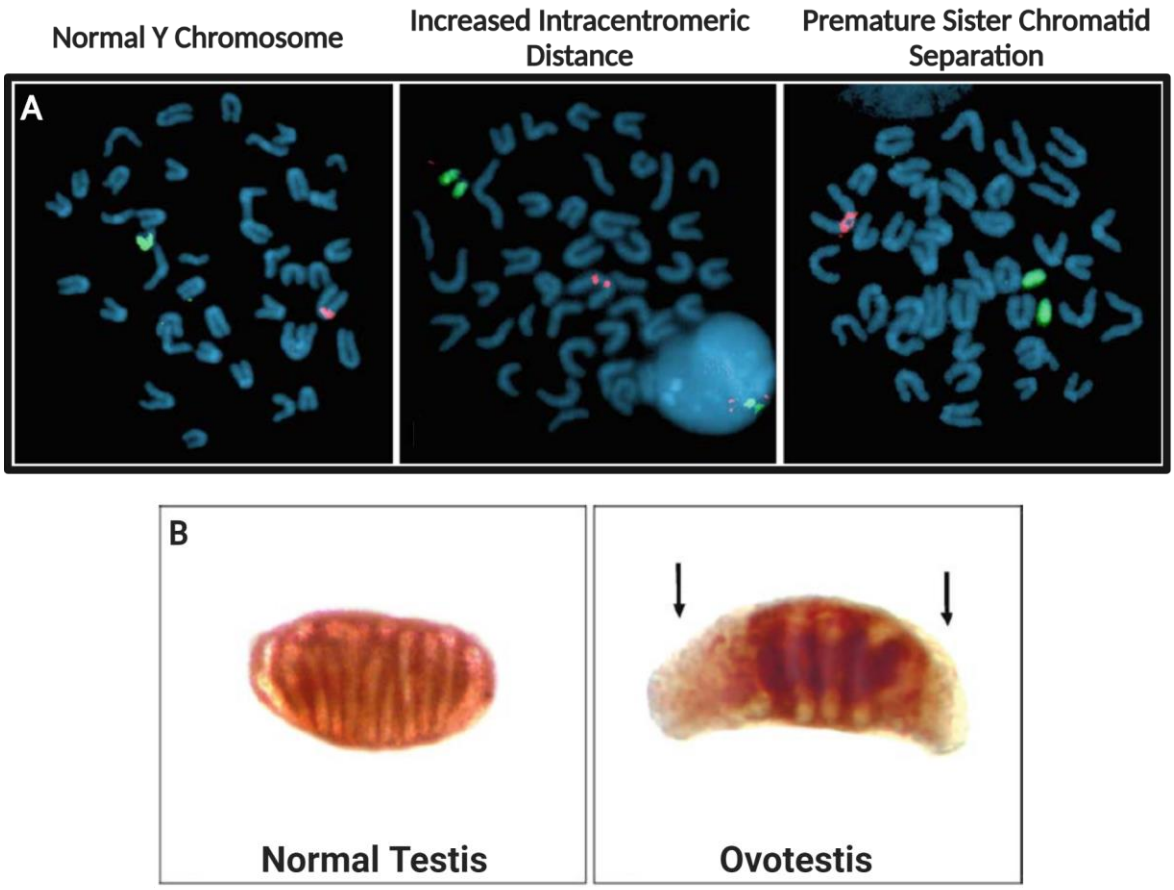

Figure 6.4 - Abnormalities Associated with the $Y^{A/HeJ}$ Chromosome from the Original Characterisation
Images modified from Hunt et al 2008[2]. (A) Images of metaphase spreads from A/HeJ male cells showing abnormalities; the $Y^{A/HeJ}$ chromosome is highlighted in green, and the X chromosome indicated by red probe signals. The left image shows a normal metaphase spread, with the duplicated sister chromatids of the $Y^{A/HeJ}$ chromosome joined at the centromere. The centre image shows an increased intracentromeric distance between the $Y^{A/HeJ}$ chromosome sister chromatids. The right image shows premature sister chromatid separation of the $Y^{A/HeJ}$ chromosome chromatids. (B) An image of a normal embryonic E14.5 C57BL/6J-$Y^{A/HeJ}$ testis (left) and an abnormal ovotestis (right) from an E14.5 C57BL/6J-$Y^{A/HeJ}$ embryo. The striated region in the centre of the ovotestis is testicular tissue, while the poles (indicated by the arrows) are composed of ovarian tissue.

6.2. Results

6.2.1. *Rbmy* Copy Number was Reduced on the $Y^{A/HeJ}$ Chromosome

The predicted structural change to the $Y^{A/HeJ}$ chromosome was hypothesised to be a deletion in the *Rbmy* tandem repeat array, reducing the number of copies of the gene between the centromere and *Sry* locus. A reduction in this array would be expected to result in a repressive effect on the expression of the *Sry* gene, due to increased proximity of *Sry* to the centromere. This would be due to the spread of repression from the heterochromatin of the centromere, with this increased repression interfering with *Sry* expression in the genital ridge during testis determination.

The *Rbmy* tandem repeat array was estimated to contain approximately 30 copies of the *Rbmy* gene on normal mouse Y chromosomes[76]. This includes the closely related A/J strain used as a control in this study (predicted to have 31 ± 1 repeats[255]). Due to the close relatedness of the A/HeJ and A/J strains[2,195], should the *Rbmy* tandem repeat array not be the site of the structural change, it would be expected that these two Y chromosomes would have a similar number of *Rbmy* gene copies.

6.2.1.1. Preliminary Indications of an *Rbmy* Copy Number Reduction in A/HeJ Males

In order to assess the *Rbmy* copy number on the $Y^{A/HeJ}$ chromosome, a preliminary assessment was performed on A/HeJ and A/J male DNA samples. A PCR-based assay was designed, in which a region of each of the *Rbmy* and *Ddx3y* genes were amplified (amplicons of 203 bp and 104 bp, respectively). *Ddx3y* was selected to be used as a reference gene, as it is known to be single copy on the Y chromosome. These two amplicons were amplified in the same reaction so that the relative amplification of *Rbmy* compared to amplification of *Ddx3y* could be compared between samples. Figure 6.5A shows the gel electrophoresis image of the products from the completed reactions, with A/HeJ and A/J male samples and a female negative control sample from each strain.

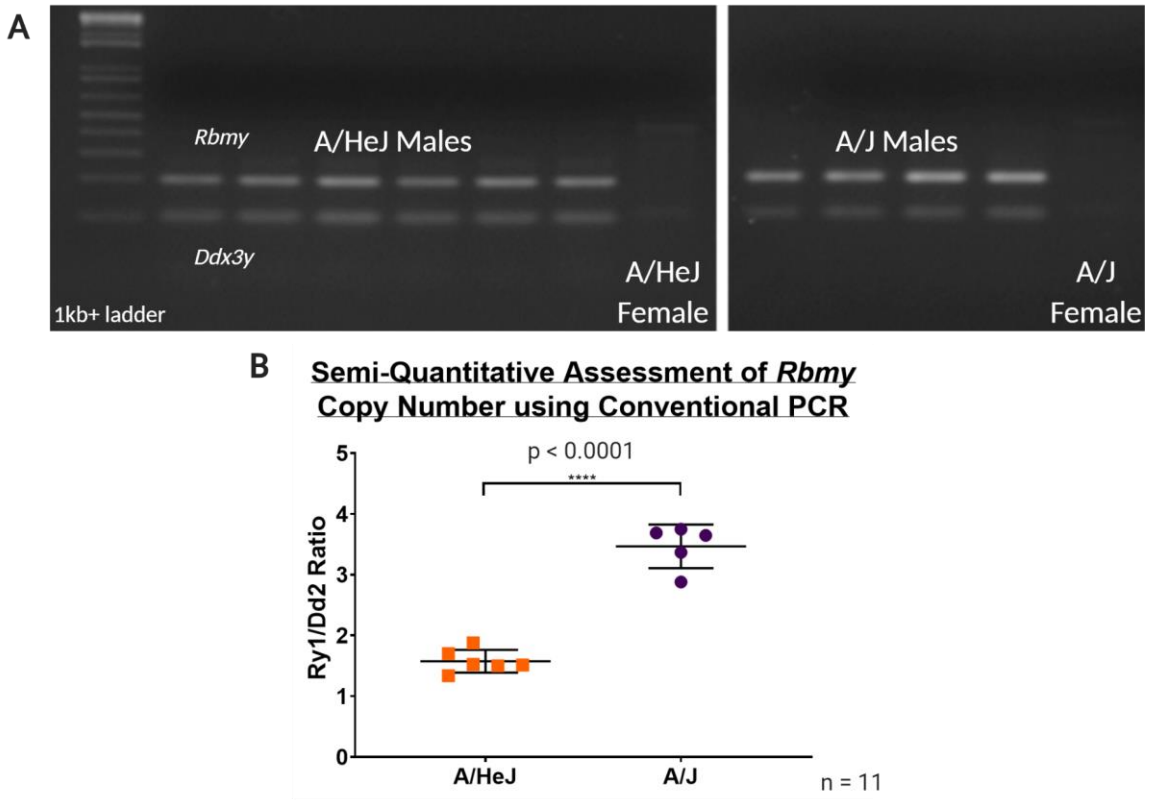

Figure 6.5 - Preliminary Semi-Quantitative Assessment of the *Rbmy* Array on the $Y^{A/HeJ}$ and $Y^{A/J}$ Chromosomes

(A) Gel image of PCR product from conventional PCR amplification of the *Ddx3y* ('Dd2' amplicon, bottom bands) and *Rbmy* ('Ry1' amplicon, top bands) from A/HeJ (left image) and A/J (right image) male DNA samples, as well as a female negative control sample from each strain. These gel images were assessed using ImageJ FIJI software (Spectral Plots in Appendix 8.2) to determine the relative amplification of both amplicons for each sample. The *Rbmy* band intensity was assessed as a ratio relative to the *Ddx3y* bands and plotted in (B). There was a statistically significant ($p < 0.0001$) reduction in the relative amplification of the A/HeJ *Rbmy* array (mean = 1.58 ± 0.19) compared to the A/J *Rbmy* array (mean = 3.47 ± 0.36), indicating a lower copy number at this locus on the $Y^{A/HeJ}$ chromosome.

The gel image was analysed using image analysis software (Section 2.1.6.1) to calculate relative band intensities between the Rbmy and Ddx3y amplicons for each sample, to yield a ratio of Rbmy band intensity relative to the Ddx3y reference band (refer to Appendix 8.2). As seen in the plot in Figure 6.5B, there was a highly significant difference ($p < 0.0001$) between the Rbmy/Ddx3y ratios of the two strains, with the mean of the A/J samples (3.47 ± 0.36) being more than double the mean of the A/HeJ samples (1.58 ± 0.19). This stark difference in the relative amplification of Rbmy between the A/HeJ and A/J male samples indicated a relative reduction in Rbmy in the A/HeJ samples. However, this method was only semi-quantitative, as the A/J Rbmy copy number has previously been shown to be 31 ± 1 copies240, not three to four copies as suggested by this analysis. The result of this semiquantitative method suggested that there was a reduction in the Rbmy array on YA/HeJ chromosome. Therefore, further analysis of this region with a more quantitative method was pursued.

6.2.1.2. *Rbmy* Copy Number was Halved on the $Y^{A/HeJ}$ Chromosome Relative to Control Strains' Y Chromosomes

The *Rbmy* and *Ddx3y* assays used in the conventional PCR semiquantitative analysis of *Rbmy* copy number were adapted to the highly quantitative Droplet Digital PCR (ddPCR) system. As this system is capable of calculating the number of amplicon copies per microlitre (µL) in a reaction, this method enabled accurate assessment of the absolute amplification of *Rbmy* and *Ddx3y*, allowing for calculation of *Rbmy* copy number. For this assessment, males from both the closely related A/J and related BALB/c strains were used as controls.

For the ddPCR analysis, the *Rbmy* and *Ddx3y* assays for each sample were run in separate reactions (representative reactions in Figure 6.6A), each in duplicate, and the concentration (copies per µL, calculated by the QuantaSoft ddPCR software, Section 2.1.6.4) was averaged across technical duplicates. The concentration for the *Rbmy* and *Ddx3y* amplicons were inserted into the equation in Section 2.7.2 to yield a number of *Rbmy* copies.

Ten A/HeJ male samples and five each of A/J and BALB/c male samples were assessed, with their *Rbmy* copy number plotted in Figure 6.6B. The mean *Rbmy* copy number was compared between the strains. The A/J and BALB/c male samples produced similar mean copy number values for *Rbmy*, 14.46 ± 1.87 [11.56, 16.32] copies and 14.07 ± 1.57 [12.09, 16.05] copies, respectively. There was no significant difference in the number of *Rbmy* copies between A/J and BALB/c mice ($p = 0.9417$).

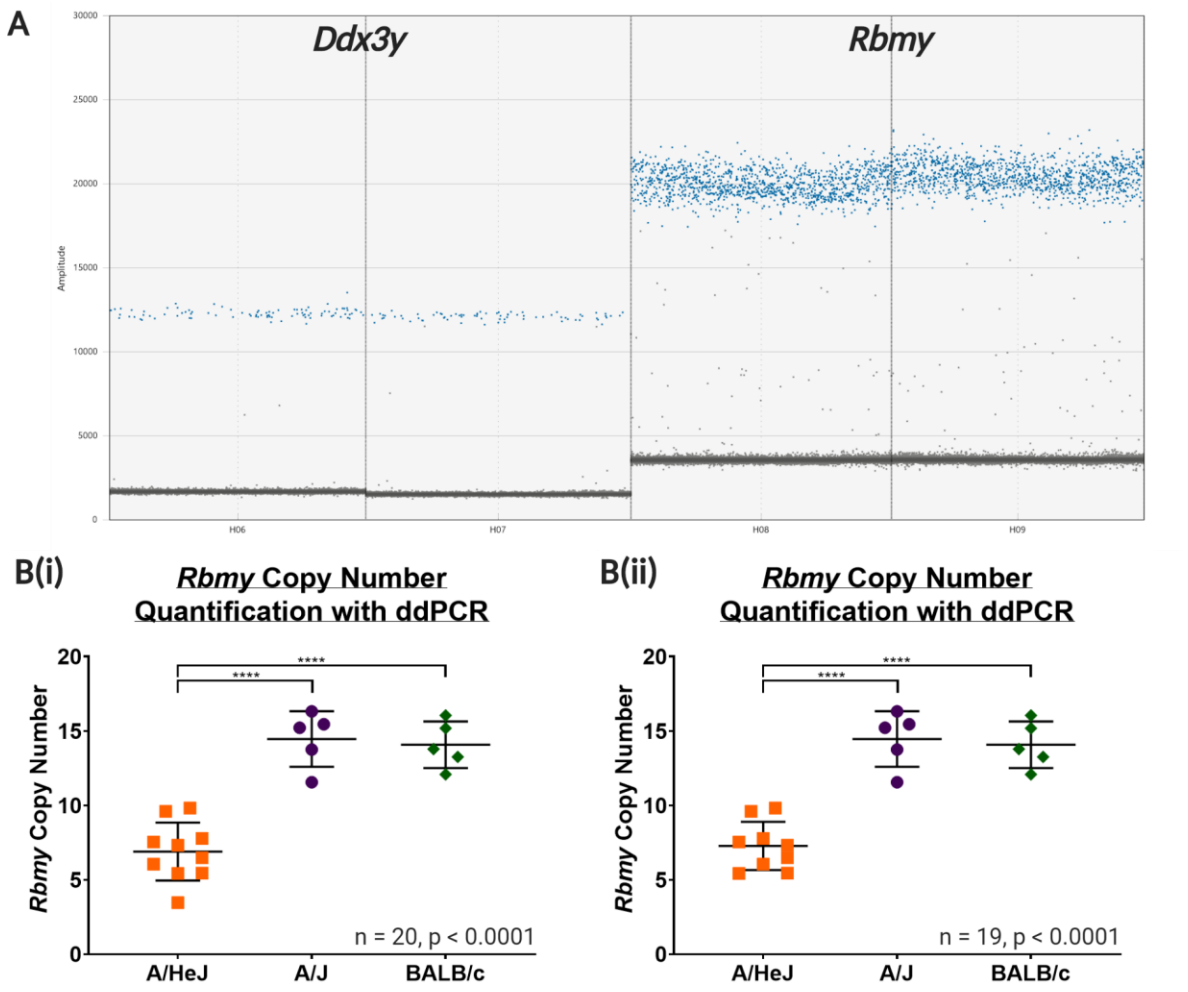

Figure 6.6 - Droplet Digital (dd)PCR Analysis of the *Rbmy* Array in A/HeJ and Control Samples

(A) Example output of ddPCR amplification of the *Ddx3y* (left) and *Rbmy* (right) amplicons. (B(i)) Plot of calculated *Rbmy* copy number in A/HeJ (orange), A/J (purple) and BALB/c (green) male samples, including an outlier of 3.47 copies in the A/HeJ cohort, lowering the mean copy number to 6.90 ± 1.95. Based on the range of results from the other samples, and assessment of its amplification plot, this outlier was excluded (B(ii)), raising the A/HeJ mean to 7.28 ± 1.62 copies. Regardless whether this outlier was included or excluded, the *Rbmy* copy number of the A/HeJ samples were significantly different from the A/J and BALB/c samples, $p < 0.0001$.

The A/HeJ samples had an outlier (shown in Figure 6.6B(i)), with one male's sample returning a value of 3.47 copies of *Rbmy*. Inclusion of this sample reduced the mean of the A/HeJ samples to 6.90 ± 1.95 copies. However, the remaining nine samples' values were within a similar-sized range as was observed in the control strains (A/HeJ = [5.43, 9.82], A/J = [11.56, 16.32], BALB/c = [12.09, 16.05]), supporting exclusion of the outlier (Figure 6.6B(ii)). This raised the A/HeJ mean *Rbmy* copy number to 7.28 ± 1.62 copies, a 49.67% and 48.27% reduction, respectively, from the A/J and BALB/c strains' mean copy number.

This result supports the hypothesis that the structural change to the $Y^{A/HeJ}$ chromosome is a deletion in the *Rbmy* tandem repeat array, as the *Rbmy* array is adjacent to the centromere, and its copy number is reduced by half on the $Y^{A/HeJ}$ chromosome.

6.2.2. *Sry* Methylation Analysis

In light of the stark reduction in *Rbmy* copy number on the $Y^{A/HeJ}$ chromosome determined in Section 6.2.1, it was predicted that *Sry* relation regulation would be affected by being brought closer to the centromere by this deletion. This was due to mouse strains which have been previously reported to have near total deletions in the *Rbmy* tandem repeat array having been shown to exhibit XY sex reversal[170-172]. This sex reversal resulted from a positional effect, repressing *Sry* gene expression due to decreased distance from the centromere[170,171].

As CpG methylation has been shown to be associated with *Sry* repression[132], the methylation of this locus was assessed in DNA from genital ridges of A/HeJ, A/J and BALB/c male embryos throughout various time points in the testis determination window. This was assessed using two methods, a novel methylation-dependent ddPCR assay and bisulfite sequencing, in order to determine whether there was disruption to the dynamic changes to *Sry* methylation in A/HeJ samples which may account for the gonadal abnormalities reported in Chapter 5.

6.2.2.1. Preliminary Indications of *Sry* Methylation Changes in A/HeJ Genital Ridges using Bisulfite Sequencing

In order to determine whether there were changes to the regulation of the *Sry* gene during testis determination in the A/HeJ strain, a preliminary assessment of *Sry* methylation in genital ridge DNA from A/HeJ, A/J and BALB/c embryos was performed using bisulfite sequencing. Bisulfite sequencing provides a quantitative assessment of the degree of methylation at individual CpGs in a given sequence, with results reported as a value between 0.0 (0% methylated) to 1.0 (100% methylated). Due to the reduction in the *Rbmy* array, it was predicted that there would be an alteration to the *Sry* methylation changes in A/HeJ genital ridges, deviating from the canonical dynamic regulation in control genital ridges (Figure 6.3).

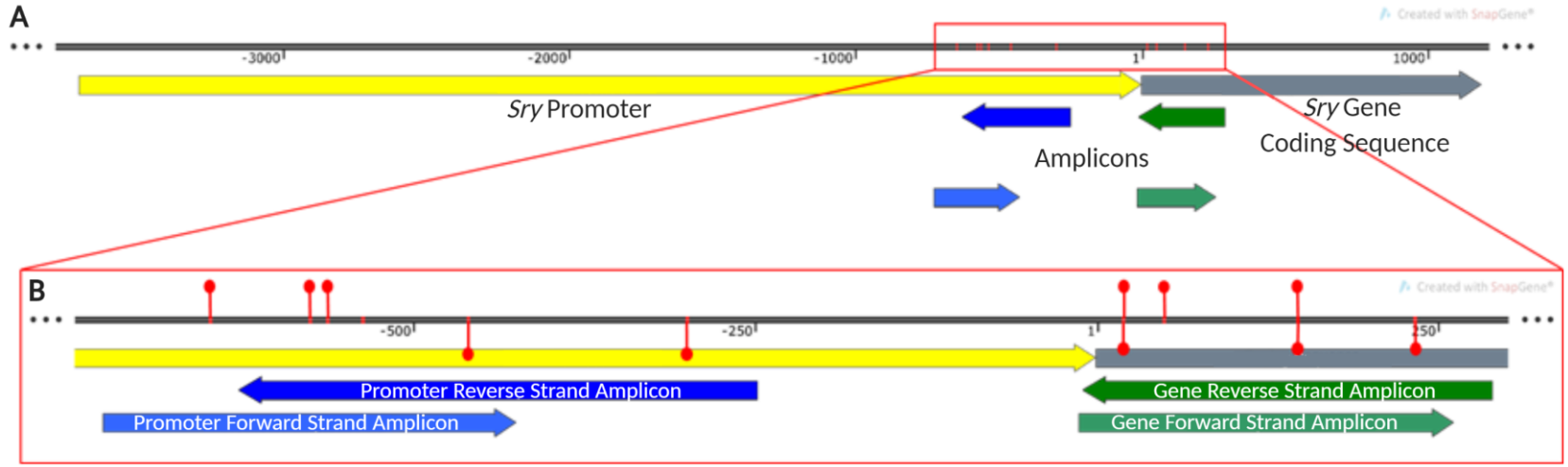

Figure 6.7 - Schematic of the Mouse *Sry* Locus as Assessed with Preliminary Bisulfite Sequencing

Schematic of the mouse *Sry* locus, including the gene promoter (yellow) and gene coding region (grey). The overall view of the region is shown in (A), including highlighting the forward and reverse amplicons in the promoter and gene assessed in the preliminary bisulfite sequencing (blue and green, respectively). (B) provides a closer view of the regions assessed, including the CpG sites assessed, indicated by red 'lollipops'. CpG markers above the sequence line were assessed in the relevant forward amplicon, and those below the line were assessed in the relevant reverse amplicon. The first base of the coding sequence was designated as +1; bases in the promoter region of the Sry locus were numbered in reverse from this point, i.e., the last base in the promoter (proximal to the first base of the coding sequence) was designated as -1.

Bisulfite sequencing of neat genital ridge DNA (mesonephros removed) from embryos at two different developmental stages: E11.5 (peak gene expression, predicted minimum methylation, assessed between 15 tail somites (ts) to 18 ts) and E12.5 (cessation of gene expression, predicted maximum methylation, assessed between 24 ts to 26 ts). Table 2.12 lists the ts of each embryo assessed in this section. Four biological samples were run for each strain/stage, and CpGs in both the *Sry* promoter and gene were assessed on both forward and reverse strands (amplicons and CpG sites shown in Figure 6.7). Mean methylation at each CpG was calculated for each stage/strain combination (Figure 6.8), and overall methylation was calculated for each amplicon as the mean of all CpGs in a given amplicon (gene/promoter, forward/reverse strand; Figure 6.9). For these results, only comparisons between different strain/stage combinations for each CpG and the overall amplicons were reported, with comparisons between different CpG sites and amplicons not reported.

Examining methylation differences between different strains and stages at individual CpG sites, all significant comparisons ($p < 0.05$) were found at CpG sites in the *Sry* promoter (Figures 6.8A and B). All comparisons performed on the gene forward and reverse strand CpGs were found to be non-significant (Figures 6.8C and D), with a high number of comparisons with p-values greater than 0.9 (see Appendix 8.3 for CpG site multiple comparison tables). Of the three CpG sites on the promoter forward strand (Figure 6.7), two (-649 and -576) yielded comparisons that were significantly different, while one (-300) of the two CpGs on the promoter reverse strand (Figure 6.7) also yielded comparisons with significant differences. These comparisons are indicated in Figures 6.8A and B by black bars.

The greatest number of significant differences in strain/stage comparisons were found at the promoter forward strand CpG -649, with the A/HeJ E11.5 value (0.576 ± 0.143) and the A/J E11.5 value (0.574 ± 0.0928) each being significantly higher than both the A/J and BALB/c E12.5 values (0.240 ± 0.114 and 0.270 ± 0.0803 respectively). Interestingly, there was no difference between the BALB/c E11.5 value and the A/HeJ E12.5 value (0.452 and 0.417 respectively, $p > 0.9999$) at this site (Figure 6.8A).

The other comparison which yielded a significant difference on the promoter forward strand was found at CpG -576 (Figure 6.8A), between BALB/c E11.5 and E12.5 values (0.745 and 0.457, $p = 0.0493$), as would be expected due to the known changes to *Sry* methylation between these two time points (Figure 6.3). All other comparisons at this CpG were non-significant. CpG -300 on the promoter reverse strand had two significant differences, with the A/HeJ E11.5 value (0.623) and the A/J E11.5 value (0.563) both being significantly different from the BALB/c E12.5 value (0.282) ($p = 0.0017$ and $p = 0.0167$, respectively, Figure 6.8B).

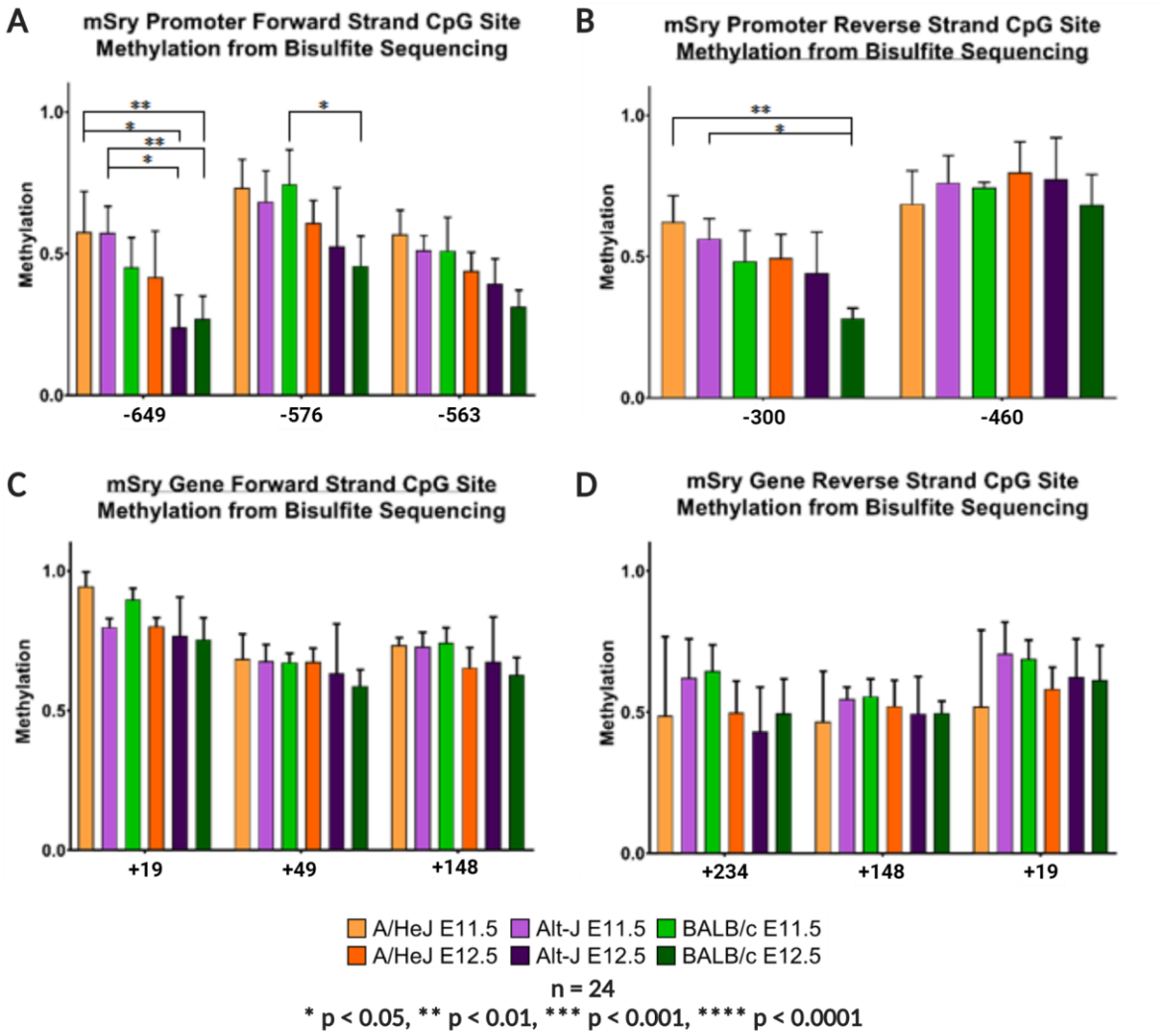

Figure 6.8 - Methylation Levels at Individual CpG Sites in the *Sry* Locus from the Preliminary Bisulfite Sequencing

The results of the preliminary bisulfite sequencing were assessed at individual CpG sites in the *Sry* promoter forward strand (A) and reverse strand (B), and in the gene forward (C) and reverse (D) strands. The only comparisons with statistically significant differences were identified in the promoter, in the forward strain (A) at CpG -649 and -576, and in the reverse strand (B) at CpG -300.

Key at the bottom of the figure.

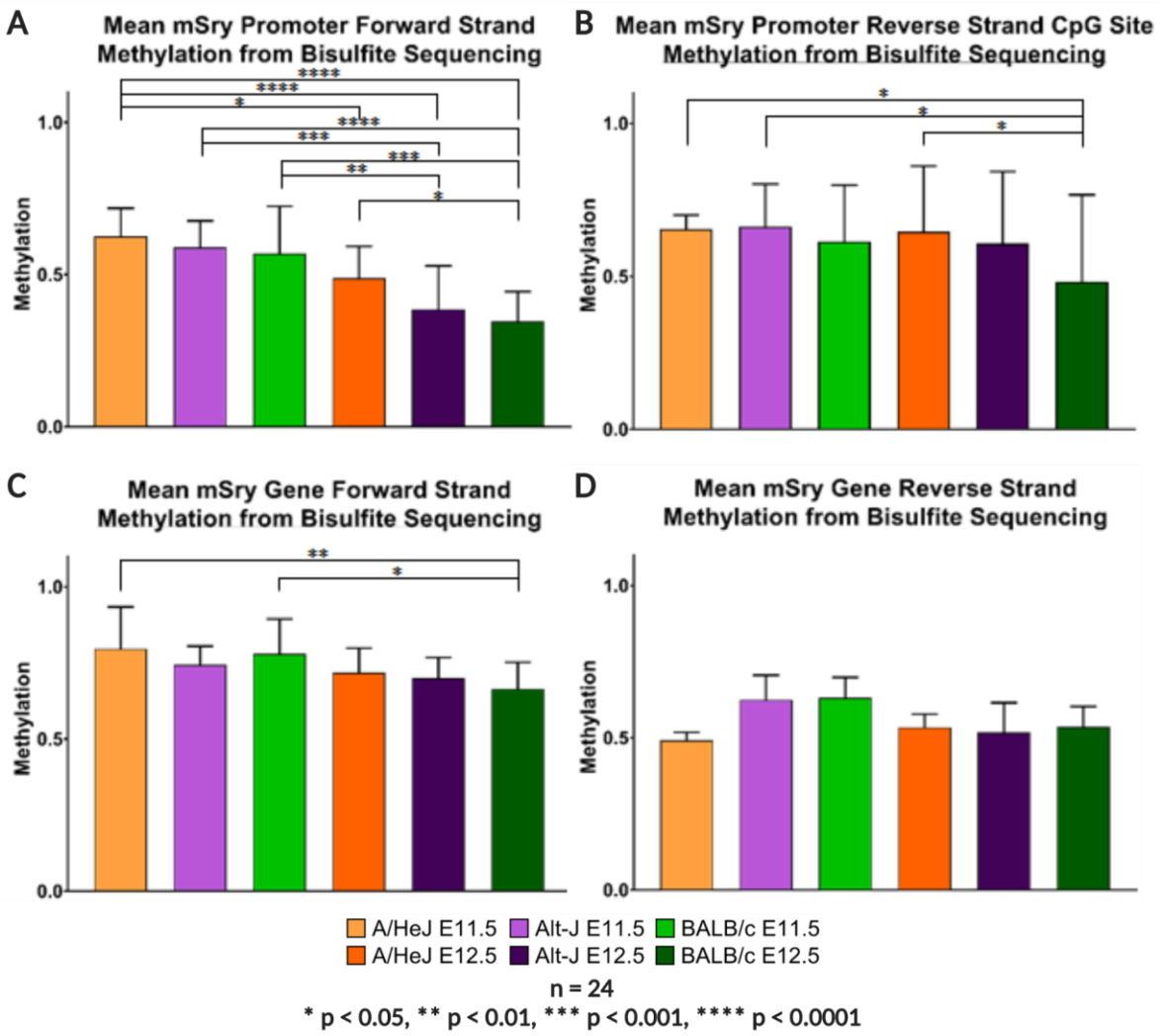

Figure 6.9 - Overall Methylation Levels of Each Amplicon Region in the *Sry* Locus from the Preliminary Bisulfite Sequencing

The results of the preliminary bisulfite sequencing were assessed for the *Sry* promoter forward strand (A) and reverse strand (B), and in the gene forward (C) and reverse (D) strands by averaging the results for each CpG site within the relevant amplicon. Comparisons with statistically significant differences were identified in all amplicons except for the gene reverse strand (D). The comparisons that were most significant were identified in the promoter forward strain (A). Of interest was that the A/HeJ E12.5 samples were significantly different from the BALB/c E12.5 samples in the promoter forward (A) and reverse (B) strands.

Key at the bottom of the figure.

The individual CpG methylation values illustrated in Figure 6.8 were used to calculate overall methylation of each amplicon (Figure 6.9, see Appendix 8.4 for amplicon multiple comparison tables). This revealed more strain/stage comparisons with statistically significant differences, on both strands of the promoter (Figure 6.9A and B), as well as on the gene forward strand (Figure 6.9C). No significant differences were identified in comparisons within the gene reverse strand amplicon (Figure 6.9D).

The amplicon with the most significantly different strain/stage comparisons was the promoter forward strand (Figure 6.9A), with all other strain/stage samples being significantly different from BALB/c E12.5 (0.346 ± 0.0977), with the exception of the A/J E12.5 (0.386 ± 0.143). This lack of difference between the BALB/c and A/J E12.5 samples was not unexpected, as both of these control strains produce normal testes, and hence would be expected to have similar methylation of *Sry*. However, the difference between BALB/c and A/HeJ E12.5 samples was of note, as it suggests a change to the methylation of the *Sry* promoter on the $Y^{A/HeJ}$ chromosome at the stage when *Sry* expression should have ceased.

The A/J E12.5 samples had the next most significant comparisons, being significantly different from all E11.5 strain/stages ($p < 0.0.1$), but not significantly different from the A/HeJ E12.5 (0.488 ± 0.105). The remaining comparison with significant difference was between the A/HeJ E12.5 and A/HeJ E11.5 (0.626 ± 0.0925, $p = 0.0414$), which was not unexpected, as these samples were from the same strain at different time points. Despite the noted abnormal gonads, the majority of A/HeJ XY gonads developed testicular tissue, indicating that *Sry* was expressed within the testis determination window, and hence that the methylation of the promoter needed to change during this time. Interestingly, A/HeJ E12.5 was not significantly different from the remaining E11.5 values (A/J and BALB/c), as would be expected between the peak and cessation of *Sry* expression.

The amplicon with the next most comparisons which were statistically different was the promoter reverse strand, yielding three significant differences, all of which were with the BALB/c E12.5 samples (0.4825 ± 0.2839). The methylation of these BALB/c samples was significantly lower than the A/HeJ E11.5 (0.655 ± 0.0454, $p = 0.0194$), A/J E11.5 (0.662 ± 0.140, $p = 0.0132$), and A/HeJ E12.5 (0.646 ± 0.214, $p = 0.0295$) samples. All methylation values, with the exception of the BALB/c E12.5 were between 0.60 and 0.66. The remaining amplicon with significant comparisons was the gene forward strand, with two significant comparisons, again with BALB/c E12.5 (0.665 ± 0.087): the A/HeJ E11.5 (0.796 ± 0.138, $p = 0.0034$) and BALB/c E11.5 (0.779 ± 0.115, $p = 0.0153$).

From these results, there were clear indications that the methylation (regulation) of the *Sry* promoter was altered on the $Y^{A/HeJ}$ chromosome, particularly when assessing the methylation of the forward promoter. While many of these significant differences were expected, as promoter has been shown to be the site of methylation changes between the two time points assessed here[119], the differences between strains of the same stage suggested that the promoter was the likely region for further analysis to determine the change in the A/HeJ samples.

6.2.2.2. Design of the Novel *Sry* Methylation Evagreen© ddPCR Assay

Based on the preliminary bisulfite sequencing results in Section 6.2.2.1, the *Sry* promoter was selected as the region of interest for further assessment, as this region yielded the greatest number of significant results. In order to assess *Sry* promoter methylation in the genital ridges without the need to bisulfite convert the DNA, a novel ddPCR-based methylation assay was designed based upon the RT-PCR methylation detection method described in Petell et al (2017)[267].

This section briefly details the design and optimisation of this novel assay, as ddPCR using the Evagreen© chemistry is not typically utilised for methylation analysis. Instead, methylation analysis with the ddPCR system is usually performed on bisulfite-converted DNA using Probe© chemistry[268,269], in which specific fluorescently-tagged probes are within the reaction mix and bind to either the converted (unmethylated) or unconverted (methylated) CpG-containing sequence. Evagreen© chemistry, in contrast, is a DNA-binding dye which fluoresces when bound to double stranded (ds)DNA, as present following PCR amplification.

The Evagreen© chemistry was selected for assessing *Sry* promoter methylation using ddPCR, as, unlike Probe© chemistry, bisulfite conversion did not need to be performed on the DNA prior to being added into the reaction. This was preferred, as the DNA yield from genital ridge pairs was quite low due to the small size of the tissue samples. By foregoing the bisulfite conversion process, a maximal amount of DNA from each sample would be available for analysis, allowing for more technical replicates. In order to assess *Sry* promoter methylation with Evagreen© chemistry, an RT-PCR methylation assay employing restriction enzyme digests[267] was adapted to the ddPCR system.

Briefly, genital ridge DNA from A/HeJ, A/J and BALB/c embryos was predigested with the restriction enzyme *Nla*III (cuts outside the sequences of interest), to improve partitioning of the template DNA in droplet synthesis, and *Msp*JI, a methylation-dependent restriction enzyme. Methylation-dependent refers to the requirement that the cytosine of the CG dinucleotide in the recognition sequence be methylated for the enzyme to cut the DNA. Refer to Section 2.8.3.1 for restriction enzyme recognition and cut sites.

*Nla*III digestion was included in all conditions (methylation-dependent (*Msp*JI and *Nla*III) and unlinked-only (*Nla*III only)) in order to unlink the two loci in the *Sry* promoter which possessed recognition sequences for *Msp*JI, at CpGs -537 and -300. The inclusion of *Nla*III was necessary to ensure that the template DNA for each of the two loci were able to assort independently into different droplets for ddPCR, particularly due to their close proximity (237 bp). Figure 6.10A shows the amplicons to amplify the each of the CpG loci, as well as highlighting the recognition and cut sites for each of the three restriction enzymes used in this experiment. Note, for *Nla*III, the restriction enzyme cuts within its recognition sequence, while *Msp*JI cuts far from its recognition site (refer to Figure 6.10A and Section 2.8.3.1).

The two amplicons (CpGs -537 and -300) were able to be duplexed, enabling both CpG sites to be assessed in a single reaction for each of the two restriction digest conditions (methylation-dependent and unlinked-only conditions) for each genital ridge sample. This was of great value in this experiment, as the assessment of methylation within each sample was to be determined as the difference in amplification in the methylation-dependent and unlinked-only conditions. This was because less amplification in the methylation-dependent condition would be indicative of higher methylation, as the template DNA would have been digested and hence unavailable for amplification[267].

Following optimisation of the ddPCR assay, the final conditions used to assess methylation in genital ridge DNA were: 10 ng of digested (*Msp*I and/or *Nla*III) template DNA per 25 µL reaction (20 µL of which was used in droplet generation, resulting in 8 ng assessed in the final reaction), annealing/extension temperature of 58°C for one minute, and the final concentration of primers being 200 nM for CpG -537 and 150 nM for CpG -300.

6.2.2.3. Quantification of Sry Methylation in Genital Ridge DNA using ddPCR

Methylation of the *Sry* promoter at CpGs -537 and -300 was assessed as the difference in amplification at each locus in the methylation-dependent digest as compared to the amplification in the unlinked-only digest. This was derived from the concentration of each amplicon in copies per µL as calculated by the QuantaSoft AP software for each digest condition, and these concentrations were used to calculate the percentage decline in the methylation-dependent digest from the unlinked-only digest. This percentage decline was considered to be the percentage of methylation, as the template DNA would have been cut at each CpG if the cytosine were methylated. Therefore, throughout this section the results are reported as percentage of methylation. Figure 6.10B shows an example ddPCR reaction amplification plot in which both of the amplicons amplified. The concentration of each amplicon was calculated by the analysis software for each reaction, averaged across technical replicates for each sample, and compared between the two digestion conditions.

It has previously been shown that methylation at the *Sry* promoter decreases between E10.5 and E11.5, with E11.5 representing peak demethylation[132], after which methylation increases to return to original (peak) methylation levels by E12.5[132], as illustrated in Figure 6.3. While the preliminary analysis of *Sry* methylation (Section 6.2.2.1) assessed E11.5 and E12.5 to determine whether there was a difference in methylation at the expected minimum and maximum methylation, the ddPCR analysis assessed additional time points. This was to better determine whether there was a shift in peak demethylation from E11.5 in the A/HeJ samples. To achieve this, DNA was extracted from genital ridge pairs with attached mesonephros from A/HeJ, A/J and BALB/c male embryos at E11.25 (14 ts to 16 ts), E11.5 (17 ts to 19 ts), E12.0 (20 ts to 23 ts) and E12.5 (25 ts to 27 ts).

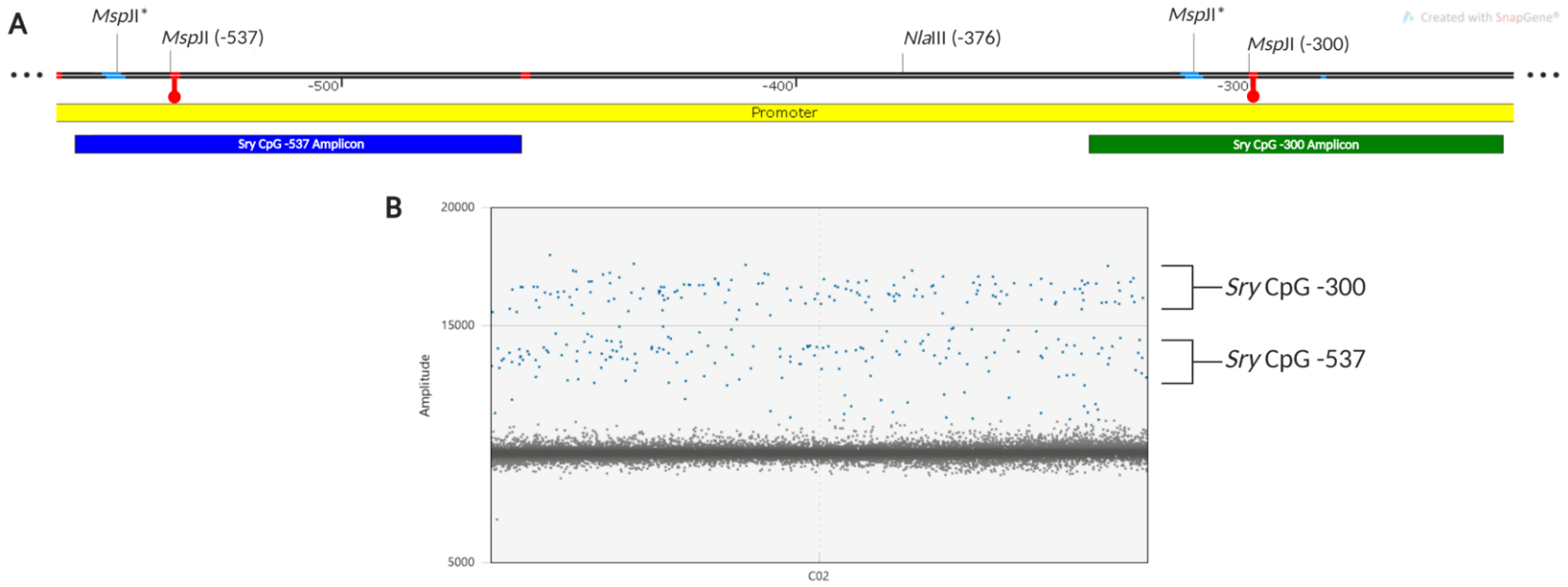

Figure 6.10 - Schematic of the Mouse *Sry* Promoter as Assessed with Droplet Digital (dd)PCR

(A) Schematic of the mouse *Sry* promoter (yellow) showing the two CpG sites assessed (red 'lollipops') and the amplicons covering these sites (blue and green). Along the sequence line, the recognition sites for the restriction enzymes utilised in the ddPCR (*Nla*III and *Msp*JI) are notated. The MspJI* site (light blue) indicates where the *Msp*JI enzyme cuts, as it does not cut at its recognition site. *Nla*III cuts within its recognition site. (B) Example output of ddPCR amplification showing the CpG -300 (top band) and -537 (bottom band) amplicons.

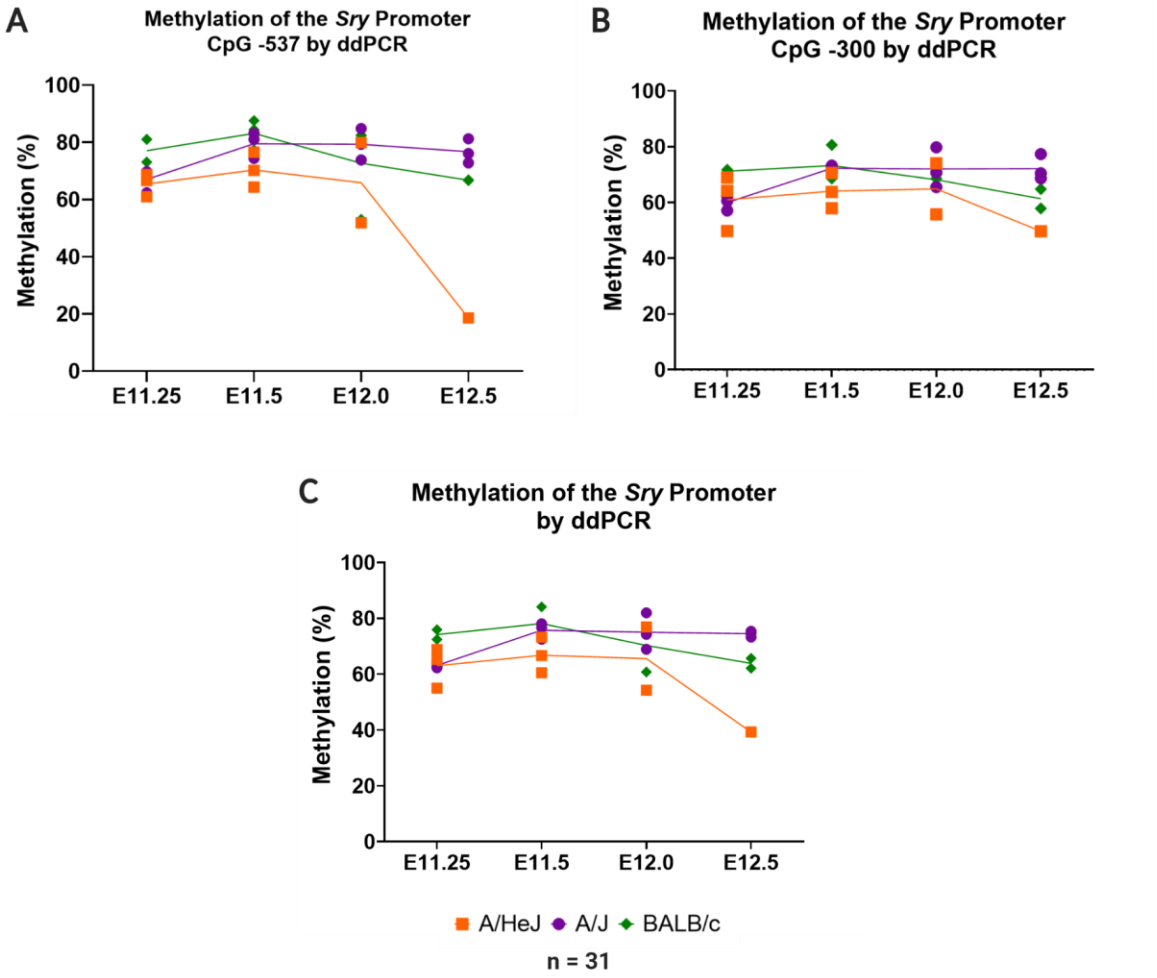

<u>Figure 6.11 - *Sry* Methylation Levels in Genital Ridge DNA from A/HeJ and Control Samples Assessed by ddPCR</u>

Methylation results from the ddPCR assessment of the *Sry* promoter at CpG -537 (A), -300 (B) and the average of the two as a proxy for the whole promoter (C). While there was change across the four time points assessed (E11.25 E11.5, E12.0 and E12.5), all strains (A to C) showed the inverse trend than expected, with methylation peaking between E11.5 and E12.0. Additionally, in none of the analyses was there a statistically significant difference between the strains at a given stage, with the exception of the A/HeJ E12.5 cohort in the CpG -537 (A) and combined (C) analyses. However, as only one A/HeJ E12.5 sample returned results, these comparisons were disregarded. Key for all graphs at the bottom of (C).

In the methylation-dependent digest reactions, it was predicted that the maximum digestion would be in DNA from E12.5 embryos, as it would be expected that the *Sry* promoter would be highly methylated. This high level of digestion would result in a low level of amplification relative to the unlinked-only control. Meanwhile, minimal digestion would be expected in the methylation-dependent digests of E11.25/E11.5 samples, as the *Sry* promoter would be expected to be unmethylated and hence not be digested, leaving the template intact for amplification. This would result in the least difference between the corresponding methylation-dependent and unlinked-only reactions.

CpGs -537 and -300 were each assessed individually for changes in methylation, and the mean of the two CpG sites was also analysed to give an overall indication of the methylation of the promoter. Figure 6.11 shows the change in methylation between E11.25 and E12.5 for all strains at the individual CpG sites (Figure 6.11A and B) and for the mean of the two CpGs (Figure 6.11C). All comparisons that were identified with statistically significant differences were comparisons with the A/HeJ E12.5 in the -537 CpG and combined CpG analyses (Figures 6.11A and C, respectively), with no comparisons with significant differences identified in the CpG -300 analysis (Figure 6.11B).

However, the A/HeJ E12.5 cohort consisted of only a single biological sample, as the remaining two biological samples failed to amplify. Additionally, the single A/HeJ E12.5 sample which amplified was a substantial outlier from the rest of the dataset, both within the A/HeJ strain and when considering all strains at all time points. Based on these factors, none of the comparisons with A/HeJ E12.5 can be considered truly significant; therefore, there were no significant differences at either CpG site between different time points.

However, a trend that could be observed in all strains at all CpG sites, as well as overall (Figure 6.11A to C), was that methylation rose between E11.25 and E11.5, and either plateaued between E12.0 and E12.5, remaining at this heightened level, or declined to a similar level as the E11.25 value (with the exception being the previously noted A/HeJ E12.5 in Figure 6.11A and C). This was the inverse of the expected pattern of methylation change across this time period, even in the control strains' genital ridge samples.

Based on these unusual results returned from the ddPCR assay for all three strains, as well as the highly variable A/HeJ results, direct quantitative assessment of the CpG sites in the *Sry* promoter was subsequently performed using bisulfite sequencing on the samples reported in this section.

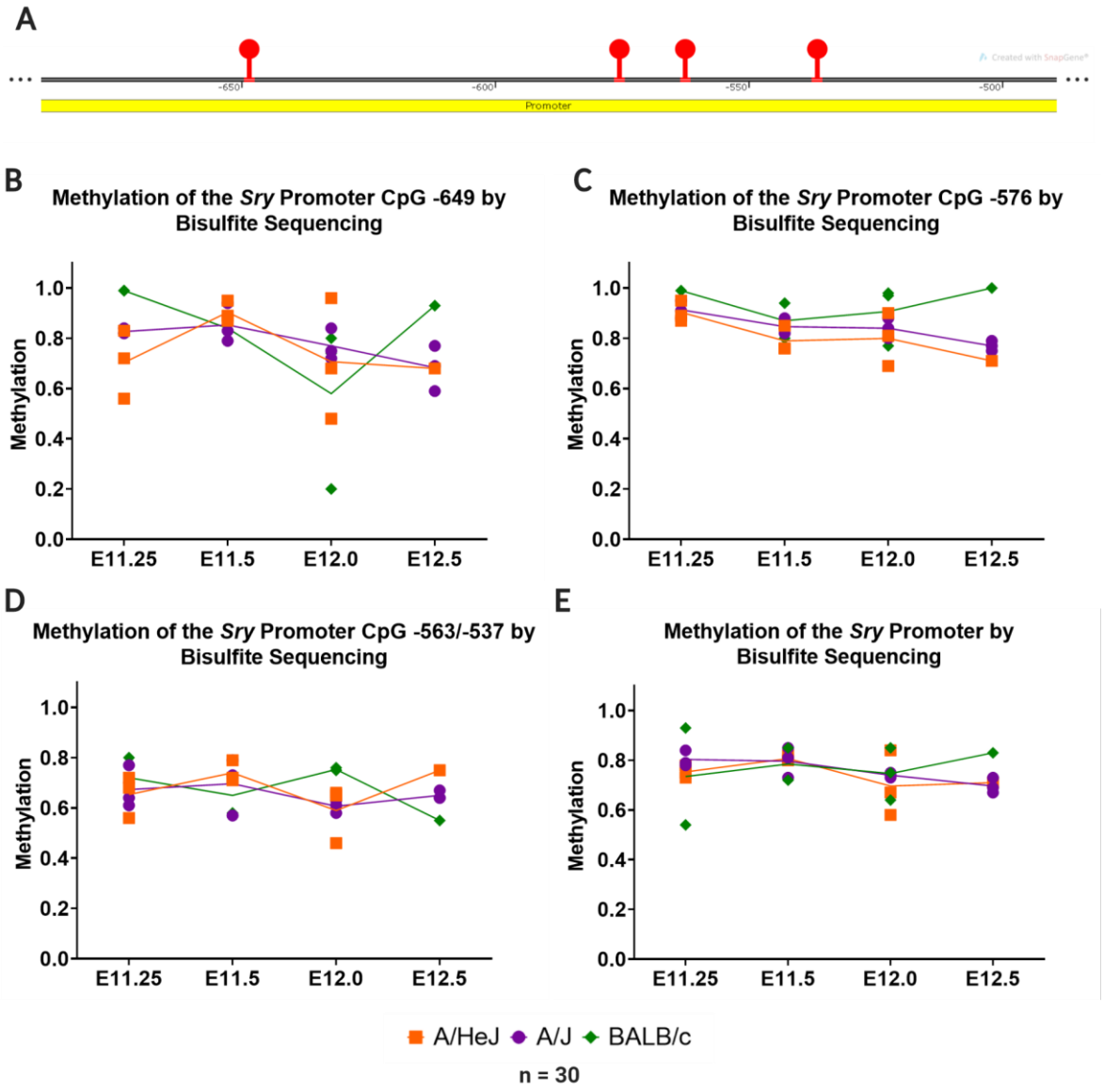

Figure 6.12 - *Sry* Methylation Levels in Genital Ridge DNA from A/HeJ and Control Samples Assessed by Bisulfite Sequencing

Methylation results from bisulfite sequencing of the *Sry* promoter. (A) shows a schematic of the CpG sites (red 'lollipops') assessed in the *Sry* promoter (yellow). Plots of the bisulfite sequencing at CpG -649 (B), -576 (C), -563/-537 (D, assessed as one site) and all CpG sites averaged to give an overall assessment of the promoter (E). As was seen in the ddPCR analysis (Section 6.2.2.3, Figure 6.11), the canonical *Sry* demethylation-remethylation pattern illustrated in Figure 6.3 was not present in the samples of any of the three strains assessed. Again, no significant comparisons between the strains at each stage were identified. Key for (B) to (E) at the bottom of the figure.

6.2.2.4. *Sry* Promoter Methylation Assessment in Genital Ridges by Bisulfite Sequencing

DNA extracted from genital ridge pairs with attached mesonephroi analysed in the ddPCR experiment in Section 6.2.2.3 was subjected to bisulfite sequencing by Australian Genomic Research Facility (AGRF) due to the abnormal ddPCR results from the control samples. This analysis was selected to give a highly quantitative direct assessment of methylation (from 0.0 to 1.0) at each CpG, and to assess methylation of all CpG sites in the *Sry* promoter, rather than focusing on the two CpGs which contained recognition sites for the relevant restriction enzyme.

The results returned assessed a region covering five CpG sites, annotated in Figure 6.12A, at positions -649, -576, -563, -537 and -460. All CpGs except -537 were assessed in the preliminary bisulfite analysis (Section 6.2.2.1); however, CpG -537 was assessed in the ddPCR methylation analysis (Section 6.2.2.3). While the bisulfite sequencing covered these five sites, only three values were obtained. CpG -460 did not return any methylation data in any sample, and the mass peaks for CpGs -563 and -567 fragments were of similar mass and hence separate values could not be obtained. Instead, the methylation was averaged between the two sites, such that both had the same methylation value. For that reason, in this section, these sites will be referred to jointly as "CpG -563/-537".

For each CpG, all strain/stage combinations were compared (Figures 6.12B to D), with no significant differences identified at any CpG site between strain/stage combinations. The mean methylation of all three CpG values was calculated for each sample (Figure 6.12E) as an indicator of overall methylation of the *Sry* promoter. When this was compared between different strain/stage comparisons, again, no comparisons with significant differences were identified.

Despite the absence of significant strain/stage comparisons yielded by the bisulfite sequencing, trends in the change in methylation were able to be noted from these results. The A/HeJ and A/J samples' variation of mean methylation with increasing stage closely mimicked one another at all CpG sites and in the whole promoter. The greatest deviation between these two strains was in the E11.25 samples at CpG -647 (Figure 6.12B), with the A/J mean methylation at 0.827 ± 0.012 and the A/HeJ mean methylation at 0.703 ± 0.136. At all other stages and CpG sites, and particularly when all CpG sites were averaged to assess the whole promoter (Figure 6.12E), the mean methylation of these two strains were highly similar.

The overall trend in methylation change over time in the BALB/c samples, meanwhile, varied between the different CpG sites. For CpG -576 (Figure 6.12C), the BALB/c trend closely followed that of the remaining two strains between E11.25 and E12.0, deviating slightly at E12.5, with the mean methylation increasing at this stage. This increase in methylation at E12.5 in the BALB/c samples resulted in an overall trend which followed the expected pattern of methylation change, with the lowest methylation observed at E11.5, and the greatest methylation occurring at E12.5 (1.0). At this

CpG, both the A/HeJ and A/J E12.5 means decreased. However, there was only a single BALB/c E12.5 sample which returned a result, and therefore this trend may change with an increased number of samples. In contrast, at CpGs -649 and -563/-537 (Figures 6.12B and D, respectively), the overall trend in BALB/c sample methylation was typically the inverse of the A/HeJ and A/J trends, with the BALB/c mean declining when the A/HeJ and A/J means increased, and vice versa.

Despite the deviation in methylation means in the BALB/c cohorts observed at the individual CpG level, once all CpG values are averaged to assess the whole *Sry* promoter (Figure 6.12E), the three strains' trends in methylation change with stage were highly similar, with similar means at all stages. Therefore, there was consistency between the three strains in changes over the entire promoter.

However, despite this consistency, the results for all three strains still maintained the abnormal results returned in the previous two analyses: that the E11.5 methylation was not the lowest level of methylation, as would be expected from the characterised methylation dynamics at this locus[132].

6.3. Discussion

This chapter detailed experiments assessing the structural and regulatory changes to the $Y^{A/HeJ}$ chromosome, comparing it to the Y chromosomes of closely related mouse strains (A/J and BALB/c). As the predicted structural change to the $Y^{A/HeJ}$ chromosome was hypothesised to be a reduction in the *Rbmy* tandem repeat array, this region was assessed for gene copy number using Droplet Digital (dd)PCR.

It was predicted that the structural change to the $Y^{A/HeJ}$ chromosome also affected the regulation of the *Sry* testis triggering gene during testis determination. Therefore, the *Sry* promoter was assessed for methylation changes in genital ridges collected in the window of testis determination. This was performed to examine whether there was a deviation from the expected pattern of demethylation-remethylation in the A/HeJ genital ridge samples following the identified *Rbmy* copy number reduction. *Sry* promoter methylation was assessed using a novel methylation ddPCR assay and bisulfite sequencing of A/HeJ and control genital ridge samples to plot methylation change over four time points ding testis determination.

6.3.1. The $Y^{A/HeJ}$ Chromosome Carries a Deletion Reducing the *Rbmy* Array by Half

The hypothesis of this study was that the abnormal testis determination phenotype observed in the A/HeJ mouse strain was the result of a copy number decrease in the *Rbmy* tandem

repeat array. This hypothesis was formed based on the speculation from the original characterisation paper[2] that there was a structural change to the $Y^{A/HeJ}$ chromosome at or near the centromere[2]. The *Rbmy* array fits this description, lying adjacent to the centromere on the short arm of the Y chromosome.

Supporting this hypothesis, large deletions within the *Rbmy* array have been previously shown to adversely affect testis determination in mice, resulting in full sex reversal[170-173]. An example of a severe *Rbmy* deletion is the Y^{d1} and Y^{d3} mouse lines[171] (Section 1.1.5.2.2.2), which had their *Rbmy* gene copy number reduced to an estimated two or three copies, respectively[170]. Both of these lines carried Y chromosomes that were positive for *Sry*[171], but due to transcriptional silencing of *Sry*[170,172], XY^d individuals developed as partially fertile female mice[173]. It was believed that this silencing of *Sry* was due to repression caused by increased proximity of the locus to the heterochromatin of the centromere (a position effect)[170,172], and that this repression manifested as an absence of *Sry* gene expression during testis determination in the genital ridges[171,172].

As XY A/HeJ mice did not exhibit full sex reversal, only abnormal gonads, all of which contained a portion of testicular tissue, it was expected that the predicted *Rbmy* reduction would be less severe than that observed in the Y^{d1} and Y^{d3} strains. As all XY A/HeJ gonads were observed to have developed testicular tissue, it was predicted that the $Y^{A/HeJ}$ chromosome structural change would result in an *Rbmy* array that retained enough repeats to allow sufficient distance between the centromere and the *Sry* gene that its expression was not totally repressed during testis determination.

In order to assess changes to the *Rbmy* region of the $Y^{A/HeJ}$ chromosome, a ddPCR assay amplifying *Rbmy* was employed to assess gene copy number in A/HeJ and control strain (A/J and BALB/c) samples. This analysis determined that the A/J and BALB/c *Rbmy* copy number was 14.46 and 14.07, respectively, while the A/HeJ *Rbmy* copy number was 7.28 copies, representing 50.33% that of A/J and 51.73% of BALB/c. This reduction in the *Rbmy* array was consistent with the prediction from the original characterisation[2] of a structural change at or near the centromere of the $Y^{A/HeJ}$ chromosome[2].

The retention of approximately seven copies of *Rbmy* on the $Y^{A/HeJ}$ chromosome likely left sufficient sequence between the heterochromatic centromere and the inverted repeat surrounding *Sry,* such that *Sry* was not entirely repressed during testis determination. The most recent estimate of the size of the *Rbmy* array determined it to span 1.1 Mb[76]. Using this value, the reduction of 48.27% to 49.67% (from BALB/c and A/J, respectively) identified here on the $Y^{A/HeJ}$ chromosome would approximate between 560 kb to 569 kb of sequence lost from between the centromere and the next coding region.

However, this array size estimate of 1.1 Mb[76] was determined by hybridisation of 38 *Rbmy*-

positive BACs to the Y chromosome[76], and taking the average clone size of 155 kb and Y chromosome coverage of 5.4 X[76], these values were used to calculate the 1.1 Mb value for this region[76]. Due to the highly repetitive nature of this region, there is currently no direct sequencing of the region between the *H2al2y* inverted repeat and the minor satellite sequence of the centromere publicly available.

The *Rbmy* gene unit was defined in the previous study as 37 kb[76], based upon 10 *Rbmy* ORFs being identified from 370 kb of sequence from the 38 *Rbmy*-positive BACs identified above[76]. The use of this repeat unit size applied to the estimated 1.1 Mb of the overall array, yielded an estimated 29.7 copies, rounded up to approximately 30 copies[76] of *Rbmy* in the reference genome.

If this gene unit size (37 kb[76]) was applied to the copy number derived in this study, it would be predicted that there was a minimum of 269 kb of sequence separating the heterochromatic centromere from the inverted repeat surrounding *Sry* on the $Y^{A/HeJ}$ chromosome, reduced from the 518 kb to 555 kb of sequence in the control strains (approximately 14 and 15 copies in BALB/c and A/J, respectively). This value, however, does not account for intergenic sequence between repeats, which would then increase the distance between *Sry* and the centromere further, potentially raising the size of the array closer to previous estimates (~1.1 Mb[76]) in the control strains.

Based upon these values, there was a stark difference in *Rbmy* copy number determined previously[76] and that determined in this study. The results from the ddPCR analysis in the control strains, A/J and BALB/c, yielded *Rbmy* copy numbers between 14 and 15, rather than the predicted 30 copies[76]. In the case of the $Y^{A/J}$ chromosome, a previous estimate of its *Rbmy* copy number was 31 ± 1[255]. However, the study that determined this value used the estimate of 30 copies as the calibration value for the $Y^{C57BL/6J}$ chromosome, against which to determine the *Rbmy* copy number of various Y chromosomes[255].

The value of 31 ± 1 *Rbmy* copies on the $Y^{A/J}$ chromosome[255] indicated that the A/J strain was a good control for assessing *Rbmy* copy number on the $Y^{A/HeJ}$ chromosome, as the A/J value falls in line with that defined in the reference (C57BL/6J) genome, confirming that the $Y^{A/J}$ chromosome did not have a reduction in the *Rbmy* array. The deviation from this value in this study to approximately 15 *Rbmy* copies on the $Y^{A/J}$ chromosome suggests that the currently used estimate of 30 copies of *Rbmy*[76] may not be accurate.

In contrast to the previous estimate[76], this study determined the number of *Rbmy* copies without assuming repeat unit or array size, and did not use the 30 copy baseline to calibrate the control estimates. Instead, sequence from the loci of both the *Rbmy* gene and the single copy *Ddx3y* reference gene were amplified directly from genomic DNA samples using ddPCR, and the relative amplification of *Rbmy* and *Ddx3y* was used to calculate *Rbmy* copy number. This was a direct experimental assessment of the *Rbmy* copy number, using a highly quantitative method (ddPCR). While the estimate of *Rbmy* copy number on the control Y chromosomes in this study (14 or 15

copies) may not be the exact number of *Rbmy* repeats, the direct experimental nature of this analysis, without making assumptions regarding the locus, supports this estimate. Additionally, the results derived from the ddPCR analysis were closer to the number of *Rbmy* ORFs that were identified in the latest estimate of the copy number (10 ORFs[76]), suggesting that there are likely to be fewer than 30 *Rbmy* repeats on the mouse Y chromosome.

Direct sequencing of the entire genomic region between *Sry* and the centromeric minor satellite DNA (Ymin) would be the ideal approach to accurately quantitate the copy number of *Rbmy*. This may now be possible with advances in sequencing such as using Oxford Nanopore™ Single Molecule sequencing, which has been able to produce ultra-long contig reads over 2 Mb[255] in length. Sequencing the *Rbmy* region in this manner would likely reduce the difficulties observed in sequencing highly repetitive regions.

Regardless of the disparity over the exact number of *Rbmy* repeats on the Y chromosome, the results of the copy number ddPCR analysis in this study identified a halving of the *Rbmy* copy number on the $Y^{A/HeJ}$ chromosome relative to normal controls. This supported the hypothesis of this study: that the structural change to the $Y^{A/HeJ}$ chromosome, predicted to be at or near the centromere, occurred as a deletion in the *Rbmy* array.

6.3.2. Methylation as the Mechanism of *Sry* Regulation

The finding that there was a reduction in *Rbmy* copy number on the $Y^{A/HeJ}$ chromosome lead to the second hypothesis of this study: that the regulation of *Sry* would be altered due to increased proximity to the centromere. This was predicted to manifest as an increased level of methylation and/or a delay in demethylation throughout the window of testis determination in the genital ridges, resulting in repression of *Sry* expression. This increased methylation would be due to position effect variegation (PEV)[165], a phenomenon in which juxtaposing euchromatin and heterochromatin allows the heterochromatin to cross its border with the euchromatin to spread repressive marks[164,165]. This had been observed in the Y^{d1} and Y^{d3} strains in which *Rbmy* had been reduced to two to three repeats[170], leading to *Sry* repression and XY sex reversal.

In order to determine whether the halving of the *Rbmy* array on the $Y^{A/HeJ}$ chromosome was exerting a similar but less extreme repressive effect on *Sry*, methylation of the locus was assessed in genital ridge DNA samples. Initially, a preliminary assessment of both the *Sry* promoter and gene was performed using bisulfite sequencing on approximately E11.5 and E12.5 genital ridge samples from A/HeJ and the two control strains (A/J and BALB/c). This experiment assessed individual CpG sites in both the promoter and gene body, with the majority of strain/stage comparisons with significant differences identified within the promoter region. This was expected due to the regulatory nature of promoters, as the role of methylation is as a regulator of gene activity[253], and consequently is frequently found in the promoter regions of genes.

As the *Sry* promoter was the region that has previously been shown to be subjected to methylation changes to regulate its gene expression[132], this was the sole region of focus for subsequent methylation assessment.

Due to all A/HeJ XY individuals developing at least some testicular tissue, with the majority observed to have wholly testicular gonads, it was predicted that the alteration to the *Sry* methylation dynamics would not substantially delay the onset of *Sry* expression. A substantial increase in *Sry* repression would be expected to result in more severe phenotype, such as a higher incidence of ovotestis development, or occurrence of full sex reversal (ovarian development). As the alteration to *Sry* methylation was predicted to be subtle, assessing methylation in genital ridges at E11.5 and E12.5 only would likely have resulted in an incomplete view of the change in the A/HeJ samples. Ideally, only A/HeJ male embryos which would develop overtly abnormal gonads, ovotestes, would be examined for changes to *Sry* methylation; however, as these embryos would only be identifiable from E14.5 or E15.5 onwards, long after the window of *Sry* action, this was not possible.

With the goal of more precisely detecting the change in *Sry* methylation changes across testis determination, genital ridge samples were collected from A/HeJ, A/J and BALB/c embryos at four time points: E11.25 (just before peak *Sry* gene expression), E11.5 (peak gene expression), E12.0 and E12.5 (decline to total cessation of *Sry* expression). These samples were assessed using a novel ddPCR methylation assay, designed and optimised in this study, and then later by bisulfite sequencing. In order to maximise the genetic material available for analysis, the mesonephroi remained attached to the genital ridges for these assessments.

It has previously been shown that methylation at the *Sry* promoter decreases as expression increases, and vice versa, increasing as expression nears cessation[132]. Further to this, it was expected that the E11.25 and E11.5 samples would return the lowest methylation scores, while E12.5 samples would return the maximum scores. E12.0 samples were expected to fall between the two. However, the preliminary bisulfite sequencing returned results in which the E11.5 samples' methylation was greater than the E12.5 samples. This reversal of expected results was replicated in both the ddPCR and bisulfite sequencing of the samples from both A/HeJ and control strains collected at four time points (Figure 6.13A to C).

While the results from all methylation analyses of the *Sry* promoter in this study were the inverse of the known pattern of demethylation and remethylation across these time points, there was consistency between the different assessment methods and between the strains. The results from the ddPCR and bisulfite analyses tended to show an increase in methylation from E11.25 to E11.5, before decreasing at E12.0 and E12.5. However, there was some variation in this pattern depending on whether individual CpGs or the overall promoter were examined. Assessment of the promoter as a whole was preferred over comparing individual CpG sites, as the individual CpGs assessed varied between analyses; however, all CpGs were assessed by at least two methods.

Additionally, there were some stages at which the methylation varied between the methods, such as A/HeJ E11.25, with the ddPCR result being approximately 25% lower than the bisulfite sequencing result (Figure 6.13A(ii)).

An important note to these results was that the preliminary bisulfite sequencing returned overall lower methylation states at each time point than either the ddPCR or subsequent bisulfite sequencing. This was due to the preliminary analysis being performed on genital ridges alone, while the subsequent analyses were performed on genital ridge with mesonephroi attached. The decision to leave the mesonephroi attached was made to reduce the risk of sample damage due to the greater number of samples when assessing four time points. It was predicted that methylation changes would still be detectable, even though the promoter was predicted to be highly methylated in mesonephric cells. As changes in methylation could be detected across the four time points, this appears to have been the case.

Recent work[266] has demonstrated that the mouse *Sry* promoter is actively demethylated during the window of testis determination in gonadal somatic cells[266]. Between 9 ts to 10 ts (E10.6) and 16 ts to 17 ts (E11.4), methylation of all CpGs in the *Sry* promoter declines from 82.5% to 65.5%[266], corresponding with a dramatic increase in relative mRNA expression from E10.6 to E11.4 in the study[266]. This work built upon previous assessment[132] of *Sry* promoter methylation, in this case quantitatively assessing both individual CpG and total promoter CpG methylation changes through bisulfite sequencing[266]. The dynamic change in methylation reported in the previous study[266] was more than that observed in this study, likely due to the fact that this study utilised not only whole genital ridges, but also left the mesonephroi attached, while the publication[266] enriched for the target cell population (pre-Sertoli cells) by dissociating and sorting genital ridges for Nr5a1-positive cells[266]. This would have removed substantial 'background' methylation from the mesonephric cells[266], as well as the pre-Leydig and germ cells in the genital ridge, which would all be expected have *Sry* highly methylated throughout testis determination.

By showing active demethylation and remethylation of the *Sry* promoter, this recent publication confirmed that the active demethylation of the *Sry* promoter positively regulates *Sry* gene expression[266]. This was demonstrated by diminished *Sry* expression in mice deficient for the demethylating enzyme (Ten-Eleven Translocation protein 2, *Tet2*). Therefore, it is clear that a reduction in methylation in pre-Sertoli cells during testis determination is required for normal *Sry* expression. In light of this, the *Sry* methylation results obtained in this study directly contradict what is known about the regulation of *Sry* in mouse testis determination. The consistency of the inverted pattern observed between the two analysis methods (ddPCR and bisulfite sequencing, Figure 6.13A to C, (ii)) and between two different collection cohorts (with and without mesonephros, Figure 6.13A to C, (i)), suggests that there was a common element between each of these analyses that lead to in this unexpected result.

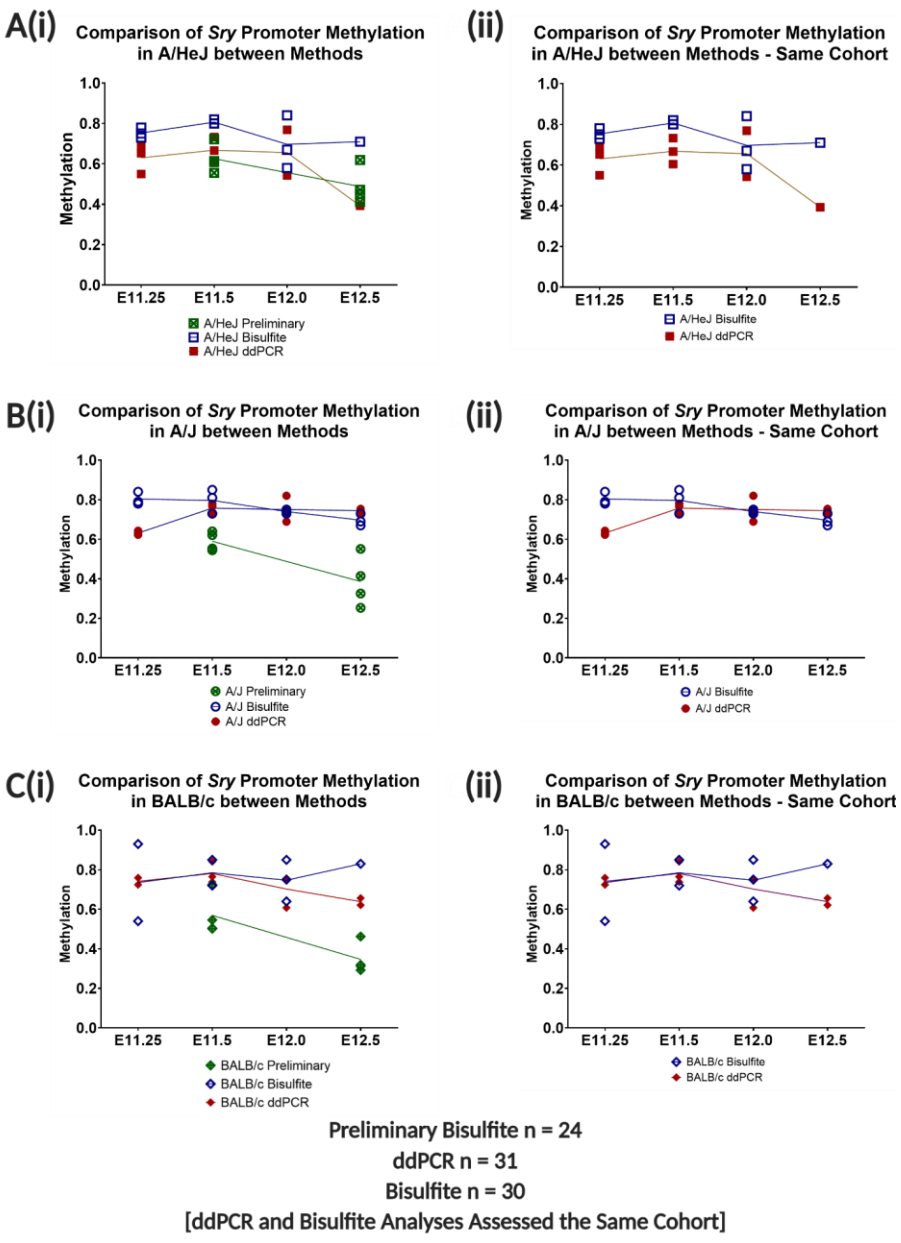

Preliminary Bisulfite n = 24
ddPCR n = 31
Bisulfite n = 30
[ddPCR and Bisulfite Analyses Assessed the Same Cohort]

Figure 6.13 - Comparison of the Results of All Three Methylation Assessment Methods

Comparison of the results of the preliminary bisulfite sequencing, ddPCR and bisulfite sequencing analyses performed on the *Sry* promoter in A/HeJ (A), A/J (B) and BALB/c (C) samples. (A to C)(i) compares all three methods, and includes two different cohorts (with and without mesonephroi), while (ii) compares the ddPCR and bisulfite sequencing methods as these assessed the same cohort. Overall the three methods gave similar results of similar trends, with the preliminary bisulfite sequencing results returning lower methylation results due to the removal of the mesonephroi from the samples in that cohort. Across the three methods, the trend of the greatest methylation being present at approximately E11.5/E12.0 was maintained, indicating that there was consistency between the methods.

As these samples were both collected at different numbers of days of gestation (11 or 12 days post-coitum), with the inclusion of precise staging by tail somite (ts) numbers, increasing the accuracy of staging these embryos, there was little chance that there has been widespread mischaracterisation of the gestational age/stage of the embryos used in these analyses. At this time, the cause of the inverted methylation dynamics over time is unknown. However, the inverted trend of methylation occurring in all three strain examined in this study did allow for comparison between the strains.

As bisulfite sequencing is regarded as the "gold standard" for assessing DNA methylation[202], the bisulfite sequencing results in this study (Figure 6.13) were considered the most accurate. Overall, there was no significant difference between the A/HeJ and control samples across the four time points, indicating that any alteration to the *Sry* methylation dynamics in the A/HeJ genital ridges was not detected in this analysis. This may be due to the grouping of samples into stages by embryonic day (E). Each grouping contained samples from embryos across three ts values, with the exception of E12.0 which covered four ts values due to sample availability (20 ts to 23 ts).

While this approach has been used previously to assess testis determination[118,124,143,266], it may not have been appropriate for this study. Somites form at an approximate rate of one pair every two to three hours in embryos at this stage[196], meaning that these stage groupings contain at least four hour windows of development, through to six to nine hours for the E12.0 samples. Due to the highly dynamic changes in *Sry* expression across the testis determination window[270,271], such that a delay in peak expression by as little as one to two ts can result in incomplete testis determination and ovotestis development, depending on genetic background[122,123,271], a slight delay to the demethylation of the *Sry* promoter could result in abnormal testis development.

Specifically, it has been shown that the critical window of Sry action is limited to approximately six hours after onset of *Sry* expression[148], with the protein only able to induce testis determination between 12 ts and 15 ts (E11.0 to E11.25)[148]. Exogenous *Sry* expression at 15 ts resulted in development of some testicular tissue, leading to ovotestes[148], believed to be due to the fact that this was the stage at which *Sry* expression reaches the poles of the genital ridges[123,148]. Beyond 15 ts, exogenous *Sry* expression failed to induce testis cord development, resulting in ovaries[148].

In light of this, the methylation analysis performed in this study had two major limitations. Firstly, the time points chosen did not cover the onset of *Sry* expression, and therefore would not show the demethylation which allows *Sry* expression. However, it would still be expected that the remethylation of the *Sry* promoter would be observable from E11.5 onwards, as the lower level of methylation has been shown to be maintained from E11.5 to E12.0[266], so the increased methylation by E12.5[132] should have been observed. The second limitation was using broad embryonic day groupings; the E11.25 samples in this study had between 14 ts and 16 ts. However, induction of

exogenous *Sry* expression at 14 ts resulted in 82% testis development[266], as this stage was immediately after the onset of endogenous *Sry* expression in XY gonads, while 15 ts induction resulted in ovotestes (as above), and induction of *Sry* at 16 ts resulted in no testicular development[266]. Therefore, as all A/HeJ XY gonads exhibited testis development to differing degrees, it would be unlikely that a delay in *Sry* demethylation would be detected by grouping these three ts stages.

To rectify this, it would be advisable to collect genital ridge samples from embryos across a broader range, E10.0 to E13.0, with a significant number of samples at each ts stage. These samples would ideally have the mesonephroi removed and/or be sorted for the pre-Sertoli cell population, then be assessed for methylation. This would allow for accurate assessment of the methylation dynamics in the A/HeJ samples. However, this would only be advisable after the cause of the inverted methylation pattern observed in this study's results has been identified and rectified.

In addition to potential changes to the canonical demethylation-remethylation dynamics of the *Sry* locus in A/HeJ XY genital ridges, the increased proximity of *Sry* to the repressive centromere may have resulted in the spread of other heterochromatic marks to the gene locus. For example, trimethylation of histone H3 lysine 9 (H3K9me3) is a mark of facultive heterochromatin[272] that have been indicated in Sry regulation[273-275]. The H3K9me3 of the *Sry* gene is demethylated by the lysine (K)-specific demethylase 3A (Kdm3a) in genital ridges at E11.5, and the absence of this demethylase results in a decrease in Sry gene expression and sex reversal[273,276]. Changes to the H3K9me3 level at the *Sry* locus in A/HeJ genital ridges across the window of testis determination is another avenue for determining whether there is heterochromatic spread outwards from the centromere as the result of the *Rbmy* interstitial deletion.

Chapter 7: Discussion

7.1. Introduction

This thesis detailed a project focused on the mouse Y chromosome, composed of two related yet different studies on two different mouse Y chromosomes. The first was the *Ddx3y*^{mKate2} Y chromosome, a transgenic fluorescent reporter Y chromosome created to serve as a tool for use in chromosome instability research. The second was the naturally occurring A/HeJ Y (Y$^{A/HeJ}$) chromosome, which results in abnormal testis determination in male embryos. The Y$^{A/HeJ}$ chromosome arose spontaneously as the A/HeJ strain split from the line leading to the closely related strain, A/J, in approximately 1930[182].

The work that was to be completed on each of these Y chromosomes differed greatly. As the *Ddx3y*^{mKate2} reporter Y chromosome was researcher-generated, the structural change from the wild-type Y chromosome was known; instead its resulting phenotype needed to be assessed. In contrast, the phenotype resulting from the Y$^{A/HeJ}$ chromosome had been previously assessed following identification of the abnormality in A/HeJ males[2]. Therefore the focus was on identification of the structural change to the Y$^{A/HeJ}$ chromosome, along with assessment of downstream epigenetic consequences of the structural change that resulted in the observed phenotype.

In order to assess each of these Y chromosomes, a series of experimental procedures were performed. To assess the *Ddx3y*^{mKate2} chromosome, it was important to first complete characterisation of the fluorescent reporter (mKate2) signal on a stable wild-type background. Therefore, the organs of a *Ddx3y*^{mKate2} male aged to one year were examined for mKate2 fluorescence, and found to exhibit a decreased fluorescence intensity than that observed in the six-week-old *Ddx3y*^{mKate2} male[5]. Additional assessments of mKate2 signal were performed in *Ddx3y*^{mKate2} embryos and adult mice to complete the characterisation of this reporter Y chromosome. To provide a comparison for the *Ddx3y*^{mKate2} mouse, another strain carrying a transgenic reporter chromosome with a red fluorescent reporter transgene was characterised. This mouse strain, *Hprt*$^{DsRed\text{-}Express}$, had its fluorescent reporter inserted onto the X chromosome at the *Hprt* locus, and the fluorescence from this reporter transgene was characterised from early preimplantation development, through midgestation embryos, and into the adult organs. The pattern of the fluorescence signal from the DsRed-Express reporter in the *Hprt*$^{DsRed\text{-}Express}$ mouse differed from that of mKate2 in the *Ddx3y*^{mKate2} adult, including the impact of X chromosome inactivation (XCI) on phenotypic differences between males and females. While there were advantages and disadvantages to both models, this comparison has served to highlight many of the strengths of the *Ddx3y*^{mKate2} mouse.

The *Ddx3y*^{mKate2} reporter Y chromosome was then crossed onto the two known chromosome instability backgrounds: *Trp53* knockout (KO)[4] and *Cenpagfp* knock-in[29]. The aim of these experiments was to demonstrate how the *Ddx3y*^{mKate2} chromosome could be used in detection of chromosome instability, as the Y chromosome can be assayed for in a presence/absence fashion by loss of fluorescence. Unfortunately, the *Trp53* KO background was a poor choice to model this, as *Trp53*$^{-/-}$ cells tend to accumulate, rather than lose chromosomes[238]. The *Cenpagfp* knock-in background posed serious difficulties, due to an increase in lethality associated with homozygosity of the knock-in allele (*Cenpa*$^{g/g}$)[29]. However, this background holds promise for further work to model the usefulness of the *Ddx3y*^{mKate2} reporter Y chromosome.

For the second study, the Y$^{A/HeJ}$ chromosome and its effect on male sex determination was assessed. To examine the effect of the Y$^{A/HeJ}$ chromosome, A/HeJ mice were assessed, both to confirm the occurrence of the previously reported phenotype[2], and to extend the characterisation of the adult phenotype by adding quantitative values, including effects on reproductive productivity and gonadal development. Following phenotype assessment, the Y$^{A/HeJ}$ chromosome itself was assessed to determine the nature of its structural change. This was confirmed to be a copy number reduction within the *Rbmy* tandem repeat array lying adjacent to the centromere, and likely resulted in the weakened cohesion observed between sister chromatids[2].

This deletion in the *Rbmy* array also served to reduce the distance between the testis-determining gene *Sry* and the repressive heterochromatin of the centromere. As it had been observed previously that increased proximity of *Sry* to the centromere results in repression of its expression in testis determination[164,170-172], this was thought to be the molecular aetiology of the A/HeJ male phenotype. As promoter CpG methylation had been shown to regulate *Sry* gene expression in testis determination, with methylation decreasing as expression increases[132,266], this was assessed in A/HeJ and control genital ridges collected at different time points during testis determination. It was predicted that A/HeJ samples would be more highly methylated than control samples at the same time point, due to a spread of repression from the centromeric heterochromatin. However, these results were inconclusive.

7.2. *Ddx3y*^{mKate2}: A Tool for Chromosome Instability Research

The first study of this project was to assess the *Ddx3y*^{mKate2} Y chromosome as a tool for chromosome instability research. As this Y chromosome was designed as a transgenic reporter chromosome, its structural changes were known and therefore did not need to be ascertained. Instead, this work focused on finalising the characterisation of its phenotype, including comparing it to another transgenic fluorescent reporter strain. In addition, the *Ddx3y*^{mKate2} reporter Y chromosome was crossed onto known chromosome instability backgrounds in order to demonstrate how it may be used as a research tool in the context of instability.

7.2.1. Characteristics and Comparison of the *Ddx3y*^{mKate2} Y Chromosome

7.2.1.1. Key Findings and Implications

7.2.1.1.1. Finalisation of the *Ddx3y*^{mKate2} Mouse Characterisation

The *Ddx3y*^{mKate2} Y chromosome was created to be a reporter chromosome for use in chromosome instability research. Its creation involved insertion of the red fluorescent protein reporter gene, *mKate2*, to allow for easy screening for cells that have lost this Y chromosome due to instability. Previous work[5] from this laboratory offered a preliminary characterisation of the phenotype of the *Ddx3y*^{mKate2} mouse. This study aimed to complete this characterisation on a chromosomally stable background, as well as characterise another transgenic fluorescent reporter mouse, *Hprt*$^{DsRed\text{-}Express}$, against which to compare the *Ddx3y*^{mKate2} mouse.

As this reporter Y chromosome and resulting mouse strain were designed to be used as a research tool, it was essential to broadly characterise the mKate2 reporter signal in the mouse in the absence of chromosome instability. To achieve this, additional assessment of the *Ddx3y*^{mKate2} phenotype was performed to finalise the characterisation begun prior to this study[5]. This included a brief examination of mKate2 signal in different tissues within embryonic body structures, as well as examining change in whole organ fluorescence with advanced age of the mouse. Additionally, whole organs were examined to determine the persistence of the mKate2 fluorescence hours post-mortem, in order to better inform on the time constraints associated with examining whole tissues.

The *Ddx3y*^{mKate2} Y chromosome had its fluorescent reporter transgene inserted adjacent to the *Ddx3y* locus on the short arm of the Y chromosome, due to the broad expression profile of *Ddx3y* (refer to Figure 3.2). It was expected that this locus would be comprised of permissive chromatin, which, combined with the strong promoter, would result in broad expression of the *mKate2* gene, and hence, broad mKate2 fluorescence in the mouse. It had previously been shown that (Figure 3.3[2]), while mKate2 fluorescence varies between adult organs, all organs examined except for the spleen were fluorescent[5].

As genomic instability, including chromosomal instability, increases with age[218,277,278] and has been associated with cancer[279], the *Ddx3y*^{mKate2} mouse was assessed for whole organ fluorescence at advanced age (one year). This revealed that there was an apparent age limitation on mKate2 fluorescence, even in previously strongly fluorescing organs such as the heart and testis, with fluorescence having declined substantially at this age (Figure 3.7). This is noteworthy when discussing the utility of the *Ddx3y*^{mKate2} Y chromosome as research tool, as any experiments using this mouse model will need to be designed to ensure mKate2 fluorescence is sufficiently present in the tissue/s of interest at the age/s of interest.

Further to this, upon examination of *Ddx3y*^{mKate2} E17.5 embryonic tissues following immunohistochemistry (IHC, Figure 3.5) staining, it was observed that different tissues within an organ or structure can differ in the level of mKate2 signal. Organs composed primarily of a single cell type, such as cardiomyocytes in the heart, exhibited consistent mKate2 signal across the entire organ, as would be expected from a homogeneous cell population. Likewise, structures comprised of many different cell types had variation in mKate2 signal due to the heterogeneous population. This was not unexpected, and underscored the necessity of determining the target cell or tissue for use of the *Ddx3y*^{mKate2} mouse model prior to beginning experimentation. It would be advisable to assess mKate2 fluorescence in chromosomally stable *Ddx3y*^{mKate2} samples of the target tissues prior to chromosome instability experiments, as the characterisation of whole organ fluorescence[5] in the *Ddx3y*^{mKate2} mouse was performed to provide a starting point for sample selection.

mKate2 fluorescence was also examined in *Ddx3y*^{mKate2} organs between five hours and nine hours post-mortem, to assess the persistence of mKate2 signal for future research. (Figure 3.6). This was performed to determine whether the fluorescence would be sufficiently maintained under chilled conditions, or whether whole organs required collection and examination and/or processing shortly after euthanasia of the mouse. While there was a moderate to low level of fluorescence in the heart, testes, liver and brain, the remaining organs examined exhibited very little to no fluorescence. Overall, while the heart maintained its fluorescence intensity the best up until nine hours post-mortem, it would be advisable that all tissues, including the heart, be collected and used for downstream purposes shortly after euthanasia in order to maximise the mKate2 fluorescence.

Overall, the *Ddx3y*^{mKate2} mouse model was observed to exhibit broad fluorescence from the reporter transgene protein, mKate2. However, this signal varied between tissue and cell types, and its utility would be maximised when samples were collected from mice from young adulthood or earlier. Additionally, these samples would require prompt entry into downstream applications to maximise the mKate2 fluorescent signal.

7.2.1.1.2. Characterisation and Comparison of the *Hprt*$^{DsRed\text{-}Express}$ Fluorescent Reporter Mouse

Following the finalisation of the *Ddx3y*^{mKate2} characterisation, the transgenic reporter mouse strain *Hprt*$^{DsRed\text{-}Express}$ was assessed to provide a similar characterisation profile as that of the *Ddx3y*^{mKate2} mouse[5]. This was performed in order to compare and contrast the phenotype of the *Ddx3y*^{mKate2} reporter mouse with that of another reporter strain which shared many similarities with the *Ddx3y*^{mKate2} Y chromosome and strain. The characterisation of the *Hprt*$^{DsRed\text{-}Express}$ mouse assessed fluorescence at preimplantation and midgestation embryonic stages, as well as assessing whole adult organs. As the X chromosome was the reporter chromosome in this strain, it was able to be inherited by both males and females. Therefore, the DsRed-Express fluorescence was examined in both sexes.

The *Hprt*$^{DsRed\text{-}Express}$ reporter chromosome was an X chromosome, created by targeted insertion of the *DsRed-Express* fluorescent protein gene into the *Hprt* locus. Likewise, the *Ddx3y*^{mKate2} reporter chromosome was created by targeted insertion of a fluorescent reporter gene into a specific locus (*Ddx3y*); in this case, the transgene was inserted onto the Y chromosome. The strains carrying each of these reporter chromosomes were maintained on the same 129S1/SvImJ background at Murdoch Children's Research Institute (MCRI), and as such had the same genomes with the exception of their respective transgenes.

However, there were differences between the *Ddx3y*^{mKate2} and *Hprt*$^{DsRed\text{-}Express}$ reporter chromosomes and strains. The most readily apparent difference was the choice of chromosome to generate the reporter chromosomes: the Y chromosome and the X chromosome. While these two chromosomes are both sex chromosomes, and are able to pair in meiosis in the male germline via the pseudoautosomal region (PAR[53,60]), they have significantly diverged from one another through evolution[21,42]. The Y chromosome became specialised for functions in the male germline, while the X chromosome retained non-sex functions, including carrying metabolic genes[21,41,42]. Of relevance to this study, the X chromosome and Y chromosome experience different inheritance patterns, with the Y chromosome only being transmitted father to son, while the X chromosome can be transmitted by either sex. In addition, while an X chromosome can be inherited by either sex, the sex of the transmitting parent affects the sex ratio of carrier offspring, with females able to pass an X chromosome to offspring of both sexes, while males only transmit to female offspring.

For both the *Ddx3y*^{mKate2} and *Hprt*$^{DsRed\text{-}Express}$ strains, in this study, both of the reporter chromosomes were hemizygous in the males, and in the *Hprt*$^{DsRed\text{-}Express}$ strain at MCRI, the reporter X chromosome was heterozygous in the females. As the X and Y chromosomes are hemizygous in the male, both chromosomes are active in every cell. In contrast, in the female, in order to balance gene dosage with males, only one X chromosome is active per cell. The inactive X chromosome is silenced by a mechanism known as X chromosome inactivation (XCI), which is applied randomly to a given X chromosome in a cell. Regarding the *Hprt*$^{DsRed\text{-}Express}$ reporter X chromosome, random XCI in a heterozygous female resulted in half of their cells inactivating the *Hprt*$^{DsRed\text{-}Express}$ X chromosome, resulting in mosaic non-fluorescence.

However, in mouse preimplantation development, while female embryos do inactivate one X chromosome, it is not random, with the paternally-inherited X chromosome being preferentially silenced[72-74]. Random XCI is not observed in the embryo proper until after implantation into the uterus[72-74]. This was observed in the *Hprt*$^{DsRed\text{-}Express}$ preimplantation embryos, as whether fluorescence was observed depended on the parental origin of the *Hprt*$^{DsRed\text{-}Express}$ X chromosome. The effect of preferential XCI on the paternal X chromosome resulted in fluorescence only being observable when the *Hprt*$^{DsRed\text{-}Express}$ reporter X chromosome was maternally-inherited.

While fluorescence from both reporter chromosomes was detectable during

preimplantation development, the timing of fluorescence onset varied greatly. The mKate2 fluorescence in *Ddx3y*^{mKate2} embryos was observable from the beginning of cavitation into a blastocyst, at approximately E3.25 to E3.5[5] (Figure 3.3A). The *Hprt*$^{DsRed\text{-}Express}$ embryos, meanwhile, exhibited fluorescence far earlier, from the late two-cell stage onwards (with a maternally-inherited *Hprt*$^{DsRed\text{-}Express}$ X chromosome, Figure 3.8). However, an unexpected observation was the presence of a low level of DsRed-Express fluorescence in all embryos throughout preimplantation, which was hypothesised to be due to persisting DsRed-Express protein from the oocyte. This was because, beyond the late two-cell stage, half of the embryos became more intensely fluorescent, which was likely due to these embryos activating their own genome and producing their own DsRed-Express protein. The embryos which retained low fluorescence were likely wild-type embryos within which DsRed-Express protein continued to persist. Of the high fluorescence *Hprt*$^{DsRed\text{-}Express}$ embryos, there was no observable difference between the sexes, as the maternal *Hprt*$^{DsRed\text{-}Express}$ X chromosome was active in all cells in both the X$^{Hprt\ DsRed\text{-}Express}$Y and X$^{Hprt\ DsRed\text{-}Express}$X embryos.

However, there were two primary similarities between these two reporter strains at the preimplantation development stage. The first was that embryos carrying either the *Ddx3y*^{mKate2} Y chromosome or the *Hprt*$^{DsRed\text{-}Express}$ X chromosome were both fluorescent before implantation. This was beneficial as it allows for selection of embryos carrying the transgenic chromosomes for downstream applications, such as implantation for gestation, or for derivation of embryonic stem (ES) cells. The second similarity was that fluorescent *Ddx3y*^{mKate2} and *Hprt*$^{DsRed\text{-}Express}$ preimplantation embryos were wholly fluorescent, with no observable difference in fluorescence between the different cell lineages of the blastocyst, indicating that both reporter chromosomes broadly expressed their reporter genes at this stage.

One notable advantage that *Ddx3y*^{mKate2} had over *Hprt*$^{DsRed\text{-}Express}$ was that, due to the *Ddx3y*^{mKate2} chromosome being a Y chromosome and therefore only present in males, the *Ddx3y*^{mKate2} strain can be used for non-invasive sex selection of preimplantation embryos. This is highly advantageous, as female (XX) preimplantation embryos are preferred for chimera generation, as only the embryonic stem (ES) cell-derived XY component of XX ↔ XY chimeras can contribute to the male germline[227]. In the *Ddx3y*^{mKate2} strain, all non-fluorescent embryos are known to be XX, whereas in the *Hprt*$^{DsRed\text{-}Express}$ strain, as the reporter X chromosome is maternally transmitted, both male and female embryos are equally likely to be fluorescent. Therefore, there is no non-invasive method to sex preimplantation *Hprt*$^{DsRed\text{-}Express}$ embryos.

Beyond implantation, midgestation embryos carrying the fluorescent reporter chromosome of both strains were fluorescent at E9.5, with the fluorescence exhibited across the entire embryo (Figure 3.3 and 3.9). Viewed at the whole-embryo level, there did not appear to be any difference in fluorescence of different tissue types in either the *Ddx3y*^{mKate2} or *Hprt*$^{DsRed\text{-}Express}$ embryos, with intensity differences instead appearing to be a function of tissue density. The *Ddx3y*^{mKate2} reporter Y chromosome resulted in all males being fluorescent at this stage. As was observed in

preimplantation embryos, the parental origin of the *Hprt*$^{DsRed\text{-}Express}$ X chromosome affected the proportion of florescent embryos observed. However, at this stage, the paternal X chromosome in XX embryos is no longer preferentially inactivated[62], and is instead subject to random XCI. This resulted in fluorescent embryos in all litters: paternal transmission of the *Hprt*$^{DsRed\text{-}Express}$ X chromosome resulted in all female embryos and no male embryos being fluorescent, while maternal transmission resulted in half of each sex being fluorescent. Of note was that the residual low DsRed-Express fluorescence observed in preimplantation embryos from heterozygous females was no longer detectable, likely as the protein had been diluted and/or degraded in wild-type embryos through development.

The effect of random XCI in XX *Hprt*$^{DsRed\text{-}Express}$ embryos was visually apparent at E9.5, with female embryos were exhibiting lower overall fluorescence than male embryos due to the *Hprt*$^{DsRed\text{-}Express}$ reporter X chromosome being silenced in half of the cells of the females. The *Hprt*$^{DsRed\text{-}Express}$ X chromosome was active in all cells of the male embryos due to the lack of XCI in XY embryos. In this way, the male *Hprt*$^{DsRed\text{-}Express}$ embryos paralleled the *Ddx3y*^{mKate2} embryos, as in both strains the reporter chromosome was active due to being hemizygous. An advantage of collecting embryos from both strains at this stage is that in both embryos can be sexed by visual assessment of fluorescence. In *Hprt*$^{DsRed\text{-}Express}$ embryos, male and female embryos carrying the maternal *Hprt*$^{DsRed\text{-}Express}$ X chromosome can be easily distinguished, with the males exhibiting approximately double the fluorescence intensity as the females. However, in the case of maternal transmission, this applied only to the fluorescent embryos, as non-fluorescent embryos were equally likely to be male or female. When the *Hprt*$^{DsRed\text{-}Express}$ reporter X chromosome was paternally-transmitted, the sex of all embryos could be determined visually, as only females were fluorescent. This was similar to the *Ddx3y*^{mKate2} strain, in which all fluorescent embryos were known to be male, with all non-fluorescent embryos being female.

It was in the adult organs, however, that the difference between the two reporter strains, and between the sexes within the *Hprt*$^{DsRed\text{-}Express}$ strain, were most clearly highlighted (Figure 3.12). While the majority of the organs examined exhibited some level of fluorescence in both *Ddx3y*^{mKate2} and *Hprt*$^{DsRed\text{-}Express}$ mice, the relative fluorescence intensity of each organ varied between the strains. While the heart and testis were the most intensely fluorescent organs in the *Ddx3y*^{mKate2} mouse, the visceral fat and liver were had the greatest intensity in the *Hprt*$^{DsRed\text{-}Express}$ mouse. The spleen was also a point of difference between the strains, with the organ fluorescing in the *Hprt*$^{DsRed\text{-}Express}$ mouse, but being non-fluorescent in the *Ddx3y*^{mKate2} mouse.

The adult organs also demonstrated the influence of random XCI in female *Hprt*$^{DsRed\text{-}Express}$ organs, with the male organs each exhibiting substantially more intense fluorescence than their female counterparts. Additionally, in some organs/tissues, most notably the visceral fat and liver, a mottled appearance of the fluorescence was observed in the female tissue, clearly showing large regions of tissue with an active (fluorescent) or inactive (non-fluorescent) *Hprt*$^{DsRed\text{-}Express}$ reporter X

chromosome. The visceral fat was the best example of this, with the female tissue having a mix of intermingled beige and pink fat visible even using white light. This pink appearance of a DsRed-Express-expressing tissue has been previously reported in other transgenic organisms[280].

Due to the presence of random XCI affecting the reporter X chromosome in females of the *Hprt*$^{\text{DsRed-Express}}$ strain, and its resulting effect on the pattern of fluorescence in whole organs, the best choice for comparison to the *Ddx3y*$^{\text{mKate2}}$ strain was the *Hprt*$^{\text{DsRed-Express}}$ male. As noted above, the hemizygosity of both the X and Y chromosomes in the male ensure that both were active in every given cell, enabling ease of comparing the fluorescence between the strains. Therefore, the remaining comparison between the *Ddx3y*$^{\text{mKate2}}$ and *Hprt*$^{\text{DsRed-Express}}$ strains (below) refers to the *Hprt*$^{\text{DsRed-Express}}$ male only.

Fluorescence intensity differed between different organs within each of the strains, a change from the apparent ubiquitous fluorescence present in E9.5 embryos. This was interesting to note, as the embryos of both strains at midgestation appeared to be similarly fluorescent, but in adulthood, the relative intensities of organs' fluorescence differed between the strains, with the most and least fluorescent organs varying between *Ddx3y*$^{\text{mKate2}}$ and *Hprt*$^{\text{DsRed-Express}}$ mice. However, despite the variation in fluorescence intensity between different organs and between the strains, it was clear that the fluorescent reporter gene of each reporter chromosomes was broadly active, with the organs' fluorescence being detectable across entire organ structures and in multiple different tissues.

This was most likely due to the target sites for insertion of the transgenes into the genome. *Hprt* and *Ddx3y* were both selected due to being broadly expressed genes, with the prediction that these loci would be composed of permissive chromatin. Additionally, the fluorescent reporters were both inserted under the control of the strong synthetic CAG promoter[174], which was predicted to be a strong driver of gene expression. This, paired with the chromatin environment of the target loci, was expected to result in high levels of fluorescence across many different tissues. The broad and easily detectable red fluorescence in each of the strains supports this prediction.

Overall, both the *Hprt*$^{\text{DsRed-Express}}$ and *Ddx3y*$^{\text{mKate2}}$ strains shared many similarities in their fluorescence patterns, indicating that both would be useful transgenic tools for researchers. However, in regards to chromosome instability research, the *Ddx3y*$^{\text{mKate2}}$ reporter Y chromosome and its strain have greater applicability. The use of a reporter Y chromosome in chromosome instability research is desirable, as its non-essential nature allows for it to be lost from an animal or cell without compromising viability. The loss of a reporter X chromosome due to chromosome instability carries greater risk of lethality due to the metabolic genes residing on the X chromosome. Also, as discussed above, a reporter Y chromosome allows for ease of visually sexing preimplantation embryos, which is of benefit in chimera generation. A reporter X chromosome fails to be of use in this context, as there is no sex difference in fluorescence in preimplantation embryos,

with the onset of random XCI not occurring until post-implantation. Therefore, regarding the stated purpose for creating the *Ddx3y*^{mKate2} reporter chromosome, the *Ddx3y*^{mKate2} strain was more advantageous for use in chromosome research than the *Hprt*$^{DsRed\text{-}Express}$ strain.

7.2.1.2. Future Directions

The primary aim of generating the *Ddx3y*^{mKate2} reporter Y chromosome was to create a tool for researchers to use in chromosome instability research. The Y chromosome was selected due to its non-essential nature, as this chromosome may be lost in mice without compromising viability. The work completed in this study was performed with three aims: (i) to complete characterisation of this reporter mouse strain; (ii) to compare and contrast the *Ddx3y*^{mKate2} mouse to another transgenic fluorescent reporter strain; and (iii) to demonstrate how this model may be of use as a chromosome instability research tool. The first two aims were addressed in this section, while the third aim was addressed in Section 7.2.2.

Regarding the *Ddx3y*^{mKate2} reporter strain, the broad characterisation of mKate2 fluorescence in the mouse is largely complete. The goal of finalising the characterisation of the *Ddx3y*^{mKate2} strain in this study was to provide an indication of tissue types from this reporter mouse that would be of use for other researchers. To achieve this, the mKate2 fluorescence has been assessed from preimplantation development[5], through to advanced age. This will allow future researchers to determine whether the *Ddx3y*^{mKate2} strain is likely to be of use in their experiments, based on the target cells or tissues of their work. Were the *Ddx3y*^{mKate2} strain to be of interest to other researchers, it would be advisable to perform further characterisation specific to the cell or tissue of interest, as the E17.5 IHC results (Section 3.2.1.1) demonstrated that different cell types within a single structure can exhibit different levels of mKate2 signal.

The *Hprt*$^{DsRed\text{-}Express}$ strain, however, does require further assessment. While this transgenic reporter strain was selected for characterisation in this study to serve as a comparison to the *Ddx3y*^{mKate2} strain, completing its characterisation would be beneficial for the reasons listed for *Ddx3y*^{mKate2} characterisation above. The *Hprt*$^{DsRed\text{-}Express}$ mouse strain was largely characterised in this study, from two-cell embryos to adulthood. However, the *Hprt*$^{DsRed\text{-}Express}$ mouse was not examined for fluorescence in advanced age; therefore, it would be advisable to examine *Hprt*$^{DsRed\text{-}Express}$ male and female organs at one year of age. This would also be beneficial due to enabling another point of comparison between the *Ddx3y*^{mKate2} and *Hprt*$^{DsRed\text{-}Express}$ strains.

Additionally, it would be ideal to perform IHC on *Hprt*$^{DsRed\text{-}Express}$ tissues, as was done on *Ddx3y*^{mKate2} tissues, to better examine the DsRed-Express signal levels of different cells within a tissue. Overall, however, the characterisation of the *Hprt*$^{DsRed\text{-}Express}$ reporter strain is near completion. Therefore, little further work is required for either the *Ddx3y*^{mKate2} or *Hprt*$^{DsRed\text{-}Express}$ strains.

7.2.2. Utility of the *Ddx3y*^{mKate2} Y Chromosome as a Tool for Chromosome Instability Research

7.2.2.1. Key Findings and Implications

The intention behind creating the *Ddx3y*^{mKate2} reporter Y chromosome was to generate a tool for chromosome instability research, as its red fluorescent reporter, mKate2, was included to allow for easy screening for cells that had lost the reporter Y chromosome. The characterisation of mKate2 signal in the *Ddx3y*^{mKate2} mouse was performed to provide a base of information regarding potential utility of the reporter strain in research. Beyond this, demonstrating how this reporter chromosome may be of use in chromosome instability experiments would also inform on potential applications of this mouse model. In order to demonstrate how the *Ddx3y*^{mKate2} reporter Y chromosome may function as a tool for chromosome instability work, it was crossed onto two known chromosome instability backgrounds: the *Trp53* knockout[4] and *Cenpagfp* fusion knock-in[29] mouse strains.

Absence of Trp53 is highly associated with tumour formation[281,282], due to increased incidence of aneuploidy and genome instability[237,238]. For this reason, the *Ddx3y*^{mKate2} Y chromosome was crossed onto the *Trp53* knockout[4] (KO) background, with the aim to be able to assay for loss of the *Ddx3y*^{mKate2} reporter Y chromosome based on loss of fluorescence in *Ddx3y*^{mKate2}/*Trp53*$^{-/-}$ mice. As there are few genes of survival or proliferative advantage on the Y chromosome, it was predicted that loss of the *Ddx3y*^{mKate2} Y chromosome due to instability would not adversely cell survival, and therefore a population of cells without the *Ddx3y*^{mKate2} Y chromosome would be detectable in the given cell population.

However, a factor not accounted for in planning this work was that *Trp53*$^{-/-}$ cells tend to accumulate chromosomes, rather than lose them, with their chromosome counts increasing up to tetraploidy (4N, 80 chromosomes)[238,240-242]. This was the likely cause of the absence of mKate2 fluorescence loss *in vivo* (thymus samples, whole embryo samples) or *in vitro* (PMEF long term culture, with and without mitotic spindle poison challenges), suggesting no loss of the *Ddx3y*^{mKate2} Y chromosome.

Despite this, examination of the *Ddx3y*^{mKate2}/*Trp53* KO mice did yield useful data. For instance, cell sorting of disaggregated *Ddx3y*^{mKate2}/*Trp53* KO midgestation embryos revealed that half of the cells in the embryo at this stage were mKate2 fluorescent, regardless of *Trp53* genotype (Figure 4.2). As this applied to the *Ddx3y*^{mKate2}/*Trp53*$^{+/+}$ embryos, this indicated that many different cell lines in midgestation *Ddx3y*^{mKate2} embryos are mKate2-positive, and therefore may be amenable for derivation for *in vitro* chromosome instability experiments. Additionally, examination and cell

sorting of the *Ddx3y*^{mKate2}/*Trp53*$^{+/+}$ and *Ddx3y*^{mKate2}/*Trp53*$^{-/-}$ thymuses added to the characterisation of the *Ddx3y*^{mKate2} mouse, by determining that the thymus was not an ideal organ to target for chromosome loss due to instability. This was because of the lack of fluorescence observed at the whole thymus level and the low percentage of mKate2-positive cells in the *Ddx3y*^{mKate2} thymus (Figure 4.5).

The primary finding from cell sorting the *Ddx3y*^{mKate2}/*Trp53*$^{-/-}$ thymuses that there was a significant increase in the proportion of mKate2-positive cells in the absence of Trp53 was also of note in this study. These cells were suspected to be a pre-malignant or malignant lineage expansion, as *Trp53*$^{-/-}$ thymic lymphomas were found to have originated from relatively immature thymocytes[4]. The identification of the increased mKate2-positive cell population in the *Ddx3y*^{mKate2}/*Trp53*$^{-/-}$ thymus suggested another potential use for the *Ddx3y*^{mKate2} reporter Y chromosome: lineage tracing. This could be of use in *in vivo* experiments, such as the *Trp53*$^{-/-}$ thymus in this experiment, in which the majority of cell types are non-fluorescent in the wild type (*Trp53*$^{+/+}$), and hence expansion of fluorescent cell types could be detected. Or, *Ddx3y*^{mKate2} cell types known to be fluorescent could be genetically modified to be prone to metastasis, such as by knockout of a tumour suppressor gene, and then implanted into an immunosuppressed nude mouse. The mKate2-positive cells could then be traced through the mouse to determine their migration from the implantation site.

Overall, the results from the *Ddx3y*^{mKate2}/*Trp53* KO intercrossed strain work did not demonstrate how the *Ddx3y*^{mKate2} Y chromosome would be of use in chromosome instability research, as absence of Trp53 did not promote chromosome loss. While some useful insight regarding the *Ddx3y*^{mKate2} reporter Y chromosome was derived from this work, the *Trp53* KO background was not an ideal selection for the aim of this study.

The second instability background selected, the *Cenpagfp* fusion knock-in[29], was more promising for assessing the *Ddx3y*^{mKate2} Y chromosome for its utility in chromosome instability work. The *Ddx3y*^{mKate2}/*Cenpagfp* intercross was generated because the *Cenpagfp* homozygous (*Cenpa*$^{g/g}$) embryos had been shown to become aneuploid[29], largely through chromosome loss due to segregation defects[29]. The known occurrence of chromosome loss in this genotype was ideal for modelling how the *Ddx3y*^{mKate2} Y chromosome could be used to assess loss rates in the presence of instability.

The high rate of aneuploidy in *Cenpa*$^{g/g}$ embryos resulted in lethality beginning just after E9.5, culminating in total absence of these embryos by E12.5[29]. As *Cenpa*$^{g/g}$ embryos had been observed at expected proportions at E9.5[29], it had been initially been the intention to collect *Ddx3y*^{mKate2}/*Cenpagfp* embryos at E9.5. It was intended that primary mouse embryonic fibroblasts (PMEFs) would be derived from the male *Ddx3y*^{mKate2}/*Cenpa*$^{g/g}$ embryos for use in *in vitro* chromosome instability assays. However, despite collecting a large number of embryos at this time point, no male *Ddx3y*^{mKate2}/*Cenpa*$^{g/g}$ embryos were recovered (Figure 4.6). Instead, a number of

resorption sites were observed at a similar frequency as female *Ddx3y*^{mKate2}/*Cenpa*$^{g/g}$ embryos, suggesting that male *Ddx3y*^{mKate2}/*Cenpa*$^{g/g}$ embryos were experiencing premature lethality. While the original description of the *Cenpagfp* transgenic strain did not assess sex ratios of E9.5 embryos[29], previous work with the *Cenpagfp* strain in this laboratory[5] had found a reduction in male *Cenpa*$^{g/g}$ embryos at this stage. However, total absence of *Ddx3y*^{mKate2}/*Cenpa*$^{g/g}$ embryos was not expected, as the fluorescent reporter protein, mKate2, would not be expected to exert any toxic or deleterious effect[214].

The occurrence of the resorption sites at the expected frequency for the male *Ddx3y*^{mKate2}/*Cenpa*$^{g/g}$ embryos indicated that the male *Ddx3y*^{mKate2}/*Cenpa*$^{g/g}$ embryos were likely surviving to implantation, before the onset of lethality between E5.0 and E9.0. As *Ddx3y*^{mKate2} embryos were known to become fluorescent from the early blastocyst onwards (Figure 3.3A), this stage was then selected to collect *Ddx3y*^{mKate2}/*Cenpagfp* embryos, with the aim to recover male *Ddx3y*^{mKate2}/*Cenpa*$^{g/g}$ blastocysts. These collections (Figure 4.7) were to confirm the presence of male *Ddx3y*^{mKate2}/*Cenpa*$^{g/g}$ blastocysts prior to implantation, with the goal for these embryos to potentially be used to derive embryonic stem (ES) cells for *in vitro* use.

By collecting blastocysts, it was confirmed that male *Ddx3y*^{mKate2}/*Cenpa*$^{g/g}$ embryos were indeed present during preimplantation development, at which point no gross morphological abnormalities were observed (Figure 4.7). While male *Ddx3y*^{mKate2}/*Cenpa*$^{g/g}$ blastocysts were reduced from the expected Mendelian proportion, this was likely an effect of a relatively small sample size, and would be expected to be resolved with a greater number of collections. The presence of these embryos prior to implantation, and their normal appearance at this stage, indicated that it was likely that the male *Ddx3y*^{mKate2}/*Cenpa*$^{g/g}$ embryos would be able to implant before the onset of lethality, accounting for the resorption sites observed at E9.5.

Due to difficulties optimising the genotyping protocol to assess the blastocysts' *Cenpa* genotypes, ES cells were unable to be derived for *in vitro* assessment in this study. However, the incidence of premature lethality in the male *Ddx3y*^{mKate2}/*Cenpa*$^{g/g}$ embryos suggests that these embryos are highly unstable. This would be highly advantageous for their use in chromosome instability research, including derivation of ES cells derived from these blastocysts, as cells that lose the *Ddx3y*^{mKate2} reporter Y chromosome would not experience lethality due to the non-essential nature of the Y chromosome. Such loss events would be able to be assayed for using cell sorting on the basis of mKate2 fluorescence, neatly illustrating the utility of the *Ddx3y*^{mKate2} Y chromosome.

Overall, despite the noted problems encountered with the *Ddx3y*^{mKate2}/*Cenpagfp* intercrossed strain, the results of this study indicate that the *Cenpagfp* knock-in transgenic background has potential for future use modelling the utility of the *Ddx3y*^{mKate2} reporter Y chromosome.

7.2.2.2. Future Directions

In order to address the final aim of this study, demonstrating the utility of the *Ddx3y*^{mKate2} reporter Y chromosome as a tool for chromosome instability research, the *Ddx3y*^{mKate2} Y chromosome was crossed onto the *Trp53* KO[4] and *Cenpagfp* knock-in[29] known instability backgrounds. This generated two intercrossed strains: *Ddx3y*^{mKate2}/*Trp53* KO and *Ddx3y*^{mKate2}/*Cenpagfp*, with the homozygotes of each strain (*Trp53*$^{-/-}$ and *Cenpa*$^{g/g}$) expected to exhibit high rates of aneuploidy.

Despite the known chromosome instability associated with each of these transgenic backgrounds, there were issues encountered when using these intercrossed strains to demonstrate how the *Ddx3y*^{mKate2} reporter Y chromosome may be of use as a research tool. The *Trp53* KO background in particular was determined to be a poor choice for this modelling, due to the propensity of cells to gain, not lose, chromosomes in the absence of Trp53. As this work did not aim to assess *Ddx3y*^{mKate2} in the context of hyperploidy, no further work is recommended on the *Ddx3y*^{mKate2}/*Trp53* KO intercrossed strain. However, as described in Section 7.2.2.1, the observation of a lineage expansion of mKate2-positive cells in the *Ddx3y*^{mKate2}/*Trp53*$^{-/-}$ thymus suggested that the *Ddx3y*^{mKate2} reporter Y chromosome may have applicability for lineage tracing. This application warrants further exploration.

The *Cenpagfp* knock-in background showed more promise for modelling the usefulness of the *Ddx3y*^{mKate2} reporter Y chromosome. This background has previously been shown to have a high propensity to lose chromosomes[29], making it a more ideal instability background for this work than the *Trp53* KO background. However, the unforeseen premature lethality present in the target (male *Ddx3y*^{mKate2}/*Cenpa*$^{g/g}$) embryos was an insurmountable issue within the timeline of this study.

Despite this difficulty, the ability to recover male *Ddx3y*^{mKate2}/*Cenpa*$^{g/g}$ embryos at the blastocyst stage indicated that the *Ddx3y*^{mKate2}/*Cenpagfp* intercrossed strain retains promise for modelling the use of the *Ddx3y*^{mKate2} reporter Y chromosome. It would be strongly recommended to collect *Ddx3y*^{mKate2}/*Cenpagfp* blastocysts for ES cell derivation. These ES cells could then be used in experiments to exacerbate chromosome instability and, ideally, loss of the *Ddx3y*^{mKate2} Y chromosome. This could be achieved by use of MSPs such as Colcemid and Nocodazole to induce chromosome missegregation events. These cell populations could then be assessed for mKate2 fluorescence using cell sorting.

Additionally, due to the pluripotent nature of ES cells[283], these *Ddx3y*^{mKate2}/*Cenpagfp* ES cells could then be differentiated into many different cell types for *in vitro* modelling of chromosome instability in different cells and tissues. This experiment would be advantageous to perform, as it would be useful to demonstrate how the *Ddx3y*^{mKate2} Y chromosome would be of use in examining chromosome instability and aneuploidy in different cell types, while reducing the need to use live

mice. Derivation of different lineages from ES cells could also be performed on *Ddx3y*^{mKate2} embryos (wild-type *Cenpa*) to perform expression analyses of the *mKate2* transgene in different tissue types, to expand on the characterisation outlined in Section 7.2.1.

Another experiment that may be useful would be to perform backcrosses with the *Cenpagfp* strain following crossing the *Ddx3y*^{mKate2} Y chromosome onto the *Cenpagfp* background. This would result in the intercrossed strain being on a pure background, rather than a mixed strain background as was used in this study. There was no indication of a reduction in *Cenpa*$^{g/g}$ embryos at E9.5 in the initial publication[29], in which the *Cenpagfp* allele was maintained on a C57BL/6J background, nor were male *Cenpa*$^{g/g}$ embryos totally absent in other work in this laboratory[5]. Therefore, it is possible that the mixed strain background in this specific intercrossed strain was responsible for the lethality observed in the *Ddx3y*^{mKate2}/*Cenpa*$^{g/g}$ embryos. However, as the *Cenpagfp* colony maintained at MCRI was on a BALB/c background, not a C57BL/6J background, it may be necessary to cross both the *Ddx3y*^{mKate2} Y chromosome and the *Cenpagfp* allele onto the C57BL/6J background in order to recover male *Ddx3y*^{mKate2}/*Cenpa*$^{g/g}$ embryos. However, if this were performed, male *Ddx3y*^{mKate2}/*Cenpa*$^{g/g}$ embryos would likely be able to be collected at E9.5, at which point PMEFs could be derived for *in vitro* assessment.

7.2.3. *Ddx3y*^{mKate2} Conclusion

The *Ddx3y*^{mKate2} reporter Y chromosome and mouse strain were created to be used as a tool in chromosome instability research. In order for this mouse model to be of use to other researchers, the fluorescence of the mouse at different stages and in different tissues from its fluorescent reporter protein, mKate2, needed to be characterised. In addition, demonstration of how the *Ddx3y*^{mKate2} Y chromosome may be of use in chromosome instability research was also performed to better inform on its utility.

The *Ddx3y*^{mKate2} mouse has several advantages as a model for use in chromosome instability research: the non-essential nature of the Y chromosome, allowing loss of the reporter Y chromosome without loss of viability; the low toxicity of the fluorescent reporter, mKate2[214]; the near-ubiquitous fluorescence observed in the adult male *Ddx3y*^{mKate2} mouse; and the ease of assaying for the reporter Y chromosome in a presence/absence fashion as it is hemizygous.

However, this model has its limitations, including the differing levels of fluorescence between whole organs in the adult, combined with the decline in fluorescence with age. Future use of the *Ddx3y*^{mKate2} mouse will likely require more direct quantification of the level of mKate2 in a given tissue or organ, such as through immunohistochemistry staining or gene expression/protein analysis, to determine the ideal samples for use of the model. Additionally, the age-related decline is yet to be explained. This may be due to a decline in Y chromosome-linked gene expression[215], or loss of the Y chromosome from cells, as it has been shown that certain cell types can be prone to

losing the non-essential sex chromosome with advanced age[218,219].

An unexpected advantage of this model may be the potential usage of cells from these mice in lineage tracing experiments. For example, crossing this reporter Y chromosome onto a tumour-prone background, then developing tumours that can then be grafted into immunocompromised mice lacking the *Ddx3y*^{mKate2} Y chromosome. As all cells that are mKate2-positive would have come from the implanted tumour, the migration of metastatic cells can be traced throughout the animal based on fluorescence. As was seen in the *Ddx3y*^{mKate2}/*Trp53* knockout mouse strain, malignant cells can tend to accumulate chromosomes, rather than lose them. This would result in low likelihood of fluorescence loss from these cells, enabling them to be traced through metastasis.

Overall, the work in this study finalised the characterisation of the *Ddx3y*^{mKate2} reporter mouse strain, and has highlighted its strengths as a tool for chromosome instability research.

7.3. A/HeJ: A Defect In Sex Determination

The A/HeJ mouse had been previously reported to experience a slight defect in its testis determination pathway[2], which was causally linked to the Y chromosome in this strain[2]. However, the specific cause of the A/HeJ male phenotype was not ascertained. The work in this study focused on adding quantitative and qualitative data to the reported A/HeJ phenotype characterisation, as well as identifying the structural change to the A/HeJ Y ($Y^{A/HeJ}$) chromosome. It was hypothesised that the structural change to the $Y^{A/HeJ}$ chromosome resulted in a change to the regulation of the testis triggering gene, *Sry*; therefore, CpG methylation of this locus on the $Y^{A/HeJ}$ chromosome was also examined.

7.3.1. The A/HeJ Male Phenotype Extends Beyond Ovotestes and Small Testes

7.3.1.1. Key Findings and Implications

The original characterisation of the A/HeJ male phenotype focused on the occurrence of ovotestes and small testes, with a particular emphasis on reporting the embryonic phenotype[2]. Assessing the A/HeJ phenotype in this study served two purposes. Firstly, to confirm that the Murdoch Children's Research Institute (MCRI) A/HeJ colony also presented the reported phenotype prior to undertaking assessment of the $Y^{A/HeJ}$ chromosome in this colony. Secondly, to supplement the previously reported characteristics of the A/HeJ males, providing data on A/HeJ adults, as the presentation of the abnormality had been well described in embryos[2].

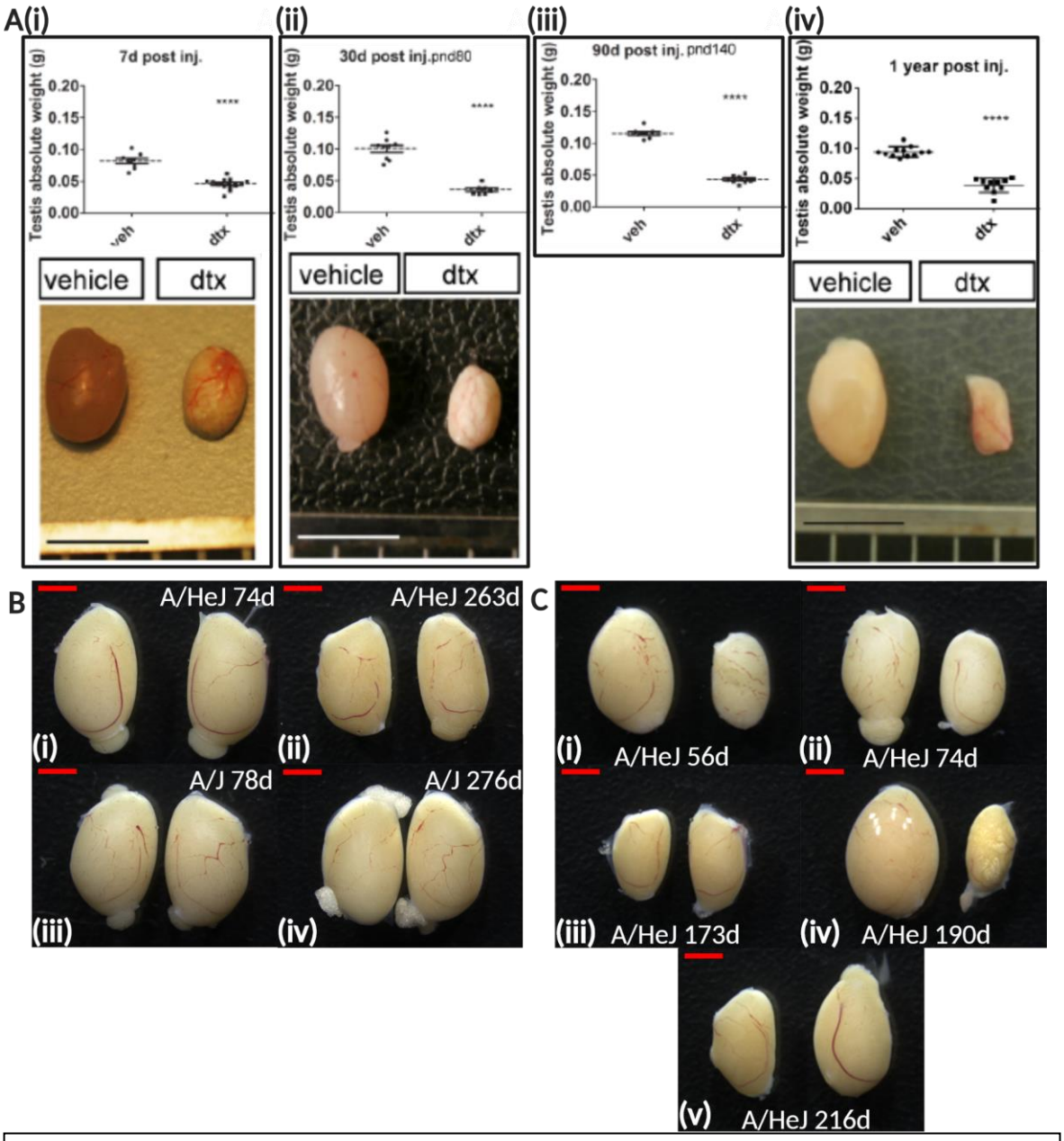

Figure 7.1 - Comparison of A/HeJ Gonads to Sertoli Cell-Ablated Testes from Rebourcet et al (2014)[1]
(A(i)) to (A(iv)) modified from Rebourcet et al[1], in which the Sertoli cell population was ablated from adult mouse testes. (A) Graphs show change in gonad mass following ablation at seven days (i), 30 days (ii), 90 days (iii) and one year (iv) post-ablation. The images show the change in testis size of ablated testes (i, ii, iv, right) relative to control testes (i, ii, iv, left). The ablated testes decrease in size and mass the longer the mouse continued after Sertoli cell ablation. For comparison, (B) shows A/HeJ young and old gonads (B(i) and (ii), respectively, (iii) and (iv) are age-matched A/J controls, Figure 5.5) and (C) the abnormal A/HeJ gonads (Figure 5.3) recovered in this study. B(i) and the abnormal gonads of (C(i)), (ii), (iii) and (v) appeared similar to the gonad image in (A(ii)). The abnormal gonad in (C(iv)) appeared to be of a similar size as that in (A(iv)); however, the external morphology differs between the gonads.

The first aspect of this study was to confirm that the A/HeJ mice in the MCRI colony were also presenting with the reported gonadal abnormalities as was previously reported[2], as this would indicate that the $Y^{A/HeJ}$ chromosome in this colony also carried the structural change. The reduction in males relative to females in the A/HeJ colony (Figure 5.1) and the incidence of abnormal genitalia and gonads in A/HeJ males (Figures 5.4 and 5.3, respectively) gave a preliminary confirmation of the A/HeJ phenotype in the MCRI colony.

However, the rate of adult males with abnormal gonads did not replicate the rate identified in the original characterisation[2], 12.8% compared to 21%[2], respectively. This discrepancy was due to the difference in selection criteria between the two analyses; in this study, males were collected opportunistically regardless of breeder status, while the original study assessed only failed breeders[2]. While the original characterisation speculated that the rate of gonadal abnormalities would increase with assessment of mice beyond failed breeders, as it was predicted that some affected mice may retain fertility or be sex reversed, and hence escape detection, the results of this study disproved this. The identification of abnormal gonads only in failed breeders or unmated males, suggested that abnormal gonads were not likely to occur in fertile A/HeJ males. Routine PCR genotyping of A/HeJ mice confirmed the absence of sex reversed XY females.

While collecting gonads in order to identify abnormal gonads in A/HeJ males, quantitative (mass) values of the gonads and bodies were recorded for all collections. This data, combined with the variable age at collection of the A/HeJ and control A/J mice, allowed for an assessment of the change in body and gonad mass with age in each of the strains. While both strains were observed to increase in total body mass with age at a similar rate, there was a stark difference in the paired gonad mass change over time. Between sexual maturity and nine months of age, A/HeJ gonads significantly decreased in mass, while A/J gonad mass remained constant across this age range (Figure 5.5). This trend had not been previously reported, and was therefore a novel finding of this study.

Additionally, it was observed that A/HeJ males tended to father fewer pups per litter on average over their lifespan compared to A/J males (Figure 5.6). However, there was no significant decline in litter size with age in the A/HeJ males, suggesting that the decline in gonad mass did not result in a decline in fertility. This may require further investigation, due to the small sample size (n = 7) of A/HeJ mice who were both breeders and collected for gonad examination.

The novel finding of age-related decline in the A/HeJ gonads indicated that the A/HeJ phenotype did not just result in a percentage of males developing abnormal testes/ovotestes. Instead, all A/HeJ males were affected by the change on the $Y^{A/HeJ}$ chromosome, with some males being more affected than others and developing overtly abnormal gonads. Due to the previous observation[3] of embryonic ovotestes in which the centre portion of the gonad was testicular tissue, with one or both poles being ovarian tissue[2], it is likely that the *Sry* gene expression wave in the

genital ridge did not reach the poles in a timely fashion before the end of testis determination. This would have resulted in a failure to convert all pre-Sertoli cells to Sertoli cells, with those that did not activate *Sry* within the testis determination window committing to ovarian development instead.

While the most apparent outcome of such a shortfall in *Sry* expression would be the ovotestes and small testes observed, it would also likely contribute to the age-related decline in gonad mass. The distinction between normal and abnormal gonads would likely be due to the extent of the *Sry* gene expression wave delay. Work from Rebourcet et al (2014)[1] demonstrated that Sertoli cells' function is to maintain testicular morphology, including gonad size[1]. This was shown through use of a mouse model of Diphtheria toxin-inducible Sertoli cell ablation[1]. Ablating the Sertoli cells in adult mice resulted in rapid testicular atrophy, with a significant decline in testicular mass within seven days of dosage[1] to similar masses observed in the oldest A/HeJ gonads examined in this study (nine months of age, Figure 5.5D). Additionally, the images of the atrophying testes in the Rebourcet et al publication at 30 days post-ablation[1] appeared visually very similar to the abnormal gonads observed in A/HeJ mice in this study. Figure 7.1 illustrates the comparison of the abnormal A/HeJ gonads recovered in this study to the ablated testes in the 2014 study[1].

The reduction in mass and size due to atrophy in treated testes was the result of Sertoli cell absence in the testis[1]. The ablation of Sertoli cells was also shown to reduce the number of Leydig cells and germ cells in the testis[1], although the overall architecture of the testis was maintained[1]. That work[1] bolsters the hypothesis that the age-related decline in the A/HeJ gonads was due to deficiency of Sertoli cells one or both poles, as the mass and size also declined in the aged A/HeJ gonads examined in this study. Therefore, it would be predicted that a small proportion of pre-Sertoli cells at the pole/s of apparently "normal" A/HeJ testes do not in fact develop into Sertoli cells, and over time, the absence of these cells is resulting in atrophy of the gonads, leading to the observed age-related decline in gonad mass in this strain. Additionally, the deficiency of Sertoli cells in such regions may also be responsible for the slightly lower productivity of A/HeJ males relative to A/J males.

7.3.1.2. Future Directions

Between this study and the original characterisation[2] of the A/HeJ mouse strain, the phenotype of these males has been largely completed. However, some additional work with this strain may be beneficial.

As a deficiency in Sertoli cells at the poles of A/HeJ gonads was speculated above to be the cause of the age-related decline in gonad mass, it would be advisable to section and stain gonads from A/HeJ and control mice collected at a variety of ages. Ideally, this would include a Sertoli cell marker, in order to detect a reduction in their abundance at the poles of A/HeJ gonads. Such staining and sectioning would also be advantageous to perform on abnormal A/HeJ gonads, to better define

the internal structure in the absence of normal testis determination.

A difference between this study and the original characterisation[2] was that the A/HeJ phenotype was originally assessed on a consomic background, C57BL/6J-$Y^{A/HeJ}$ [2]. This was performed in order to specifically link the phenotype to the $Y^{A/HeJ}$ chromosome[2]. This study, meanwhile, assessed the phenotype resulting from the $Y^{A/HeJ}$ chromosome on the A/HeJ strain background. This resulted in a different genetic background between the experimental (A/HeJ) and control (A/J and BALB/c) mice, rather than simply examining the difference in phenotype due to different Y chromosomes. Therefore, it would be ideal to repeat the collection of quantitative data (body and gonad masses) with consomic strains carrying either $Y^{A/HeJ}$, $Y^{A/J}$ or $Y^{BALB/c}$ on a C57BL/6J background. However, the occurrence of the phenotype in the consomic C57BL/6J-$Y^{A/HeJ}$ strain in the original characterisation[2] suggests that it is unlikely that the A/HeJ background beyond the $Y^{A/HeJ}$ chromosome contributed to the observed phenotype.

One unresolved facet of the A/HeJ male phenotype was the observed sex skewing in the colony, reducing the percentage of males. The original characterisation of the A/HeJ strain[2] determined that the $Y^{A/HeJ}$ chromosome did not exhibit any segregation issues in meiosis[2], with similar proportions of X chromosome-bearing and Y chromosome-bearing metaphase II testis cells (transition from secondary spermatocytes to spermatids, refer to Section 1.1.5.2.1) from C57BL/6J-$Y^{A/HeJ}$ and C57BL/6J-$Y^{C57BL/6J}$ males[2]. Therefore, it can be concluded that the reduction in A/HeJ males was not the result of fewer $Y^{A/HeJ}$ chromosome-carrying sperm. Additionally, it was observed that the rate of $Y^{A/HeJ}$ chromosome aneuploidy between C57BL/6J-$Y^{A/HeJ}$ males and hermaphrodites was similar in both cell types assessed[2], with aneuploidy rate not predictive of the gonadal phenotype[2]. Therefore, it would be unlikely that the reduced proportion of male A/HeJ mice was the result of $Y^{A/HeJ}$ chromosome loss in the early embryos.

As no satisfactory explanation for the sex skew has yet been determined, it would be advisable to investigate this aspect of the A/HeJ phenotype. One method to explore this would be to perform timed matings of preimplantation A/HeJ embryos from fertilisation to implantation. At each stage, embryos could be sexed by PCR to determine whether there is a deficiency of males from fertilisation (fewer $XY^{A/HeJ}$ conceptions), or whether male embryos decline in proportion as development progresses (fewer $XY^{A/HeJ}$ embryos surviving preimplantation development). The results of such analysis would then inform the next step of the investigation, such as assessing A/HeJ sperm function/motility.

Overall, however, the A/HeJ male phenotype has been explored in both the original characterisation[2] and this study. With the exception of the gonadal staining detailed above to explore the aetiology of the gonad mass change over time, little further work regarding the phenotype is necessary.

7.3.2. The $Y^{A/HeJ}$ Chromosome Carries a Structural Change

7.3.2.1. Key Findings and Implications

The hypothesis of this study was that the A/HeJ male phenotype reported in both the original characterisation[2] and this study was the result of a copy number reduction in the *Rbmy* gene tandem repeat array on the $Y^{A/HeJ}$ chromosome. Such a deletion was hypothesised to be the predicted structural change at/near the $Y^{A/HeJ}$ centromere[2], as it would likely account for the cytological abnormalities (weakened cohesion at the centromere[2]), as well as the abnormal gonadal phenotype. Depending on whereabouts in the *Rbmy* array the deletion occurred, a reduction in the array may have adversely affected the function of the $Y^{A/HeJ}$ centromere due to its close proximity to the centromere. Additionally, large deletions of the *Rbmy* array have been previously linked to XY sex reversal in mice[170-173].

In assessing the $Y^{A/HeJ}$ chromosome in this study, the first task was to determine whether a copy number reduction in the *Rbmy* array was indeed the structural change to the $Y^{A/HeJ}$ chromosome, as hypothesised. Mouse strains in which the *Rbmy* array was reduced to only two to three copies (the Y^{d1} and Y^{d3} strains, respectively)[170-173] had been observed to undergo XY sex reversal[170-173]. As no sex reversal was observed in the A/HeJ strain, it was predicted that a reduction in the *Rbmy* copy number on the $Y^{A/HeJ}$ chromosome would not be as severe as that in the Y^{d1} and Y^{d3} strains[170-173]. It was predicted that the $Y^{A/HeJ}$ chromosome could instead retain several copies of *Rbmy*, due to the development of testicular tissue in all A/HeJ gonads, including ovotestes.

Through use of a copy number variance (CNV) droplet digital (dd)PCR on A/HeJ and control strain male DNA samples, it was determined that there was a stark reduction in *Rbmy* copy number of the $Y^{A/HeJ}$ chromosome. The $Y^{A/HeJ}$ chromosome was found to carry approximately half the number of *Rbmy* gene repeats as the two closely related control strains (A/J and BALB/c, Figure 6.6). This represented approximately seven *Rbmy* copies on the $Y^{A/HeJ}$ chromosome, aligning with the prediction that the $Y^{A/HeJ}$ chromosome would retain a greater number of repeats than the Y^{d1} and Y^{d3} strains. However, the ddPCR analysis performed in this study returned an *Rbmy* copy number of between 14 and 15 copies on the $Y^{A/J}$ and $Y^{BALB/c}$ chromosomes. The $Y^{A/J}$ chromosome had been previously shown to carry the same number of *Rbmy* repeats as the Y chromosome of the reference genome ($Y^{C57BL/6J}$)[255], previously estimated at 30 copies[76], with the $Y^{A/J}$ chromosome calculated to carry 31 ± 1 copies[255].

The most recent estimate of the copy number at the *Rbmy* locus on the mouse Y chromosome was quantified from bacterial artificial chromosomes (BACs) carrying $Y^{C57BL/6J}$ chromosome material[76]. From 38 *Rbmy*-positive BACs, 10 copies of *Rbmy* were identified across 370 kb of sequence, leading to characterisation of the *Rbmy* gene unit size as 37 kb[76]. Dividing the calculated size of the *Rbmy* array (1.1 Mb) by this value gave the 30 *Rbmy* copy estimate[76]. This

estimate has formed the basis for quantification of this locus across multiple mouse strains[255], with the reference C57BL/6J genome set at 30 copies to serve as the calibrator value for calculating the copy number on other Y chromosomes, including the estimate of the $Y^{A/J}$ chromosome noted above[255]. However, the *Rbmy* copy number identified in this study for the $Y^{A/J}$ chromosome was half that of the published copy number[255]. Despite this apparent reduction, the A/J mice in the MCRI colony did not exhibit abnormalities or sex reversal, nor have they been reported as such[183]. Therefore, it is highly likely that the A/J samples assessed in this study carried the same number of *Rbmy* copies as samples assessed in other studies, despite the different results obtained in this study.

This discrepancy between this study's assessment of the *Rbmy* array and other studies likely lies within the methodology utilised. Due to the highly repetitive nature of the *Rbmy* tandem repeat array, sequencing this region has previously been challenging. This has resulted in reliance on estimates of the gene copy number in this region, which have ranged from 50 copies[170], to the most recent estimate of 30 copies[76]. Previous assessments of mouse strains bearing *Rbmy* deletions, such as the Y^{d1} and Y^{d3} sex reversed mice, calculated their *Rbmy* copy number values assuming that the Y^{d1} chromosome carried at least two copies *Rbmy*[170,284].

In contrast, the assessment of *Rbmy* copy number performed in this study did not rely on previous estimates. As a result, this analysis had two main strengths: firstly, the samples analysed were genomic DNA isolated directly from mouse tissue samples, rather than cloned DNA sources such as BACs. Second, this analysis did not presume the number of *Rbmy* repeats in the control samples, as was the case in other analyses[170,255]. Instead, *Rbmy* copy number was assessed relative to another gene on the Y chromosome, *Ddx3y*, which was known to be in a single copy. This both controlled for input sample concentration, as well as enabled the *Rbmy* copy number to be calculated directly from experimental data. While there are limitations to PCR-based assays, such as the potential difference in efficiency between amplification of the target and reference amplicons, the highly quantitative nature of the ddPCR technology suggests that the *Rbmy* copy number values obtained in this study were likely to be representative of the true number of repeats on the mouse Y chromosome.

Regardless of the exact number of *Rbmy* copies on the $Y^{A/HeJ}$ chromosome, what can be concluded from the results of the ddPCR CNV analysis in this study is that there was a halving of the *Rbmy* copy number on the $Y^{A/HeJ}$ chromosome relative to the control Y chromosomes. This deletion resulted in the distance between the *Sry* gene and the heterochromatin of the centromere being at least halved, depending on the size of intergenic sequence between the *Rbmy* repeats (not assessed here). Previous work on the mouse Y chromosome has demonstrated that severely reducing the distance between *Sry* and the centromere through deletion of almost the entire *Rbmy* array resulted in near complete repression of *Sry* gene expression in the genital ridges at E11.5[172], resulting in XY sex reversal. Retention of a small number of repeats, meanwhile, was found to result in lower levels

of *Sry* expression at this time point, manifesting as incomplete sex reversal (hermaphroditism)[172].

The cause of *Sry* gene expression disruption or repression in these mouse strains was the increased proximity of the euchromatic *Sry* gene locus to the heterochromatic Y chromosome centromere[170-173]. The juxtaposition of euchromatin and constitutive heterochromatin causes a phenomenon called position effect variegation (PEV)[165,285], in which repressive epigenetic marks extend out from the heterochromatin to the euchromatic regions, resulting in repression of gene expression[165]. One such repressive marker is methylation of a cytosine residue when followed immediately by a guanine, called a CpG site.

CpG methylation is both a marker of constitutive heterochromatin, such as that found in the centromeric region[286-288], and is an epigenetic mechanism for gene silencing[289,290]. In particular, as CpG methylation has been previously been shown to play a role in *Sry* gene regulation[132,266], this was the likely mechanism at play in the positional effect on *Sry*, reducing its expression in the context of *Rbmy* array deletions in the Y^{d1} and Y^{d3} strains[170,171]. Previous work has shown that heterochromatin is able to spread into neighbouring regions in a sequence-independent manner when boundary elements surrounding the heterochromatin are disrupted[291].

It was hypothesised that the deletion event that resulted in halving of the *Rbmy* copy number on the $Y^{A/HeJ}$ chromosome disturbed a boundary element which protected the remainder of the Y chromosome short arm from heterochromatic spreading from the centromere. CpG methylation has been studied as a regulator of *Sry* regulation, with the demethylation and remethylation dynamics of the *Sry* promoter having been characterised[132]. In the preliminary assessment of the *Sry* locus on the $Y^{A/HeJ}$ chromosome, both the gene body and promoter were assessed for CpG methylation differences between E11.5 and E12.5 (Figures 6.8 and 6.9). As significant comparisons were only identified in the promoter region, methylation of CpG sites in the *Sry* promoter were the focus of the remainder of the work in this study.

The *Sry* promoter is actively demethylated in the somatic cells of the genital ridge during the window of testis determination[266], with overall methylation declining from the onset of testis determination, through the peak of gene expression (approximately E11.5)[266]. It has been demonstrated that the methylation level of the *Sry* promoter in pre-Sertoli cells declines from the E10.6 (9 tail somites (ts) to 10 ts) level of 82.5%[266] to 65.5% at E11.4 (16 ts to 17 ts)[266]. The methylation level of the promoter remains at a similar level at E12.0 (22 ts to 23 ts, 60.5%)[266]. This decreased methylation of the promoter reflects the increased *Sry* gene expression during this time frame[91,132], as it indicates the removal of the repressive marks. It was predicted that spreading of repression from the centromere on the $Y^{A/HeJ}$ chromosome would result in a delay in reaching the lowest methylation values in pre-Sertoli cells within the window of testis determination. This was speculated to be due to a higher baseline level of methylation prior to E10.5 due to spread of repression from the centromere, which would then result in the demethylation mechanisms, such

as TET2[266], requiring more time to demethylate the promoter to below a threshold that would allow for gene expression.

While the *Sry* promoter and the CpG sites it contains were assessed in multiple ways (novel methylation-dependent ddPCR and bisulfite sequencing, Figure 6.13), from two different cohorts with differing sample collections methods (with and without mesonephroi attached to genital ridges), all analyses of this locus on the $Y^{A/HeJ}$ chromosome returned a similar overall trend. In all analyses, the greatest methylation was observed at approximately E11.5 to E12.0, when methylation should be at its lowest[132,266] in order to allow for *Sry* gene expression. This result was contrary to the known regulation dynamics of the *Sry* promoter[132,266]. Beyond that point, at E12.0 to E12.5, methylation values tended to either remain at approximately the E11.5 value, or decreased from this value. This, again, was a deviation from the known dynamics of *Sry* methylation, as promoter methylation should increase at E12.5[132].

This abnormal pattern in the methylation dynamics was observed in the A/HeJ and control (A/J and BALB/c) strains. As the *Sry* promoter is hypermethylated (> 90%) in mesonephric cells at all stages assessed[266], the analyses that assessed genital ridges with the mesonephroi left attached returned higher overall methylation values than samples which removed the mesonephroi. Despite this, the above abnormal trend was still observable (Figure 6.13). The consistency between the methods and cohorts suggests that there is an unknown factor resulting in this abnormal trend in *Sry* methylation values, even in controls, rather than it being the result of technical error. As recent work demonstrated that CpGs in the *Sry* promoter are actively demethylated by TET2 in somatic cells during testis determination[266], the values returned in this study's analyses cannot reflect the events transpiring within the genital ridges collected. As the development of testes/testicular tissue in males of all three strains indicates that *Sry* is being expressed within the testis determination window, highly increased repression in the form of increased methylation cannot be transpiring.

While the cause of this deviated pattern is as yet unknown, the analyses performed in this study differ from other assessments of the methylation dynamics of the mouse *Sry* promoter in a few notable ways. Firstly, regarding the second cohort examined: the decision to leave the mesonephroi attached to the genital ridge samples. This is not typical of *Sry* methylation assessment in testis determination, as the high methylation of the promoter in the mesonephric cells[266] raises the reported methylation value of the sample, as all cells (genital ridge and mesonephros) contribute to the DNA sample analysed. The mesonephroi were left attached in the second round of collections to reduce the risk of loss or damage to the genital ridge samples, particularly at the earlier collection time points. Another consideration regarding the retention of the mesonephros in these samples was that the relative proportion of the mesonephros to the genital ridge in the sample can change between time points, as the genital ridge increases in size as testis determination progresses, with accelerated growth a noted feature of the early testis[119]. This change in proportion within the DNA sample potentially affected the methylation values obtained in this study; however,

the extent of this effect is unknown, as the relative proportions of mesonephric to genital ridge cells was not quantified. As similar trends in *Sry* methylation changes across the time points assessed with mesonephroi removed were observed when the mesonephroi remained attached, the retention of the mesonephroi did not appear to be the sole cause the unexpected *Sry* methylation results.

The second way this study's assessment of the *Sry* promoter differed from other studies also pertained to the samples. The choice to use whole genital ridges as the sample source for DNA isolation is less commonly applied to promoter methylation analysis, and more frequently used for assessment of Sry expression such as *in situ* staining[123]. Typically, the pre-Sertoli somatic cells are isolated from the genital ridge samples following disaggregation of the tissue[132,266], with the methylation of this subpopulation being assessed. This approach is advantageous as it removes the interference of the higher methylation state of the promoter in not only the mesonephric cells, but also the germ cells and steroidogenic (pre-Leydig) cells, and therefore gives a more detailed assessment of the methylation dynamics in the cell of interest, the pre-Sertoli cell.

However, despite these two aspects, combined with the overall abnormal trend observed, the results of the *Sry* promoter methylation analyses in this study could still be assessed by comparison between the strains and stages assessed. While there was an indication of a significant difference between A/HeJ and BALB/c E12.5 promoter methylation in the preliminary assessment (Figure 6.8 and 6.9), subsequent analyses did not yield any significant comparisons. Therefore, the methylation of this locus requires further assessment.

The hypothesised structural change to the $Y^{A/HeJ}$ chromosome in the form of a deletion within the *Rbmy* gene tandem repeat array was predicted to have a deleterious effect on the regulating of the *Sry* gene during testis determination. Despite the difficulties in assessing *Sry* methylation in this study, it is still hypothesised that the *Rbmy* copy number reduction on the $Y^{A/HeJ}$ chromosome has resulted in a deviation of the canonical demethylation/remethylation pattern of the *Sry* promoter in A/HeJ genital ridges. As the function of *Sry* is to trigger commitment of the pre-Sertoli cells to differentiate into Sertoli cells, and thus to begin the reorganisation of the bipotential genital ridge into a testis[107,119], a change to the regulation of *Sry* expression would result in incomplete testis determination, as seen in the A/HeJ mice.

If, as hypothesised here, the *Rbmy* copy number reduction is delaying the demethylation of the *Sry* promoter in the A/HeJ genital ridges, it is predicted that there is a subpopulation of pre-Sertoli cells which do not commit to the testis development pathway in XY A/HeJ embryos. This would account for both the incidence of ovotestes and small testes, and likely also explains the age-related decline in gonad mass observed in males of this strain, with the difference being in the proportion of uncommitted pre-Sertoli cells from a given gonad.

7.3.2.2. Future Directions

The focus of the A/HeJ study was to assess the phenotype of the A/HeJ males (Section 7.3.1) and to assess the $Y^{A/HeJ}$ chromosome (Section 7.3.2). The purpose of assessing the $Y^{A/HeJ}$ chromosome was to (i) determine whether a copy number change in the *Rbmy* array was the predicted structural change to this Y chromosome, and (ii) determine whether this structural change had an adverse effect on regulation of the *Sry* gene during testis determination.

This work has demonstrated that a halving of the number of *Rbmy* copies on the $Y^{A/HeJ}$ chromosome was indeed the structural change that was predicted in the original characterisation of the A/HeJ mouse[2]. However, as alluded to in Section 7.3.2.1, the precise number of *Rbmy* repeats on the $Y^{A/HeJ}$ chromosome, as well as other strains' Y chromosomes, cannot be determined, as there has previously been no direct quantification of the *Rbmy* repeat locus in mice from primary DNA sources. This study has provided a quantitative value for *Rbmy* copy number with the CNV ddPCR assay, and this has served to enable comparison of A/HeJ and control strains. However, a limitation of this analysis was that it has not been tested on a positive control which contains a known number of repeats of both the target and reference genes (*Rbmy* and *Ddx3y*, respectively), such as a plasmid. Therefore, it cannot be definitively stated that the copy numbers calculated here were a precise assessment of the number of repeats on the Y chromosome of the three strains assessed.

While it would be advantageous to perform such a quality control experiment to assess utility of the assay, a better avenue to pursue would be to sequence *Rbmy* array directly from the Y chromosome, directly from genomic samples. This would be the far superior method, not only regarding the $Y^{A/HeJ}$ chromosome, but also to benefit the broader research community. Directly sequencing this array not only on the $Y^{C5BL/6J}$ chromosome from the reference genome, but as well on Y chromosomes from other classic inbred strains such as A/J, BALB/c and 129/S1, would eliminate gaps in the mouse Y chromosome map. This would improve the resources available to researchers interested in the mouse Y chromosome.

This sequencing has previously not been performed due to known difficulties sequencing highly repetitive regions[292]. The Oxford Nanopore™ Single Molecule sequencing system has currently been used to sequence the longest single read (over 2 Mb)[293]. This should be more than sufficient to sequence across the *Rbmy* repeat array (estimated at 1.1 Mb[76]) in a single read, rather than using short reads which will require assembly into a single contiguous sequence. This would be the ideal sequencing strategy, as the repetitive nature of this gene array could pose difficulties in assembling a contiguous sequence, as similar repeat units can often be mistakenly regarded as covering the same sequence rather than neighbouring repeats[292]. This would be avoidable through use of single molecule sequencing.

As described in Section 7.3.2.1, it was the hypothesis of this study that the *Rbmy* copy

number reduction resulted in a spread of repression from the centromere to the *Sry* locus. Such repressive spread would be expected to adversely affect *Sry* gene expression during testis determination[164]. To examine this, this study attempted to assess methylation at the *Sry* promoter in genital ridge DNA samples from A/HeJ and control embryos collected between E11.25 and E12.5. However, the results returned from these analyses for the control samples deviated significantly from the known dynamics of *Sry* promoter methylation during this window[132,266] for unknown reasons. Therefore, this aspect of assessing the $Y^{A/HeJ}$ chromosome requires further investigation.

In order to complete assessment of the methylation of the *Sry* promoter on the $Y^{A/HeJ}$ chromosome, the cause of the abnormal methylation results must first be ascertained, particularly regarding the control samples. From there, another methylation experiment can be designed to avoid the problem, and the $Y^{A/HeJ}$ and control Y chromosomes may then be assessed for changes in promoter methylation across the testis determination window.

Additionally, future assessments of *Sry* promoter methylation would benefit from modification of the sample collection method. This would entail collection of A/HeJ and control embryos at individual tail somite (ts) values for the given time frame, rather than grouping multiple ts values into embryonic day cohorts/stages. This would allow for more detailed assessment of the dynamic changes in *Sry* methylation across this time window, which would ideally be extended from the E11.25 to E12.5 examined here, to E10.5 to E13.0 (approximately 8 ts to 30 ts). It would also be advantageous to collect a larger number of samples at each ts value; as the rate of embryonic abnormal gonads observed in this study was 17.24% of XY gonads, at least six XY embryos would need to be examined to identify one abnormal embryo. In order to maximise the likelihood of identifying one to two XY embryos which would have developed abnormal gonads, 10 to 12 XY embryos would need to be assessed at each ts value.

While this would require a substantially large number of embryos, it is likely that this would be the only way to detect any deviation in *Sry* methylation dynamics in A/HeJ embryos, as there is still development of testicular tissue in all XY mice. It has been demonstrated that the critical time period for Sry action in the mouse genital ridge is only approximately six hours, between 12 and 15 ts (approximately E11.0 to E11.25)[148]. Through the use of an *Sry* heat shock-inducible model, Hiramatsu et al[148] demonstrated that at 16 ts and beyond, expression of *Sry* in the genital ridge was not able to trigger testis determination (zero of 15 samples exhibited testicular development)[148], with only 27% (three of 11) of those expressing *Sry* at 15 ts having developed as testes[148]. Of those induced to express *Sry* at 15 ts, an additional two gonads developed as ovotestes[148].

Therefore, accounting for this critical window of Sry action and the abnormal gonadal phenotype observed in A/HeJ males, it is hypothesised that that there is a delay of *Sry* expression of only two to four hours in the A/HeJ genital ridges. There may be some potential variation between embryos to account for the incidence of ovotestes and small testes, as well as normally formed

testes. As there is approximately two to three hours between the development of sequential tail somites[196], a two to four hour delay would represent a delay of one to two tail somites. This is the reason for the recommendation that samples be collected at individual ts values, as this predicted delay would likely be masked in broad embryonic day/stage assessments.

Additionally, as detailed in Section 7.3.2.1, much of the previous assessment of the changes in *Sry* promoter methylation have previously been performed on pre-Sertoli cells that have been sorted from disaggregated genital ridges. It would be ideal to perform future methylation analyses on this cell population only, as this would also give a more precise assessment of the degree of methylation at each time point assessed by removing the other cell types with the genital ridge which do not demethylate *Sry*. Additionally, to supplement analysis of *Sry* CpG methylation, this gene locus could also be assessed for changes to other heterochromatic markers, such as H3K9me3 (refer to Section 6.3.2), which may also indicate spreading of repression from the heterochromatic centromere.

Another experiment that would be highly beneficial to assessing the *Sry* locus the $Y^{A/HeJ}$ chromosome would be to directly assess *Sry* gene expression in A/HeJ and control genital ridges. Such gene expression analysis would benefit from a sample collection method similar to that recommended above for the methylation analysis: collection of a large number of XY embryos at each ts value between 8 ts and 30 ts, ideally sorting for the pre-Sertoli cell population only. Quantifying *Sry* gene expression in the genital ridges during testis determination would bolster the methylation data, demonstrating the predicted deviation in *Sry* dynamics in the A/HeJ males. For this gene expression analysis, it would be recommended that *Sry* expression be normalised to expression of the gene *Sdha* (Succinate Dehydrogenase Complex, Subunit A), which has been shown to be a suitable normalising gene for expression analyses in embryonic mouse gonads[121].

Additionally, as there was a substantial deletion of *Rbmy* repeats on the $Y^{A/HeJ}$ chromosome, it may be worth assessing whether there is a significant decrease in the gene expression level of *Rbmy* in the gonads of male and hermaphrodite mice. This expression data could be combined with breeding data to determine whether any observed decrease correlates with reduced reproductive capacity of these mice. It is likely that the reduced productivity of the A/HeJ mice was due to the slight defects in otherwise 'normal' A/HeJ testes relative to A/J and BALB/c control testes. However, a change to the expression of *Rbmy* may be a contributing factor, as deletions of *Rbmy* in mice has been linked to sperm abnormalities[170], and therefore is worthy of exploration.

While this study was able to confirm that the predicted structural change to the $Y^{A/HeJ}$ chromosome was indeed a reduction in the *Rbmy* array, the downstream consequences of this reduction were unable to be satisfactorily quantified. This work, particularly assessment of *Sry* promoter methylation, would be of great value in completing assessment of the $Y^{A/HeJ}$ chromosome.

7.3.3. A/HeJ Conclusion

The A/HeJ mouse strain had been previously reported to exhibit gonadal abnormalities in males, causatively linked to the $Y^{A/HeJ}$ chromosome[2]. The exact cause of this phenotype had not been determined, but was predicted to be a structural change at or near the centromere of the $Y^{A/HeJ}$ chromosome[2].

Assessment of the A/HeJ mouse in this study had two main focuses. Firstly, to assess the phenotype of the male A/HeJ mice in the MCRI colony, both to confirm the occurrence of the phenotype and to generate quantitative data on that phenotype. The second focus was on assessing the $Y^{A/HeJ}$ chromosome for the predicted structural change, hypothesised to be within the *Rbmy* array, and to determine whether there was a regulatory change to the *Sry* gene as a consequence.

The A/HeJ male phenotype of mice with abnormal gonads and a sex skew reducing males in the population was observed in the MCRI A/HeJ colony. Through examination of A/HeJ mice to confirm this phenotype, quantitative and qualitative data was recorded to better inform on the phenotype, with an emphasis on extending the A/HeJ adult phenotype. This data revealed a novel age-related decline in gonad mass in A/HeJ males, indicating that the phenotype affected all A/HeJ males, not only those with overtly abnormal gonads.

This was followed by assessment of the $Y^{A/HeJ}$ chromosome, in which it was determined that there was indeed a reduction within the *Rbmy* tandem repeat array on the short arm of the chromosome. This reduction resulted in a halving of the *Rbmy* gene copy number on the $Y^{A/HeJ}$ chromosome relative to control Y chromosomes. As previously assessed mouse strains with near complete deletion of the *Rbmy* array experienced XY sex reversal[170-172], the reduction in this array on the $Y^{A/HeJ}$ chromosome was expected to be the cause of the abnormal gonads observed in A/HeJ males. This was hypothesised to be due to spread of repression from the heterochromatic centromere to the *Sry* gene locus, affecting its demethylation during testis determination. Unfortunately, this was unable to be adequately assessed, and will require further investigation.

Overall, this study better characterised the phenotypic abnormalities in the A/HeJ strain, and defined the structural abnormality on the Y chromosome of this strain ($Y^{A/HeJ}$).

7.4. Conclusion

The two studies that comprise this project focused on two different mouse Y chromosomes: the $Ddx3y^{mKate2}$ Y chromosome and the $Y^{A/HeJ}$ chromosome. As both of these were Y chromosomes, both of these studies focused on male mice and the impact that inheriting their respective Y chromosome had on the males of each strain.

The transgenic fluorescent reporter *Ddx3y*^{mKate2} Y chromosome was designed to be a tool for use in chromosome instability research. This study finalised the characterisation of this Y chromosome's fluorescence reporter in the mouse, and attempted to demonstrate the utility of the *Ddx3y*^{mKate2} Y chromosome in an instability context. Overall, this work highlighted the strengths of the *Ddx3y*^{mKate2} reporter Y chromosome and mouse strain as tools for researchers.

The $Y^{A/HeJ}$ chromosome, meanwhile, was naturally occurring, and both its structural abnormality and the resulting phenotype required assessment. This assessment increased the known characteristics of the A/HeJ phenotype, including the novel finding of an age-related phenotype in the A/HeJ males, and confirmed the presence of a deletion within the *Rbmy* tandem repeat array. The $Y^{A/HeJ}$ chromosome requires further assessment of the impact of the *Rbmy* reduction on the methylation dynamics of the *Sry* promoter in genital ridges during testis determination.

Overall, this project explored different facets of research involving the mouse Y chromosome.

Appendix

8.1. Additional Data Pertaining to the A/HeJ Abnormal Gonad Pairs

Gonad volumes calculated using estimates of length and width obtained from image analysis of gonads. These values were inserted into the equation for the volume of a prolate spheroid[294]:

$$Volume\ of\ Prolate\ Spheroid = Width^2 \times Length \times 0.523$$

Table A1 - Comparison of Masses and Volumes of Abnormal A/HeJ Gonad Pairs with Age-Matched A/J Control Gonad Pairs

Age (days, (A/HeJ)/ (A/J))	A/HeJ (Mass in mg) (Volume in mm^3)		A/J (Mass in mg) (Volume in mm^3)		A/HeJ Change from A/J (Mass, Percentage Mass) (Volume, Percentage Volume)	
	Left	**Right**	**Left**	**Right**	**Left**	**Right**
56 d/48 d *volumes only*	– 25.2 mm^3	– 71.0 mm^3	– 65.8 mm^3	– 63.4 mm^3	– -40.6 mm^3, -61.7%	– +7.6 mm^3, +12.0%
74 d/78 d	33.0 mg 33.3 mm^3	53.4 mg 47.7 mm^3	70.0 mg 63.3 mm^3	76.1 mg 67.2 mm^3	-37.0 mg, -52.1% -30 mm^3, -47.4%	-22.7 mg, -29.8% -19.5 mm^3, -29.0%
173 d/173 d	24.8 mg 25.0 mm^3	22.2 mg 23.7 mm^3	70.6 mg 64.7 mm^3	69.6 mg 64.7 mm^3	-45.8 mg, -64.9%- 39.7 mm^3, -61.4%	-47.4 mg, -68.1% -41.0 mm^3, -63.4%
190 d/196 d	14.0 mg 14.2 mm^3	65.4 mg 82.5 mm^3	77.1 mg 73.5 mm^3	75.6 mg 76.0 mm^3	-63.1 mg, -81.8% -59.2 mm^3, -76.9%	-10.2 mg, -13.5% +6.5 mm^3, +8.6%
216 d/209 d	50.8 mg 53.7 mm^3	32.6 mg 32.4 mm^3	78.2 mg 86.8 mm^3	74.3 mg 83.3 mm^3	-27.4 mg, -35.0% -33.1 mm^3, -38.1%	-41.7 mg, -56.1% -50.9 mm^3, -61.1%

Table A2 - Comparison of Abnormal A/HeJ Gonads to Their Normal Counterparts

Age (days)	Mass (mg) Volume (mm^3)		Difference (Normal-Abnormal) (Mass, Percentage Mass) (Volume, Percentage Volume)
	Left	Right	
56 d *volumes only*	– 25.2 mm^3	– 71.0 mm^3	– -45.8 mm^3, -64.5% (Right - Left)
74 d	33.0 mg 33.3 mm^3	53.4 mg 47.7 mm^3	-20.4 mg, -38.2% -14.4 mm^3, -30.2% (Right - Left)
173 d	24.8 mg 25.0 mm^3	22.2 mg 23.7 mm^3	N/A
190 d	14.0 mg 14.2 mm^3	65.4 mg 82.5 mm^3	-51.4 mg, -78.6% -68.3 mm^3, -82.8% (Right - Left)
216 d	50.8 mg 53.7 mm^3	32.6 mg 32.4 mm^3	-18.2 mg, -35.8% -21.3 mm^3, -39.7% (Left - Right)

8.2. Spectral Plots from Conventional Rbmy CNV Analysis

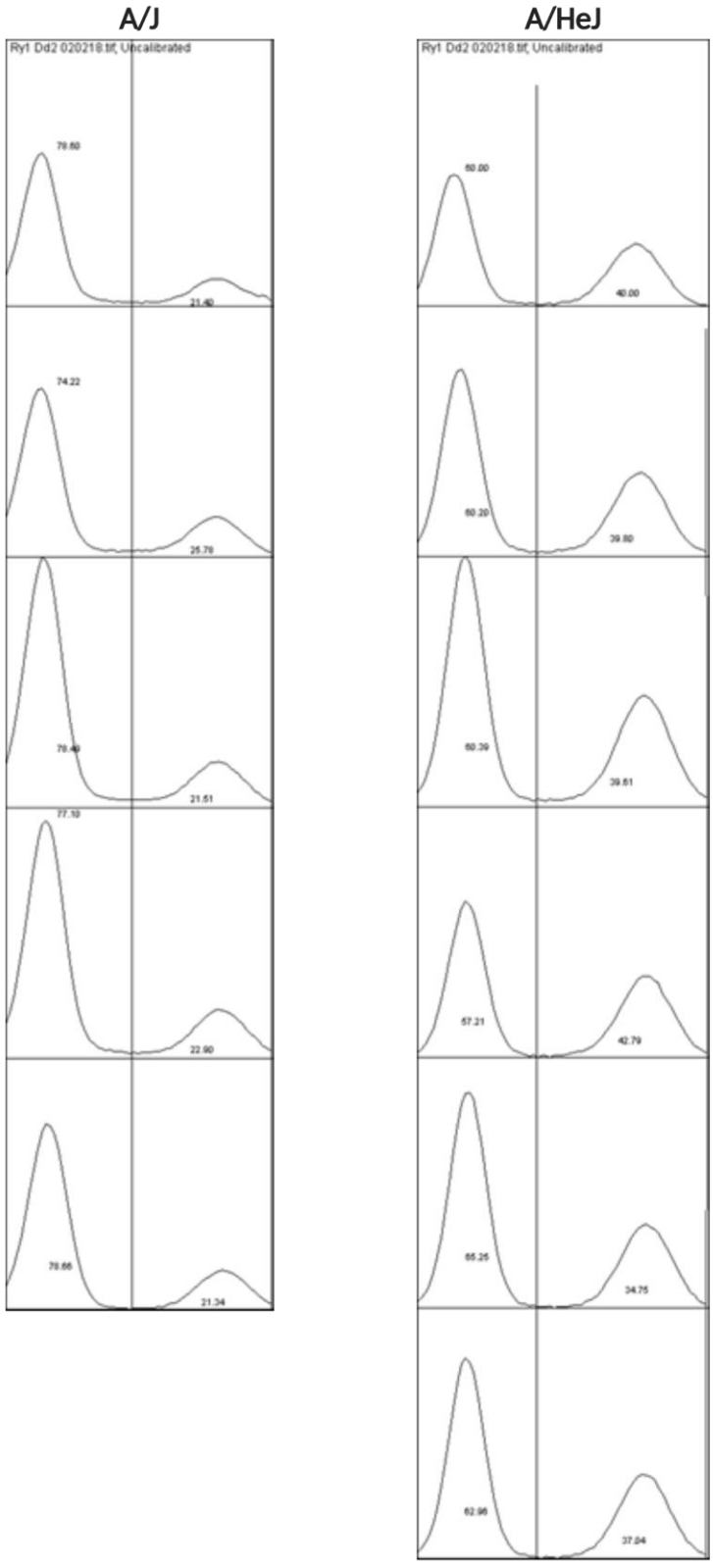

8.3. Strain/Stage Comparisons for Individual CpG Sites in the Sry Promoter and Gene from Preliminary Bisulfite Sequencing

Table A3 - Multiple Comparisons of *Sry* Methylation at CpG +19 in the Gene Forward Strand

mSry Gene Forward Strand CpG +19						
	A/HeJ E11.5 0.9525	**A/J E11.5 0.8075**	**BALB/c E11.5 0.9058**	**A/HeJ E12.5 0.8100**	**A/J E12.5 0.7750**	**BALB/c E12.5 0.7630**
A/HeJ E11.5 0.9525						
A/J E11.5 0.8075	0.5478					
BALB/c E11.5 0.9058	>0.9999	0.961				
A/HeJ E12.5 0.8100	0.5780	>0.9999	0.9690			
A/J E12.5 0.7750	0.2149	>0.9999	0.7162	>0.9999		
BALB/c E12.5 0.7630	0.1376	>0.9999	0.575	>0.9999	>0.9999	

Table A4 - Multiple Comparisons of *Sry* Methylation at CpG +49 in the Gene Forward Strand

mSry Gene Forward Strand CpG +49						
	A/HeJ E11.5 0.6938	**A/J E11.5 0.6858**	**BALB/c E11.5 0.6808**	**A/HeJ E12.5 0.6825**	**A/J E12.5 0.6148**	**BALB/c E12.5 0.5965**
A/HeJ E11.5 0.6938						
A/J E11.5 0.6858	>0.9999					
BALB/c E11.5 0.6808	>0.9999	>0.9999				
A/HeJ E12.5 0.6825	>0.9999	>0.9999	>0.9999			
A/J E12.5 0.6148	>0.9999	>0.9999	>0.9999	>0.9999		
BALB/c E12.5 0.5965	0.9644	0.9840	0.9910	0.9889	>0.9999	

Table A5 - Multiple Comparisons of *Sry* Methylation at CpG +148 in the Gene Forward Strand

mSry Gene Forward Strand CpG +148						
	A/HeJ E11.5 0.7425	**A/J E11.5 0.7358**	**BALB/c E11.5 0.7515**	**A/HeJ E12.5 0.6625**	**A/J E12.5 0.6825**	**BALB/c E12.5 0.6355**
A/HeJ E11.5 0.7425						
A/J E11.5 0.7358	>0.9999					
BALB/c E11.5 0.7515	>0.9999	>0.9999				
A/HeJ E12.5 0.6625	0.9948	0.9978	0.9844			
A/J E12.5 0.6825	0.9998	>0.9999	0.9991	>0.9999		
BALB/c E12.5 0.6355	0.9217	0.9497	0.8601	>0.9999	>0.9999	

Table A6 - Multiple Comparisons of *Sry* Methylation at CpG +234 in the Gene Reverse Strand

mSry Gene Reverse Strand CpG +234						
	A/HeJ E11.5 0.4875	**A/J E11.5 0.6218**	**BALB/c E11.5 0.6463**	**A/HeJ E12.5 0.4988**	**A/J E12.5 0.4318**	**BALB/c E12.5 0.4960**
A/HeJ E11.5 0.4875						
A/J E11.5 0.6218	0.9955					
BALB/c E11.5 0.6463	0.9751	>0.9999				
A/HeJ E12.5 0.4988	>0.9999	0.9983	0.9878			
A/J E12.5 0.4318	>0.9999	0.8912	0.7645	>0.9999		
BALB/c E12.5 0.4960	>0.9999	0.9978	0.9853	>0.9999	>0.9999	

Table A7 - Multiple Comparisons of *Sry* Methylation at CpG +148 in the Gene Reverse Strand

mSry Gene Reverse Strand CpG +148						
	A/HeJ E11.5 0.4663	**A/J E11.5 0.5468**	**BALB/c E11.5 0.5568**	**A/HeJ E12.5 0.5213**	**A/J E12.5 0.4950**	**BALB/c E12.5 0.4970**
A/HeJ E11.5 0.4663						
A/J E11.5 0.5468	>0.9999					
BALB/c E11.5 0.5568	>0.9999	>0.9999				
A/HeJ E12.5 0.5213	>0.9999	>0.9999	>0.9999			
A/J E12.5 0.4950	>0.9999	>0.9999	>0.9999	>0.9999		
BALB/c E12.5 0.4970	>0.9999	>0.9999	>0.9999	>0.9999	>0.9999	

Table A8 - Multiple Comparisons of *Sry* Methylation at CpG +19 in the Gene Reverse Strand

mSry Gene Reverse Strand CpG +19						
	A/HeJ E11.5 0.5200	**A/J E11.5 0.7073**	**BALB/c E11.5 0.6895**	**A/HeJ E12.5 0.5825**	**A/J E12.5 0.6243**	**BALB/c E12.5 0.6133**
A/HeJ E11.5 0.5200						
A/J E11.5 0.7073	0.9020					
BALB/c E11.5 0.6895	0.9555	>0.9999				
A/HeJ E12.5 0.5825	>0.9999	0.9980	0.9997			
A/J E12.5 0.6243	0.9998	>0.9999	>0.9999	>0.9999		
BALB/c E12.5 0.6133	>0.9999	>0.9999	>0.9999	>0.9999	>0.9999	

Table A9 - Multiple Comparisons of *Sry* Methylation at CpG -649 in the Promoter Forward Strand

mSry Promoter Forward Strand CpG -649						
	A/HeJ E11.5 0.5760	**A/J E11.5 0.5743**	**BALB/c E11.5 0.4520**	**A/HeJ E12.5 0.4168**	**A/J E12.5 0.2400**	**BALB/c E12.5 0.2700**
A/HeJ E11.5 0.5760						
A/J E11.5 0.5743	>0.9999					
BALB/c E11.5 0.4520	0.9790	0.9816				
A/HeJ E12.5 0.4168	0.8443	0.8552	>0.9999			
A/J E12.5 0.2400	0.0086	0.0092	0.4082	0.7149		
BALB/c E12.5 0.2700	0.0267	0.0285	0.6704	0.9120	>0.9999	

Table A10 - Multiple Comparisons of *Sry* Methylation at CpG -576 in the Promoter Forward Strand

mSry Promoter Forward Strand CpG -576						
	A/HeJ E11.5 0.7323	**A/J E11.5 0.6830**	**BALB/c E11.5 0.7450**	**A/HeJ E12.5 0.6085**	**A/J E12.5 0.5250**	**BALB/c E12.5 0.4565**
A/HeJ E11.5 0.7323						
A/J E11.5 0.6830	>0.9999					
BALB/c E11.5 0.7450	>0.9999	>0.9999				
A/HeJ E12.5 0.6085	0.9794	>0.9999	0.9504			
A/J E12.5 0.5250	0.4479	0.8521	0.3450	0.9998		
BALB/c E12.5 0.4565	0.0751	0.2979	0.0493	0.8864	>0.9999	

Table A11 - Multiple Comparisons of *Sry* Methylation at CpG -563 in the Promoter Forward Strand

mSry Promoter Forward Strand CpG -563						
	A/HeJ E11.5 0.5683	**A/J E11.5 0.5118**	**BALB/c E11.5 0.5103**	**A/HeJ E12.5 0.4385**	**A/J E12.5 0.3933**	**BALB/c E12.5 0.3128**
A/HeJ E11.5 0.5683						
A/J E11.5 0.5118	>0.9999					
BALB/c E11.5 0.5103	>0.9999	>0.9999				
A/HeJ E12.5 0.4385	0.9681	>0.9999	>0.9999			
A/J E12.5 0.3933	0.7293	0.9864	0.9881	>0.9999		
BALB/c E12.5 0.3128	0.1394	0.5198	0.5331	0.9760	0.9999	

Table A12 - Multiple Comparisons of *Sry* Methylation at CpG -300 in the Promoter Reverse Strand

mSry Promoter Reverse Strand CpG -300						
	A/HeJ E11.5 0.6225	**A/J E11.5 0.5633**	**BALB/c E11.5 0.4833**	**A/HeJ E12.5 0.4950**	**A/J E12.5 0.4418**	**BALB/c E12.5 0.2818**
A/HeJ E11.5 0.6225						
A/J E11.5 0.5633	0.9994					
BALB/c E11.5 0.4833	0.7273	0.9919				
A/HeJ E12.5 0.4950	0.8195	0.9989	>0.9999			
A/J E12.5 0.4418	0.3609	0.8597	>0.9999	0.9998		
BALB/c E12.5 0.2818	0.0017	0.0167	0.2191	0.1591	0.5404	

Table A13 - Multiple Comparisons of *Sry* Methylation at CpG -460 in the Promoter Reverse Strand

mSry Promoter Reverse Strand CpG -460						
	A/HeJ E11.5 0.6868	**A/J E11.5 0.7610**	**BALB/c E11.5 0.7440**	**A/HeJ E12.5 0.7975**	**A/J E12.5 0.7738**	**BALB/c E12.5 0.6833**
A/HeJ E11.5 0.6868						
A/J E11.5 0.7610	0.9956					
BALB/c E11.5 0.7440	0.9996	>0.9999				
A/HeJ E12.5 0.7975	0.9177	>0.9999	0.9998			
A/J E12.5 0.7738	0.9844	>0.9999	>0.9999	>0.9999		
BALB/c E12.5 0.6833	>0.9999	0.9936	0.9993	0.9008	0.9790	

8.4. Strain/Stage Comparisons for Amplicons in the Sry Promoter and Gene

Table A14 - Multiple Comparisons of *Sry* Methylation in the Gene Forward Strand

mSry Gene Forward Strand						
	A/HeJ E11.5 0.7963	**A/J E11.5 0.7433**	**BALB/c E11.5 0.7793**	**A/HeJ E12.5 0.7183**	**A/J E12.5 0.6998**	**BALB/c E12.5 0.6650**
A/HeJ E11.5 0.7963						
A/J E11.5 0.7433	0.6191					
BALB/c E11.5 0.7793	0.9959	0.8909				
A/HeJ E12.5 0.7183	0.2052	0.9754	0.4657			
A/J E12.5 0.6998	0.0616	0.7859	0.1865	0.9936		
BALB/c E12.5 0.6650	0.0034	0.2004	0.0153	0.6111	0.9046	

Table A15 - Multiple Comparisons of *Sry* Methylation in the Gene Reverse Strand

mSry Gene Reverse Strand						
	A/HeJ E11.5 0.4913	**A/J E11.5 0.6253**	**BALB/c E11.5 0.6308**	**A/HeJ E12.5 0.5342**	**A/J E12.5 0.5170**	**BALB/c E12.5 0.5354**
A/HeJ E11.5 0.4913						
A/J E11.5 0.6253	0.1941					
BALB/c E11.5 0.6308	0.1598	>0.9999				
A/HeJ E12.5 0.5342	0.9743	0.6056	0.5427			
A/J E12.5 0.5170	0.9975	0.4162	0.3598	0.9997		
BALB/c E12.5 0.5354	0.9709	0.6196	0.5567	>0.9999	0.9995	

Table A16 - Multiple Comparisons of *Sry* Methylation in the Promoter Forward Strand

mSry Promoter Forward Strand						
	A/HeJ E11.5 0.6255	**A/J E11.5 0.5897**	**BALB/c E11.5 0.5691**	**A/HeJ E12.5 0.4879**	**A/J E12.5 0.3861**	**BALB/c E12.5 0.3464**
A/HeJ E11.5 0.6255						
A/J E11.5 0.5897	0.9683					
BALB/c E11.5 0.5691	0.8141	0.9975				
A/HeJ E12.5 0.4879	0.0414	0.2369	0.4825			
A/J E12.5 0.3861	<0.0001	0.0005	0.0023	0.2361		
BALB/c E12.5 0.3464	<0.0001	<0.0001	0.0001	0.0331	0.9513	

Table A17 - Multiple Comparisons of *Sry* Methylation in the Promoter Reverse Strand

mSry Promoter Reverse Strand						
	A/HeJ E11.5 0.6546	**A/J E11.5 0.6621**	**BALB/c E11.5 0.6136**	**A/HeJ E12.5 0.6463**	**A/J E12.5 0.6078**	**BALB/c E12.5 0.4825**
A/HeJ E11.5 0.6546						
A/J E11.5 0.6621	>0.9999					
BALB/c E11.5 0.6136	0.9642	0.9287				
A/HeJ E12.5 0.6463	>0.9999	0.9996	0.9868			
A/J E12.5 0.6078	0.9377	0.8893	>0.9999	0.9726		
BALB/c E12.5 0.4825	0.0194	0.0132	0.1275	0.0295	0.1607	

8.5. Issues in the MCRI A/HeJ Colony

A major difficulty in this study was the occurrence of a serious adverse event in the A/HeJ mouse colony. The A/HeJ mouse strain is particularly prone to the development of congenital eye problems[183]. In August 2018, the MCRI Animal Facility had a change of practice, introducing a veterinary disinfectant called F10. When used in a spray bottle, there was the potential for irritation of the eyes. This irritation combined with the pre-existing eye issues in this strain resulted in many animals having developed corneal lesions and ulceration. As these conditions were quite painful, in the interest of managing animal welfare, the affected individuals were euthanised on the direction of the Animal Welfare Officer. This reduced the size of the colony by approximately 75%, with none of the remaining animals being active breeders, instead being old relative to the norms for breeding this strain (females must be mated between six and eight weeks of age to trigger maternal behaviour towards the pups). Beyond this, while the females are capable to becoming pregnant, they tend to cannibalise their litters in the few days following birth.

Nonetheless, due to the extenuating circumstances, matings were set up to attempt to recover mouse numbers in the colony. As all surviving females were already older than eight weeks, it was arranged that they would mate with the remaining A/HeJ males, with any pups born to be reared by foster mothers from another strain. One litter was born from the matings with the remaining animals, and was transferred to a foster mother; however, the pups did not survive to weaning. No further litters were born.

Once the remaining A/HeJ mice's ages were advanced to the point that it was no longer ethically viable to continue with breeding attempts, the mice were culled and reproductive material (eggs and sperm) were preserved and used for *in vitro* fertilisation (IVF) by experienced Animal Facility staff. From this material, 89 embryos were conceived, and were transferred into pseudopregnant recipient females in two batches: 40 embryos between two females, and 49 embryos between three females. One litter was born from the first transfer; however, of six pups born, all were male. Hence, there were no new breeding pairs with which to attempt to rebuild the colony. The second transfer yielded no pregnancies. To rebuild the colony, an order for cryorecovery of the A/HeJ strain from the Jackson Laboratory was placed in November 2018. The first attempt at cryorecovery was deemed a failure as of February 2019. The second cryorecovery yielded pups, with one male and four females received at MCRI in early May 2019. Once the mice arrived at the facility, matings were set up with the new mice and the IVF-derived males to rebuild the colony.

Reference List

1 Rebourcet, D. *et al.* Sertoli cells maintain Leydig cell number and peritubular myoid cell activity in the adult mouse testis. *PloS one* **9**, e105687-e105687, doi:10.1371/journal.pone.0105687 (2014).

2 Hunt, P. A. *et al.* The mouse A/HeJ Y chromosome: another good Y gone bad. *Chromosome research : an international journal on the molecular, supramolecular and evolutionary aspects of chromosome biology* **16**, 623-636, doi:10.1007/s10577-008-1216-8 (2008).

3 Yue, F. *et al.* A comparative encyclopedia of DNA elements in the mouse genome. *Nature* **515**, 355-364, doi:10.1038/nature13992 (2014).

4 Jacks, T. *et al.* Tumor spectrum analysis in p53-mutant mice. *Current biology : CB* **4**, 1-7 (1994).

5 Robinson, J. *Characterisation of the Y-GFPd2 and Y-RFP Mouse Strains and their Utility in Chromosome Instability Studies* Bachelor of Science Honours thesis, The University of Melbourne, (2015).

6 Lambert, T. J. FPbase: a community-editable fluorescent protein database. *Nat Methods* **16**, 277-278, doi:10.1038/s41592-019-0352-8 (2019).

7 Xie, Z.-X. *et al.* Design and chemical synthesis of eukaryotic chromosomes. *Chemical Society Reviews* **46**, 7191-7207, doi:10.1039/C7CS00208D (2017).

8 Oliferenko, S. Understanding eukaryotic chromosome segregation from a comparative biology perspective. *Journal of cell science* **131**, jcs203653, doi:10.1242/jcs.203653 (2018).

9 Fritz, A. J. *et al.* Chromosomes at Work: Organization of Chromosome Territories in the Interphase Nucleus. *J Cell Biochem* **117**, 9-19, doi:10.1002/jcb.25280 (2016).

10 Cremer, T. & Cremer, M. Chromosome territories. *Cold Spring Harbor perspectives in biology* **2**, a003889-a003889, doi:10.1101/cshperspect.a003889 (2010).

11 Cremer, T. *et al.* Chromosome territories--a functional nuclear landscape. *Curr Opin Cell Biol* **18**, 307-316, doi:10.1016/j.ceb.2006.04.007 (2006).

12 Krivega, I. & Dean, A. Enhancer and promoter interactions-long distance calls. *Current opinion in genetics & development* **22**, 79-85, doi:10.1016/j.gde.2011.11.001 (2012).

13 Batty, P. & Gerlich, D. W. Mitotic Chromosome Mechanics: How Cells Segregate Their Genome. *Trends in Cell Biology* **29**, 717-726, doi:10.1016/j.tcb.2019.05.007 (2019).

14 Hirano, T. Chromosome Dynamics during Mitosis. *Cold Spring Harbor perspectives in biology* **7**, a015792, doi:10.1101/cshperspect.a015792 (2015).

15 Kalitsis, P., Zhang, T., Marshall, K. M., Nielsen, C. F. & Hudson, D. F. Condensin, master organizer of the genome. *Chromosome research : an international journal on the molecular, supramolecular and evolutionary aspects of chromosome biology* **25**, 61-76, doi:10.1007/s10577-017-9553-0 (2017).

16 Kouzarides, T. Chromatin modifications and their function. *Cell* **128**, 693-705, doi:10.1016/j.cell.2007.02.005 (2007).

17 Kanka, J. Gene expression and chromatin structure in the pre-implantation embryo. *Theriogenology* **59**, 3-19, doi:10.1016/s0093-691x(02)01267-0 (2003).

18 Kornberg, R. D. & Lorch, Y. Twenty-five years of the nucleosome, fundamental particle of the eukaryote chromosome. *Cell* **98**, 285-294, doi:10.1016/s0092-8674(00)81958-3 (1999).

19 Hübner, M. R., Eckersley-Maslin, M. A. & Spector, D. L. Chromatin organization and transcriptional regulation. *Current opinion in genetics & development* **23**, 89-95, doi:10.1016/j.gde.2012.11.006 (2013).
20 Felsenfeld, G. & Groudine, M. Controlling the double helix. *Nature* **421**, 448-453, doi:10.1038/nature01411 (2003).
21 Pertile, M. D., Graham, A. N., Choo, K. H. A. & Kalitsis, P. Rapid evolution of mouse Y centromere repeat DNA belies recent sequence stability. *Genome research* **19**, 2202-2213, doi:10.1101/gr.092080.109 (2009).
22 Anthony JF Griffiths, Jeffrey H Miller, David T Suzuki, Richard C Lewontin & Gelbart, W. M. in *An Introduction to Genetic Analysis* (ed W. H. Freeman) (2007).
23 Kalitsis, P., Griffiths, B. & Choo, K. H. A. Mouse telocentric sequences reveal a high rate of homogenization and possible role in Robertsonian translocation. *Proceedings of the National Academy of Sciences of the United States of America* **103**, 8786-8791, doi:10.1073/pnas.0600250103 (2006).
24 Graham, A. N. & Kalitsis, P. Chromosome Y centromere array deletion leads to impaired centromere function. *PloS one* **9**, e86875-e86875, doi:10.1371/journal.pone.0086875 (2014).
25 Willard, H. F. Evolution of alpha satellite. *Current Opinion in Genetics & Development* **1**, 509-514, doi:https://doi.org/10.1016/S0959-437X(05)80200-X (1991).
26 Sato, H., Masuda, F., Takayama, Y., Takahashi, K. & Saitoh, S. Epigenetic inactivation and subsequent heterochromatinization of a centromere stabilize dicentric chromosomes. *Current biology : CB* **22**, 658-667, doi:10.1016/j.cub.2012.02.062 (2012).
27 Earnshaw, W. C. *et al.* Esperanto for histones: CENP-A, not CenH3, is the centromeric histone H3 variant. *Chromosome research : an international journal on the molecular, supramolecular and evolutionary aspects of chromosome biology* **21**, 101-106, doi:10.1007/s10577-013-9347-y (2013).
28 Westhorpe, F. G. & Straight, A. F. Functions of the centromere and kinetochore in chromosome segregation. *Curr Opin Cell Biol* **25**, 334-340, doi:10.1016/j.ceb.2013.02.001 (2013).
29 Kalitsis, P. *et al.* Partially functional Cenpa-GFP fusion protein causes increased chromosome missegregation and apoptosis during mouse embryogenesis. *Chromosome research : an international journal on the molecular, supramolecular and evolutionary aspects of chromosome biology* **11**, 345-357 (2003).
30 Putkey, F. R. *et al.* Unstable Kinetochore-Microtubule Capture and Chromosomal Instability Following Deletion of CENP-E. *Dev Cell* **3**, 351-365, doi:https://doi.org/10.1016/S1534-5807(02)00255-1 (2002).
31 Bakhoum, S. F. & Compton, D. A. Kinetochores and disease: keeping microtubule dynamics in check! *Curr Opin Cell Biol* **24**, 64-70, doi:10.1016/j.ceb.2011.11.012 (2012).
32 Fryns, J. P. & Lukusa, T. P. *Monosomies*. (2006).
33 Kyriakidou, M., Tai, H. H., Anglin, N. L., Ellis, D. & Strömvik, M. V. Current Strategies of Polyploid Plant Genome Sequence Assembly. *Frontiers in Plant Science* **9**, doi:10.3389/fpls.2018.01660 (2018).
34 Griffiths, A. J., Miller, J. H., Suzuki, D. T., Lewontin, R. C. & Gelbart, W. M. in *An Introduction to Genetic Analysis* (ed W. H. Freeman) (2007).
35 Yamamoto, M., Wakata, A., Aoki, Y., Miyamae, Y. & Kodama, S. Induction of a whole chromosome loss by colcemid in human cells elucidated by discrimination between FISH

signal overlap and chromosome loss. *Mutation research* **749**, 39-48, doi:10.1016/j.mrfmmm.2013.06.001 (2013).
36 Nagaoka, S. I., Hassold, T. J. & Hunt, P. A. Human aneuploidy: mechanisms and new insights into an age-old problem. *Nat Rev Genet* **13**, 493-504, doi:10.1038/nrg3245 (2012).
37 Panning, B. X-chromosome inactivation: the molecular basis of silencing. *Journal of Biology* **7**, 30, doi:10.1186/jbiol95 (2008).
38 Armoskus, C. *et al.* Identification of sexually dimorphic genes in the neonatal mouse cortex and hippocampus. *Brain Res* **1562**, 23-38, doi:10.1016/j.brainres.2014.03.017 (2014).
39 Salo, P., Kääriäinen, H., Page, D. C. & de la Chapelle, A. Deletion mapping of stature determinants on the long arm of the Y chromosome. *Hum Genet* **95**, 283-286, doi:10.1007/bf00225194 (1995).
40 Quintana-Murci, L. & Fellous, M. The Human Y Chromosome: The Biological Role of a "Functional Wasteland". *J Biomed Biotechnol* **1**, 18-24, doi:10.1155/S1110724301000080 (2001).
41 Bachtrog, D. Y-chromosome evolution: emerging insights into processes of Y-chromosome degeneration. *Nat Rev Genet* **14**, 113-124, doi:10.1038/nrg3366 (2013).
42 Morgan, A. P. & Pardo-Manuel de Villena, F. Sequence and Structural Diversity of Mouse Y Chromosomes. *Molecular Biology and Evolution* **34**, 3186-3204, doi:10.1093/molbev/msx250 (2017).
43 Freriks, K. *et al.* Buccal cell FISH and blood PCR-Y detect high rates of X chromosomal mosaicism and Y chromosomal derivatives in patients with Turner syndrome. *European journal of medical genetics* **56**, 497-501, doi:10.1016/j.ejmg.2013.07.008 (2013).
44 Nishi, M. Y., Costa, E. M. F., Oliveira, S. B., Mendonca, B. B. & Domenice, S. The role of SRY mutations in the etiology of gonadal dysgenesis in patients with 45,X/46,XY disorder of sex development and variants. *Horm Res Paediatr* **75**, 26-31, doi:10.1159/000316536 (2011).
45 Patsalis, P. C. *et al.* Identification of high frequency of Y chromosome deletions in patients with sex chromosome mosaicism and correlation with the clinical phenotype and Y-chromosome instability. *American journal of medical genetics. Part A* **135**, 145-149, doi:10.1002/ajmg.a.30712 (2005).
46 Yamamoto, S. *et al.* Rapid selection of XO embryonic stem cells using Y chromosome-linked GFP transgenic mice. *Transgenic Res* **23**, 757-765, doi:10.1007/s11248-014-9813-0 (2014).
47 Graves, J. Sex Chromosome Specialization and Degeneration in Mammals. *Cell* **124**, 901-914, doi:10.1016/j.cell.2006.02.024 (2006).
48 Bachtrog, D. *et al.* Sex Determination: Why So Many Ways of Doing It? *PLOS Biology* **12**, e1001899, doi:10.1371/journal.pbio.1001899 (2014).
49 Luo, Z. X., Yuan, C. X., Meng, Q. J. & Ji, Q. A Jurassic eutherian mammal and divergence of marsupials and placentals. *Nature* **476**, 442-445, doi:10.1038/nature10291 (2011).
50 Graves, J. A. M. Did sex chromosome turnover promote divergence of the major mammal groups?: De novo sex chromosomes and drastic rearrangements may have posed reproductive barriers between monotremes, marsupials and placental mammals. *Bioessays* **38**, 734-743, doi:10.1002/bies.201600019 (2016).
51 Veyrunes, F. *et al.* Bird-like sex chromosomes of platypus imply recent origin of mammal sex chromosomes. *Genome research* **18**, 965-973, doi:10.1101/gr.7101908 (2008).
52 Ross, M. T. *et al.* The DNA sequence of the human X chromosome. *Nature* **434**, 325-337, doi:10.1038/nature03440 (2005).

53 Handel, M. A. The XY body: a specialized meiotic chromatin domain. *Exp Cell Res* **296**, 57-63, doi:10.1016/j.yexcr.2004.03.008 (2004).
54 Otto, S. P. *et al.* About PAR: the distinct evolutionary dynamics of the pseudoautosomal region. *Trends Genet* **27**, 358-367, doi:10.1016/j.tig.2011.05.001 (2011).
55 Alföldi, J. Sequence of the mouse Y chromosome. (2008).
56 Perry, J., Palmer, S., Gabriel, A. & Ashworth, A. A short pseudoautosomal region in laboratory mice. *Genome research* **11**, 1826-1832, doi:10.1101/gr.203001 (2001).
57 Fernandez-Capetillo, O. *et al.* H2AX is required for chromatin remodeling and inactivation of sex chromosomes in male mouse meiosis. *Dev Cell* **4**, 497-508, doi:10.1016/s1534-5807(03)00093-5 (2003).
58 Hinch, A. G., Altemose, N., Noor, N., Donnelly, P. & Myers, S. R. Recombination in the human Pseudoautosomal region PAR1. *PLoS Genet* **10**, e1004503-e1004503, doi:10.1371/journal.pgen.1004503 (2014).
59 Graves, J. A. The origin and function of the mammalian Y chromosome and Y-borne genes--an evolving understanding. *Bioessays* **17**, 311-320, doi:10.1002/bies.950170407 (1995).
60 Khalil, A. M., Boyar, F. Z. & Driscoll, D. J. Dynamic histone modifications mark sex chromosome inactivation and reactivation during mammalian spermatogenesis. *Proceedings of the National Academy of Sciences of the United States of America* **101**, 16583-16587, doi:10.1073/pnas.0406325101 (2004).
61 Santos, F. R. *et al.* A polymorphic L1 retroposon insertion in the centromere of the human Y chromosome. *Human molecular genetics* **9**, 421-430, doi:10.1093/hmg/9.3.421 (2000).
62 Disteche, C. M. & Berletch, J. B. X-chromosome inactivation and escape. *J Genet* **94**, 591-599, doi:10.1007/s12041-015-0574-1 (2015).
63 Barr, M. L. & Bertram, E. G. A morphological distinction between neurones of the male and female, and the behaviour of the nucleolar satellite during accelerated nucleoprotein synthesis. *Nature* **163**, 676-676, doi:10.1038/163676a0 (1949).
64 Li, M., Zou, C. & Zhao, Z. Triple x syndrome with short stature: case report and literature review. *Iran J Pediatr* **22**, 269-273 (2012).
65 Bonomi, M. *et al.* Klinefelter syndrome (KS): genetics, clinical phenotype and hypogonadism. *J Endocrinol Invest* **40**, 123-134, doi:10.1007/s40618-016-0541-6 (2017).
66 Ross, J. L. *et al.* Behavioral and social phenotypes in boys with 47,XYY syndrome or 47,XXY Klinefelter syndrome. *Pediatrics* **129**, 769-778, doi:10.1542/peds.2011-0719 (2012).
67 Okamoto, I. *et al.* Evidence for de novo imprinted X-chromosome inactivation independent of meiotic inactivation in mice. *Nature* **438**, 369-373, doi:10.1038/nature04155 (2005).
68 Behringer, R., Gertsenstein, M., Nagy, K. V. & Nagy, A. *Manipulating the Mouse Embryo: A Laboratory Manual*. (Cold Spring Harbor Laboratory Press, 2014).
69 Hamatani, T., Carter, M. G., Sharov, A. A. & Ko, M. S. H. Dynamics of global gene expression changes during mouse preimplantation development. *Dev Cell* **6**, 117-131, doi:10.1016/s1534-5807(03)00373-3 (2004).
70 Schultz, R. M. The molecular foundations of the maternal to zygotic transition in the preimplantation embryo. *Hum Reprod Update* **8**, 323-331, doi:10.1093/humupd/8.4.323 (2002).
71 Ram, P. T. & Schultz, R. M. Reporter gene expression in G2 of the 1-cell mouse embryo. *Dev Biol* **156**, 552-556, doi:10.1006/dbio.1993.1101 (1993).

72 Oikawa, M. *et al.* Understanding the X chromosome inactivation cycle in mice: a comprehensive view provided by nuclear transfer. *Epigenetics* **9**, 204-211, doi:10.4161/epi.26939 (2014).
73 Sado, T. & Sakaguchi, T. Species-specific differences in X chromosome inactivation in mammals. *Reproduction (Cambridge, England)* **146**, R131-139, doi:10.1530/rep-13-0173 (2013).
74 Sado, T., Wang, Z., Sasaki, H. & Li, E. Regulation of imprinted X-chromosome inactivation in mice by Tsix. *Development (Cambridge, England)* **128**, 1275-1286 (2001).
75 Mak, W. *et al.* Reactivation of the paternal X chromosome in early mouse embryos. *Science* **303**, 666-669, doi:10.1126/science.1092674 (2004).
76 Soh, Y. Q. *et al.* Sequencing the mouse Y chromosome reveals convergent gene acquisition and amplification on both sex chromosomes. *Cell* **159**, 800-813, doi:10.1016/j.cell.2014.09.052 (2014).
77 Singh, N. P. *et al.* Epigenetic profile of the euchromatic region of human Y chromosome. *Nucleic acids research* **39**, 3594-3606, doi:10.1093/nar/gkq1342 (2011).
78 Moens, P. B. & Spyropoulos, B. Immunocytology of chiasmata and chromosomal disjunction at mouse meiosis. *Chromosoma* **104**, 175-182, doi:10.1007/bf00352182 (1995).
79 Oh, B., Hwang, S. Y., Solter, D. & Knowles, B. B. Spindlin, a major maternal transcript expressed in the mouse during the transition from oocyte to embryo. *Development (Cambridge, England)* **124**, 493-503 (1997).
80 Lee, K. H. *et al.* Ubiquitin-specific protease activity of USP9Y, a male infertility gene on the Y chromosome. *Reprod Fertil Dev* **15**, 129-133, doi:10.1071/rd03002 (2003).
81 Nakasuji, T. *et al.* Complementary Critical Functions of Zfy1 and Zfy2 in Mouse Spermatogenesis and Reproduction. *PLoS Genet* **13**, e1006578-e1006578, doi:10.1371/journal.pgen.1006578 (2017).
82 Vernet, N. *et al.* Mouse Y-Encoded Transcription Factor Zfy2 Is Essential for Sperm Head Remodelling and Sperm Tail Development. *PloS one* **11**, e0145398-e0145398, doi:10.1371/journal.pone.0145398 (2016).
83 Matsubara, Y. *et al.* TALEN-Mediated Gene Disruption on Y Chromosome Reveals Critical Role of EIF2S3Y in Mouse Spermatogenesis. *Stem Cells Dev* **24**, 1164-1170, doi:10.1089/scd.2014.0466 (2015).
84 Mazeyrat, S. *et al.* The mouse Y chromosome interval necessary for spermatogonial proliferation is gene dense with syntenic homology to the human AZFa region. *Human molecular genetics* **7**, 1713-1724, doi:10.1093/hmg/7.11.1713 (1998).
85 Kotov, A. A., Olenkina, O. M., Godneeva, B. K., Adashev, V. E. & Olenina, L. V. Progress in understanding the molecular functions of DDX3Y (DBY) in male germ cell development and maintenance. *Biosci Trends* **11**, 46-53, doi:10.5582/bst.2016.01216 (2017).
86 Vong, Q. P. *et al.* Structural characterization and expression studies of Dby and its homologs in the mouse. *J Androl* **27**, 653-661, doi:10.2164/jandrol.106.000471 (2006).
87 Yao, C. J. *et al.* The role of Dby mRNA in early development of male mouse zygotes. *Asian journal of andrology* **12**, 567-577, doi:10.1038/aja.2010.28 (2010).
88 Ditton, H. J., Zimmer, J., Kamp, C., Rajpert-De Meyts, E. & Vogt, P. H. The AZFa gene DBY (DDX3Y) is widely transcribed but the protein is limited to the male germ cells by translation control. *Human molecular genetics* **13**, 2333-2341, doi:10.1093/hmg/ddh240 (2004).

89 Chen, C.-P. *et al.* Prenatal diagnosis and molecular cytogenetic characterization of a small marker chromosome derived from Y chromosome. *Taiwan J Obstet Gynecol* **50**, 253-257, doi:10.1016/j.tjog.2011.04.007 (2011).
90 Bernardi, M. L., Cotinot, C., Payen, E. & Delouis, C. Transcription of Y- and X-linked genes in preimplantation ovine embryos. *Mol Reprod Dev* **45**, 132-138, doi:10.1002/(SICI)1098-2795(199610)45:2<132::AID-MRD4>3.0.CO;2-U (1996).
91 Kashimada, K. & Koopman, P. Sry: the master switch in mammalian sex determination. *Development (Cambridge, England)* **137**, 3921-3930, doi:10.1242/dev.048983 (2010).
92 Elliott, D. J. *et al.* An RBM Homologue Maps to the Mouse Y Chromosome and is Expressed in Germ Cells. *Human molecular genetics* **5**, 869-874, doi:10.1093/hmg/5.7.869 (1996).
93 Zeng, M. *et al.* Identification of target messenger RNA substrates for mouse RBMY. *Mol Hum Reprod* **14**, 331-336, doi:10.1093/molehr/gan024 (2008).
94 Houdebine, L.-M. in *The Laboratory Mouse* (eds Hans J. Hedrich & Gillian Bullock) 97-110 (Academic Press, 2004).
95 Davisson, M. T. & Linder, C. C. in *The Laboratory Mouse* (eds Hans J. Hedrich & Gillian Bullock) 15-24 (Academic Press, 2004).
96 Flurkey, K. & Currer, J. M. in *The Jackson Laboratory Handbook on Genetically Standardized Mice* (eds Kevin Flurkey, Joanne M. Currer, Edward H. Leiter, & Barbara Witham) Ch. 1, (2009).
97 Guénet, J.-L. & Bonhomme, F. in *The Laboratory Mouse* (eds Hans J. Hedrich & Gillian Bullock) 3-13 (Academic Press, 2004).
98 Group, T. M. G. D. *Mouse Genome Database (MGD) 2019, MGI 6.15*, <http://www.informatics.jax.org/mgihome/homepages/stats/all_stats.shtml> (2019).
99 Alam, M. M., Haque, S. M. & Ghosh, B. Karyomorphological studies of six commercially cultivated edible cucurbits: bitter gourd, sponge gourd, ridge gourd, snake gourd, ash gourd and cucumber. *Caryologia* **71**, 150-159, doi:10.1080/00087114.2018.1450800 (2018).
100 Li, L., Zheng, P. & Dean, J. Maternal control of early mouse development. *Development (Cambridge, England)* **137**, 859-870, doi:10.1242/dev.039487 (2010).
101 Pasantes, J. J. *et al.* 47,X,idic(Y),inv dup(Y): a non-mosaic case of a phenotypically normal boy with two different Y isochromosomes and neocentromere formation. *Cytogenetic and genome research* **136**, 157-162, doi:10.1159/000335705 (2012).
102 Aoki, F., Worrad, D. M. & Schultz, R. M. Regulation of transcriptional activity during the first and second cell cycles in the preimplantation mouse embryo. *Dev Biol* **181**, 296-307, doi:10.1006/dbio.1996.8466 (1997).
103 Bean, C. J., Hunt, P. A., Millie, E. A. & Hassold, T. J. Analysis of a malsegregating mouse Y chromosome: evidence that the earliest cleavage divisions of the mammalian embryo are non-disjunction-prone. *Human molecular genetics* **10**, 963-972 (2001).
104 Whitten, W. K. Chromosomal basis for hermaphrodism in mice. *The developmental biology of reproduction*, 189 (1975).
105 Kang, M., Piliszek, A., Artus, J. & Hadjantonakis, A.-K. FGF4 is required for lineage restriction and salt-and-pepper distribution of primitive endoderm factors but not their initial expression in the mouse. *Development (Cambridge, England)* **140**, 267-279, doi:10.1242/dev.084996 (2013).

106 Murashima, A., Xu, B. & Hinton, B. T. Understanding normal and abnormal development of the Wolffian/epididymal duct by using transgenic mice. *Asian journal of andrology* **17**, 749-755, doi:10.4103/1008-682X.155540 (2015).
107 Tanaka, S. S. & Nishinakamura, R. Regulation of male sex determination: genital ridge formation and Sry activation in mice. *Cell Mol Life Sci* **71**, 4781-4802, doi:10.1007/s00018-014-1703-3 (2014).
108 Yisheng, Y., Stephanie, W. & Megan, J. W. The molecular pathways underlying early gonadal development. *Journal of Molecular Endocrinology* **62**, R47-R64, doi:10.1530/JME-17-0314 (2019).
109 Morais da Silva, S. *et al.* Sox9 expression during gonadal development implies a conserved role for the gene in testis differentiation in mammals and birds. *Nature genetics* **14**, 62-68, doi:10.1038/ng0996-62 (1996).
110 Kent, J., Wheatley, S. C., Andrews, J. E., Sinclair, A. H. & Koopman, P. A male-specific role for SOX9 in vertebrate sex determination. *Development (Cambridge, England)* **122**, 2813-2822 (1996).
111 Karl, J. *et al.* Three-dimensional structure of the developing mouse genital ridge. *Philosophical Transactions of the Royal Society of London. Series B: Biological Sciences* **350**, 235-242, doi:doi:10.1098/rstb.1995.0157 (1995).
112 Martineau, J., Nordqvist, K., Tilmann, C., Lovell-Badge, R. & Capel, B. Male-specific cell migration into the developing gonad. *Current Biology* **7**, 958-968, doi:10.1016/S0960-9822(06)00415-5 (1997).
113 Coveney, D., Cool, J., Oliver, T. & Capel, B. Four-dimensional analysis of vascularization during primary development of an organ, the gonad. *Proceedings of the National Academy of Sciences* **105**, 7212-7217, doi:10.1073/pnas.0707674105 (2008).
114 Hu, Y.-C., Okumura, L. M. & Page, D. C. Gata4 Is Required for Formation of the Genital Ridge in Mice. *PLoS Genet* **9**, e1003629, doi:10.1371/journal.pgen.1003629 (2013).
115 Doitsidou, M. *et al.* Guidance of Primordial Germ Cell Migration by the Chemokine SDF-1. *Cell* **111**, 647-659, doi:10.1016/S0092-8674(02)01135-2 (2002).
116 Molyneaux, K. A., Stallock, J., Schaible, K. & Wylie, C. Time-Lapse Analysis of Living Mouse Germ Cell Migration. *Dev Biol* **240**, 488-498, doi:https://doi.org/10.1006/dbio.2001.0436 (2001).
117 Tam, P. P. & Snow, M. H. Proliferation and migration of primordial germ cells during compensatory growth in mouse embryos. *Journal of embryology and experimental morphology* **64**, 133-147 (1981).
118 Hacker, A., Capel, B., Goodfellow, P. & Lovell-Badge, R. Expression of Sry, the mouse sex determining gene. *Development (Cambridge, England)* **121**, 1603-1614 (1995).
119 Svingen, T. & Koopman, P. Building the mammalian testis: origins, differentiation, and assembly of the component cell populations. *Genes & development* **27**, 2409-2426, doi:10.1101/gad.228080.113 (2013).
120 Schmahl, J., Eicher, E. M., Washburn, L. L. & Capel, B. Sry induces cell proliferation in the mouse gonad. *Development (Cambridge, England)* **127**, 65-73 (2000).
121 Svingen, T., Spiller, C. M., Kashimada, K., Harley, V. R. & Koopman, P. Identification of suitable normalizing genes for quantitative real-time RT-PCR analysis of gene expression in fetal mouse gonads. *Sexual development : genetics, molecular biology, evolution, endocrinology, embryology, and pathology of sex determination and differentiation* **3**, 194-204, doi:10.1159/000228720 (2009).

122 Albrecht, K. H., Young, M., Washburn, L. L. & Eicher, E. M. Sry expression level and protein isoform differences play a role in abnormal testis development in C57BL/6J mice carrying certain Sry alleles. *Genetics* **164**, 277-288 (2003).
123 Bullejos, M. & Koopman, P. Delayed Sry and Sox9 expression in developing mouse gonads underlies B6-Y(DOM) sex reversal. *Dev Biol* **278**, 473-481, doi:10.1016/j.ydbio.2004.11.030 (2005).
124 Nagamine, C. M., Morohashi, K., Carlisle, C. & Chang, D. K. Sex reversal caused by Mus musculus domesticus Y chromosomes linked to variant expression of the testis-determining gene Sry. *Dev Biol* **216**, 182-194, doi:10.1006/dbio.1999.9436 (1999).
125 Albrecht, K. H. & Eicher, E. M. Evidence that Sry is expressed in pre-Sertoli cells and Sertoli and granulosa cells have a common precursor. *Dev Biol* **240**, 92-107, doi:10.1006/dbio.2001.0438 (2001).
126 Wilhelm, D. *et al.* Sertoli cell differentiation is induced both cell-autonomously and through prostaglandin signaling during mammalian sex determination. *Dev Biol* **287**, 111-124, doi:10.1016/j.ydbio.2005.08.039 (2005).
127 Sekido, R., Bar, I., Narváez, V., Penny, G. & Lovell-Badge, R. SOX9 is up-regulated by the transient expression of SRY specifically in Sertoli cell precursors. *Dev Biol* **274**, 271-279, doi:10.1016/j.ydbio.2004.07.011 (2004).
128 Zirkin, B. R. & Papadopoulos, V. Leydig cells: formation, function, and regulation†. *Biol Reprod* **99**, 101-111, doi:10.1093/biolre/ioy059 (2018).
129 Liu, C.-F., Barsoum, I., Gupta, R., Hofmann, M.-C. & Yao, H. H.-C. Stem cell potential of the mammalian gonad. *Front Biosci (Elite Ed)* **1**, 510-518, doi:10.2741/e47 (2009).
130 Polanco, J. C. & Koopman, P. Sry and the hesitant beginnings of male development. *Dev Biol* **302**, 13-24, doi:10.1016/j.ydbio.2006.08.049 (2007).
131 Jeske, Y. W., Bowles, J., Greenfield, A. & Koopman, P. Expression of a linear Sry transcript in the mouse genital ridge. *Nature genetics* **10**, 480-482, doi:10.1038/ng0895-480 (1995).
132 Nishino, K., Hattori, N., Tanaka, S. & Shiota, K. DNA methylation-mediated control of Sry gene expression in mouse gonadal development. *The Journal of biological chemistry* **279**, 22306-22313, doi:10.1074/jbc.M309513200 (2004).
133 She, Z.-Y. & Yang, W.-X. Sry and SoxE genes: How they participate in mammalian sex determination and gonadal development? *Semin Cell Dev Biol* **63**, 13-22, doi:10.1016/j.semcdb.2016.07.032 (2017).
134 Whitfield, L. S., Lovell-Badge, R. & Goodfellow, P. N. Rapid sequence evolution of the mammalian sex-determining gene SRY. *Nature* **364**, 713-715, doi:10.1038/364713a0 (1993).
135 Harley, V. R. & Goodfellow, P. N. The biochemical role of SRY in sex determination. *Mol Reprod Dev* **39**, 184-193, doi:10.1002/mrd.1080390211 (1994).
136 Koopman, P., Gubbay, J., Vivian, N., Goodfellow, P. & Lovell-Badge, R. Male development of chromosomally female mice transgenic for Sry. *Nature* **351**, 117-121, doi:10.1038/351117a0 (1991).
137 Gubbay, J. *et al.* A gene mapping to the sex-determining region of the mouse Y chromosome is a member of a novel family of embryonically expressed genes. *Nature* **346**, 245-250, doi:10.1038/346245a0 (1990).
138 Zhao, L., Quinn, A., Ng, E. T., Veyrunes, F. & Koopman, P. Reduced Activity of SRY and its Target Enhancer Sox9-TESCO in a Mouse Species with X*Y Sex Reversal. *Sci Rep* **7**, 41378-41378, doi:10.1038/srep41378 (2017).

139 Zhao, L. & Koopman, P. SRY protein function in sex determination: thinking outside the box. *Chromosome Research* **20**, 153-162, doi:10.1007/s10577-011-9256-x (2012).
140 Bowles, J., Cooper, L., Berkman, J. & Koopman, P. Sry requires a CAG repeat domain for male sex determination in Mus musculus. *Nature genetics* **22**, 405-408, doi:10.1038/11981 (1999).
141 Zhao, L. *et al.* Structure-function analysis of mouse Sry reveals dual essential roles of the C-terminal polyglutamine tract in sex determination. *Proceedings of the National Academy of Sciences of the United States of America* **111**, 11768-11773, doi:10.1073/pnas.1400666111 (2014).
142 Bishop, C. E., Boursot, P., Baron, B., Bonhomme, F. & Hatat, D. Most classical Mus musculus domesticus laboratory mouse strains carry a Mus musculus musculus Y chromosome. *Nature* **315**, 70-72, doi:10.1038/315070a0 (1985).
143 Wilhelm, D. *et al.* Antagonism of the testis- and ovary-determining pathways during ovotestis development in mice. *Mech Dev* **126**, 324-336, doi:10.1016/j.mod.2009.02.006 (2009).
144 Washburn, L. L. & Eicher, E. M. Normal testis determination in the mouse depends on genetic interaction of a locus on chromosome 17 and the Y chromosome. *Genetics* **123**, 173-179 (1989).
145 Yokoyama, T. *et al.* Genetic differences between C57BL/6 substrains affect the process of testis differentiation in Y(POS) mice. *J Vet Med Sci* **81**, 608-611, doi:10.1292/jvms.18-0621 (2019).
146 Eicher, E. M., Washburn, L. L., Whitney, J. B., 3rd & Morrow, K. E. Mus poschiavinus Y chromosome in the C57BL/6J murine genome causes sex reversal. *Science* **217**, 535-537, doi:10.1126/science.7089579 (1982).
147 Albrecht, K. H. & Eicher, E. M. DNA sequence analysis of Sry alleles (subgenus Mus) implicates misregulation as the cause of C57BL/6J-Y(POS) sex reversal and defines the SRY functional unit. *Genetics* **147**, 1267-1277 (1997).
148 Hiramatsu, R. *et al.* A critical time window of Sry action in gonadal sex determination in mice. *Development (Cambridge, England)* **136**, 129-138, doi:10.1242/dev.029587 (2009).
149 Turner, J. M. A. Meiotic sex chromosome inactivation. *Development (Cambridge, England)* **134**, 1823-1831, doi:10.1242/dev.000018 (2007).
150 Fayomi, A. P. & Orwig, K. E. Spermatogonial stem cells and spermatogenesis in mice, monkeys and men. *Stem Cell Research* **29**, 207-214, doi:https://doi.org/10.1016/j.scr.2018.04.009 (2018).
151 Oatley, J. M. & Brinster, R. L. The germline stem cell niche unit in mammalian testes. *Physiological reviews* **92**, 577-595, doi:10.1152/physrev.00025.2011 (2012).
152 Lee, J. T. Sex chromosome inactivation: the importance of pairing. *Current biology : CB* **15**, R249-R252, doi:10.1016/j.cub.2005.03.024 (2005).
153 Turner, J. M. A. *et al.* Silencing of unsynapsed meiotic chromosomes in the mouse. *Nature genetics* **37**, 41-47, doi:10.1038/ng1484 (2005).
154 Namekawa, S. H. *et al.* Postmeiotic sex chromatin in the male germline of mice. *Current biology : CB* **16**, 660-667, doi:10.1016/j.cub.2006.01.066 (2006).
155 Baarends, W. M. *et al.* Histone ubiquitination and chromatin remodeling in mouse spermatogenesis. *Dev Biol* **207**, 322-333, doi:10.1006/dbio.1998.9155 (1999).

156 Hendriksen, P. J. *et al.* Postmeiotic transcription of X and Y chromosomal genes during spermatogenesis in the mouse. *Dev Biol* **170**, 730-733, doi:10.1006/dbio.1995.1252 (1995).
157 Escalier, D. & Garchon, H. J. XMR is associated with the asynapsed segments of sex chromosomes in the XY body of mouse primary spermatocytes. *Chromosoma* **109**, 259-265, doi:10.1007/s004120000075 (2000).
158 Kim, K. S. & Kim, J. Disorders of sex development. *Korean J Urol* **53**, 1-8, doi:10.4111/kju.2012.53.1.1 (2012).
159 Chaboissier, M.-C. *et al.* Functional analysis of Sox8 and Sox9 during sex determination in the mouse. *Development (Cambridge, England)* **131**, 1891-1901, doi:10.1242/dev.01087 (2004).
160 Barseghyan, H. *et al.* Identification of novel candidate genes for 46,XY disorders of sex development (DSD) using a C57BL/6J-Y (POS) mouse model. *Biol Sex Differ* **9**, 8-8, doi:10.1186/s13293-018-0167-9 (2018).
161 Meyer, K. F. *et al.* The XY female and SWYER syndrome. *Urology Case Reports* **26**, 100939, doi:https://doi.org/10.1016/j.eucr.2019.100939 (2019).
162 Michala, L. & Creighton, S. M. The XY female. *Best Pract Res Clin Obstet Gynaecol* **24**, 139-148, doi:10.1016/j.bpobgyn.2009.09.009 (2010).
163 Feingold, K. *et al.* 46, XY Disorders of Sexual Development--Endotext. (2000).
164 Gimelli, G., Giorda, R., Beri, S., Gimelli, S. & Zuffardi, O. A 46,X,inv(Y) young woman with gonadal dysgenesis and gonadoblastoma: cytogenetics, molecular, and methylation studies. *American journal of medical genetics. Part A* **140**, 40-45, doi:10.1002/ajmg.a.31044 (2006).
165 Elgin, S. C. R. & Reuter, G. Position-effect variegation, heterochromatin formation, and gene silencing in Drosophila. *Cold Spring Harbor perspectives in biology* **5**, a017780-a017780, doi:10.1101/cshperspect.a017780 (2013).
166 Elliott, D. J. *et al.* Dynamic changes in the subnuclear organisation of pre-mRNA splicing proteins and RBM during human germ cell development. *Journal of cell science* **111 (Pt 9)**, 1255-1265 (1998).
167 Abid, S., Sagare-Patil, V., Gokral, J. & Modi, D. Cellular ontogeny of RBMY during human spermatogenesis and its role in sperm motility. *J Biosci* **38**, 85-92, doi:10.1007/s12038-012-9281-8 (2013).
168 Abid, S. *et al.* Clinical and laboratory evaluation of idiopathic male infertility in a secondary referral center in India. *J Clin Lab Anal* **22**, 29-38, doi:10.1002/jcla.20216 (2008).
169 Foresta, C., Moro, E. & Ferlin, A. Y chromosome microdeletions and alterations of spermatogenesis. *Endocr Rev* **22**, 226-239, doi:10.1210/edrv.22.2.0425 (2001).
170 Mahadevaiah, S. K. *et al.* Mouse homologues of the human AZF candidate gene RBM are expressed in spermatogonia and spermatids, and map to a Y chromosome deletion interval associated with a high incidence of sperm abnormalities. *Human molecular genetics* **7**, 715-727 (1998).
171 Capel, B. *et al.* Deletion of Y chromosome sequences located outside the testis determining region can cause XY female sex reversal. *Nature genetics* **5**, 301-307, doi:10.1038/ng1193-301 (1993).
172 Laval, S. H. *et al.* Y chromosome short arm-Sxr recombination in XSxr/Y males causes deletion of Rbm and XY female sex reversal. *Proceedings of the National Academy of Sciences of the United States of America* **92**, 10403-10407 (1995).

173 Vernet, N. *et al.* The expression of Y-linked Zfy2 in XY mouse oocytes leads to frequent meiosis 2 defects, a high incidence of subsequent early cleavage stage arrest and infertility. *Development (Cambridge, England)* **141**, 855-866, doi:10.1242/dev.091165 (2014).
174 Alexopoulou, A. N., Couchman, J. R. & Whiteford, J. R. The CMV early enhancer/chicken beta actin (CAG) promoter can be used to drive transgene expression during the differentiation of murine embryonic stem cells into vascular progenitors. *BMC Cell Biol* **9**, 2-2, doi:10.1186/1471-2121-9-2 (2008).
175 Hense, A., Nienhaus, K. & Nienhaus, G. U. Exploring color tuning strategies in red fluorescent proteins. *Photochemical & Photobiological Sciences* **14**, 200-212, doi:10.1039/C4PP00212A (2015).
176 Evrogen. *Far-red fluorescent protein mKate2*, <http://evrogen.com/products/mKate2/mKate2_Detailed_description.shtml> (2002-2020).
177 Rohozinski, J., Agoulnik, A. I., Boettger-Tong, H. L. & Bishop, C. E. Successful targeting of mouse Y chromosome genes using a site-directed insertion vector. *Genesis* **32**, 1-7, doi:10.1002/gene.10020 (2002).
178 Bevis, B. J. & Glick, B. S. Rapidly maturing variants of the Discosoma red fluorescent protein (DsRed). *Nat Biotechnol* **20**, 83-87, doi:10.1038/nbt0102-83 (2002).
179 Tang, S.-H. E., Silva, F. J., Tsark, W. M. K. & Mann, J. R. A Cre/loxP-deleter transgenic line in mouse strain 129S1/SvImJ. *Genesis* **32**, 199-202, doi:10.1002/gene.10030 (2002).
180 Strack, R. L. *et al.* A noncytotoxic DsRed variant for whole-cell labeling. *Nat Methods* **5**, 955-957, doi:10.1038/nmeth.1264 (2008).
181 Deng, C. & Capecchi, M. R. Reexamination of gene targeting frequency as a function of the extent of homology between the targeting vector and the target locus. *Mol Cell Biol* **12**, 3365-3371, doi:10.1128/mcb.12.8.3365 (1992).
182 Festing, M. F. *Inbred Strains of Mice: A*, <http://www.informatics.jax.org/inbred_strains/mouse/docs/A.shtml> (1998).
183 *Mouse Strain Datasheet - 000646*, <https://www.jax.org/strain/000646> (2020).
184 Zhao, X. *et al.* Identification of the Sex of Pre-implantation Mouse Embryos Using a Marked Y Chromosome and CRISPR/Cas9. *Sci Rep* **9**, 14315, doi:10.1038/s41598-019-50731-x (2019).
185 Kent WJ, S. C., Furey TS, Roskin KM, Pringle TH, Zahler AM, Haussler D. The human genome browser at UCSC. *Genome Res.* **12**, 996-1006 (2002 Jun).
186 Ye J, C. G., Zaretskaya I, Cutcutache I, Rozen S, Madden T. Primer-BLAST: A tool to design target-specific primers for polymerase chain reaction. *BMC Bioinformatics* **13** (2012).
187 *Mouse Strain Datasheet - 002448*, <https://www.jax.org/strain/002448> (2020).
188 Clapcote, S. J. & Roder, J. C. Deletion polymorphism of Disc1 is common to all 129 mouse substrains: implications for gene-targeting studies of brain function. *Genetics* **173**, 2407-2410, doi:10.1534/genetics.106.060749 (2006).
189 Vasudevan, K. & Sztein, J. M. In vitro fertility rate of 129 strain is improved by buserelin (gonadotropin-releasing hormone) administration prior to superovulation. *Lab Anim* **46**, 299-303, doi:10.1258/la.2012.012073 (2012).
190 *Mouse Strain Datasheet - 002101*, <https://www.jax.org/strain/002101> (2020).
191 *Mouse Strain Datasheet - 000664*, <https://www.jax.org/strain/000664> (2020).

192 Bult, C. J. *et al.* Mouse Genome Database (MGD) 2019. *Nucleic Acids Research* **8**, (D1): D801–D806 (2019).
193 *Mouse Strain Datasheet - 000651*, <https://www.jax.org/strain/000651> (2020).
194 *Mouse Strain Datasheet - 000645*, <https://www.jax.org/strain/000645> (2019).
195 Potter, M. History of the BALB/c family. *Curr Top Microbiol Immunol* **122**, 1-5, doi:10.1007/978-3-642-70740-7_1 (1985).
196 Tam, P. P. L. The control of somitogenesis in mouse embryos. *Journal of embryology and experimental morphology* **65**, 103-128 (1981).
197 Theiler, K. The house mouse : atlas of embryonic development. (1989).
198 Scavizzi, F. *et al.* Blastocyst genotyping for quality control of mouse mutant archives: an ethical and economical approach. *Transgenic Res* **24**, 921-927, doi:10.1007/s11248-015-9897-1 (2015).
199 Brown, W. E., Hu, J. C. & Athanasiou, K. A. Ammonium-Chloride-Potassium Lysing Buffer Treatment of Fully Differentiated Cells Increases Cell Purity and Resulting Neotissue Functional Properties. *Tissue Eng Part C Methods* **22**, 895-903, doi:10.1089/ten.TEC.2016.0184 (2016).
200 Bio-Rad Laboratories, I. Vol. Bulletin 6407, version B.
201 Li, Y. & Tollefsbol, T. O. DNA methylation detection: bisulfite genomic sequencing analysis. *Methods Mol Biol* **791**, 11-21, doi:10.1007/978-1-61779-316-5_2 (2011).
202 Wreczycka, K. *et al.* Strategies for analyzing bisulfite sequencing data. *J Biotechnol* **261**, 105-115, doi:10.1016/j.jbiotec.2017.08.007 (2017).
203 Saiz, N. & Plusa, B. Early cell fate decisions in the mouse embryo. *Reproduction (Cambridge, England)* **145**, R65-R80, doi:10.1530/REP-12-0381 (2013).
204 Laboratory, T. J. in *A Jackson Laboratory Resource Manual* (2007).
205 Jinnah, H. A. Lesch-Nyhan disease: from mechanism to model and back again. *Dis Model Mech* **2**, 116-121, doi:10.1242/dmm.002543 (2009).
206 O'Leary, N. A. *et al.* Reference sequence (RefSeq) database at NCBI: current status, taxonomic expansion, and functional annotation. *Nucleic acids research* **44**, D733-D745, doi:10.1093/nar/gkv1189 (2016).
207 Jiralerspong, S. & Patel, P. I. Regulation of the hypoxanthine phosphoribosyltransferase gene: in vitro and in vivo approaches. *Proc Soc Exp Biol Med* **212**, 116-127, doi:10.3181/00379727-212-43998 (1996).
208 Cvetkovic, B., Yang, B., Williamson, R. A. & Sigmund, C. D. Appropriate tissue- and cell-specific expression of a single copy human angiotensinogen transgene specifically targeted upstream of the HPRT locus by homologous recombination. *The Journal of biological chemistry* **275**, 1073-1078, doi:10.1074/jbc.275.2.1073 (2000).
209 Guillot, P. V. *et al.* Targeting of human eNOS promoter to the Hprt locus of mice leads to tissue-restricted transgene expression. *Physiol Genomics* **2**, 77-83, doi:10.1152/physiolgenomics.2000.2.2.77 (2000).
210 Capecchi, M. R. Altering the genome by homologous recombination. *Science* **244**, 1288-1292, doi:10.1126/science.2660260 (1989).
211 Barakat, T. S. & Gribnau, J. in *The Cell Biology of Stem Cells* (eds Eran Meshorer & Kathrin Plath) 132-154 (Springer US, 2010).
212 *DAB staining*, <https://www.abcam.com/kits/dab-staining> (1998-2020).
213 Pinto, A. R. *et al.* Revisiting Cardiac Cellular Composition. *Circ Res* **118**, 400-409, doi:10.1161/CIRCRESAHA.115.307778 (2016).

214 Shcherbo, D. *et al.* Far-red fluorescent tags for protein imaging in living tissues. *Biochemical Journal* **418**, 567-574, doi:10.1042/bj20081949 (2009).
215 Lund, J. B. *et al.* Age-dependent DNA methylation patterns on the Y chromosome in elderly males. *Aging Cell* **n/a**, e12907, doi:10.1111/acel.12907 (2019).
216 Berletch, J. B., Yang, F. & Disteche, C. M. Escape from X inactivation in mice and humans. *Genome biology* **11**, 213, doi:10.1186/gb-2010-11-6-213 (2010).
217 Belmont, J. W. Genetic control of X inactivation and processes leading to X-inactivation skewing. *Am J Hum Genet* **58**, 1101-1108 (1996).
218 Faggioli, F., Wang, T., Vijg, J. & Montagna, C. Chromosome-specific accumulation of aneuploidy in the aging mouse brain. *Human molecular genetics* **21**, 5246-5253, doi:10.1093/hmg/dds375 (2012).
219 Pierre, R. V. & Hoagland, H. C. Age-associated aneuploidy: loss of Y chromosome from human bone marrow cells with aging. *Cancer* **30**, 889-894, doi:10.1002/1097-0142(197210)30:4<889::aid-cncr2820300405>3.0.co;2-1 (1972).
220 Turner, V. M. & Mabbott, N. A. Influence of ageing on the microarchitecture of the spleen and lymph nodes. *Biogerontology* **18**, 723-738, doi:10.1007/s10522-017-9707-7 (2017).
221 Delire, B. *et al.* Aging enhances liver fibrotic response in mice through hampering extracellular matrix remodeling. *Aging (Albany NY)* **9**, 98-113, doi:10.18632/aging.101124 (2016).
222 Lim, J. H. *et al.* Age-Associated Molecular Changes in the Kidney in Aged Mice. *Oxidative Medicine and Cellular Longevity* **2012**, 171383, doi:10.1155/2012/171383 (2012).
223 Razzaque, M. S. Does renal ageing affect survival? *Ageing Research Reviews* **6**, 211-222, doi:https://doi.org/10.1016/j.arr.2007.06.001 (2007).
224 Schulte, H., Mühlfeld, C. & Brandenberger, C. Age-Related Structural and Functional Changes in the Mouse Lung. *Front Physiol* **10**, 1466-1466, doi:10.3389/fphys.2019.01466 (2019).
225 Kobayashi, S. *et al.* Live imaging of X chromosome reactivation dynamics in early mouse development can discriminate naïve from primed pluripotent stem cells. *Development (Cambridge, England)* **143**, 2958-2964, doi:10.1242/dev.136739 (2016).
226 Nichols, J. & Smith, A. Naive and primed pluripotent states. *Cell Stem Cell* **4**, 487-492, doi:10.1016/j.stem.2009.05.015 (2009).
227 Patek, C. E. *et al.* Sex chimaerism, fertility and sex determination in the mouse. *Development (Cambridge, England)* **113**, 311-325 (1991).
228 Utomo, A. R., Nikitin, A. Y. & Lee, W. H. Temporal, spatial, and cell type-specific control of Cre-mediated DNA recombination in transgenic mice. *Nat Biotechnol* **17**, 1091-1096, doi:10.1038/15073 (1999).
229 Thompson, S. L., Bakhoum, S. F. & Compton, D. A. Mechanisms of chromosomal instability. *Current biology : CB* **20**, R285-R295, doi:10.1016/j.cub.2010.01.034 (2010).
230 Chiang, A. C. & Massagué, J. Molecular basis of metastasis. *N Engl J Med* **359**, 2814-2823, doi:10.1056/NEJMra0805239 (2008).
231 Segre, J. A., Nemhauser, J. L., Taylor, B. A., Nadeau, J. H. & Lander, E. S. Positional Cloning of the nude Locus: Genetic, Physical, and Transcription Maps of the Region and Mutations in the Mouse and Rat. *Genomics* **28**, 549-559, doi:https://doi.org/10.1006/geno.1995.1187 (1995).
232 Arnold, A. P. & Disteche, C. M. Sexual Inequality in the Cancer Cell. *Cancer Res* **78**, 5504-5505, doi:10.1158/0008-5472.CAN-18-2219 (2018).

233 Toufektchan, E. & Toledo, F. The Guardian of the Genome Revisited: p53 Downregulates Genes Required for Telomere Maintenance, DNA Repair, and Centromere Structure. *Cancers (Basel)* **10**, 135, doi:10.3390/cancers10050135 (2018).
234 Lane, D. P. Cancer. p53, guardian of the genome. *Nature* **358**, 15-16, doi:10.1038/358015a0 (1992).
235 Vogelstein, B., Lane, D. & Levine, A. J. Surfing the p53 network. *Nature* **408**, 307-310, doi:10.1038/35042675 (2000).
236 Zilfou, J. T. & Lowe, S. W. Tumor suppressive functions of p53. *Cold Spring Harbor perspectives in biology* **1**, a001883-a001883, doi:10.1101/cshperspect.a001883 (2009).
237 Hanel, W. & Moll, U. M. Links between mutant p53 and genomic instability. *J Cell Biochem* **113**, 433-439, doi:10.1002/jcb.23400 (2012).
238 Woo, R. A. & Poon, R. Y. Activated oncogenes promote and cooperate with chromosomal instability for neoplastic transformation. *Genes & development* **18**, 1317-1330, doi:10.1101/gad.1165204 (2004).
239 Eischen, C. M. Genome Stability Requires p53. *Cold Spring Harb Perspect Med* **6**, a026096, doi:10.1101/cshperspect.a026096 (2016).
240 Lanni, J. S. & Jacks, T. Characterization of the p53-dependent postmitotic checkpoint following spindle disruption. *Mol Cell Biol* **18**, 1055-1064, doi:10.1128/mcb.18.2.1055 (1998).
241 Cross, S. M. *et al.* A p53-dependent mouse spindle checkpoint. *Science* **267**, 1353-1356, doi:10.1126/science.7871434 (1995).
242 Gualberto, A., Aldape, K., Kozakiewicz, K. & Tlsty, T. D. An oncogenic form of p53 confers a dominant, gain-of-function phenotype that disrupts spindle checkpoint control. *Proceedings of the National Academy of Sciences of the United States of America* **95**, 5166-5171, doi:10.1073/pnas.95.9.5166 (1998).
243 Xing, Y. & Hogquist, K. A. Isolation, identification, and purification of murine thymic epithelial cells. *J Vis Exp*, e51780-e51780, doi:10.3791/51780 (2014).
244 Irla, M. *et al.* Three-Dimensional Visualization of the Mouse Thymus Organization in Health and Immunodeficiency. *The Journal of Immunology* **190**, 586-596, doi:10.4049/jimmunol.1200119 (2013).
245 Su, D.-m. & Manley, N. R. Stage-specific changes in fetal thymocyte proliferation during the CD4-8- to CD4+8+ transition in wild type, Rag1-/-, and Hoxa3,Pax1 mutant mice. *BMC Immunol* **3**, 12-12, doi:10.1186/1471-2172-3-12 (2002).
246 Rezzani, R., Nardo, L., Favero, G., Peroni, M. & Rodella, L. F. Thymus and aging: morphological, radiological, and functional overview. *Age (Dordr)* **36**, 313-351, doi:10.1007/s11357-013-9564-5 (2014).
247 Aw, D. & Palmer, D. B. It's not all equal: a multiphasic theory of thymic involution. *Biogerontology* **13**, 77-81, doi:10.1007/s10522-011-9349-0 (2012).
248 Song, H. *et al.* Cytosolic phospholipase A2alpha is crucial [correction of A2alpha deficiency is crucial] for 'on-time' embryo implantation that directs subsequent development. *Development (Cambridge, England)* **129**, 2879-2889 (2002).
249 Eicher, E. M., Beamer, W. G., Washburn, L. L. & Whitten, W. K. A cytogenetic investigation of inherited true hermaphroditism in BALB/cWt mice. *Cytogenetics and cell genetics* **28**, 104-115, doi:10.1159/000131518 (1980).
250 Phillips, T. R., Wright, D. K., Gradie, P. E., Johnston, L. A. & Pask, A. J. A Comprehensive Atlas of the Adult Mouse Penis. *Sexual development : genetics, molecular biology,*

evolution, endocrinology, embryology, and pathology of sex determination and differentiation **9**, 162-172, doi:10.1159/000431010 (2015).
251 Blaschko, S. D. *et al.* Analysis of the effect of estrogen/androgen perturbation on penile development in transgenic and diethylstilbestrol-treated mice. *Anat Rec (Hoboken)* **296**, 1127-1141, doi:10.1002/ar.22708 (2013).
252 Hotchkiss, A. K. & Vandenbergh, J. G. The anogenital distance index of mice (Mus musculus domesticus): an analysis. *Contemp Top Lab Anim Sci* **44**, 46-48 (2005).
253 Jang, H. S., Shin, W. J., Lee, J. E. & Do, J. T. CpG and Non-CpG Methylation in Epigenetic Gene Regulation and Brain Function. *Genes* **8**, doi:10.3390/genes8060148 (2017).
254 Szot, M. *et al.* Does Rbmy have a role in sperm development in mice? *Cytogenetic And Genome Research* **103**, 330-336 (2003).
255 Case, L. K. *et al.* Copy number variation in Y chromosome multicopy genes is linked to a paternal parent-of-origin effect on CNS autoimmune disease in female offspring. *Genome biology* **16**, 28, doi:10.1186/s13059-015-0591-7 (2015).
256 Wilhelm, D., Palmer, S. & Koopman, P. Sex Determination and Gonadal Development in Mammals. *Physiological Reviews* **87**, 1-28, doi:10.1152/physrev.00009.2006 (2007).
257 Rato, L. *et al.* Metabolic regulation is important for spermatogenesis. *Nat Rev Urol* **9**, 330-338, doi:10.1038/nrurol.2012.77 (2012).
258 Harley, V. R., Lovell-Badge, R. & Goodfellow, P. N. Definition of a consensus DNA binding site for SRY. *Nucleic acids research* **22**, 1500-1501, doi:10.1093/nar/22.8.1500 (1994).
259 Ono, M. & Harley, V. R. Disorders of sex development: new genes, new concepts. *Nature Reviews Endocrinology*, 79, doi:10.1038/nrendo.2012.235 (2013).
260 Koopman, P., Münsterberg, A., Capel, B., Vivian, N. & Lovell-Badge, R. Expression of a candidate sex-determining gene during mouse testis differentiation. *Nature* **348**, 450-452, doi:10.1038/348450a0 (1990).
261 Dolci, S., Grimaldi, P., Geremia, R., Pesce, M. & Rossi, P. Identification of a promoter region generating Sry circular transcripts both in germ cells from male adult mice and in male mouse embryonal gonads. *Biol Reprod* **57**, 1128-1135, doi:10.1095/biolreprod57.5.1128 (1997).
262 Nishino, K. *et al.* Non-CpG methylation occurs in the regulatory region of the Sry gene. *J Reprod Dev* **57**, 586-593, doi:10.1262/jrd.11-033a (2011).
263 Capel, B. *et al.* Circular transcripts of the testis-determining gene Sry in adult mouse testis. *Cell* **73**, 1019-1030, doi:10.1016/0092-8674(93)90279-y (1993).
264 Rossi, P., Dolci, S., Albanesi, C., Grimaldi, P. & Geremia, R. Direct evidence that the mouse sex-determining gene Sry is expressed in the somatic cells of male fetal gonads and in the germ cell line in the adult testis. *Mol Reprod Dev* **34**, 369-373, doi:10.1002/mrd.1080340404 (1993).
265 Lahr, G. *et al.* Transcription of the Y chromosomal gene, Sry, in adult mouse brain. *Brain Res Mol Brain Res* **33**, 179-182, doi:10.1016/0169-328x(95)00136-g (1995).
266 Okashita, N., Kuroki, S., Maeda, R. & Tachibana, M. TET2 catalyzes active DNA demethylation of the Sry promoter and enhances its expression. *Sci Rep* **9**, 13462-13462, doi:10.1038/s41598-019-50058-7 (2019).
267 Petell, C. J., Loiseau, G., Gandy, R., Pradhan, S. & Gowher, H. A refined DNA methylation detection method using MspJI coupled quantitative PCR. *Analytical biochemistry* **533**, 1-9, doi:10.1016/j.ab.2017.06.006 (2017).

268 Pharo, H. D. *et al.* A robust internal control for high-precision DNA methylation analyses by droplet digital PCR. *Clinical Epigenetics* **10**, 24, doi:10.1186/s13148-018-0456-5 (2018).
269 Van Wesenbeeck, L., Janssens, L., Meeuws, H., Lagatie, O. & Stuyver, L. Droplet digital PCR is an accurate method to assess methylation status on FFPE samples. *Epigenetics* **13**, 207-213, doi:10.1080/15592294.2018.1448679 (2018).
270 Quinn, A. *et al.* A Site-Specific, Single-Copy Transgenesis Strategy to Identify 5′ Regulatory Sequences of the Mouse Testis-Determining Gene Sry. *PLOS ONE* **9**, e94813, doi:10.1371/journal.pone.0094813 (2014).
271 Warr, N. *et al.* Transgenic expression of Map3k4 rescues T-associated sex reversal (Tas) in mice. *Human molecular genetics* **23**, 3035-3044, doi:10.1093/hmg/ddu020 (2014).
272 Saksouk, N., Simboeck, E. & Déjardin, J. Constitutive heterochromatin formation and transcription in mammals. *Epigenetics & Chromatin* **8**, 3, doi:10.1186/1756-8935-8-3 (2015).
273 Kuroki, S. *et al.* Rescuing the aberrant sex development of H3K9 demethylase Jmjd1a-deficient mice by modulating H3K9 methylation balance. *PLoS Genet* **13**, e1007034, doi:10.1371/journal.pgen.1007034 (2017).
274 Garcia-Moreno, S. A., Plebanek, M. P. & Capel, B. Epigenetic regulation of male fate commitment from an initially bipotential system. *Mol Cell Endocrinol* **468**, 19-30, doi:10.1016/j.mce.2018.01.009 (2018).
275 Katoh-Fukui, Y. *et al.* Cbx2, a polycomb group gene, is required for Sry gene expression in mice. *Endocrinology* **153**, 913-924, doi:10.1210/en.2011-1055 (2012).
276 Kuroki, S. *et al.* Epigenetic Regulation of Mouse Sex Determination by the Histone Demethylase Jmjd1a. *Science* **341**, 1106-1109, doi:10.1126/science.1239864 (2013).
277 López-Otín, C., Blasco, M. A., Partridge, L., Serrano, M. & Kroemer, G. The hallmarks of aging. *Cell* **153**, 1194-1217, doi:10.1016/j.cell.2013.05.039 (2013).
278 White, M. C. *et al.* Age and cancer risk: a potentially modifiable relationship. *Am J Prev Med* **46**, S7-S15, doi:10.1016/j.amepre.2013.10.029 (2014).
279 Hanahan, D. & Weinberg, R. A. Hallmarks of cancer: the next generation. *Cell* **144**, 646-674, doi:10.1016/j.cell.2011.02.013 (2011).
280 Zhang, Q., Walawage, S. L., Tricoli, D. M., Dandekar, A. M. & Leslie, C. A. A red fluorescent protein (DsRED) from Discosoma sp. as a reporter for gene expression in walnut somatic embryos. *Plant Cell Rep* **34**, 861-869, doi:10.1007/s00299-015-1749-1 (2015).
281 Baker, S. J. *et al.* p53 Gene Mutations Occur in Combination with 17p Allelic Deletions as Late Events in Colorectal Tumorigenesis. *Cancer Res* **50**, 7717-7722 (1990).
282 Olivier, M. *et al.* The clinical value of somatic TP53 gene mutations in 1,794 patients with breast cancer. *Clinical Cancer Research* **12**, 1157-1167, doi:10.1158/1078-0432.Ccr-05-1029 (2006).
283 Chen, C.-Y., Cheng, Y.-Y., Yen, C. Y. T. & Hsieh, P. C. H. Mechanisms of pluripotency maintenance in mouse embryonic stem cells. *Cell Mol Life Sci* **74**, 1805-1817, doi:10.1007/s00018-016-2438-0 (2017).
284 Navin, A. *et al.* Mouse Y-Specific Repeats Isolated by Whole Chromosome Representational Difference Analysis. *Genomics* **36**, 349-353, doi:https://doi.org/10.1006/geno.1996.0473 (1996).
285 Berloco, M., Palumbo, G., Piacentini, L., Pimpinelli, S. & Fanti, L. Position Effect Variegation and Viability Are Both Sensitive to Dosage of Constitutive Heterochromatin in

Drosophila. *G3: Genes|Genomes|Genetics* **4**, 1709-1716, doi:10.1534/g3.114.013045 (2014).

286 Magaraki, A. *et al.* Silencing markers are retained on pericentric heterochromatin during murine primordial germ cell development. *Epigenetics & Chromatin* **10**, 11, doi:10.1186/s13072-017-0119-3 (2017).

287 Richards, E. J. & Elgin, S. C. R. Epigenetic codes for heterochromatin formation and silencing: rounding up the usual suspects. *Cell* **108**, 489-500, doi:10.1016/s0092-8674(02)00644-x (2002).

288 Rountree, M. R. & Selker, E. U. DNA methylation and the formation of heterochromatin in Neurospora crassa. *Heredity (Edinb)* **105**, 38-44, doi:10.1038/hdy.2010.44 (2010).

289 Curradi, M., Izzo, A., Badaracco, G. & Landsberger, N. Molecular mechanisms of gene silencing mediated by DNA methylation. *Mol Cell Biol* **22**, 3157-3173, doi:10.1128/mcb.22.9.3157-3173.2002 (2002).

290 De Smet, C., Lurquin, C., Lethé, B., Martelange, V. & Boon, T. DNA methylation is the primary silencing mechanism for a set of germ line- and tumor-specific genes with a CpG-rich promoter. *Mol Cell Biol* **19**, 7327-7335, doi:10.1128/mcb.19.11.7327 (1999).

291 Wang, J., Lawry, S. T., Cohen, A. L. & Jia, S. Chromosome boundary elements and regulation of heterochromatin spreading. *Cell Mol Life Sci* **71**, 4841-4852, doi:10.1007/s00018-014-1725-x (2014).

292 De Bustos, A., Cuadrado, A. & Jouve, N. Sequencing of long stretches of repetitive DNA. *Sci Rep* **6**, 36665, doi:10.1038/srep36665 (2016).

293 Payne, A., Holmes, N., Rakyan, V. & Loose, M. Whale watching with BulkVis: A graphical viewer for Oxford Nanopore bulk fast5 files. *bioRxiv*, 312256, doi:10.1101/312256 (2018).

294 Shoemaker, M. B. & Heideman, P. D. Reduced body mass, food intake, and testis size in response to short photoperiod in adult F344 rats. *BMC Physiol* **2**, 11-11, doi:10.1186/1472-6793-2-11 (2002).